# Decays of Hadrons as Probes of the Standard Model and Beyond

A thesis submitted in partial fulfilment of
the requirements for the degree of

**Doctor of Philosophy**

*by*


**Girish Kumar**

(Roll No. 11330021)


Under the guidance of


**Dr. Namit Mahajan**

Associate Professor

Theoretical Physics Division

Physical Research Laboratory, Ahmedabad, India.



DEPARTMENT OF PHYSICS

INDIAN INSTITUTE OF TECHNOLOGY GANDHINAGAR



2016

*to*

*my mother*

# Declaration

I declare that this written submission represents my ideas in my own words and where others' ideas or words have been included, I have adequately cited and referenced the original sources. I also declare that I have adhered to all principles of academic honesty and integrity and have not misrepresented or fabricated or falsified any idea/data/fact/source in my submission. I understand that any violation of the above will be cause for disciplinary action by the Institute and can also evoke penal action from the sources which have thus not been properly cited or from whom proper permission has not been taken when needed.

(Signature)

(Name: Girish Kumar)

(Roll No: 11330021)

Date: September 2, 2016

# CERTIFICATE

It is certified that the work contained in this thesis titled **"Decays of Hadrons as Probes of the Standard Model and Beyond"** by **Mr. Girish Kumar** (Roll No. 11330021), has been carried out under my supervision and that this work has not been submitted elsewhere for a degree.

Dr. Namit Mahajan
(Thesis Supervisor)
Associate Professor,
Theoretical Physics Division,
Physical Research Laboratory,
Ahmedabad, India.

Date: September 2, 2016

# Acknowledgements

*I would like to express my deepest gratitude and heartiest respect towards my thesis supervisor, Dr. Namit Mahajan, for his guidance, patience and support throughout these last five years. It has been a pleasure working under his supervision. I have greatly benefitted from his understanding, expertise and clean approach on the subject. I truly appreciate his willingness to discuss any idea or thought on the subject (or even completely different subject, for that matter), which has been instrumental in creating an amiable working relationship. His continued support and encouragement has kept me going and inspired me to work harder. I am also grateful for his personal concern and support towards my well-being during these five years. I feel myself privileged and lucky to have got the opportunity to work under his supervision.*

*I would like to extend my sincere gratitude to Prof. Anjan Joshipura, Prof. Saurabh Rindani, and Prof. Hiranmaya Mishra for reviewing my thesis work, and for their many valuable advice, comments, and suggestions which were critical in improving the quality of my research work. I am obliged to Prof. Srubabati Goswami, Prof. Raghavan Rangarajan, Prof. Angom Dilip, Dr. Bijaya Sahoo, Dr. Partha Konar, and Dr. Navinder Singh for teaching courses during my course work at PRL. Here, I also owe thanks to Prof. Subhendra Mohanty for teaching many useful high energy physics courses which had helped me in grasping many intricate things on the subject.*

*I am very much indebted to Chandan Hati and Diganta Das, with whom I have enjoyed working on various research projects. I wholeheartedly acknowledge their help and support.*

*I am thankful to the Director and the Dean of PRL for their support and for providing necessary facilities to carry out research work. In this regard, I would also like to thank Prof. Utpal Sarkar and Prof. J. Goswami, former Directors, PRL for their support. I would like to convey my sincere thanks to the members of Academic Committee, PRL for timely reviewing the progress of this thesis and giving valuable inputs.*

*I would like to extend my thanks to all the academic and administrative staff* *members of PRL and IIT Gandhinagar. I gratefully acknowledge their efforts and readiness to sort out any problem that I faced during my doctoral study.*

*My most heartfelt thanks go to my dearest friends Arun, Manu, Guru, Abhaya, Tanmoy, Alok, Sanjay, Anirban, Shradhha, Ikshu, Kuldeep and Chithrabhanu. Without their love, support, and companionship, my life would not have been so much fun and enjoyable in these long years. I would like to especially thank Naveen Negi who is like a brother to me and has been very supportive and affectionate towards me. Over the course of last five years, I have met some really awesome people here in PRL. Special mention to my seniors Bhaswar, Saumya, Pankaj, Ketan, Vimal, Suman, Arko, Gaurav Tomar, Bhavya, Priyanka, Shweta, Tanmoy Chattopadhyay, Monojit, Dillip, Avdhesh, Girish C, Yashpal, for being warm and helpful to me. I would like to thank Arko, Chandan H, Avdhesh, Chandan G for being wonderful officemates. I would also like to thank Dipti, Deepak, Venky, Newton, Lalit, Bivin, Rukmani, Navpreet, Rupa, Satish, Prahlad, Kuldeep, Jabir, Bharti, Bhavesh and Varun for their support and friendship.*

*Finally, I would like to thank my parents for their unconditional love and support, and for everything they had to put up with so that I could pursue higher education. I will always remain grateful to them. I would also like to thank: my grandparents who raised me up; my sister, Swati, for always sticking by me; my little brother, Ani, for making me watch "Doraemon" and "Chhota Bheem" whenever I visit home; and my uncle, Rakesh, for believing in me.*

***( Girish Kumar )***

# Abstract

Flavor physics is the study of quark "flavors" and their interactions involving change of one type of flavor to another type of flavor. It is known that, historically, the study of flavor physics has played a key role in the development of the Standard Model (SM) of particle physics. The recent discovery of the last missing piece, the Higgs boson, in the first run of the Large Hadron Collider (LHC) marks the completion of the SM. The SM has been exceptionally successful in explaining the experimental data collected so far. However, there are many experimental measurements which point towards the existence of physics beyond the SM. Therefore, it is natural to consider SM as the low-energy limit of a more general theory above the electroweak scale. The next important task is then to look for hints of the physics beyond the SM. In this endeavour, the study of flavor physics continues to be an integral part of the searches at the intensity frontier. The study of flavor physics offers unique possibilities to study the weak interactions operating at the fundamental level governing the decays in conjunction with the strong forces responsible for keeping the constituents bound in various colorless hadronic states. In recent years, due to dedicated efforts by the Belle, BaBar, CDF, and LHC$b$ experiments, a great theoretical understanding of the flavor dynamics of the SM has been achieved, and severe constraints on the new physics parameters have been imposed. The rare and flavor changing neutral current processes of b quark have been quite instrumental and valuable probes of new physics, thanks to their suppressed nature in the SM and high sensitivity to the new physics effects.

In this context, the exclusive semileptonic decay $B \to K^* \ell^+ \ell^-$ governed by the quark-level transition $b \to s \ell^+ \ell^-$ is one of the most interesting candidates, which has received great attention, experimentally as well as theoretically. The analysis of the angular distribution of its four-body final state gives access to a large number of experimentally accessible observables as a function of invariant mass squared of the dilepton system ($q^2$). Interestingly, the LHC$b$ collaboration has found deviations from the SM predictions in the measurement of angular observables of $B \to K^* \mu^+ \mu^-$. These measurements are reported in bins of $q^2$.

Particularly, the discrepancy in one of the angular observables, $P_5'$, in two of low $q^2$ bins is quite intriguing. However, in order to be certain that the reported deviations are hints of new physics or artifacts of underestimated theoretical uncertainties, it is necessary to measure the observables which are as insensitive to hadronic effects as possible with more precision. In this thesis, we study some of these "theoretically cleaner" observables which are independent of hadronic form factors within the heavy quark effective framework. We show that zero crossing points of observables $P_5'$, $P_4'$, and of a new observable, $O_T^{\mathrm{L,R}}$, are independent of form factors, and are functions of short-distance Wilson coefficients in the considered limit. The zero crossing of $O_T^{\mathrm{L,R}}$ in the standard model coincides with the zero crossing of the forward-backward asymmetry ($A_{\mathrm{FB}}$) of the lepton pair. But in the presence of new physics contributions they show different behaviors. Moreover, we show that there exist relations between the zeros of $P_5'$, $P_4'$, $O_T^{\mathrm{L,R}}$, and the zero of $A_{\mathrm{FB}}$, which are also independent of hadronic uncertainties. We point out that precise measurements of these zeros in the near future would provide a crucial test of the standard model and would be useful in distinguishing between different possible new physics contributions to the Wilson coefficients. If the experimental observations are in fact due to NP in $b \to s\ell\ell$, then similar effects must also be seen in other $b \to s\ell\ell$ transitions involving different hadronic states. This fact sets the tone for our next work in which we study the semileptonic baryonic $b \to s$ decay, $\Lambda_b \to \Lambda\ell^+\ell^-$. We construct new angular observables and asymmetries; all of which have zero crossing points in the large $q^2$ region. The zeros of proposed observables in the heavy quark and large $q^2$ limit are again functions of Wilson coefficients only, and therefore have less sensitivity to hadronic effects. We discuss the potential of the decay $\Lambda_b \to \Lambda\ell^+\ell^-$ in probing the new physics effects in $b \to s\ell^+\ell^-$ along with the decays $B \to K^{(*)}\ell^+\ell^-$.

In the second part of the thesis, we present the explanation of some of the experimentally observed anomalies in the flavor sector within the framework of left-right symmetric gauge theories motivated by one of the low-energy subgroups of $E_6$ naturally accommodating leptoquarks. First, we explain the enhanced decay rates of $B \to D^{(*)}\tau\nu$ in $E_6$ motivated Alternative Left-Right Symmetric

Model. We discuss the constraints from the flavor sector on the couplings involved in explaining the experimental data. We further consider the framework of $E_6$ motivated Neutral Left-Right Symmetric Model, and give simultaneous explanation for B decay anomalies in $B \to D^{(*)}\tau\nu$ and $\bar{B} \to \bar{K}\ell^+\ell^-$ together with the anomalous magnetic moment of the muon, consistent with the constraints from other flavor data.

In the last part of the thesis, we carry out a detailed study of the effects of new physics originating from a scalar leptoquark model on the kaon sector. It is known that kaon decays provide some of the most stringent constraints on various extensions of the SM. We consider a simple extension of the SM by a scalar leptoquark of charge $-1/3$ with $(\mathrm{SU(3)_C}, \mathrm{SU(2)_L})$ quantum numbers $(3, 1)$, which is able to account for the deviations observed in B decays. The leptoquark we consider is a TeV-scale particle and within the reach of the LHC. We use the existing experimental data on the several kaon processes including $K^0 - \bar{K}^0$ mixing, rare decays $K^+ \to \pi^+\nu\bar{\nu}$, $K_L \to \pi\nu\bar{\nu}$, the short-distance part of $K_L \to \mu^+\mu^-$, and lepton-flavor-violating decay $K_L \to \mu^\pm e^\mp$ to obtain useful constraints on the model.

**Keywords:** flavor physics, rare decays, semileptonic B decays, Kaon decays, baryonic b decay, effective field theory, Wilson coefficients, beyond the Standard Model, leptoquarks.

# Acronyms and Abbreviations

| | |
|---|---|
| GWS | Glashow-Weinberg-Salam |
| SM | Standard Model |
| BSM | Beyond Standard Model |
| QCD | Quantum Chromodynamics |
| SSB | Spontaneous Symmetry Breaking |
| VEV | Vacuum Expectation Value |
| CKM | Cabibbo-Kobayashi-Maskawa |
| CP | Charge-Parity |
| CPV | CP Violation |
| LFV | Lepton Flavor Violation |
| PDG | Particle Data Group |
| UT | Unitarity Triangle |
| EFT | Effective Field Theory |
| OPE | Operator Product Expansion |
| RG | Renormalization Group |
| LLA | Leading-Logarithmic Approximation |
| NLO | Next-to-Leading Order |
| NNLO | Next-to-Next-Leading Order |
| HQET | Heavy Quark Effective Theory |
| GIM | Glashow-Iliopoulos-Maiani |
| FCNC | Flavor Changing Neutral Current |
| NP | New Physics |
| LHC | Large Hadron Collider |
| QCDF | QCD Factorization |
| FFs | Form Factors |
| C.L. | Confidence Level |
| 2HDM | two-Higgs Doublet Model |
| MSSM | Minimal Supersymmetric Standard Model |
| RPV | R-Parity Violating |
| ALRSM | Alternative Left-Right Symmetric Model |
| NLRSM | Neutral Left-Right Symmetric Model |
| HFAG | Heavy Flavor Averaging Group |
| GUT | Grand Unified Theory |

# Contents

# List of Figures

# List of Tables

# Chapter 1

# Introduction

## 1.1 The Glashow-Weinberg-Salam Model

The Glashow-Weinberg-Salam (GWS) model, also known as the Standard Model (SM) [1–3], is a theoretical framework which describes how the fundamental constituents of matter—elementary particles—interact with each other through the strong and electroweak forces. Since its inception in the 1960s, the SM has withstood the test of time, and has been extremely successful in explaining the experimental data. It has predicted many particles and phenomena which were confirmed afterwards in experiments; the Higgs boson being the last missing particle which was discovered recently in 2012 [4, 5], and therefore completing the SM. The SM contains in total 17 fundamental degrees of freedom: 12 spin half elementary particles (fermions), 4 spin-1 particles (gauge bosons), and one scalar particle, the Higgs boson. All the known matter in the universe is comprised of fermions, which are further divided as quarks and leptons in the SM. The gauge bosons: photon ($\gamma$), weak gauge bosons ($W^{\pm}$, $Z$), and gluon ($g$), are the carriers of electromagnetic, weak and strong forces, respectively, through the exchange of which the fermions interact with each other. The leptons and quarks both have three families in the SM with the members of the third family being the heaviest and that of the first family being the lightest. The quarks come in six "flavors": *up*, *down*, *charm*, *strange*, *top*, and *bottom*. The quarks do not exist independently, rather combine together to form two-quark bound states (mesons), and three-quark bound states (baryons). The SM Lagrangian is invariant under the gauge group $\mathrm{SU(3)_C \times SU(2)_L \times U(1)_Y}$ which spontaneously breaks down to $\mathrm{SU(3)_C \times U(1)_Q}$,

$$\mathrm{SU(3)_C \times SU(2)_L \times U(1)_Y} \xrightarrow[\text{breaking}]{\text{spontaneous}} \mathrm{SU(3)_C \times U(1)_Q}, \tag{1.1.1}$$

where 'C' refers to *color* charge, 'Q' refers to *electric* charge, and 'Y' refers to *hypercharge* quantum number. The subscript L signifies that generators of SU(2) act only on left-handed fermions. The matter content of the SM, *i.e.*, leptons and quarks, are grouped into multiplets of the SM gauge group. The weak interaction violates parity, and this feature is embedded in the SM by assigning different quantum numbers to the left- and right-handed part of particles. The left-handed quarks transform under the SM group $\big(\mathrm{SU(3)_C, SU(2)_L}\big)_\mathrm{Y}$ as $(3,2)_{1/6}$,

$$q_{iL} \;\equiv\; \begin{pmatrix} u'_L \\ d'_L \end{pmatrix}, \quad \begin{pmatrix} c'_L \\ s'_L \end{pmatrix}, \quad \begin{pmatrix} t'_L \\ b'_L \end{pmatrix}, \tag{1.1.2}$$

where $u'$, $c'$, $t'$ are called 'up-type' quarks and have electric charge +2/3, and the 'down-type' quarks $d'$, $s'$, $b'$ have electric charge -1/3 in the units of proton charge. On the other hand, the right-handed quarks transform trivially under SU(2). The up-type right-handed quarks $u'_{iR}$ transform as $(3,1)_{2/3}$, whereas the down-type right-handed quarks $d'_{iR}$ transform as $(3,1)_{-1/3}$. Here the subscripts L and R refer to the left-handed and right-handed projections,

$$\psi_{\mathrm{L/R}} = \frac{1 \mp \gamma_5}{2}\,\psi. \tag{1.1.3}$$

Similarly, the left-handed leptons transform under the SM group as $(1,2)_{-1/2}$,

$$\ell_{iL} \;\equiv\; \begin{pmatrix} \nu_{eL} \\ e^-_L \end{pmatrix}, \quad \begin{pmatrix} \nu_{\mu L} \\ \mu^-_L \end{pmatrix}, \quad \begin{pmatrix} \nu_{\tau L} \\ \tau^-_L \end{pmatrix}. \tag{1.1.4}$$

The right-handed charged leptons $e_{iR}$ transform as $(1,1)_{-1}$, whereas the neutral leptons (neutrinos), do not have right-handed part, and therefore are massless in the SM. The leptons do not have color quantum number as they don't participate in strong interaction.

The most general gauge-invariant GWS Lagrangian is comprised of the following parts,

$$\mathcal{L}_{\rm SM} = \mathcal{L}_{\rm Fermion} + \mathcal{L}_{\rm Gauge} + \mathcal{L}_{\rm Yukawa} + \mathcal{L}_{\rm Higgs}. \tag{1.1.5}$$

The first term $\mathcal{L}_{\rm Fermion}$ contains the kinetic part of the leptons and quarks, and is given by,

$$\mathcal{L}_{\rm Fermion} = \bar{\ell}^i i\gamma^\mu \mathcal{D}_\mu \ell^i + \bar{q}^i i\gamma^\mu \mathcal{D}_\mu q^i, \tag{1.1.6}$$

with the covariant derivative $\mathcal{D}_\mu$ defined as

$$\mathcal{D}_\mu = \partial_\mu - ig_s A^a_\mu \frac{\lambda^a}{2} - ig_2 W^i_\mu \frac{\tau^i}{2} - ig_1 \frac{Y}{2} B_\mu, \tag{1.1.7}$$

where $A^a_\mu$ $(a = 1, 2, ..., 8)$ are eight gluon fields corresponding to $\mathrm{SU(3)_C}$, $W^i_\mu$ are three weak fields corresponding to gauge group $\mathrm{SU(2)_L}$, and $B_\mu$ is the gauge boson corresponding to $\mathrm{U(1)_Y}$. The $\lambda^a$ and $\tau^i$ are the Gell-Mann and Pauli matrices, the generators of SU(3) and SU(2), respectively. For fermion fields transforming as singlet under $\mathrm{SU(3)_C}$ and $\mathrm{SU(2)_L}$, the terms containing matrices $\lambda^i$ and $\tau^i$ vanish. The parameters $g_s$, $g_2$, and $g_1$ are the $\mathrm{SU(3)_C}$, $\mathrm{SU(2)_L}$, and $\mathrm{U(1)_Y}$ gauge coupling constants, respectively.

The second term in Eq. (1.1.5), $\mathcal{L}_{\rm Gauge}$, contains the gauge part of the model, and is given by

$$\mathcal{L}_{\rm Gauge} = -\frac{1}{4} G^{\mu\nu}_a G^a_{\mu\nu} - \frac{1}{4} F^{\mu\nu}_i F^i_{\mu\nu} - \frac{1}{4} B^{\mu\nu} B_{\mu\nu}, \tag{1.1.8}$$

where $G^{\mu\nu}_a$, $F^{\mu\nu}_i$ and $B^{\mu\nu}$ are the field strengths of $\mathrm{SU(3)_C}$, $\mathrm{SU(2)_L}$, and $\mathrm{U(1)_Y}$, respectively. In terms of gauge boson fields $A^i_\mu$, $W^i_\mu$, and $B_\mu$, field strengths are defined as

$$\begin{aligned}
G^a_{\mu\mu} &= \partial_\mu A^a_\nu - \partial_\nu A^a_\mu + g_s \epsilon^{abc} A^b_\mu A^c_\nu, \\
F^i_{\mu\mu} &= \partial_\mu W^i_\nu - \partial_\nu W^i_\mu + g_2 \epsilon^{ijk} W^j_\mu W^k_\nu, \\
B_{\mu\nu} &= \partial_\mu B_\nu - \partial_\nu B_\mu.
\end{aligned} \tag{1.1.9}$$

The third term in Eq. (1.1.5), $\mathcal{L}_{\rm Yukawa}$, describes the interaction of fermions with the Higgs field $(\phi)$, and is given by

$$\mathcal{L}_Y = Y^d_{ij}\ \bar{q}_{iL} \Phi d'_{jR} + Y^u_{ij}\ \bar{q}_{iL} \tilde{\Phi} u'_{jR} + Y^e_{ij}\ \bar{\ell}_{iL} \Phi e_{jR} + \text{h.c.}, \tag{1.1.10}$$

where $Y_{ij}^d$, $Y_{ij}^u$, and $Y_{ij}^\ell$ are the arbitrary Yukawa couplings and $\tilde{\Phi}$ ($\equiv i\tau_2\Phi^*$) is the charge conjugate to the Higgs field doublet $\Phi$ (Y = +1),

$$\Phi = \begin{pmatrix} \phi^+ \\ \phi^0 \end{pmatrix}. \tag{1.1.11}$$

The last part of Eq. (1.1.5), $\mathcal{L}_{\text{Higgs}}$, is the Lagrangian for the Higgs sector and describes the interaction of the Higgs with the gauge bosons,

$$\mathcal{L}_{\text{Higgs}} = (\mathcal{D}_\mu\Phi)^\dagger(\mathcal{D}^\mu\Phi) - V(\Phi), \tag{1.1.12}$$

with $V(\Phi)$ being the self-interaction part,

$$V(\Phi) = -\mu^2\Phi^\dagger\Phi + \lambda(\Phi^\dagger\Phi)^2, \tag{1.1.13}$$

where $\lambda$ is a positive number which ensures the vacuum stability, and $\mu^2$ is chosen to be positive. The local gauge invariance of the SM forbids to have the mass terms in the $\mathcal{L}_{\text{SM}}$. The mass generation for the bosons and fermions is achieved by means of the so-called 'Higgs mechanism' [6] which spontaneously breaks the gauge symmetry $\text{SU}(2)_\text{L} \times \text{U}(1)_\text{Y}$ to $\text{U}(1)_\text{Q}$. The Higgs potential is chosen in such a way that the Higgs field $\Phi$ develops a non-zero vacuum expectation value (VEV) which respects the conservation of electric charge,

$$\langle\Phi\rangle_0 = \frac{1}{\sqrt{2}}\begin{pmatrix} 0 \\ v \end{pmatrix}; \qquad v = \sqrt{\mu^2/\lambda}. \tag{1.1.14}$$

It should be noted here that the neutral diagonal generator $\frac{\tau_3}{2}$ of SU(2) and generator of U(1) acting on scalar VEV give

$$\frac{\tau_3}{2}\langle\Phi\rangle_0 \neq 0, \qquad \frac{Y}{2}\langle\Phi\rangle_0 \neq 0, \tag{1.1.15}$$

but the combination

$$\left(\frac{\tau_3}{2} + \frac{Y}{2}\right)\langle\Phi\rangle_0 = 0. \tag{1.1.16}$$

can be identified with the unbroken electromagnetic charge generator $Q$ of $U(1)_\text{Q}$: $Q\langle\Phi\rangle_0 = 0$ implying that the vacuum remains invariant under $U(1)_\text{Q}$ symmetry and therefore the corresponding gauge boson (photon) is massless. The charge equation is, then, given by

$$Q = T_3 + \frac{Y}{2}, \tag{1.1.17}$$

where $T_3$ is the third component of weak isospin of $\mathrm{SU}(2)_\mathrm{L}$.

After spontaneous symmetry breaking (SSB), the fermions and bosons acquire masses from their interaction terms with the Higgs in $\mathcal{L}_\mathrm{SM}$. The masses of gauge bosons can be obtained by substituting Eq. (1.1.14) in the scalar kinetic term of Eq. (1.1.12) giving

$$\mathcal{L}^{\mathrm{mass}}_{W^\pm,Z,A} = \frac{1}{4}g_2^2 v^2 W^{+\mu} W^-_\mu + \frac{1}{8}v^2 \begin{pmatrix} W^3_\mu & B_\mu \end{pmatrix} \begin{pmatrix} g_2^2 & -g_2 g_1 \\ -g_2 g_1 & g_1^2 \end{pmatrix} \begin{pmatrix} W^3_\mu \\ B_\mu \end{pmatrix}. \tag{1.1.18}$$

Therefore the charged gauge bosons $W^\pm_\mu$ which are combinations of gauge bosons $W^1_\mu$ and $W^2_\mu$ corresponding to off-diagonal generators of $\mathrm{SU}(2)_\mathrm{L}$:

$$W^\pm_\mu = \frac{1}{\sqrt{2}}\left(W^1_\mu \mp i W^2_\mu\right), \tag{1.1.19}$$

acquire mass

$$M_{W^\pm} = \frac{1}{2}g_2 v. \tag{1.1.20}$$

The SSB induces mixing between neutral gauge bosons $W^3_\mu$ and $B_\mu$ and the resulting spectrum of neutral gauge bosons has one massive neutral weak boson $Z$

$$Z_\mu = \frac{-g_1 B_\mu + g_2 W^3_\mu}{\sqrt{g_2^2 + g_1^2}}, \tag{1.1.21}$$

with

$$M_Z = \frac{1}{2}v\sqrt{g_2^2 + g_1^2}. \tag{1.1.22}$$

while the other neutral gauge boson, identified with photon field $A_\mu$, remains massless:

$$A_\mu = \frac{g_2 B_\mu + g_1 W^3_\mu}{\sqrt{g_2^2 + g_1^2}}. \tag{1.1.23}$$

Introducing the weak mixing angle, $\theta_W$, also called Weinberg angle, given by

$$\theta_W = \arctan\left(\frac{g_1}{g_2}\right), \tag{1.1.24}$$

one can rewrite $Z_\mu$ and $A_\mu$ as

$$\begin{aligned} A_\mu &= \sin\theta_W \; W_\mu^3 + \cos\theta_W \; B_\mu, \\ Z_\mu &= \cos\theta_W \; W_\mu^3 - \sin\theta_W \; B_\mu. \end{aligned} \tag{1.1.25}$$

The charged- and neutral-current interactions of gauge bosons with the fermions in the SM are described by Eq. (1.1.6). The charged current interaction involving first generation of family of fermions is given by

$$\mathcal{L}_{\rm int}^{\rm CC} = \frac{g_2}{\sqrt{2}} \left(\bar{\nu}_L \gamma^\mu e_L + \bar{u}'_L \gamma^\mu d'_L\right) W_\mu^+ + \text{h.c.}\,, \tag{1.1.26}$$

whereas the neutral-current interaction part in terms of physical gauge fields $Z_\mu$ and $A_\mu$ is given by

$$\mathcal{L}_{\rm int}^{\rm NC} = eQ_{f_i} \bar{f}_i \gamma^\mu f_i A_\mu + \frac{g_2}{2\cos\theta_W} \bar{f}_i \gamma^\mu \left[ (T_3^{f_i} - 2Q_{f_i} \sin^2\theta_W) - T_3^{f_i} \gamma_5 \right] f_i Z_\mu, \tag{1.1.27}$$

where sum over repeated indices is implied. The first term corresponds to electromagnetic current, while the second one corresponds to weak neutral current. Here, $Q_f$ is the charge of fermion $f$ in units of $e$, and $T_3^f$ is the third component of weak isospin of $f$ as discussed in the text earlier.

## 1.2 Mixing of the quarks and the CKM mechanism

Following the SSB, the mass terms for the quarks can be obtained from the $\mathcal{L}_{\rm Yukawa}$ by replacing the Higgs field with its VEV,

$$\mathcal{L}_{\rm Yukawa}^{\rm mass} = \frac{v}{\sqrt{2}} \; M_{ij}^u \; \overline{u}'_{iL} u'_{jR} + \frac{v}{\sqrt{2}} \; M_{ij}^d \; \overline{d}'_{iL} d'_{jR} + \text{h.c.}, \tag{1.2.1}$$

where the quark fields, $u'_i$ and $d'_i$, are written in the flavor eigenstate basis, and $M_{ij}^{u,d}$ are $3 \times 3$ generational coupling matrices. In general, these matrices are not diagonal and contain off-diagonal elements which are responsible for the flavor violating transitions among quarks. These Yukawa matrices can always be diagonalized by means of the biunitary transformations on the fields. The fields in the flavor eigenstates and in the mass eigenstates are related through the following linear transformations,

$$u'_{iL,R} = (V^u_{L,R})_{ij}\ u_{jL,R}, \tag{1.2.2}$$

$$d'_{iL,R} = (V^d_{L,R})_{ij}\ d_{jL,R}, \tag{1.2.3}$$

where the unprimed quark fields, $u_i$ and $d_i$, correspond to the mass basis. In the mass basis, by definition, the Yukawa matrices are diagonal, and given by

$$M^u_{\text{diag.}} = V^{u\dagger}_L\ M^u\ V^u_R, \tag{1.2.4}$$

$$M^d_{\text{diag.}} = V^{d\dagger}_L\ M^d\ V^d_R. \tag{1.2.5}$$

The non-trivial implications of the fields transformation from flavor to mass basis are realized in the Lagrangian containing gauge interaction of the quark fields. In the mass basis, the weak charged current interaction for the quarks, $\mathcal{L}^{\text{CC}}_{\text{int}}$, is given by,

$$\mathcal{L}^{\text{CC}}_{\text{int}} = \frac{g_2}{\sqrt{2}} \begin{pmatrix} \bar{u}_L & \bar{c}_L & \bar{t}_L \end{pmatrix} \gamma^\mu\ V_{\text{CKM}} \begin{pmatrix} d_L \\ s_L \\ b_L \end{pmatrix} W^+_\mu + \text{ h.c.}\,, \tag{1.2.6}$$

where $V_{\text{CKM}}$ is a $3 \times 3$ unitary matrix which appears as a result of redefining the quark fields in the mass eigenstate basis, and is the genesis of flavor-violating quark interactions in the SM. $V_{\text{CKM}}$ is referred to as the Cabibbo-Kobayashi-Maskawa (CKM) matrix [7,8], and is defined by,

$$V_{\text{CKM}} = V^{u\dagger}_L V^d_L \equiv \begin{pmatrix} V_{ud} & V_{us} & V_{ub} \\ V_{cd} & V_{cs} & V_{cb} \\ V_{td} & V_{ts} & V_{tb} \end{pmatrix}. \tag{1.2.7}$$

### 1.2.1 Parametrization of the CKM matrix

A general $\text{N} \times \text{N}$ unitary matrix contains $\text{N}^2$ real-valued parameters. Out of $\text{N}^2$, $\text{N}(\text{N}-1)/2$ are the Euler angles and the remaining $\text{N}^2 - \text{N}(\text{N}-1)/2 = \text{N}(\text{N}+1)/2$ are the phases. However, some of the phases are spurious, and do not have any physical significance. The spurious phases arise because one has the freedom to redefine the fermion fields by a phase,

$$\psi_\alpha \to \exp(i\alpha)\ \psi_\alpha; \qquad \alpha = 1, 2, ..., \mathrm{N}. \tag{1.2.8}$$

By rephasing of the quark fields, one can eliminate $(2\mathrm{N}-1)$ phases from the $V_{\mathrm{CKM}}$. Therefore the final counting for the physical phases reads

$$\frac{1}{2}\mathrm{N}(\mathrm{N}+1) - (2\mathrm{N}-1) = \frac{1}{2}(\mathrm{N}-1)(\mathrm{N}-2). \tag{1.2.9}$$

Thus, in the two-generation SM, there are no physical phases. A $2 \times 2$ quark mixing matrix has only one parameter known as the Cabibbo angle $\theta_C$ [7]. In the case of $\mathrm{N} = 3$ generations, the $V_{\mathrm{CKM}}$ matrix has four parameters. Of these, three are the angles and one is the physical phase. This phase is the only source of CP violation (CPV) in the SM. This mechanism of naturally incorporating the CPV in the SM via the three-generation quark mixing was first proposed by Kobayashi and Maskawa in 1973 [8], and is known as the CKM mechanism.

There are various ways to represent the CKM matrix using the four parameters. One of parameterizations of $V_{\mathrm{CKM}}$, also recommended by the Particle Data Group (PDG) [9], employs three mixing angles $\theta_{12}$, $\theta_{13}$, $\theta_{23}$, and one CPV phase $\delta$ in the following way,

$$V_{\mathrm{CKM}} = \begin{pmatrix} c_{12}c_{13} & s_{12}c_{13} & s_{13}e^{-i\delta} \\ -s_{12}c_{23} - c_{12}s_{23}e^{i\delta} & c_{12}c_{23} - s_{12}s_{23}s_{13}e^{i\delta} & s_{23}c_{13} \\ s_{12}s_{23} - c_{12}c_{23}s_{13}e^{i\delta} & -c_{12}s_{23} - s_{12}c_{23}s_{13}e^{i\delta} & c_{23}c_{13} \end{pmatrix}, \tag{1.2.10}$$

where the abbreviations are $s_{ij} = \sin(\theta_{ij})$, $c_{ij} = \cos(\theta_{ij})$, with the indices i and j being the family labels. By appropriately choosing the quark field phases, all the angles can be constrained to lie in the range $0 \leq \theta_{ij} \leq \pi/2$. The phase $\delta$ lies in the range $0 \leq \delta \leq 2\pi$.

Another popular parametrization of $V_{\mathrm{CKM}}$, known as the Wolfenstein parametrization [10], utilizes the experimental information on CKM elements. From experiments, it is known that quark flavor transitions within the family are favored, *i.e.*, the diagonal entries in the $V_{\mathrm{CKM}}$ are of order unity. On the other hand, the inter-generation quark transitions are suppressed, implying the off-diagonal entries in the $V_{\mathrm{CKM}}$ to be small. Therefore, each element in the $V_{\mathrm{CKM}}$ can be written as an expansion in powers of the small parameter $\lambda$ ($\equiv \sin(\theta_{12})$) in the following way,

$$V_{\text{CKM}} = \begin{pmatrix} 1-\lambda^2/2 & \lambda & A\lambda^3(\rho - i\eta) \\ -\lambda & 1-\lambda^2/2 & A\lambda^2 \\ A\lambda^3(1-\rho-i\eta) & -A\lambda^2 & 1 \end{pmatrix} + \mathcal{O}(\lambda^4) \qquad (1.2.11)$$

In the Wolfenstein parametrization, the four parameters are $\lambda$, $A$, $\rho$, and $\eta$. The present experimental results on the CKM elements give [9]

$$\lambda = 0.22537 \pm 0.00061, \qquad A = 0.814^{+0.023}_{-0.024}, \qquad (1.2.12)$$

$$\bar{\rho} = 0.117 \pm 0.021, \qquad \bar{\eta} = 0.353 \pm 0.013, \qquad (1.2.13)$$

where the parameters $\bar{\rho}$, and $\bar{\eta}$ in terms of $\rho$, and $\eta$ are given by

$$\bar{\rho} \simeq \left(1 - \frac{\lambda^2}{2}\right)\rho + \mathcal{O}(\lambda^4), \qquad \bar{\eta} \simeq \left(1 - \frac{\lambda^2}{2}\right)\eta + \mathcal{O}(\lambda^4). \qquad (1.2.14)$$

and appear in $V_{\text{CKM}}$ if the $\mathcal{O}(\lambda^5)$ terms are also included in Eq. (1.2.11). The Wolfenstein parametrization in Eq. (1.2.11) is true upto $\mathcal{O}(\lambda^4)$, and therefore, the unitarity of $V_{\text{CKM}}$ holds approximately. The Wolfenstein parameters are related to the set $(\theta_{12}, \theta_{13}, \theta_{23}, \delta)$ of the standard parametrization through the following relations,

$$s_{12} = \lambda, \quad s_{23} = A\lambda^2, \quad s_{13}\, e^{-i\delta} = A\lambda^3(\rho - i\eta). \qquad (1.2.15)$$

The above relations are valid to all orders in $\lambda$. The exact parametrization of $V_{\text{CKM}}$ in terms of $(\lambda, A, \rho, \eta)$ can be obtained from the standard parametrization in Eq. (1.2.10) by replacing the parameters $(\theta_{12}, \theta_{13}, \theta_{23}, \delta)$ with the Wolfenstein parameters using the above relations.

### 1.2.2 The Unitarity triangle

The unitarity of the CKM matrix ( $V_{\text{CKM}}V^{\dagger}_{\text{CKM}} = V^{\dagger}_{\text{CKM}}V_{\text{CKM}} = \hat{\mathbb{I}}$ ) implies that there are several orthonormal relations between the rows and columns of the $V_{\text{CKM}}$. For a three-generation matrix, this leads to a set of 12 bilinear relations between combinations of the CKM elements,

$$V_{ij}V^{*}_{ik} = \delta_{jk}, \qquad (1.2.16)$$

$$V_{ij}V_{kj}^* = \delta_{ik}, \tag{1.2.17}$$

where i, j = 1, 2, 3 and repeated indices are summed over. The first relation corresponds to the orthonormality of the rows, and the second relation corresponds to orthonormality of the columns of the $V_{\text{CKM}}$. Since the CKM elements are, in general, complex, these relations can be geometrically represented as triangles in the complex plane. For example, the product of the first and the third columns of $V_{\text{CKM}}$ gives the following condition,

$$V_{ud}V_{ub}^* + V_{cd}V_{cb}^* + V_{td}V_{tb}^* = 0 \tag{1.2.18}$$

If each of the complex number is viewed as a vector in the complex plane, the above relation can be represented as a triangle in the complex plane as shown in Fig 1.1. Since the orthonormal conditions are born out of the unitarity of $V_{\text{CKM}}$, these triangles are known as unitarity triangles (UTs). The conditions in Eq. (1.2.16) and Eq. (1.2.17) give six UTs for a $3 \times 3$ $V_{\text{CKM}}$. In Fig 1.1, the angles $\alpha$, $\beta$, $\gamma$ in the triangle are given by,

$$\alpha \equiv \arg\left(-\frac{V_{td}V_{tb}^*}{V_{ud}V_{ub}^*}\right), \tag{1.2.19}$$

$$\beta \equiv \arg\left(-\frac{V_{cd}V_{cb}^*}{V_{td}V_{tb}^*}\right), \tag{1.2.20}$$

$$\gamma \equiv \arg\left(-\frac{V_{ud}V_{ub}^*}{V_{cd}V_{cb}^*}\right). \tag{1.2.21}$$

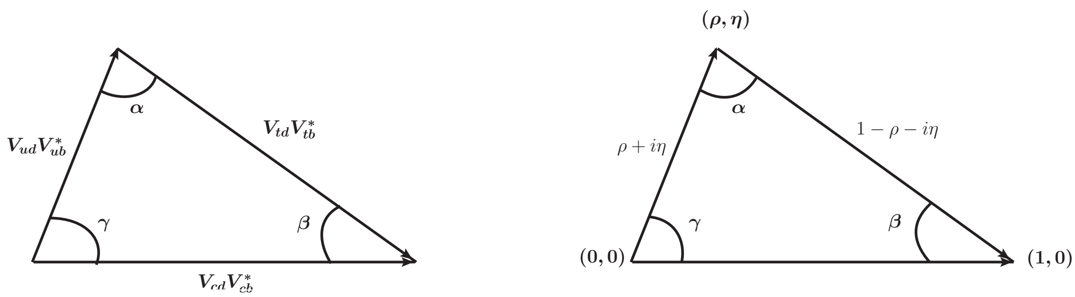


Figure 1.1: The Unitarity triangles (UTs). The UT (left) represents the Eq. (1.2.18) in the complex plane. The UT (right) corresponds to the same equation with each side being rescaled by $|V_{cd}V_{cb}|$ in the $(\rho, \eta)$ plane.

By definition, it follows that the sum of three angles is $\alpha + \beta + \gamma = \pi$. All the six triangles have different shapes which depend on its angles and the magnitude of its sides. The angles of the UT are invariant under the rephasing of the quark fields, and therefore the shape of the triangle does not change. The rephasing only rotates the triangle in the plane. Another important feature of all UTs is that despite their different shapes, the area of every UT is the same and is given by,

$$\text{Area of UT} = \frac{1}{2}\,|J|, \tag{1.2.22}$$

where J is a rephasing invariant quantity and is called the Jarlskog invariant [11]. It is defined as,

$$J = \sum_m \epsilon_{ikm} \sum_n \epsilon_{j\ell n}\ \mathrm{Im}(V_{ij}V^*_{kj}V_{k\ell}V^*_{i\ell}). \tag{1.2.23}$$

It is more convenient to work with the rescaled version of the UT as shown in Fig 1.1. The equation representing the rescaled UT is obtained from Eq. (1.2.18) by dividing the length of each side by $V_{cd}V^*_{cb}$, and choosing a phase convention such that $V_{cd}V^*_{cb}$ is real. With this choice of phase convention, in the leading order in Wolfenstein parametrization, we obtain

$$-\frac{V_{ud}V^*_{ub}}{V_{cd}V^*_{cb}} = \rho + i\eta, \tag{1.2.24}$$

$$-\frac{V_{td}V^*_{tb}}{V_{cd}V^*_{cb}} = 1 - \rho - i\eta. \tag{1.2.25}$$

Therefore, one side of UT aligns with the real axis in the complex plane, and has a length of unity. The coordinates of the two vertices of the rescaled UT are $(0,\ 0)$ and $(1,\ 0)$, while the coordinates of the third vertex are given by the Wolfenstein parameters $(\rho,\ \eta)$. The shape of the triangle remains unaltered. In the $(\rho,\ \eta)$ plane, the lengths of other two sides are $\sqrt{\rho^2+\eta^2}$, and $\sqrt{(1-\rho)^2+\eta^2}$.

## 1.3 Weak decays of hadrons in effective field theory

An effective field theory (EFT) is an approximation to a more complete field theory that is sufficiently accurate to describe the dynamics of the physical system up to a limited energy scale $E$. The basic concept of EFT is that in order to describe the physical phenomena at a low-energy scale $E$, one needs to know only the degrees of freedom which are relevant up to the mass scale $E$; it is not necessary to know the details of the theory at a heavy scale $\Lambda \gg E$. Therefore, one can construct an effective Lagrangian which describes low-energy physics with only degrees of freedom relevant up to the scale under consideration, while the degrees of freedom corresponding to short-distance physics (equivalent to high-energy scale) do not appear explicitly in the Lagrangian. The EFTs are more convenient and useful to study the physical systems in which widely separated energy scales are present; $E$ corresponds to the natural scale of the process under consideration, and $\Lambda_i$ ($\gg E$) are the other mass scales involved in the system. For example, in the weak decays of mesons $K$, $B$, $D$, etc., there are two disparate mass scales present: mass of the decaying meson ($\sim 1\,\mathrm{GeV}$), and the electroweak scale $\sim 100\,\mathrm{GeV}$. The heavier degrees of freedom are integrated out and the the action for the process can be described as an expansion in powers of $E/\Lambda_i$, and contains only the light degrees of freedom. The effect of removing the heavy degrees of freedom from the theory is that the renormalizable "full" theory now can be written as an effective theory with infinite numbers of non-renormalizable interactions suppressed by powers of high-energy scales $\Lambda_i$. These effects being suppressed in general can be neglected, which is in accord with the statement of the "decoupling theorem." There are several advantages of studying a physical system using the effective theory over the "full" description of the system. Since in the effective theory only light degrees of freedom are dynamical, description of the physics becomes rather simple. The other key advantage of using the effective theory is that long-distance physics and short-distance physics get separated; the contribution of light degrees and heavier degrees can be treated independent of each other. We will discuss more about this feature later in the section.

### 1.3.1 The Effective Hamiltonian

A convenient framework to parametrize the low-energy effects of the full theory in terms of fewer degrees of freedom is known as the operator product expansion (OPE) [12–14]. The basic idea of OPE can be grasped from the simple example of the decay $b \to c\bar{u}d$. It is a weak charged-current transition which proceeds at tree level via the mediation of $W$-boson in the SM as shown in Fig 1.2. The tree-level amplitude in the full theory is given by,

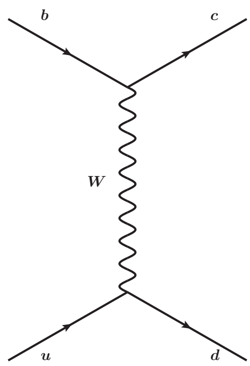


Figure 1.2: Feynman diagram corresponding to quark transition $b \to c\bar{u}d$ at tree level in the full theory.

$$A^{\text{full}} = -\frac{g_2^2}{2} V_{cb}^* V_{ud} (\bar{c}\gamma^\mu \frac{1-\gamma_5}{2} b) \; \frac{g_{\mu\nu}}{q^2 - M_W^2} \; (\bar{d}\gamma^\nu \frac{1-\gamma_5}{2} u), \tag{1.3.1}$$

where $V_{cb}^*$, $V_{ud}$ are CKM elements, and $q$ is the is the momentum flowing through W-propagator. Since the decaying meson has mass $m_b \simeq 5\,\text{GeV}$, the momentum-transfer $q^2$ is small compared with $M_W^2$. Therefore the propagator can be written as a expansion in powers of $q^2/M_W^2 \ll 1$,

$$\frac{1}{q^2 - M_W^2} = \frac{-1}{M_W^2} \left(1 + \frac{q^2}{M_W^2} + \ldots\right), \tag{1.3.2}$$

and the tree-level amplitude in the full theory can be approximated by ignoring the higher-order terms in the $q^2/M_W^2$ expansion,

$$A \simeq \frac{g_2^2}{8M_W^2} V_{cb}^* V_{ud} (\bar{c}\gamma^\mu (1-\gamma_5) b) \; (\bar{d}\gamma_\mu (1-\gamma_5) u) + \mathcal{O}(\frac{q^2}{M_W^2}), \tag{1.3.3}$$

However, the leading term in Eq. (1.3.3) can also be obtained by sandwiching the following local effective Hamiltonian between initial and final states,

$$\mathcal{H}_{\text{eff}} = \frac{g_2^2}{8M_W^2} V_{cb}^* V_{ud} (\bar{c}\gamma^\mu (1-\gamma_5) b) \; (\bar{d}\gamma_\mu (1-\gamma_5) u), \tag{1.3.4}$$

which corresponds to the Feynman diagram in Fig 1.3. The operator $(\bar{c}\gamma^\mu(1-\gamma_5)b)\;(\bar{d}\gamma_\mu(1-\gamma_5)u)$ in Eq. (1.3.4) is a dimension-six operator. The effects of the terms $\mathcal{O}(q^2/M_W^2)$ or higher can be taken into account by including the higher

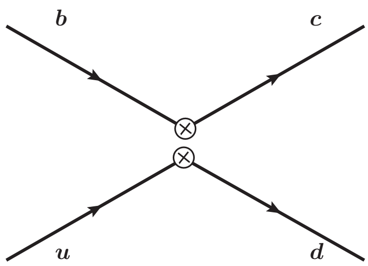


Figure 1.3: Feynman diagram corresponding to quark transition $b \to c\bar{u}d$ at tree level in effective theory.

dimensional operators in the $\mathcal{H}_{\text{eff}}$. In the low-energy effective description of the decay, the external quark fields which constitute the local operators are the dynamical degrees of freedom, and the heavy degrees, like W-boson in this example, have been 'integrated out' and are no longer a dynamical degree of the theory. The heavy degrees, though, do not appear explicitly in the $\mathcal{H}_{\text{eff}}$, but their effects are embodied in the effective coupling strengths of the local operators. In the example above, there is only one dimension-six operator in the effective Hamiltonian $\mathcal{H}_{\text{eff}}$, but in general there can be a number of effective local operators $(O_i)$ with different Dirac structures governing the process in question. A list of operators relevant for weak decays of hadrons has been given in Appendix A. The series in local operators is known as the operator product expansion (OPE). The expansion is based on the fact that effects of high energy appear local when viewed at low energy. Let us consider two local operators which have coordinates $x$ and $y$ in the position space. The product of operators $\mathcal{O}(x)\mathcal{O}(y)$ is a non-local quantity and the separation between the operators $O(x)$ and $O(y)$ corresponds to energy scale $\sim 1/(x-y)$. However, in low-energy systems with characteristic energy scale $\ll 1/(x-y)$, the product of operators $\mathcal{O}(x)\mathcal{O}(y)$ becomes a local quantity, and therefore, in the limit $(x-y) \to 0$, the product can be expressed as,

$$\mathcal{O}(x)\mathcal{O}(y) \approx \sum_i C_i(x-y)O_i(\frac{x+y}{2}). \tag{1.3.5}$$

Here, $O_i$ are the local operators. The distance scale $(x+y)/2$ corresponds to the intrinsic scale of the low-energy theory. The coefficients of these operators, $C_i$, are complex valued numbers, and are known as the Wilson coefficients. $C_i$ contain the short-distance, *i.e.*, $x \to y$ information. Therefore, in the OPE framework, one can write the effective Hamiltonian as a series of local operators weighted by the Wilson coefficients,

$$\mathcal{H}_{\text{eff}} = \sum_i C_i(\mu) O_i. \tag{1.3.6}$$

The Wilson coefficients $C_i$ as well as matrix elements of local operators $\langle O_i \rangle$ depend on an arbitrary scale $\mu$. The scale $\mu$ has the dimension of mass and is chosen appropriately to separate the contribution of long-distance (low-energy part) and short-distance (high-energy part). In the $\mathcal{H}_{\text{eff}}$, all the contributions above the scale $\mu$ belong to short-distance physics and are contained in the Wilson coefficients, while the contributions below $\mu$ belong to long-distance physics and are contained in the matrix elements $\langle O_i \rangle$. The origin of the $\mu$-dependence of $C_i$ and $\langle O_i \rangle$ lies in the quantum loop corrections they receive due to short-distance QCD effects. For example, in the decay $b \to c\bar{u}d$ we discussed above, the effective Hamiltonian given in Eq. (1.3.4) does not include the QCD effects, and can be rewritten in a compact form as,

$$\mathcal{H}_{\text{eff}} \text{ (without QCD)} = \frac{4\mathrm{G_F}}{\sqrt{2}} \mathrm{V^*_{cb} V_{ud}\ C_a\ O_a}, \tag{1.3.7}$$

with $O_a = (\bar{c}_i \gamma^\mu \mathrm{L} b_i)\ (\bar{d}_j \gamma_\mu \mathrm{L} u_j)$, and $C_a = 1$. Here $i,\ j$ are the color indices. Since quarks are involved in the problem, one has to take inevitable QCD quantum corrections into consideration as well. The one-loop QCD corrections to the the effective current-current operators are shown in Fig 1.4. The operator $O_a$ is comprised of two color-singlet currents with $(\mathrm{V-A}) \otimes (\mathrm{V-A})$ Dirac structure. However, a gluon connecting the two color-singlet weak-current lines, as shown in Fig 1.4, induces the mixing of the color indices owing to the following relation,

$$T^a_{ik} T^b_{jl} = -\frac{1}{2N} \delta_{ik} \delta_{jl} + \frac{1}{2} \delta_{il} \delta_{jk}. \tag{1.3.8}$$

The QCD effects induce a new four-quark operator $(O_b)$ with different color structure in addition to the color-singlet operator $O_a$ given in the $\mathcal{H}_{\text{eff}}$. This results in modifying the $\mathcal{H}_{\text{eff}}$ to the following form,

$$\mathcal{H}_{\text{eff}} = \frac{4G_F}{\sqrt{2}} V^*_{cb} V_{ud} (C_a O_a + C_b O_b), \tag{1.3.9}$$

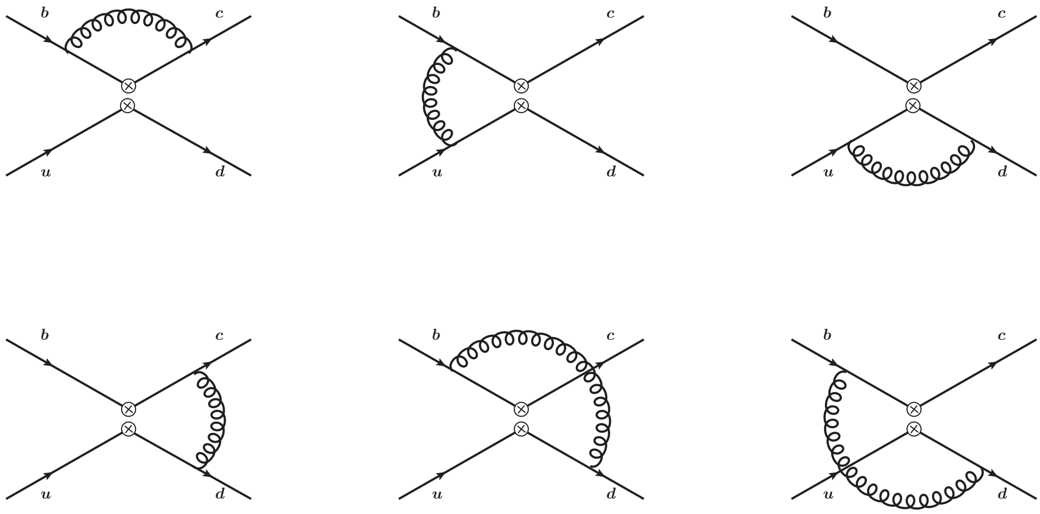


Figure 1.4: One-loop QCD corrections to current-current operators $Q_a$ and $Q_b$.

with $O_b = (\bar{c}_i \gamma^\mu L b_j)\ (\bar{d}_j \gamma_\mu L u_i)$, and $O_a$ given in Eq. (1.3.7), with the corresponding Wilson coefficient $C_b$ and $C_a$, respectively, which develop dependence on scale $\mu$ due to short-distance QCD corrections. A crucial point here is the asymptotic freedom of QCD [15,16] that allows one to use perturbation theory in calculating the QCD short-distance corrections. The calculation of the Wilson coefficients $C_i$ at the low-energy scale in effective theory involves several steps. The first step is to calculate the amplitude $A^{\rm full}$ corresponding to the process $M \to F$ in the full theory upto the desired order in the $\alpha_s$. Here $M$ stands for meson such as $K$, $B$, $D$, etc., and $F$ stands for final state which in general can include hadrons as well as leptons. Now, since the effective theory should be able to reproduce the physics of full theory at the low-energy scale, the amplitude $A(M \to F)$ in the full theory and in the effective one are set equal to each other,

$$\begin{aligned} A(M \to F)_{\rm full} &= A(M \to F)_{\rm eff} \\ &= \langle F|H_{\rm eff}|M\rangle \ \equiv\ \sum_i c_i(\mu)\ \langle F|O_i(\mu)|M\rangle. \end{aligned} \quad (1.3.10)$$

This matching of the amplitudes is done at a typical scale ($\mu_h$) of the full theory (for weak interaction processes, it is the mass of W-boson, $M_W$ ), and this step of comparing the full amplitude to the effective amplitude is called “the matching of the full theory onto the effective theory”. It should be stressed here that the Wilson coefficients do not depend on the external states. Their extraction is independent of the external states in the problem. In order to extract the correct Wilson coefficients from the matching procedure, the external states in both, the full and the effective theory, should be dealt alike. The matching gives the Wilson coefficients at the scale $\mu \sim \mu_h$, which are now functions of heavy masses, gauge couplings $\alpha_{\rm em}$, $\alpha_s$, and renormalization scale $\mu$. The Wilson coefficients extracted from the matching condition can be written as a series in $\alpha_s$ and $\alpha_{\rm em}$ in ordinary perturbation theory. For example in pure QCD case, the general form of the Wilson coefficients is given by [17],

$$\begin{aligned} C_i(\mu_h,\mu,\alpha_s) &= a_i^{00} \\ &+ a_i^{11}\left(\frac{\alpha_s}{4\pi}\right)\log\frac{\mu_h}{\mu} + a_i^{10}\left(\frac{\alpha_s}{4\pi}\right) \\ &+ a_i^{22}\left(\frac{\alpha_s}{4\pi}\right)^2\log^2\frac{\mu_h}{\mu} + a_i^{21}\left(\frac{\alpha_s}{4\pi}\right)^2\log\frac{\mu_h}{\mu} + a_i^{20}\left(\frac{\alpha_s}{4\pi}\right)^2 \\ &+ a_i^{33}\left(\frac{\alpha_s}{4\pi}\right)^3\log^3\frac{\mu_h}{\mu} + a_i^{32}\left(\frac{\alpha_s}{4\pi}\right)^3\log\frac{\mu_h}{\mu} + a_i^{31}\left(\frac{\alpha_s}{4\pi}\right)^3\log\frac{\mu_h}{\mu} + \ldots \end{aligned} \tag{1.3.11}$$

Although the scale $\mu$ is arbitrary, it is typically chosen to be the characteristic scale appearing in the matrix elements of operators. This generally corresponds to the mass of the decaying hadrons. But, the value of $\mu$ should not be chosen smaller than $\sim 1\,\text{GeV}$ as below this QCD is expected to become non-perturbative and the perturbative expansion in $\alpha_s$ would no longer be valid. However, this choice of $\mu$ also poses another problem. The general expression for the Wilson coefficients given in Eq. (1.3.11) contains logarithmic terms involving ratios $\alpha_s^m \log^n(\mu_h/\mu)$. As long as $\mu$ is in the vicinity of $\mu_h$, the smallness of $\alpha_s$ ensures the validity of perturbative expansion in $\alpha_s$ in Eq. (1.3.11). But, for the values of $\mu \sim 1-5\,\text{GeV}$ corresponding to the masses of decaying hadrons, the logarithmic values can become large enough to compensate the smallness of the strong coupling $\alpha_s$. For example, for the decays of hadrons containing b quark, the high scale $\mu_h$ is of the order of $M_W$, and choosing $\mu$ to be the mass of b quark, $m_b \sim 5\,\text{GeV}$, one finds that $\log(M_W/m_b) \sim 3$. This implies that, despite $\alpha_s$ being a justified expansion parameter in Eq. (1.3.11), the logarithmic terms $\alpha_s^m \log^n(M_W/m_b)$ can be large, and therefore, might spoil the ordinary perturbative treatment of the short-distance QCD corrections. This problem is solved by resumming the large logarithms to all orders in $\alpha_s$ by utilizing the renormalization group (RG) machinery. The solution of the RG equations allows one to sum the large logarithms automatically. In particular, the summation of the terms $(\alpha_s)^n \log(\mu_h/\mu)^n$ to orders in $n$ is called the leading-logarithmic approximation (LO). Including the summation of the terms $(\alpha_s)^n \log(\mu_h/\mu)^{n-1}$ to all orders in $n$ corresponds to the next-to-leading logarithmic approximation (NLO), and so on. The resulting RG improved perturbation series does not contain large logarithms and therefore a more trustworthy calculation for the Wilson coefficients can be performed.

The RG equations for the matrix elements and the Wilson coefficients follows from the requirement that a physical amplitude cannot depend on the arbitrary scale $\mu$. Therefore, the matrix element of the effective Hamiltonian, *i.e.*, $\langle F|\mathcal{H}_{\rm eff}|M\rangle$, should not change under change of scale $\mu$. The RG equations for the Wilson coefficients are given by,

$$\frac{d}{d\log\mu} C_i(\mu) = \gamma_{ij}^T \, C_j(\mu), \tag{1.3.12}$$

where $\gamma$ is the anomalous dimension matrix which depends on $\alpha_s$ and $\alpha_{\rm em}$. The solution of above RG equations, with initial conditions determined from the matching condition at the scale $\mu_h$, $C(\mu_h)$, gives the evolution of the Wilson coefficients from high scale $\mu_h$ to the desired low-energy scale $\mu$. The general form of the solution can be written as,

$$C\ (\mu) = U(\mu,\mu_h)\ C(\mu_h), \tag{1.3.13}$$

where the evolution matrix $U(\mu,\mu_h)$ is given by,

$$U(\mu,\mu_h) \;=\; 1 + \int_{g(\mu_h)}^{g(\mu)} dg_1 \frac{\gamma^T(g_1)}{\beta(g_1)} + \int_{g(\mu_h)}^{g(\mu)} dg_1 \int_{g(\mu_h)}^{g_1} dg_2 \frac{\gamma^T(g_1)}{\beta(g_1)} \frac{\gamma^T(g_2)}{\beta(g_2)} + \ldots\ , \tag{1.3.14}$$

where $g$ is the QCD coupling constant, and $\beta(g)$ determines the flow of the coupling $g$ with the change in $\mu$, and is defined as,

$$\beta(g) = \frac{d}{d\log\mu} g(\mu) \tag{1.3.15}$$

This implies that the $\mu$ dependence of the Wilson coefficients $C_i(\mu)$ must cancel the $\mu$ dependence of matrix elements of operators, $\langle F|O_i(\mu)|M\rangle$.

However, in order to calculate the amplitude $\langle F|\mathcal{H}_{\text{eff}}|M\rangle$, the matrix elements of local operators $\langle F|O_i(\mu)|M\rangle$ also need to be calculated. The main limitation in the calculations of $\langle F|O_i(\mu)|M\rangle$ is that these objects are inherently nonperturbative. Around the scale $\Lambda_{\text{QCD}}$, QCD becomes non-perturbative; the quarks and gluons hadronize and are no longer dynamical degrees of the theory. Since the matrix elements $\langle O_i(\mu)\rangle$ contain the contribution below the scale $\mu$, the so-called long-distance physics, one can not really use the tools of the perturbation theory to calculate them. Therefore, one has to rely on nonperturbative methods such as lattice calculations, heavy quark effective theory (HQET) [18–20], the 1/N expansion [21–23], QCD sum rules [24–26], chiral perturbation theory etc. to evaluate the matrix elements $\langle O_i(\mu)\rangle$. Although there have been considerable improvements in evaluating these hadronic objects using these non-perturbative techniques, the computations still have some limitations. Therefore, the theoretical uncertainties in the calculations of the matrix elements $\langle O_i(\mu)\rangle$ account for the major source of error in the theoretical predictions of the amplitude $A(M \to F)$.

### 1.3.2 Effective Hamiltonian for $|\Delta F| = 1$ transitions

In this subsection we will discuss the effective Hamiltonian for flavor transitions, $|\Delta F| = 1$, which involve change in the flavor quantum number by one unit. The processes relevant for our discussion are decays of bottom, strange and charm hadrons. Since the mass of decaying particles ($\sim 1-5$ GeV) are much smaller than the mass of $W^\pm$, $Z$ and top quark, these heavy particles can be integrated out and the processes can be studied in an effective theory framework. We start by discussing first the effective Hamiltonian for nonleptonic $b \to s$ transition which is a $|\Delta B| = |\Delta S| = 1$, $|\Delta C| = 0$ process. The effective Hamiltonian consists of four current-current operators $(O_1^c, O_2^c)$ and $(O_1^u, O_2^u)$ corresponding to

$b \to sc\bar{c}$ and $b \to su\bar{u}$ transitions, respectively:

$$O_1^u = (\bar{s}_i\gamma^\mu \mathrm{L} u_j)(\bar{u}_j\gamma_\mu \mathrm{L}\ b_i), \qquad O_2^u = (\bar{s}_i\gamma^\mu \mathrm{L} u_i)(\bar{u}_j\gamma_\mu \mathrm{L}\ b_j), \tag{1.3.16}$$

$$O_1^c = (\bar{s}_i\gamma^\mu \mathrm{L} c_j)(\bar{c}_j\gamma_\mu \mathrm{L} b_i), \qquad O_2^c = (\bar{s}_i\gamma^\mu \mathrm{L} c_i)(\bar{c}_j\gamma_\mu \mathrm{L} b_j). \tag{1.3.17}$$

In addition to these operators, the u and c quarks can also form a loop, emitting a gluon which can couple to quark-antiquark pair. The resulting penguin diagrams (see Appendix A) generate the following four QCD penguin operators:

$$Q_3 = (\bar{s}_i\gamma^\mu \mathrm{L} b_i)\sum_q(\bar{q}_j\gamma_\mu \mathrm{L} q_j), \qquad Q_4 = (\bar{s}_i\gamma^\mu \mathrm{L} b_j)\sum_q(\bar{q}_j\gamma_\mu \mathrm{L} q_i), \tag{1.3.18}$$

$$Q_3 = (\bar{s}_i\gamma^\mu \mathrm{L} b_i)\sum_q(\bar{q}_j\gamma_\mu \mathrm{R} q_j), \qquad Q_3 = (\bar{s}_i\gamma^\mu \mathrm{L} b_j)\sum_q(\bar{q}_j\gamma_\mu \mathrm{R} q_i). \tag{1.3.19}$$

The operator basis also includes the so-called "Electro-weak penguin" operators ($O^{\mathrm{EW}}_{7,8,9,10}$) which are generated by diagrams similar to gluon-penguin diagrams but with gluon replaced by a photon or $Z$ boson. The expression of these operators and the corresponding diagrams in the full theory are collected in Appendix A. Therefore, the effective Hamiltonian for nonleptonic $b \to s$ transitions is given by

$$\begin{aligned}\mathcal{H}_{\mathrm{eff}} &= \frac{4G_F}{\sqrt{2}}\Bigg\{V_{cb}V_{cs}^*\left(C_1O_1^c + C_2O_2^c\right) + V_{ub}V_{us}^*\left(C_1O_1^u + C_2O_2^u\right) \\ &\qquad - V_{tb}V_{ts}^*\left(\sum_{i=3}^{6} C_iO_i + \sum_{i=7}^{10} C_i^{\mathrm{EW}}O_i^{\mathrm{EW}}\right)\Bigg\} + \text{h.c.}\,,\end{aligned} \tag{1.3.20}$$

For radiative and (semi) leptonic $b \to s$ transitions ($b \to s\gamma, b \to s\ell^+\ell^-$), the operator basis is further extended to include the following operators:

$$O_7 = \frac{e}{16\pi^2}m_b(\bar{s}_i\sigma_{\mu\nu}\mathrm{R} b_i)F^{\mu\nu}, \qquad O_8 = \frac{g_s}{16\pi^2}m_b(\bar{s}_iT^a_{ij}\sigma_{\mu\nu}Rb_j)G^{a\mu\nu}, \tag{1.3.21}$$

$$O_9 = \frac{e^2}{16\pi^2}(\bar{s}_i\gamma^\mu \mathrm{L} b_i)(\bar{\ell}\gamma_\mu\ell), \qquad O_{10} = \frac{e^2}{16\pi^2}(\bar{s}_i\gamma^\mu \mathrm{L} b_i)(\bar{\ell}\gamma_\mu\gamma_5\ell). \tag{1.3.22}$$

Here, $O_7$ and $O_8$ corresponds to magnetic-penguin operators, whereas operators $O_{9,10}$ are called semileptonic operators. After including these operators and using the unitarity condition of CKM elements ($V_{ub}V_{us}^* + V_{cb}V_{cs}^* + V_{tb}V_{ts}^* = 0$), the general effective Hamiltonian for $b \to s$ transition can be expressed as

$$\begin{aligned}\mathcal{H}_{\mathrm{eff}} &= -\frac{4G_F}{\sqrt{2}}\Bigg\{V_{ub}V_{us}^*\Big(C_1(O_1^c - O_1^u) + C_2(O_2^c - O_2^u)\Big) \\ &\qquad + V_{tb}V_{ts}^*\left(\sum_{i=1}^{10} C_iO_i + \sum_{i=7}^{10} C_i^{\mathrm{EW}}O_i^{\mathrm{EW}}\right)\Bigg\} + \text{h.c.}\,,\end{aligned} \tag{1.3.23}$$

where terms in the first line of above equation are doubly-cabibbo suppressed with respect to terms in the second line and are generally omitted. The effective Hamiltonian for other $\Delta F = 1$ flavor transitions can be obtained by suitable change of quark fields given in Eq. (1.3.23). For example, for the flavor transition $\Delta B = 1$, $\Delta C = \Delta S = 0$, the corresponding effective Hamiltonian and the operator basis is obtained by replacing $s$ quark field with $d$ quark field in Eq. (1.3.23). It should be pointed out here that for transitions which involve four different quark flavors, the penguin operators cannot be generated and the corresponding effective Hamiltonian consists of current-current operators only. For example, for the case of flavor transition $\Delta B = \Delta C = 1$, $\Delta S = 0$, the corresponding effective Hamiltonian involves current-current operators only as given in Eq. (1.3.9).

### 1.3.3 Effective Hamiltonian for $|\Delta F| = 2$ transitions

The effective Hamiltonian for flavor transitions $\Delta F = 2$ (*e.g.,* $K^0$-$\bar{K}^0$, $B^0$-$\bar{B}^0$ mixing) in the SM consists of one four-quark operator only. The effective operator for $\Delta F = 2$ in the leading order in electroweak interaction is induced by box diagrams (see Appendix A). For $\Delta S = 2$ transition, the effective Hamiltonian is given by

$$\begin{aligned}\mathcal{H}_{\text{eff}}^{|\Delta S|=2} &= \frac{G_F^2 M_W^2}{4\pi^2}\Big\{(V_{cs}^* V_{cd})^2 \eta_{cc} S_0(x_c) + (V_{ts}^* V_{td})^2 \eta_{tt} S_0(x_t) \\ &\qquad + 2\,(V_{ts}^* V_{td})(V_{cs}^* V_{cd})\eta_{ct} S_0(x_c, x_t)\Big\} K(\mu)(\bar{s}\gamma_\mu \mathrm{L}d)(\bar{s}\gamma^\mu \mathrm{L}d),\end{aligned} \tag{1.3.24}$$

where $x_i = m_i^2/M_W^2$, $\eta_i$ are the QCD-correction factors (see Chapter 6 for details), $K(\mu)$ is a short-distance factor defined in Eq. (6.2.3) such that the product $K(\mu)(\bar{s}\gamma_\mu \mathrm{L}d)(\bar{s}\gamma^\mu \mathrm{L}d)$ is independent of $\mu$, and $S_0(x)$ and $S_0(x_i, x_j)$ are loop functions given in Eq. (6.2.2).

Similarly, the effective Hamiltonian for $\Delta B = 2$ transition corresponding to $B_d^0 - \bar{B}_d^0$ mixing is given by

$$\mathcal{H}_{\text{eff}}^{|\Delta B|=2} = \frac{G_F^2 M_W^2}{4\pi^2}(V_{tb}^* V_{td})^2 \eta_{tt} S_0(x_t) B(\mu)(\bar{b}\gamma_\mu \mathrm{L}d)(\bar{b}\gamma^\mu \mathrm{L}d). \tag{1.3.25}$$

The corresponding effective Hamiltonian for $B_s^0 - \bar{B}_s^0$ is obtained by replacing $d$ quark field with $s$ quark field in the above equation. Here, $B(\mu)$, similar to $K(\mu)$

in the case of $K^0 - \bar{K}^0$, is a short-distance factor which is required to make the product $B(\mu)(\bar{b}\gamma_\mu \mathrm{L}d)(\bar{b}\gamma^\mu \mathrm{L}d)$ independent of $\mu$, and is defined in terms of the bag parameter $B_{B_q}$ (q = s, d) and the decay constant $f_{B_q}$ as [27]

$$B_{B_q} = \frac{3}{2} B(\mu) \frac{\langle \bar{B}_q^0 | (\bar{b}\gamma_\mu \mathrm{L}q)(\bar{b}\gamma^\mu \mathrm{L}q) | B_q^0 \rangle}{f_{B_q}^2 m_{B_q}^2}. \tag{1.3.26}$$

## 1.4 Flavor physics as a tool to probe the SM and beyond

The study of flavor physics, in particular, the decays of $K$ and $B$ mesons, has played a crucial role in the development of the SM to its present form. For example, the first observation of breaking of CP-invariance in the weak interactions came from the decays $K \to 2\pi,\ 3\pi$ [28]. This experimental discovery later led Kobayashi and Maskawa to predict three generations of quarks in the SM even before the discovery of the charm quark. In 1970, to explain the small branching ratio of $K_L \to \mu^+\mu^-$, S. L. Glashow, J. Iliopoulos and L. Maiani proposed the famous GIM mechanism responsible for the suppression of FCNC transitions [29]. This also required them to predict the existence of the fourth quark, charm, which was discovered four years later. By incorporating the charm contribution in the calculation of $K^0 - \bar{K}^0$ mass-difference, $\Delta M_K$, Gaillard and Lee predicted the mass of the charm quark before its experimental discovery. Similarly, the first hint towards the large mass of the top quark came from the experimental measurement of semileptonic decays of the B meson and the $B_d - \bar{B}_d$ oscillations. Moreover, the study of various charged current and FCNC processes of the K and B mesons has provided important information for the determination of the elements of CKM matrix. The precision measurements of the flavor transitions $b \to d$, $b \to u$, and time-dependent CPV asymmetries in the B sector at the B factories Belle and BaBar have further established the CKM mechanism to be the dominant source of CPV in the SM. Subsequently, with the availability of high precision experiments at experimental facilities such as LHC$b$, the role of flavor physics has shifted to constraining the parameter space of the SM, and possibly even discovering the new physics (NP).

Despite the fact that the SM has explained the experimental data upto the electroweak scale ($\sim$ 100 GeV) with remarkable success, there are many theoretical motivations as well as experimental evidences which point towards the existence of NP. Here, the term NP is used for physics which lies beyond the SM, and is able to correct the shortcomings of the SM. A partial list of deficiencies of the SM includes the following. The scalar sector of the SM is unnatural. In order to prevent the Higgs mass from getting a large radiative correction, one has to extend the SM to include NP at a scale $\sim$ 1 TeV. This problem is known as the fine-tuning problem of the Higgs mass or the hierarchy problem of the SM. Neutrinos in the SM are massless, which is in contradiction with the experimental observation of neutrino oscillations. The SM does not have any dark matter candidate. The SM also does not explain the matter-antimatter asymmetry of the universe. In the SM, there is only one source of the CP violation, namely, the complex CKM phase. However, the CKM mechanism fails to account for the required amount of CP violation needed to explain the matter-antimatter asymmetry. Also, the SM does not include the gravitational force and hence does not unify all known forces in a single framework. Therefore, there must exist a more general unified theory above the electroweak scale. Since the SM does explain the low-energy phenomena involving the strong and electroweak interactions, it is natural to consider the SM as an effective low energy description of the general theory. Broadly, there are two approaches to search for NP. Of these, one is the collider searches of new particles at high energies, known as the searches at the energy frontier. In this approach, particle beams are produced and collided at the ever higher energies achievable at state of the art experimental facilities. If the centre-of-mass energies are high enough, new particles can be produced and detected. The other approach is the so-called indirect searches for NP at the intensity frontier. In such searches, the basic idea is to measure the low-energy processes with high precision and then confront the measurements with the SM predictions. The deviation between theory and the experimental measurements will indicate the presence of NP. The most promising processes for indirect searches are the ones which are suppressed in the SM, in particular, the processes which occur at the loop level in the SM. The amplitude of such processes, e.g., neutral meson mixing, FCNC decays of $K$, $B$, and $D$, etc., are suppressed due to loop and CKM factors and therefore have a very small value in the SM. Now, since these processes proceed at loop level, the so-far unknown heavy particles can also contribute to them via the quantum corrections. The effects due to new particles can be in principle large relative to the very small prediction in the SM, and therefore, are easier to be identified at the high precision experiments.

The direct collider searches at the high-energy frontier ( TeV scale) have not found any new particle but, interestingly, there are some tantalizing hints towards NP from high-precision low-energy experiments in the flavor sector. In particular, the experimental measurements in the semileptonic decays of the B meson have reported some deviations with respect to the SM predictions. To be specific, in 2012, BaBar measured the ratios of branching fractions for the semi-tauonic decay of $B$ meson, $R_{D^{(*)}} = \mathrm{BR}(\bar{B} \to D^{(*)}\tau\bar{\nu})/\mathrm{BR}(\bar{B} \to D^{(*)}\ell\bar{\nu}_\ell)$ with $\ell = e, \mu$, and reported $2.0\sigma$ and $2.7\sigma$ excesses over the SM predictions in the measurement of $R_D$ and $R_{D^*}$, respectively [30,31]. The Belle [32] and LHC$b$ [33] collaborations have also reported measurements of these decays recently. These measurements also show deviations from the SM. Another interesting indirect hint of NP has been reported in the $b \to s\mu^+\mu^-$ processes. The LHC$b$ collaboration has seen a $2.6\sigma$ departure from the SM prediction in lepton flavor universality ratio $R_K = \mathrm{BR}(\bar{B} \to \bar{K}\mu^+\mu^-)/\mathrm{BR}(\bar{B} \to \bar{K}e^+e^-) = 0.745^{+0.090}_{-0.074} \pm 0.036$ in the dilepton invariant mass bin $1\,\mathrm{GeV}^2 < q^2 < 6\,\mathrm{GeV}^2$ [34]. Though the individual branching fractions for $\bar{B} \to \bar{K}\mu^+\mu^-$ and $\bar{B} \to \bar{K}e^+e^-$ are marred with large hadronic uncertainties in the SM [35], their ratio is a very clean observable and predicted to be $R_K = 1.0003 \pm 0.0001$ [35,36]. Also, the recent data on angular observables of four-body distribution in the process $B \to K^*(\to K\pi)\ell^+\ell^-$ indicate some tension with the SM, particularly the deviation of $\sim 3\sigma$ in two of $q^2$ bins of the angular observable $P_5'$ [37–39]. In the decay $B_s \to \phi\mu^+\mu^-$, a deviation of $3.5\sigma$ significance with respect to the SM prediction has also been reported by LHC$b$ [40].

# Chapter 2

# $B \to K^*\ell^+\ell^-$ : Zeros of Angular Observables

## 2.1 Introduction

Rare B decays are mediated by FCNC transitions which are absent in the SM at tree level. The leading contributions come from one-loop diagrams. Being suppressed by GIM- and CKM-suppressed factors, their predictions in the SM are very small. As these processes are very sensitive to heavy particles in the loops, any effect of NP will potentially show significant deviation from the SM predictions. This makes these decays assets in probing NP. So far data collected on rare B decays by dedicated particle physics experiments (*e.g.*, B-factories, LHC$b$) are in excellent agreement with the SM predictions. The data have been used to retrieve information on flavor structure of possible NP and to put stringent constraints on beyond Standard Model (BSM) scenarios, but expectations of looking for any definitive hints of NP have not met with success. The results seem to be consistent with the CKM mechanism of the SM [8]. However, recent data on angular observables of four-body distribution in the rare decay, $B \to K^*(\to K\pi)\ell^+\ell^-$, indicate a plausible change in this situation. In 2013, LHC$b$ reported measurements of several form-factor independent angular observables of $B \to K^*\mu^+\mu^-$ as a binned function of the dilepton invariant mass squared ($q^2$) using dataset corresponding to an integrated luminosity of 1 fb$^{-1}$. Interestingly, the analysis showed a discrepancy of $3.7\sigma$ significance with respect to the SM in the measurement of angular observable $P_5'$ in the low $q^2$ bin $4.30 < q^2 < 8.68$ GeV$^2$ [37]. Later in 2015, this result was confirmed by LHC$b$ in its updated analysis using 3 fb$^{-1}$ integrated luminosity data and observed discrepancy of $2.8\sigma$ and $3.0\sigma$ significance with respect to the SM in $P_5'$ in bins $4 < q^2 < 6$ GeV$^2$ and $6 < q^2 < 8$ GeV$^2$, respectively [38]. Very recently, Belle Collaboration [41] has also reported a deviation in $P_5'$ in a long bin $4 < q^2 < 8$ GeV$^2$ consistent with LHC$b$ measurement. These discrepancies might be a result of statistical fluctuations or inevitable theoretical uncertainties inherent in the calculation of these observables [42–47]. One has to wait for more experimental data and a more careful analysis of theoretical uncertainties to clear the smoke. Assuming that these discrepancies are solely due to NP effects, there have been attempts in the literature to resolve this tension between theory and experimental data (see, for example, [48–70]).

In this chapter, we study some of the angular observables, $P_4'$, $P_5'$, $A_{\rm FB}$, and a new observable, which we call $\mathcal{O}_T^{\rm L,R}$, with a different approach. We look at the zeros of these observables. The expressions, under certain reasonable assumptions, are more or less independent of theoretical uncertainties, and depend solely on the short distance Wilson coefficients, and thus have very clean predictions in the SM. The precise measurements of these quantities gives certain relations (experimentally testable) among the Wilson coefficients, and therefore provide tests of short-distance physics. The most favored solutions to the present data explaining these deviations generally point towards new physics in the Wilson coefficient ($C_9^{\rm eff}$) of the semi-leptonic operator $O_9$ [39, 48, 49, 71, 72]. Since these zeros essentially probe new contributions to the Wilson coefficients, their experimental measurement in the near future can be worthwhile.

The chapter is organized in the following way. In the next section, we discuss the effective Hamiltonian for $b \to s\ell^+\ell^-$. In section 2.3, we describe the four-body angular distribution of $B \to K^*(\to K\pi)\ell^+\ell^-$, and various observables in the large energy recoil limit. In section 2.4, we calculate zeros of the observables $P_4'$, $P_5'$, $\mathcal{O}_T^{\rm L,R}$, and obtain correlations among them. In section 2.5, we give the

SM predictions for the zeros of the considered observables, and discuss the implications of the zeros and their correlations in providing the new constraints on the BSM scenarios. The NP sensitivity of these zeros is discussed in detail. In section 2.6, we summarize the results of this chapter.

## 2.2 The effective Hamiltonian for $b \to s\ell^+\ell^-$

The rare decay $B \to K^*\ell^+\ell^-$ proceeds via the transition $b \to s\ell^+\ell^-$ at the quark level, and is governed by the effective Hamiltonian

$$\mathcal{H}_{\text{eff}} = -\frac{4G_F}{\sqrt{2}} V_{ts}^* V_{tb} \sum_i (C_i(\mu) O_i + C_i^{'}(\mu) O_i^{'}) + \text{h.c.}\,, \tag{2.2.1}$$

where the contribution of the Cabibbo-suppressed term ($\propto \frac{V_{ub}V_{us}^*}{V_{tb}V_{ts}^*}$) has been ignored. $O_i^{(\prime)}$ are the effective local operators, and $C_i^{(\prime)}(\mu)$ are the Wilson coefficients evaluated at scale $\mu$. At the leading order in the SM, the process $B \to K^*\ell^+\ell^-$ is induced by the $\gamma$, $Z$-penguins, and $W$-box diagrams as shown in Fig 2.1, which generate the following effective operators

$$O_7 = \frac{e}{16\pi^2} m_b (\bar{s}_\alpha \sigma_{\mu\nu} \mathrm{R} b_\alpha) F^{\mu\nu}, \tag{2.2.2}$$

$$O_9 = \frac{e^2}{16\pi^2} (\bar{s}_\alpha \gamma^\mu \mathrm{L} b_\alpha)(\bar{l}\gamma_\mu l), \tag{2.2.3}$$

$$O_{10} = \frac{e^2}{16\pi^2} (\bar{s}_\alpha \gamma^\mu \mathrm{L} b_\alpha)(\bar{l}\gamma_\mu \gamma_5 l). \tag{2.2.4}$$

Here $\alpha,\ \beta$ are the color indices, $\mathrm{L/R} = (1 \mp \gamma_5)/2$ represent chiral projections, $e$ is the electric charge, and $m_b$ is the b-quark mass. The primed operators have chirality opposite to that of the unprimed operators. Their contribution within the SM is either severely suppressed or not present.

The operators $O_i$, (i = 1,2,..,6), do contribute to the process $b \to s\ell^+\ell^-$, and their effects can be parametrized in terms of effective Wilson coefficients of operators $O_7$ and $O_9$. The effective Wilson coefficients $C_7^{\text{eff}}$ and $C_9^{\text{eff}}$ are defined as

$$C_7^{\text{eff}} = C_7 - \frac{1}{3}C_3 - \frac{4}{9}C_4 - \frac{20}{3}C_5 - \frac{80}{9}C_6, \tag{2.2.5}$$

$$C_9^{\text{eff}} = C_9 + Y(\hat{s}), \tag{2.2.6}$$

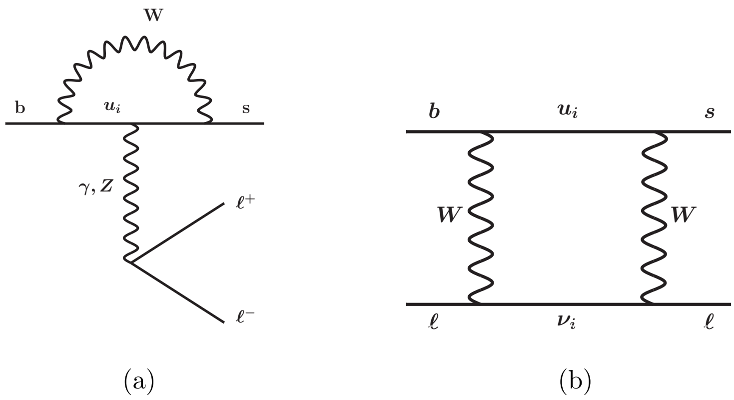


Figure 2.1: Feynman diagrams for $b \to s\ell^+\ell^-$ in the SM. (a) the penguin diagram, and (b) box diagram.

Here $s$ ($\equiv q^2$) is dilepton invariant mass and $\hat{s}$ is the invariant mass ($s$) normalized by B-meson mass square, *i.e.*, $\hat{s} = s/m_B^2$. $Y(\hat{s})$ is a loop function containing the contribution from one-loop matrix elements of operators $O_i$, i= 1,...6, and is given by [73]

$$Y(\hat{s}) = \frac{4}{3}\, C_3 + \frac{64}{9}\, C_5 + \frac{64}{27}\, C_6 + h(z, \hat{s})\; T_9 + h(1, \hat{s})\; U_9 + h(0, \hat{s})\; W_9, \tag{2.2.7}$$

where

$$\begin{aligned} h(z, \hat{s}) \;\; &= \;\; -\frac{4}{9}\ln(z) + \frac{8}{27} + \frac{16}{9}\frac{z}{\hat{s}} - \frac{2}{9}(2 + \frac{4z}{\hat{s}}) \\ &\quad \times \begin{cases} 2\ \arctan\sqrt{\hat{s}/(4z-\hat{s})}, & \hat{s} < 4z, \\ \ln[(\sqrt{\hat{s}} + \sqrt{\hat{s}-4z})/(\sqrt{\hat{s}} - \sqrt{\hat{s}-4z})] - i\pi, & \hat{s} > 4z, \end{cases} \end{aligned} \tag{2.2.8}$$

and

$$T_9 \;=\; \frac{4}{3}\; C_1 + C_2 + 6\; C_3 + 60\; C_5, \tag{2.2.9}$$

$$U_9 \;=\; -\frac{7}{2}\; C_3 - \frac{2}{3}\; C_4 - 38 C_5 - \frac{32}{3}\; C_6, \tag{2.2.10}$$

$$W_9 \;=\; -\frac{1}{2}\; C_3 - \frac{2}{3}\; C_4 - 8 C_5 - \frac{32}{3}\; C_6, \tag{2.2.11}$$

where $z = m_c^2/m_b^2$. Due to $Y(\hat{s})$, $C_9^{\rm eff}$ is not real but has a small imaginary part. In the analytic relations below, $Y(\hat{s})$ is neglected and all the Wilson coefficients are assumed to be real, but for numerical calculations, we include $Y(\hat{s})$ in $C_9^{\rm eff}$. As we will see, this turns out to be a good working approximation.

To calculate observables for the $B \to K^*$ process, one needs to calculate matrix elements of the local operators $O_i$'s. These matrix elements are generally parametrized in terms of seven form factors $V$, $A_{0,1,2}$, $T_{1,2,3}$, which are functions of squared momentum transfer ($q^2$) between initial and final meson, and are given as [74]

$$\begin{aligned}\langle \bar{K}^*(k)|\bar{s}\gamma_\mu(1-\gamma_5)b|\bar{B}(p)\rangle &= -i\epsilon^*_\mu(m_B+m^*_K)A_1(q^2)+i(2p-q)(\epsilon^*.q)\\ &\times \frac{A_2(q^2)}{m_B+m^*_K}+iq_\mu(\epsilon^*.q)\frac{2m^*_K}{q^2}[A_3(q^2)-A_0(q^2)]\\ &+\epsilon_{\mu\nu\rho\sigma}\epsilon^{*\nu}p^\rho k^\sigma\frac{2V(q^2)}{m_B+m^*_K},\end{aligned} \tag{2.2.12}$$

$$\begin{aligned}\langle \bar{K}^*(k)|\bar{s}\sigma_{\mu\nu}(1+\gamma_5)b|\bar{B}(p)\rangle &= i\epsilon_{\mu\nu\rho\sigma}\epsilon^{*\nu}p^\rho k^\sigma 2T_1(q^2)+T_2(q^2)\Big[\epsilon^*_\mu(m_B^2-m_{K^*}^2)\\ &-(\epsilon^*.q)(2p-q)_\mu\Big]+T_3(q^2)(\epsilon^*.q)\Big[q_\mu\\ &-\frac{q^2}{m_B^2-m_{K^*}^2}(2p-q)_\mu\Big],\end{aligned} \tag{2.2.13}$$

with

$$A_3(q^2)=\frac{m_B+m^*_K}{2m^*_K}A_1(q^2)-\frac{m_B-m^*_K}{2m^*_K}A_2(q^2), \tag{2.2.14}$$

$$A_0(0)=A_3(0), \quad T_1(0)=T_2(0), \tag{2.2.15}$$

where $q^\mu=(p-k)^\mu$, and $\epsilon^\mu$ is the polarization vector of $K^*$. These form factors are calculated via non-perturbative methods like QCD sum rules on the light cone (LCSRs) [75]. Working in the QCD factorization (QCDF) framework and heavy quark and large recoil limit (low $q^2$ region), all seven "full" form factors can be written in terms of only two independent universal "soft" form factors: $\xi_\perp$ and $\xi_\parallel$ [76–79]. The two sets of form factors are related to each other as (see, for example, [79])

$$\xi_\perp=\frac{m_B}{m_B+m_{K^*}}V(q^2), \tag{2.2.16}$$

$$\xi_\parallel=\frac{m_B+m_{K^*}}{2E_{K^*}}A_1(q^2)-\frac{m_B-m_{K^*}}{m_B}A_2(q^2), \tag{2.2.17}$$

where $E_{K^*}=(m_B^2+m_{K^*}^2-q^2)/2m_B$ is the energy of the $K^*$ meson.

## 2.3 Angular distribution and observables of $B \to K^*\ell^+\ell^-$

The angular distribution of $B \to K^*(\to K\pi)\ell^+\ell^-$ offers a plethora of experimentally accessible observables which are independent of form factors in certain limits, and therefore are theoretically cleaner. The fully differential decay distribution can be completely described in terms of four kinematic variables: dilepton invariant mass $q^2$, $\theta_\ell$, $\theta_K$, and $\phi$, and is given by [74, 80, 81]

$$
\begin{aligned}
\frac{d^4\Gamma(\bar{B} \to \bar{K}^*(\to K\pi)\ell^+\ell^-)}{\mathrm{d}q^2\,\mathrm{d}\cos\theta_{K^*}\,\mathrm{d}\cos\theta_l\,\mathrm{d}\phi} &= \frac{9}{32\pi} J(q^2, \theta_\ell, \theta_K, \phi) \\
&= J_1^s \sin^2\theta_K + J_1^c \cos^2\theta_K \\
&+ \left(J_2^s \sin^2\theta_K + J_2^c \cos^2\theta_K\right)\cos 2\theta_\ell \\
&+ J_3 \sin^2\theta_K \sin^2\theta_\ell \cos 2\phi + J_4 \sin 2\theta_K \sin 2\theta_\ell \cos\phi \\
&+ J_5 \sin 2\theta_K \sin\theta_\ell \cos\phi \\
&+ \left(J_6^s \sin^2\theta_K + J_6^c \cos^2\theta_K\right)\cos\theta_\ell + J_7 \sin 2\theta_K \sin\theta_\ell \sin\phi \\
&+ J_8 \sin 2\theta_K \sin 2\theta_\ell \sin\phi + J_9 \sin^2\theta_K \sin^2\theta_\ell \sin 2\phi, \\
&= \sum_i J_i(q^2) f_i(\theta_\ell, \theta_{K^*}, \phi),
\end{aligned} \tag{2.3.1}
$$

where $\theta_\ell$ is the angle between $\bar{K}^{*0}$ and $\ell^-$ in the rest frame of lepton pair, $\theta_K$ is the angle between $\bar{K^{*0}}$ and $K^-$ in the centre mass of frame of $(K^- - \pi^+)$ pair, and $\phi$ denotes the angle between the planes containing lepton pair and $(K^- - \pi^+)$ pair in the $B$ meson rest frame as depicted in Fig 2.2.

There are in total 24 angular coefficients [$J_i(q^2)$ and $\bar{J}_i(q^2)$]. The CP conjugated coefficients $\bar{J}_i$ (corresponding to CP conjugate mode of $B \to K^*(\to K\pi)\ell^+\ell^-$) are given by $J_i$ with the weak phases conjugated. To obtain decay distribution of CP conjugated mode, one has to make the replacements: $J_{1,2,3,4,7} \to \bar{J}_{1,2,3,4,7}$ and $J_{5,6,8,9} \to -\bar{J}_{5,6,8,9}$. These angular coefficients, $J_i(q^2)$, are expressed in terms of complex transversity amplitudes $A^{L,R}_{\perp,0,\|}$, $A_t$ and $A_s$. For

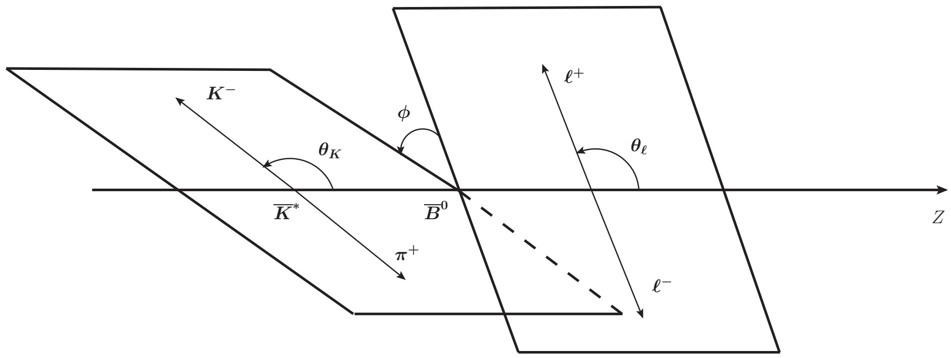


Figure 2.2: Topology of the four-body angular distribution of $\bar{B} \to \bar{K}^*(\to K^-\pi^+)\ell^+\ell^-$ with the description of the angles $\theta_\ell$, $\theta_K$, and $\phi$.

$m_\ell \neq 0$, we have [80, 82]

$$J_1^s = \frac{(2+\beta_\ell^2)}{4}[|A_\perp^L|^2 + |A_\parallel^L|^2 + (L \to R)] + \frac{4m_\ell^2}{q^2}\mathrm{Re}(A_\perp^L A_\perp^{R*} + A_\parallel^L A_\parallel^{R*}), \tag{2.3.2}$$

$$J_1^c = |A_0^L|^2 + |A_0^R|^2 + \frac{4m_\ell^2}{q^2}[|A_t|^2 + 2\mathrm{Re}(A_0^L A_0^{R*})] + \beta_\ell^2|A_s|^2, \tag{2.3.3}$$

$$J_2^s = \frac{\beta_\ell^2}{4}[|A_\perp^L|^2 + |A_\parallel^L|^2 + (L \to R)], \tag{2.3.4}$$

$$J_2^c = -\beta_\ell^2[|A_0^L|^2 + (L \to R), \tag{2.3.5}$$

$$J_3 = \frac{1}{2}\beta_\ell^2[|A_\perp^L|^2 - |A_\parallel^L|^2 + (L \to R)], \tag{2.3.6}$$

$$J_4 = \frac{\beta_\ell^2}{\sqrt{2}}[\mathrm{Re}(A_0^L A_\parallel^{L*}) + (L \to R)], \tag{2.3.7}$$

$$J_5 = \sqrt{2}\beta_\ell[\mathrm{Re}(A_0^L A_\perp^{L*}) - (L \to R) - \frac{m_\ell}{\sqrt{q^2}}\mathrm{Re}(A_\parallel^L A_s^* + A_\parallel^R A_s^*)], \tag{2.3.8}$$

$$J_6^s = 2\beta_\ell[\mathrm{Re}(A_\parallel^L A_\perp^{L*}) - (L \to R)], \tag{2.3.9}$$

$$J_6^c = 4\beta_\ell\frac{m_\ell}{\sqrt{q^2}}\mathrm{Re}[A_0^L A_s^* + (L \to R)], \tag{2.3.10}$$

$$J_7 = \sqrt{2}\beta_\ell[\mathrm{Im}(A_0^L A_\parallel^{L*} - (L \to R) + \frac{m_\ell}{\sqrt{q^2}}\mathrm{Im}(A_\perp^L A_s^* + A_\perp^R A_s^*)], \tag{2.3.11}$$

$$J_8 = \frac{1}{\sqrt{2}}\beta_\ell^2[\mathrm{Im}(A_0^L A_\perp^{L*}) + (L \to R)], \tag{2.3.12}$$

$$J_9 = \beta_\ell^2[\mathrm{Im}A_\parallel^{L*}A_\perp^L) + (L \to R)], \tag{2.3.13}$$

$$\tag{2.3.14}$$

where $\beta_\ell = \sqrt{1 - \frac{4m_\ell^2}{q^2}}$.

Note that $A_s$ contributes only when scalar operators are taken into account. In this chapter, we do not consider contributions from scalar operators. However, for the sake of generality, we include $A_s$ in the expressions of $J_i(q^2)$. Also, we have dropped the explicit $q^2$ dependence of the transversity amplitudes for notational simplicity. The eight transversity amplitudes, $A^{\rm L,R}_{\perp,\parallel,0}$, and $A_{s,t}$ in terms of $B \to K^*$ form factors and the Wilson coefficients are given by the following expressions:

$$
\begin{aligned}
A_\perp^{\rm L,R} &= N\sqrt{2}\lambda^{1/2}\Bigg[\bigg((C_9^{\rm eff}+C_9^{\rm eff\prime})\mp(C_{10}^{\rm eff}+C_{10}^{\rm eff\prime})\bigg)\frac{V}{m_B+m_{K^*}} \\
&\quad + \frac{2m_b}{q^2}(C_7^{\rm eff}+C_7^{\rm eff\prime})T_1\Bigg] \qquad (2.3.15)\\
A_\parallel^{\rm L,R} &= -N\sqrt{2}(m_B^2-m_{K^*}^2)\Bigg[\bigg((C_9^{\rm eff}-C_9^{\rm eff\prime})\mp(C_{10}^{\rm eff}-C_{10}^{\rm eff\prime})\bigg)\frac{A_1}{m_B-m_{K^*}} \\
&\quad + \frac{2m_b}{q^2}(C_7^{\rm eff}-C_7^{\rm eff\prime})T_2\Bigg] \qquad (2.3.16)\\
A_0^{\rm L,R} &= -\frac{N}{2m_{K^*}\sqrt{q^2}}\Bigg[\bigg((C_9^{\rm eff}-C_9^{\rm eff\prime})\mp(C_{10}^{\rm eff}-C_{10}^{\rm eff\prime})\bigg)\bigg((m_B^2-m_{K^*}^2-q^2) \\
&\quad (m_B+m_{K^*})A_1-\lambda\,\frac{A_2}{m_B+m_{K^*}}\bigg)+2m_b(C_7^{\rm eff}-C_7^{\rm eff\prime}) \\
&\quad \times\bigg((m_B^2+3m_{K^*}^2-q^2)\,T_2-\frac{\lambda}{m_B^2-m_{K^*}^2}T_3\bigg)\Bigg], \qquad (2.3.17)\\
A_t &= \frac{N}{\sqrt{q^2}}\lambda^{1/2}\bigg(2(C_{10}^{\rm eff}-C_{10}^{\rm eff\prime})+\frac{q^2}{2m_\mu}(C_P-C_P')\bigg)A_0, \qquad (2.3.18)\\
A_s &= -N\lambda^{1/2}(C_s-C_s')A_0. \qquad (2.3.19)
\end{aligned}
$$

In the above expressions,

$$
N=\left[\frac{G_F^2\alpha^2}{3\cdot 2^{10}\pi^5 m_B^3}|V_{tb}V_{ts}^*|^2q^2\lambda^{1/2}\beta_\ell\right]^{1/2}, \qquad (2.3.20)
$$

and $\lambda = m_B^4+m_{K^*}^4+q^4-2(m_B^2m_{K^*}^2+m_{K^*}^2q^2+m_B^2q^2)$, $\hat m_b = m_b/m_B$. $C_s^{(\prime)}$ and $C_P^{(\prime)}$ are the Wilson coefficients of scalar and pseudoscalar operators which, as mentioned before, have been ignored in this analysis. Interestingly, in the heavy quark and large recoil limit, the transversity amplitude can be written simply in terms of two universal form factors $\xi_\perp$ and $\xi_\parallel$. At the leading order in $1/m_b$ and $\alpha_s$, the transversity amplitudes read

$$
\begin{aligned}
A_\perp^{L,R} &= \sqrt{2}Nm_B(1-\hat s)\Bigg[(C_9^{\rm eff}+C_9^{\prime\rm eff})\mp(C_{10}+C_{10}^{\prime}) \\
&\quad + 2\frac{\hat m_b}{\hat s}(C_7^{\rm eff}+C_7^{\prime\rm eff})\Bigg]\xi_\perp(E_{K^*}), \qquad (2.3.21)
\end{aligned}
$$

$$
\begin{aligned}
A_{\parallel}^{L,R} &= -\sqrt{2}Nm_B(1-\hat{s})\Big[(C_9^{\rm eff}-C_9^{\prime\rm eff}) \mp (C_{10}-C_{10}^{\prime}) \\
&\quad + 2\frac{\hat{m}_b}{\hat{s}}(C_7^{\rm eff}-C_7^{\prime\rm eff})\Big]\xi_{\perp}(E_{K^*}), \qquad (2.3.22)\\
A_0^{L,R} &= -\frac{Nm_b}{2\hat{m}_{K^*}\sqrt{\hat{s}}}(1-\hat{s})^2\Big[(C_9^{\rm eff}-C_9^{\prime\rm eff}) \mp (C_{10}-C_{10}^{\prime}) \\
&\quad + 2\hat{m}_b(C_7^{\rm eff}-C_7^{\prime\rm eff})\Big]\xi_{\parallel}(E_{K^*}), \qquad (2.3.23)\\
A_t &= \frac{Nm_b}{\hat{m}_{K^*}\sqrt{\hat{s}}}(1-\hat{s})^2\left[C_{10}-C_{10}^{\prime}\right]\xi_{\parallel}(E_{K^*}). \qquad (2.3.24)
\end{aligned}
$$

In writing the above expressions, terms of $\mathcal{O}(\hat{m}_{K^*}^2)$ have been neglected. However, it is worth mentioning that these relations hold only in the kinematic region $1 < q^2\ (\mathrm{GeV}^2) < 6$, which is precisely the region of interest.

As mentioned before, one can extract 24 angular coefficients $J_i(q^2)$ from the full fit of $B \to K^*\mu^+\mu^-$ (including its' CP conjugated mode). The key observables like branching ratio, longitudinal polarization fraction $F_L$, forward-backward asymmetry of lepton pair $A_{\rm FB}$ can be expressed in terms of functions $J_i(q^2)$ integrated in $q^2$- bins. For example, the dilepton mass distribution can be written in terms of $J_i$ as

$$
\frac{d\Gamma}{dq^2} = \frac{1}{4}\left(3J_{1c}+6J_{1s}-J_{2c}-2J_{2s}\right). \qquad (2.3.25)
$$

and the $q^2$-binned observables $A_{\rm FB}$ and $F_L$ are given as,

$$
\begin{aligned}
A_{\rm FB} &= -\frac{3}{4}\frac{\int dq^2(J_{6s}+\bar{J}_{6s})}{\int dq^2(d\Gamma/dq^2+d\bar{\Gamma}/dq^2)}, \qquad (2.3.26)\\
F_L &= -\frac{\int dq^2(J_{2c}+\bar{J}_{2c})}{\int dq^2(d\Gamma/dq^2+d\bar{\Gamma}/dq^2)}. \qquad (2.3.27)
\end{aligned}
$$

Apart from these observables, one can also construct new observables by considering ratios of certain combinations of coefficients $J_i(q^2)$ in such a way that LO hadronic uncertainties get canceled in particular $q^2$ region and therefore these observables are theoretically under more control. In literature, several such "optimized" observables $P_i^{(\prime)}$ have been constructed and studied. For example, observable $P_1$ [83] was proposed to probe the right-handed structure in $B \to K^*\ell^+\ell^-$. Due to left-handed structure of the SM, $P_1$ vanishes in the SM and therefore a nonzero measurement of this quantity immediately points towards the departure from the SM. $P_2$ [81] is theoretically more cleaner observable than $A_{\rm FB}$. On the other hand, observable $P_3$ [84] has the capability to probe weak as well strong phases in the SM and beyond. Below, we list interesting "optimized" observables defined in terms of $q^2$ -integrated $J_i's$ [85],

$$\begin{aligned}
P_1 &= \frac{1}{2}\frac{\int dq^2(J_3+\bar{J}_3)}{\int dq^2(J_{2s}+\bar{J}_{2s})}, \qquad & P_2 &= \frac{1}{8}\frac{\int dq^2(J_{6s}+\bar{J}_{6s})}{\int dq^2(J_{2s}+\bar{J}_{2s})},\\
P_3 &= -\frac{1}{4}\frac{\int dq^2(J_9+\bar{J}_9)}{\int dq^2(J_{2s}+\bar{J}_{2s})}, & P_4' &= \frac{1}{\mathcal{N}}\int dq^2(J_4+\bar{J}_4),\\
P_5' &= \frac{1}{2\mathcal{N}}\int dq^2(J_5+\bar{J}_5), & P_6' &= -\frac{1}{2\mathcal{N}}\int dq^2(J_7+\bar{J}_7),
\end{aligned} \tag{2.3.28}$$

with $\mathcal{N} = \sqrt{-\int dq^2(J_{2s}+\bar{J}_{2s})\int dq^2(J_{2c}+\bar{J}_{2c})}$. The "optimized" observables are sensitive to combinations of different short-distance Wilson coefficients (for example, see [72] for a recent and detailed discussion on observables $P_i$'s sensitivity to NP Wilson coefficients) and therefore their precise measurement holds a good chance of unraveling patterns of NP in this mode.

## 2.4 Zeros of angular observables and relations in the SM

The zero crossing of the forward-backward asymmetry of the lepton pair ($\hat{s}_0$) is known to be highly insensitive to form factors. This was first pointed out in [86] where a number of form-factor models were considered, and was noted that the value of $\hat{s}_0$ is practically independent of hadronic form factors. Later Ali *et. al.* [87] in their analysis showed that $\hat{s}_0$ depends on the Wilson coefficients and ratios of form factors, and in the heavy quark limit and large $E_{K^*} \sim \mathcal{O}(m_B/2)$, the hadronic uncertainties in ratios of form factors drop out, and $\hat{s}_0$ essentially depends on a combination of short distance parameters only. This leads to a nearly model-independent relation between the Wilson coefficients. The position of the zero crossing is thus heralded as a test of the SM.

In the SM, $\hat{s}_0$ is given by [87]

$$\mathrm{Re}(C_9^{\rm eff}(\hat{s}_0)) = -2\frac{\hat{m}_b}{\hat{s}_0}C_7^{\rm eff}\frac{1-\hat{s}_0}{1+\hat{m}_{K^*}^2-\hat{s}_0} \sim -2\frac{\hat{m}_b}{\hat{s}_0}C_7^{\rm eff}. \tag{2.4.1}$$

Note that existence of zero from the above Eq. (2.4.1) necessarily requires the condition Sign $\left[\mathrm{Re}(C_9^{\mathrm{eff}})\,C_7^{\mathrm{eff}}\right] = -1$ to be satisfied. For NP models where $C_7^{\mathrm{eff}}$ has the same sign as $C_9^{\mathrm{eff}}$, there will then be no zero crossing. The LHC$b$ collaboration [88, 89] has measured the zero of forward-backward asymmetry of the lepton pair to be $q_0^2 = 3.7^{+0.8}_{-1.1}$ GeV$^2$. which, within errors, is consistent with the SM predictions, typically lying in the range (3.7 - 4.3) GeV$^2$ which in units normalized by mass of the B-meson ($\hat{s} = q^2/m_B^2$) translates to the range (0.13 - 0.16), and have relative uncertainties below 10% level [79, 90, 91].

We now discuss the angular observables of interest and work in the basis where the SM operators are augmented with their helicity flipped counterparts. We retain contributions of the helicity-flipped Wilson coefficients so that analysis done includes a subset of NP models involving primed Wilson coefficients*. The expressions below clearly show the power of the zero crossing point of these angular observables to probe different NP scenarios.

The value of $\hat{s}_0$ can be easily obtained from integrated $q^2$ angular observable, $A_{\mathrm{FB}}$. In terms of the angular coefficients $[J_i(q^2)]$, $A_{\mathrm{FB}}$ is defined as

$$A_{\mathrm{FB}} = -\frac{3}{4}\frac{\int dq^2 (J_{6s} + \bar{J}_{6s})}{\int dq^2 (d\Gamma/dq^2 + d\bar{\Gamma}/dq^2)}. \tag{2.4.2}$$

To calculate $\hat{s}_0$, we use the expressions for the transversity amplitudes given in Eqs. (2.3.21 -2.3.24), which are valid in the large recoil region. The zero crossing of any observable is easily obtained by equating the numerator to zero. From Eq. (2.4.2), we obtain

$$\hat{s}_0 = -2\,\frac{(C_{10}C_7^{\mathrm{eff}} - C_{10}'C_7')}{(C_{10}C_9^{\mathrm{eff}} - C_{10}'C_9')}\hat{m}_b \tag{2.4.3}$$

Within the SM ($C_i' \to 0$), dependence on $C_{10}$ cancels out, and the expression reduces to Eq. (2.4.1), sensitive to the ratio of $C_7^{\mathrm{eff}}$ and $C_9^{\mathrm{eff}}$.

The angular observables $P_5'$ and $P_4'$ both have zero crossing point in their mass spectrum. The value of zero crossing for both lies in the "theoretically clean" low-$q^2$ region; interestingly the same region where the LHC$b$ has measured deviation from the SM prediction for the angular observable $P_5'$.

---

*We reiterate that in the analytic relations, we assume $C_i$'s to be real but retain the complex nature in numerical analysis.

Observable $P_5'$ is related to the angular coefficient $J_5$ through the following relation

$$P_5' = \frac{\int dq^2 (J_5 + \bar{J}_5)}{2\sqrt{-\int dq^2 (J_{2s} + \bar{J}_{2s}) \int dq^2 (J_{2c} + \bar{J}_{2c})}} \tag{2.4.4}$$

The numerator of $P_5'$ in the massless lepton limit is proportional to $[\mathrm{Re}(A_0^L A_\perp^{L*}) - (L \leftrightarrow R)]$. Then the zero of $P_5'$, in the large recoil region, is given by the following combination of short-distance parameters

$$\hat{s}_0^{P_5} = \frac{(C_7^{\rm eff} + C_7')(C_{10}' - C_{10})}{[C_{10}C_9^{\rm eff} - C_{10}'C_9' + (C_7^{\rm eff} - C_7')(C_{10} + C_{10}')\hat{m}_b]}\hat{m}_b \tag{2.4.5}$$

The zero of $P_5'$ turns out to be insensitive to hadronic form factors similar to the zero of $A_{\rm FB}$. In the SM limit, $C_{10}$ dependence disappears and the expression reduces to a very simple relation between value of zero and the Wilson coefficient $C_7^{\rm eff}$ and $C_9^{\rm eff}$,

$$\hat{s}_0^{P_5,SM} = -\frac{C_7^{\rm eff}}{C_9^{\rm eff} + C_7^{\rm eff}\hat{m}_b}\hat{m}_b \tag{2.4.6}$$

Interestingly enough, we find that within the SM, the zero of $P_5'$ can be written solely in terms of $\hat{s}_0$, the zero of $A_{\rm FB}$

$$\hat{s}_0^{P_5,SM} = \frac{\hat{s}_0^{SM}/2}{1 - \hat{s}_0^{SM}/2} \tag{2.4.7}$$

We find this correlation between zero of $A_{\rm FB}$ and that of $P_5'$ an important result. Eq. (2.4.7) can be expanded in a Taylor series, and dropping out terms of order $\mathcal{O}\left((\hat{s}_0^{SM}/2)^2\right)$ and higher, the relation predicts that zero of $P_5'$ is approximately half of the value of $\hat{s}_0$ in the SM.

A similar analysis can also be done for the observable $P_4'$. In terms of angular coefficients $J_i's$, observable $P_4'$ is written as

$$P_4' = \frac{\int dq^2 (J_4 + \bar{J}_4)}{\sqrt{-\int dq^2 (J_{2s} + \bar{J}_{2s}) \int dq^2 (J_{2c} + \bar{J}_{2c})}} \tag{2.4.8}$$

The numerator of $P_4'$ is $\propto [\mathrm{Re}(A_0^L A_\parallel^{L*}) + (L \leftrightarrow R)]$. Using expressions in Eqs. (2.3.22) and (2.3.23) for transversity amplitudes $A_\parallel^L$ and $A_0^L$ , we find the zero of $P_4'$ to be

$$\hat{s}_0^{P_4} = -2\frac{(C_7^{\rm eff} - C_7')[C_9^{\rm eff} - C_9' + 2(C_7^{\rm eff} - C_7')\hat{m}_b]}{[(C_9^{\rm eff} - C_9')^2 + (C_{10} - C_{10}')^2 + 2(C_7^{\rm eff} - C_7')(C_9^{\rm eff} - C_9')\hat{m}_b]}\hat{m}_b \tag{2.4.9}$$

The expression is again very 'clean' and has a non-trivial dependence on short-distance parameters in the large recoil region. In the SM limit, this relation yields

$$\hat{s}_0^{P_4,SM} = -2\frac{C_7^{\text{eff}}C_9^{\text{eff}} + 2(C_7^{\text{eff}})^2\hat{m}_b}{C_{10}^2 + (C_9^{\text{eff}})^2 + 2C_7^{\text{eff}}C_9^{\text{eff}}\hat{m}_b}\hat{m}_b \tag{2.4.10}$$

The zero of $P_4^{\prime}$ can also be written in terms of $\hat{s}_0$ (utilizing the fact that within the SM, $C_{10} = -C_9$)

$$\hat{s}_0^{P_4,SM} = \frac{\hat{s}_0^{\text{SM}}(1-\hat{s}_0^{SM})}{(2-\hat{s}_0^{SM})} \tag{2.4.11}$$

Again using the fact that the value of $\hat{s}_0$ is very small compared to unity, we find the value of the zero of $P_4^{\prime}$ to be approximately half of $\hat{s}_0$, similar to the case of $P_5^{\prime}$. However, if we keep effects of higher order terms in $\hat{s}_0$, the value of zero of $P_5^{\prime}$ and that of $P_4^{\prime}$ turns out be a bit larger and smaller than $\hat{s}_0^{\text{SM}}/2$ respectively and the leading effect is of order $(\hat{s}_0)^2$. From the experimental point of view, this accuracy is currently not there and therefore the effect can be safely neglected. The correlation between zeros of $A_{\text{FB}}$, $P_4^{\prime}$, $P_5^{\prime}$ is quite intriguing since in a chosen optimal basis of observables, $A_{\text{FB}}$, $P_5{}'$ and $P_4^{\prime}$ are independent observables, and there is no *a priori* reason for their zero crossing points to develop this dependence on each other.

With enough data available, one would be able to perform a full angular analysis of the final state distribution in the decay $B \to K^*(\to K\pi)\ell^+\ell^-$, and this would allow complete determination of the $K^*$ spin amplitudes. Therefore one can use the spin amplitudes to design observables which are sensitive to specific NP and have relatively controlled theoretical uncertainties. With this in mind, we propose a new CP conserving observable which we call $\mathcal{O}_T^{\text{L,R}}$. It has the following form

$$\mathcal{O}_T^{L,R} = \frac{|A_\perp^L|^2 + |A_\parallel^L|^2 - (L \leftrightarrow R)}{8(J_{2s} + \bar{J}_{2s})} \tag{2.4.12}$$

This new observable is constructed out of both parallel and perpendicular spin amplitudes of $K^*$ and has not been explored before in the literature. The ratio of amplitudes is chosen such that theoretical uncertainties due to the hadronic form factors cancel at the leading order. The profile of $\mathcal{O}_T^{\text{L,R}}$ also has a zero in low-$q^2$ region. In a basis where the SM operator structure is augmented with right-handed currents, the zero of $\mathcal{O}_T^{\rm L,R}$ has NP sensitivity different from that of $A_{\rm FB}$. Its zero crossing point occurs at

$$\hat{s}_0^{\mathcal{O}_T^{L,R}} = -2\,\frac{(C_{10}C_7^{\rm eff} + C_{10}^{\prime}C_7^{\prime})}{(C_{10}C_9^{\rm eff} + C_{10}^{\prime}C_9^{\prime})}\hat{m}_b \qquad (2.4.13)$$

The expressions $\hat{s}_0$ [Eq. (2.4.3)] and $\hat{s}_0^{\mathcal{O}_T^{L,R}}$ [Eq. (2.4.13)] have some interesting features. By definition, observables $A_{\rm FB}$ and $\mathcal{O}_T^{L,R}$ have non-identical dependence on invariant mass $\hat{s}$ and therefore vary differently as functions of $\hat{s}$. But within the SM, despite $q^2$ profiles being different, the values of zero crossings, $\hat{s}_0^{SM}$ and $\hat{s}_0^{\mathcal{O}_T^{L,R},SM}$, are degenerate. However, in the presence of helicity flipped operators, the positions of zero crossing shift in a dissimilar fashion and the degeneracy gets lifted. This rather utilitarian feature can be used to probe contributions from helicity flipped operators once the values of $\hat{s}_0$ and $\hat{s}_0^{\mathcal{O}_T^{L,R}}$ are known experimentally with good precision.

Let us remark that all the expressions and relations obtained above have been worked out under the hypothesis of no scalar and tensor contributions. Observables $A_{\rm FB}$, $P_4^{\prime}$ and the proposed new observable $\hat{s}_0^{\mathcal{O}_T^{L,R}}$ are blind to the presence of scalar/tensor contributions. Therefore, the expressions for zeros will remain unaltered even in the presence of these new contributions. The observable $P_5^{\prime}$, however, does receive contributions from the scalar component of $K^*$-spin amplitudes. But the sensitivity to this contribution is highly suppressed ( $m_\mu^2/q^2$ is the suppression factor) and in the limit of negligible leptons mass, these contributions vanish.

## 2.5 Constraining New Physics

All the Wilson coefficients are assumed to be real in this analysis, *i.e.*, NP does not introduce any new weak phase in the Wilson coefficients and we assume that the sign of $C_7$ is as in the SM. We will ignore NP scenarios where $C_7$ and $C_9$ have the same sign. The expressions of zeros of these observables depend only on the Wilson coefficients, practically independent of form factors, thereby leading to theoretically clean predictions. To calculate these zeros, we use $C_9 = 4.2297$,

$C_{10}$ = -4.2068, $C_7^{\rm eff}$ = -0.2974 [71] at scale $m_b$. Other input parameters are: $m_b^{\rm pole}$ = 4.80 GeV, $G_F = 1.166 \times 10^{-5}$, $m_B$ = 5.280GeV, $m_{K^*}$ = 0.895GeV, $m_\mu = 0.106$GeV, $\alpha = 1/129$, $\alpha_s = 0.21$.

| Observable | Value of zero using analytic relations | Exact values of zero crossings | |
|---|---|---|---|
| | | using "full" form factors ($V$, $A_{0,1,2}$, $T_{1,2,3}$) | using "soft" form factors ($\xi_\perp$, $\xi_\parallel$) |
| $A_{FB}$ | 0.128 | 0.122 | 0.125 |
| $P_5'$ | 0.068 | 0.069 | 0.069 |
| $P_4'$ | 0.059 | 0.054 | 0.056 |
| $\mathcal{O}_T^{L,R}$ | 0.128 | 0.122 | 0.125 |

Table 2.1: Zeros in the SM. In column II, we quote the values calculated using relations [Eq. (2.4.3), Eq. (2.4.7), Eq. (2.4.11), Eq. (2.4.13)], while the third and fourth columns have entries predicted in the SM using form factors ($V$, $A_{0,1,2}$, $T_{1,2,3}$) and ($\xi_\perp$, $\xi_\parallel$), respectively.

In Table 2.1, we give the numerical values of zeros of the observables in the SM. The values in the second column are obtained using the relations in Eq. (2.4.3), Eq. (2.4.7), Eq. (2.4.11), and Eq. (2.4.13). To compare with the exact predictions in the SM and to have a consistency check of these relations, we also calculate values of these zeros in the SM using form factors and retaining $Y(\hat{s})$ in $C_9^{\rm eff}$, which we had ignored for obtaining analytic relations among the zeros. We use "full" form factors ($V$, $A_{0,1,2}$, $T_{1,2,3}$) calculated in [75] using light-cone sum rule and tabulate the results in the third column of Table 2.1 whereas in the last column we tabulate the same results using "soft" form factors ($\xi_\perp$, $\xi_\parallel$) given in Refs. [76–78] (see appendix B for more details). As is evident, the two sets of form factors yield very similar values, thereby confirming that these zeros are (almost) independent of form factors. Clearly, the employed analytic relations yield values close to those when no approximations are made, showing the robustness of these relations. All the zeros lie in the low-$q^2$ region, where form factors are known with relatively greater precision. At LO, soft form factors cancel precisely and predictions of zeros are clean. Largest corrections to the values of zeros come from form factor uncertainties when NLO effects are included (as noted in [78] for the case of $\hat{s}_0$). The typical error on form factors is $\sim$ 10-12% (see [75]). Assuming the size of errors in all the form factors of the same order, we find the relative uncertainties in our estimates of these zeros to be $\sim$ 30%. So far experimentally as well as theoretically only $\hat{s}_0$ has received attention. The experimental value of $\hat{s}_0$ has large relative uncertainties (of order 35%) [88,89]. Though we have ignored $\mathcal{O}(\alpha_s)$ contributions in favor of obtaining form-factor insensitive correlations among the zeros, our theoretical estimate of $\hat{s}_0$ is still competitive with the experimental value with current precision as discussed above. The zeros and the relations among them can be used to constrain the Wilson coefficients in the following ways:

- Under the hypothesis of no NP-induced right-handed currents and real Wilson coefficients, all the zeros including that of the new observable $\mathcal{O}_T^{L,R}$ are functions of $C_7^{\text{eff}}$ and $C_9^{\text{eff}}$ only. With the magnitude of $C_7^{\text{eff}}$ stringently constrained from branching ratio of decay $B \to K^*\gamma$ (and $B \to X_s\gamma$), the zeros provide new information on $C_9^{\text{eff}}$.

- Some of the zero crossing points are sensitive to right-handed currents (more details below). These contributions can be probed once the precise measurements of zero crossings are made.

Global fits to recently updated data on angular analysis of the $B \to K^*\mu\mu$ indicate significant tension with the SM [39,48,49,71,72]. It has been suggested that solutions having destructive NP contribution to $C_9$ or with $C_9^{\text{NP}} = -C_{10}^{\text{NP}} < 0$ are in very good agreement with the data. From this perspective, the measurement of these zero crossing points would provide a very clean and good test of the hypothesis of NP contribution to $C_9$. In Fig 2.3, we show the constrained region in $C_7$ and $C_9$ plane in the SM-like operator basis. The most stringent bounds on $C_7$ come from the decay $B \to X_s\gamma$. The formula for branching ratio of $B \to X_s\gamma$

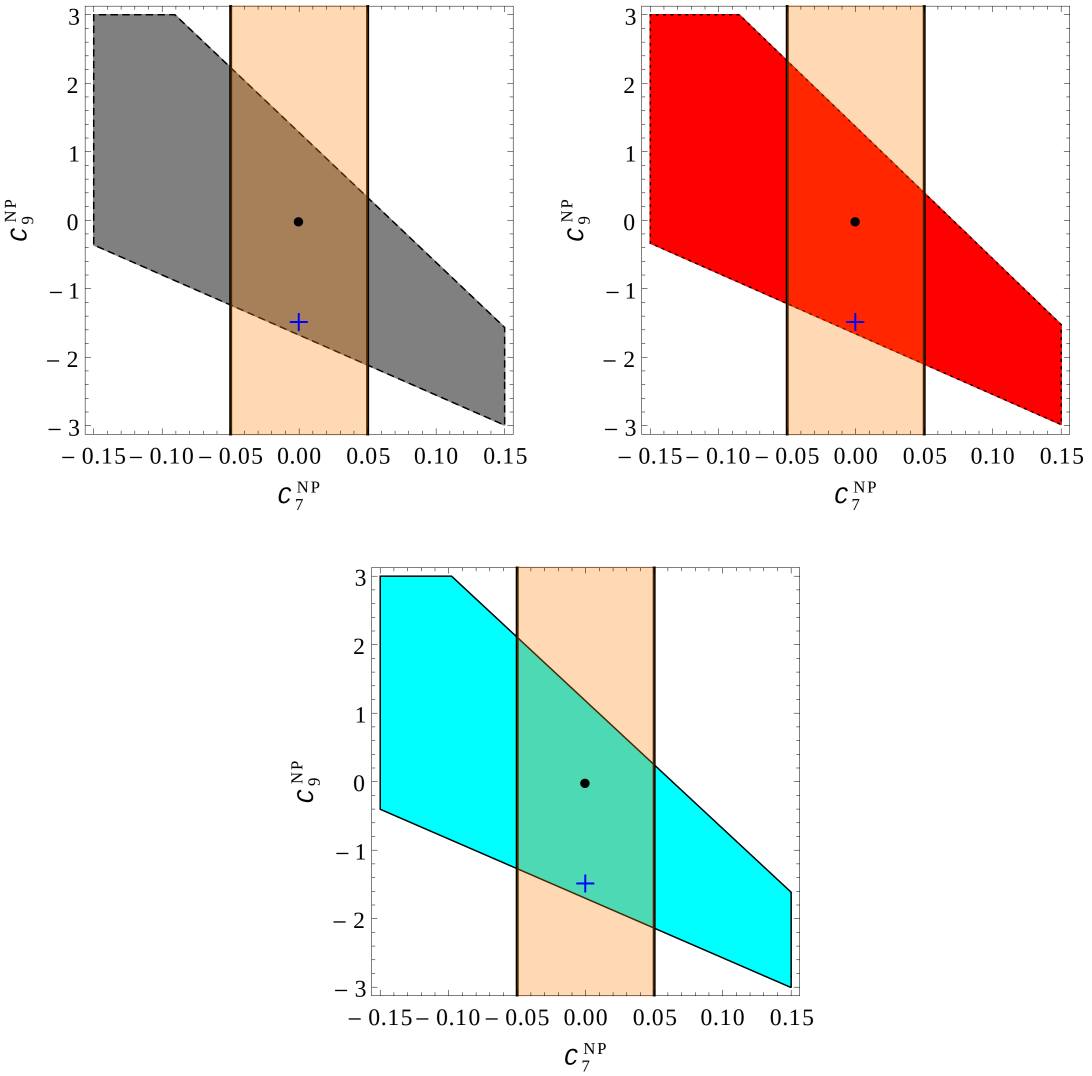


Figure 2.3: Constraints on $C_7^{\rm NP} - C_9^{\rm NP}$ from zeros of observables $A_{FB}$ (Gray), $P_5^{\prime}$ (Red) and $P_4^{\prime}$ (Cyan) using analytic relations Eq. (2.4.1), Eq. (2.4.6), Eq. (2.4.10). The light orange band shows the constraints on the values of $C_7$ from the inclusive and exclusive $b \to s\gamma$ modes as discussed in the text. The black filled circle shows the SM point whereas the blue colored '+' in the plots corresponds to the simplest possible NP solution $C_9^{\rm NP} = -1.5$ to explain the observed tension in the experimental data on $b \to s\mu^+\mu^-$. The NP solution $C_9^{\rm NP} = -1.5$ corresponds to 'BSM1' scenario and has been discussed in detail later in the text.

with photon energy cut $E_0 = 1.6$ defining the threshold is given by [92],

$$BR(B \to X_s\gamma)_{E_\gamma > E_0} = BR(B \to X_c e\bar{\nu}) \left| \frac{V_{tb}V_{ts}^*}{V_{cb}} \right|^2 \frac{6\alpha_{\rm em}}{\pi C}(P(E_0) + \delta_{\rm nonp.}), \tag{2.5.1}$$

where $C$ is a semileptonic phase-space factor given by [93]

$$C = \left|\frac{V_{ub}}{V_{cb}}\right|^2 \frac{\Gamma(\bar{B} \to X_c e\bar{\nu})}{\Gamma(\bar{B} \to X_u e\bar{\nu})} = 0.58 \pm 0.01, \tag{2.5.2}$$

and $\delta_{\text{nonp.}}$ is the nonperturbative contribution estimated in Ref. [94]. At LO, $P(E_0) = |C_7|^2$ and NNLO QCD corrections have been computed in Ref. [95–97]. The formula for branching ratio for exclusive $B \to K^*\gamma$ is given by [98]

$$BR(B \to K^*\gamma) = \tau_B \frac{G_F^2 \alpha_{\text{em}} m_B^3 m_b^2}{32\pi^3} \left(1 - \frac{m_{K^*}^2}{m_B^2}\right)^3 |V_{tb}V_{ts}^*|^2 \left(|C_7|^2 + |C_7'|^2\right) T_1(0), \tag{2.5.3}$$

where form factor $T_1(0)$ is the main source of uncertainty in the prediction of branching ratio. The updated LCSR calculation of the full QCD form factors gives $T_1(0) = 0.282 \pm 0.031$ [99], and combined fit of the LCSR and lattice calculation gives $T_1(0) = 0.312 \pm 0.027$ [100]. Constraint on the real part of NP Wilson coefficient $C_7^{\text{NP}}$ from updated data on inclusive as well as exclusive $b \to s\gamma$ processes allows $-0.043 \leq \text{Re } C_7^{\text{NP}} \leq 0.030$ at 95% C.L [98]. In Fig 2.3, we have taken a more conservative value of this constraint and allowed for $-0.05 \leq \text{Re } C_7^{\text{NP}} \leq 0.05$.

Then the precise measurement of $\hat{s}_0$ essentially determines the effective coefficient $C_9^{\text{eff}}$. The recently measured value of $\hat{s}_0$ currently involves large errors ( $\sim 35\%$) [88]. Therefore, bounds on $C_9^{\text{eff}}$ are not as stringent. But a qualitative analysis shows that $\hat{s}_0$ is compatible with models having NP contribution to $C_9$. We also provide constrained region in $C_7 - C_9$ plane using bounds from zero of $P_4'$ and $P_5'$. However, we must mention that constraints from zero of $P_4'$ and $P_5'$ in Fig 2.3 are not to be taken at the face value (as the experimental measurements of zeros of $P_4'$ and $P_5'$ are not available[†]) and are shown for illustrative purpose only. This exercise shows that the measurement of these zeros will provide equally efficient constraints on $C_9$ as drawn from $\hat{s}_0$.

Finally, we investigate the BSM reach of these zeros by carrying out a numerical study of the $\hat{s}_0^{P_5'}$, $\hat{s}_0^{P_4'}$ and $\hat{s}_0^{\mathcal{O}_T^{L,R}}$ in Table 2.2. In the SM, their values lie in the large recoil region and therefore these observables, like the zero of $A_{\text{FB}}$, are

[†]LHC$b$ has now started measuring these zeros and the reported measurements, which came after the publication of this work, have been discussed at the end of this Chapter.

expected to be very clean. These zeros also have sensitivity to BSM effects induced by right-handed currents. The BSM scenarios we have chosen in Table 2.2 are motivated from the analysis [39] of the updated data on $B \to K^*\mu\mu$ and are obtained by allowing variation in single Wilson coefficient at a time. The case BSM1 is most favored while the cases BSM2 and BSM3 are less favorable. The three columns in Table 2.2 correspond to these scenarios as follows:

- The scenario BSM1 corresponds to a negative contribution of $-1.5$ to the SM value of $C_9$ (shown in Fig 2.3 by the symbol '+'). This kind of scenario could, for example, be generated by a $Z'$ boson which has vector like coupling to muons [53], where $C_9$ has a non-zero contribution while the NP contribution to the Wilson coefficient $C_{10}$ vanishes.

- The other two columns correspond to cases where NP enters in a correlated way in two Wilson coefficients. The second scenario, BSM2, has new physics in the $SU(2)_L$ invariant direction $C_9^{\rm NP} = -C_{10}^{\rm NP}$ and can be realized in $Z'$ models with the $Z'$ boson having coupling to left-handed muons [53]. A scalar leptoquark $\phi$ transforming as $(3, 3)_{-1/3}$ with couplings to left-handed muons can also generate this scenario [101].

- The third scenario stems from new contributions from helicity-flipped semileptonic operators $O_9'$ and $O_{10}'$. This case was specifically chosen to show the distinguishing features of these zeros when only right-handed currents have new physics contributions.

In each of the BSM scenarios, estimates of uncertainties are the same as discussed for the SM case. Our numerical analysis explicitly shows that the observables $\hat{s}_0^{P_5'}$, $\hat{s}_0^{P_4'}$ and $\hat{s}_0^{\mathcal{O}_T^{L,R}}$ along with $\hat{s}_0$ can certainly distinguish between the SM case (the SM predictions for zeros are given in Table 2.1) and different BSM hypotheses. An important point we would like to make here is that from Table 2.2, it is clear that $\hat{s}_0$ has very similar values as $\hat{s}_0^{\mathcal{O}_T^{L,R}}$ in all scenarios. This is true only when there is no contribution from right-handed currents (like the cases BSM1 and BSM2). The values of zero crossing points would not be identical when right-handed currents are invoked (like in the case BSM3). However, the difference between $\hat{s}_0$ and $\hat{s}_0^{\mathcal{O}_T^{L,R}}$ in the case BSM3 is arising only beyond third decimal place and therefore, at present, can be neglected in favor of experimental errors. We would be able to identify distinctions among different NP scenarios more

| Observable | BSM1 | BSM2 | BSM3 |
|---|---|---|---|
| | $C_9^{\rm NP} = -1.5$ | $C_9^{\rm NP} = -C_{10}^{\rm NP} = -0.53$ | $C_9' = C_{10}' = -0.10$ |
| $\hat{s}_0$ | 0.198 | 0.146 | 0.127(76) |
| $\hat{s}_0^{P_5'}$ | 0.109 | 0.078 | 0.067 |
| $\hat{s}_0^{P_4'}$ | 0.050 | 0.067 | 0.061 |
| $\hat{s}_0^{\mathcal{O}_T^{L,R}}$ | 0.198 | 0.146 | 0.127(91) |

Table 2.2: Values of zeros compared between different BSM scenarios. Only non-zero NP Wilson coefficients are shown in each scenario. The values in the parenthesis correspond to beyond the third decimal place. See Table 2.1 for values in the SM.

accurately once these zeros are precisely measured. Experimentally, only $\hat{s}_0$ has received attention. We stress that the other zeros are equally important and should be measured or extracted experimentally, since this could already yield crucial information about NP, if present. Further, it may happen that some of the observable profiles (i.e. values in experimentally measured bins) turn out to be different from the SM, as is the case say with $P_5'$. In such a situation, a further check would be the position of the zero. These two pieces of information put together will clearly point out to any NP present.

## 2.6 Summary and Conclusions

The radiative and semi-leptonic $b \to s$ decays have a potential sensitivity to effects beyond the SM. With LHC$b$'s dedicated efforts to measure the decay $B \to K^*\ell\ell$ and associated angular observables extensively, the decay $B \to K^*\ell\ell$ seems to be a promising field to identify patterns of NP which can be probed by experimental data. Recent data shows some discrepancies in comparison to the SM predictions but due to uncertainties inherent in the theoretical calculations of such processes, at present, it is difficult to infer the same in affirmation. Precise measurements of theoretically clean observables hold the best chance of unambiguously revealing the presence of physics beyond the SM, if any. The zero of the forward-backward asymmetry ($\hat{s}_0$) is known to fall under this category of observables. But the current measurement is not precise enough to say anything definitive and is totally consistent with the SM. It may be useful to have more such observables measured with precision. In this chapter, we have pointed out that along with $\hat{s}_0$, the zeros of observables $P_5'$, $P_4'$ and $\mathcal{O}_T^{L,R}$ (a new angular observable proposed) are suitable candidates in this regard. The zeros of these observables, like the case of $\hat{s}_0$, have good theoretical control over hadronic uncertainties and can provide crucial tests of the SM. We noted that there exist correlations among zeros of different observables within the SM, and the positions of all the zeros are essentially fixed by $\hat{s}_0$, up to small corrections. We further used these relations to model-independently constrain the $C_7^{\rm NP} - C_9^{\rm NP}$ plane. To this end, we defined our framework by considering that NP enters in electromagnetic ($O_7$) and semileptonic operators $O_9$, and $O_{10}$, together with their chirally-flipped counterparts. We have assumed the Wilson coefficients to be real, but generalization to complex coefficients is straightforward.

We studied the implications of these zeros on $C_7^{\rm NP} - C_9^{\rm NP}$ plane in the SM like operator basis. The conservative bounds on $C_7^{\rm NP}$ are taken from $B \to X_s\gamma$ experimental data. Owing to the rather large uncertainties in the current measured value of $\hat{s}_0$, the constraints on the Wilson coefficient $C_9$ are rather weak and the deviations of up to $\sim -1.5$ in $C_9$ are compatible with experimental data within the $1\sigma$ range. We showed that observables $\hat{s}_0^{P_5'}$, $\hat{s}_0^{P_4'}$ have equally good sensitivity to $C_9$ and $C_7$ as $\hat{s}_0$. In addition to the SM-like basis scenario, we further investigated the cases where the operator basis is augmented by helicity-flipped operators. We noted that the zeros of these observables are quite sensitive to the effects stemming from BSM scenarios. This can be observed from the numerical analysis we performed in Table 2.2. The analysis clearly shows that the zeros have the capability to discriminate between different BSM scenarios. This sensitivity can be further exploited to test such scenarios once more precise data on the zeros of discussed observables become available. To date, only $\hat{s}_0$ has received attention but we have shown that zeros of other angular observables also carry important and complementary information on short-distance parameters. We thus hope that these observables will be measured precisely by the LHC$b$ collaboration, and data on these observables can certainly be used to put strong constraints on NP physics. The relations are obtained in the large recoil region in the large energy limit where theoretical uncertainties are supposed to be minimal. To the best of our knowledge, this is the first attempt to use such correlations as a stringent test of the SM itself. A simultaneous accurate determination of these zeros will surely provide conclusive evidence of any NP present. Moreover, in a general setting, the zeros by themselves carry complementary information about the Wilson coefficients and their measurement, together with the existing data can be used to pinpoint the class of NP scenarios which can give rise to such predictions. This is clearly evident from the position of $\hat{s}_0^{\mathcal{O}_T^{L,R}}$ which in the standard model limit yields the same value as $\hat{s}_0$ but when the helicity flipped operators are included, leads to complementary information on the Wilson coefficients compared to what can be inferred from $\hat{s}_0$.

In the end, we must mention that following the suggestion of this work that apart from the zero of $A_{\rm FB}$, the zeros of observables $P_5'$ and $P_4'$ can also provide new and theoretically cleaner tests of the SM, the LHC$b$ collaboration has started measuring the zeros of observables $P_4'$ and $P_5'$ (see [38] ). However, the associated experimental errors are still large to draw any conclusions on the presence of NP, and the values of zero crossings are consistent with the SM. The zero crossing points determined from the decay amplitude fit are [38]

$$\begin{aligned} s_0^{P_5'} &\in [2.49, 3.95]\,\mathrm{GeV}^2 \;\text{ at } 68\% \text{ confidence level (C.L.)}, \\ s_0 &\in [3.40, 4.87]\,\mathrm{GeV}^2 \text{ at } 68\% \text{ C.L.}, \\ s_0^{P_4'} &< 2.65\,\mathrm{GeV}^2 \text{ at } 95\% \text{ C.L.} \end{aligned}$$

We hope that with more data, not just the position of various zeros, but also the complete profiles of angular observables will be known with high precision, which can be used further as a crucial test of the SM.

# Chapter 3

# Angular Observables and Asymmetries for $\Lambda_b \to \Lambda\ell^+\ell^-$

## 3.1 Introduction

As discussed in the previous chapter, semileptonic decays mediated by the quark level transition $b \to s\ell^+\ell^-$ offer cleaner probes compared to nonleptonic exclusive hadronic decays. In the latter case, theoretical calculations are more difficult in general and they are also marred by issues related to QCD effects, both perturbative and nonperturbative, in a bigger way. Semileptonic decays on the other hand are somewhat easier at the theoretical level as the leptonic sub-system factorizes as far as the QCD effects between the final state subsystems go. Further, since LHC$b$ observations hint at deviations from the SM predictions in observables related to $B \to K^{(*)}\mu^+\mu^-$ channels (see [37, 38, 41] for anomalies in $K^*$ channel and [34] for hints of lepton universality violation in $K$ channel), which proceed at the quark level by the same $b \to s$ semi-leptonic decay, it is of utmost importance to study any other such semi-leptonic decay modes to clarify the situation and pin point the source of these deviations. Since the hadronic effects bring along large uncertainties, the above mentioned hints cannot be conclusively taken as evidence for new physics, which is part of the short distance structure. However, if a similar pattern emerges for decays with different hadronic particles but governed by the same $b \to s\ell^+\ell^-$ quark level transition, then that would amount to an unambiguous signal for physics beyond the SM. The baryonic decay $\Lambda_b \to \Lambda \ell^+ \ell^-$ satisfies all these requirements, and therefore, it is useful to study it in detail. This decay has been studied theoretically in the past [102–123] but the emphasis has been somewhat different from that in this chapter. This decay mode, like $B \to K^* \ell^+ \ell^-$, has many angular observables to offer as probes. This fact was utilized to some extent in Ref. [124]. Here we take it further and also construct some new angular observables which can be used to extract information on the short-distance structure which is theoretically clean and less sensitive to the hadronic form factors. On the experimental side, this decay was observed at the Tevatron [125]. Recently, LHC$b$ has measured the branching fraction along with some angular coefficients [126, 127]. The errors are still quite large but one hopes to have better results in the near future.

## 3.2 Effective Hamiltonian and the decay $\Lambda_b \to \Lambda \ell^+ \ell^-$

Since the decay $\Lambda_b \to \Lambda \ell^+ \ell^-$, at the quark level, is governed by FCNC transition $b \to s \ell^+ \ell^-$, the effective Hamiltonian is identical to that given in Section 2.2 in the previous chapter,

$$\mathcal{H}_{\text{eff}} = -\frac{4G_F}{\sqrt{2}} V_{ts}^* V_{tb} \sum_i (C_i(\mu) O_i + C_i^{'}(\mu) O_i^{'}) + \text{h.c.}\,, \qquad (3.2.1)$$

The operators contributing significantly in the SM are the semileptonic vector operator $O_9$, the axial vector operator $O_{10}$, and the magnetic photon penguin operator $O_7$.

Taking into account the polarizations of $\Lambda_b$ and $\Lambda$, there are a host of form factors that enter the calculations. The $\Lambda_b \to \Lambda$ form factors parametrize the (axial-)vector, (pseudo-) scalar and (pseudo-) tensor matrix elements and are defined in the helicity basis as follows [128]. For vector and axial-vector currents, we have

$$\begin{aligned}
\langle \Lambda(k, s_\Lambda)|\bar{s}\gamma^\mu b|\Lambda_b(p, s_{\Lambda_b})\rangle &= \bar{u}_\Lambda(k, s_\Lambda)\Bigg[f_t^V(q^2)(m_{\Lambda_b} - m_\Lambda)\frac{q^\mu}{q^2} \\
&+ f_0^V(q^2)\frac{m_{\Lambda_b} + m_\Lambda}{s_+}\left(p^\mu + k^\mu - (m_{\Lambda_b}^2 - m_\Lambda^2)\frac{q^\mu}{q^2}\right) \\
&+ f_\perp^V(q^2)\left(\gamma^\mu - \frac{2m_\Lambda}{s_+}p^\mu - \frac{2m_{\Lambda_b}}{s_+}k^\mu\right)\Bigg] u_{\Lambda_b}(p, s_{\Lambda_b}),
\end{aligned} \tag{3.2.2}$$

and

$$\begin{aligned}
\langle \Lambda(k, s_\Lambda)|\bar{s}\gamma^\mu\gamma_5 b|\Lambda_b(p, s_{\Lambda_b})\rangle &= -\bar{u}_\Lambda(k, s_\Lambda)\gamma_5\Bigg[f_t^A(q^2)(m_{\Lambda_b} + m_\Lambda)\frac{q^\mu}{q^2} \\
&+ f_0^A(q^2)\frac{m_{\Lambda_b} - m_\Lambda}{s_-}\left(p^\mu + k^\mu - (m_{\Lambda_b}^2 - m_\Lambda^2)\frac{q^\mu}{q^2}\right) \\
&+ f_\perp^A(q^2)\left(\gamma^\mu + \frac{2m_\Lambda}{s_-}p^\mu - \frac{2m_{\Lambda_b}}{s_-}k^\mu\right)\Bigg] u_{\Lambda_b}(p, s_{\Lambda_b}),
\end{aligned} \tag{3.2.3}$$

with the condition $f_t^V(0) = f_0^V(0)$, $f_t^A(0) = f_0^A(0)$, where $q^\mu = (p-k)^\mu$ is the momentum transfer and $s_\pm = (m_{\Lambda_b} \pm m_\Lambda)^2 - q^2$.

The form factor parametrization for scalar and pseudo-scalar current can be obtained from Eq. (3.2.2) and Eq. (3.2.3) via use of the equations of motion. These are given by,

$$\langle \Lambda(k, s_\Lambda)|\bar{s}b|\Lambda_b(p, s_{\Lambda_b})\rangle = f_t^V(q^2)\left(\frac{m_{\Lambda_b} - m_\Lambda}{m_b - ms}\right)\bar{u}_\Lambda(k, s_\Lambda)\; u_{\Lambda_b}(p, s_{\Lambda_b}), \tag{3.2.4}$$

and

$$\langle \Lambda(k, s_\Lambda)|\bar{s}\gamma_5 b|\Lambda_b(p, s_{\Lambda_b})\rangle = f_t^A(q^2)\left(\frac{m_{\Lambda_b} + m_\Lambda}{m_b + ms}\right)\bar{u}_\Lambda(k, s_\Lambda)\; \gamma_5 u_{\Lambda_b}(p, s_{\Lambda_b}), \tag{3.2.5}$$

For tensor and pseudo-tensor current, we have

$$\begin{aligned}
&\langle \Lambda(k, s_\Lambda)|\bar{s}i\sigma^{\mu\nu}q_\nu b|\Lambda_b(p, s_{\Lambda_b})\rangle \\
&\quad = -\bar{u}_\Lambda(k, s_\Lambda)\Bigg[f_0^T(q^2)\frac{q^2}{s_+}\left(p^\mu + k^\mu - (m_{\Lambda_b}^2 - m_\Lambda^2)\frac{q^\mu}{q^2}\right) \\
&\quad + f_\perp^T(q^2)(m_{\Lambda_b} + m_\Lambda)\left(\gamma^\mu - \frac{2m_\Lambda}{s_+}p^\mu - \frac{2m_{\Lambda_b}}{s_+}k^\mu\right)\Bigg] u_{\Lambda_b}(p, s_{\Lambda_b}),
\end{aligned} \tag{3.2.6}$$

and

$$\begin{aligned}
&\langle \Lambda(k, s_\Lambda) | \bar{s} i \sigma^{\mu\nu} q_\nu \gamma_5 b | \Lambda_b(p, s_{\Lambda_b}) \rangle \\
&\qquad = -\bar{u}_\Lambda(k, s_\Lambda) \gamma_5 \left[ f_0^{T_5}(q^2) \frac{q^2}{s_-} \left( p^\mu + k^\mu - (m_{\Lambda_b}^2 - m_\Lambda^2) \frac{q^\mu}{q^2} \right) \right. \\
&\qquad\qquad \left. + f_\perp^{T_5}(q^2)(m_{\Lambda_b} - m_\Lambda) \left( \gamma^\mu + \frac{2m_\Lambda}{s_-} p^\mu - \frac{2m_{\Lambda_b}}{s_-} k^\mu \right) \right] u_{\Lambda_b}(p, s_{\Lambda_b}).
\end{aligned} \tag{3.2.7}$$

Note that our notations for form factors are identical to the ones used in Ref. [124] but differ from the ones used in Ref. [128]. The two sets of notations used in Ref. [124] and Ref. [128] can be translated into each other via the following change: $f_t^V = f_0$, $f_0^V = f_+$, $f_\perp^V = f_\perp$, $f_t^A = g_0$, $f_0^A = g_+$, $f_\perp^A = g_\perp$, $f_0^T = h_+$, $f_\perp^T = h_\perp$, $f_0^{T_5} = \tilde{h}_+$, $f_\perp^{T_5} = \tilde{h}_\perp$.

At first sight the decay $\Lambda_b \to \Lambda \ell^+ \ell^-$ may seem not to be too useful owing to larger uncertainties in the transition form factors involved, when compared to the mesonic counterpart $B \to K^* \ell^+ \ell^-$. However, this decay offers a larger number of observables. For example, in contrast to $K^* \to K\pi$ decay in the mesonic counterpart which is parity conserving, $\Lambda \to N\pi$ is a parity violating decay and hence brings along the possibility of measuring forward-backward asymmetry in the hadronic system as well. This decay has been studied theoretically, but the emphasis in most of those studies was mainly on the lepton forward-backward asymmetry and/or lepton polarization asymmetry. Since the decay was observed at Tevatron, there has been some activity, both on the form factors [128–137] as well as on exploiting the angular observables [124]. In the present work, we extend the analysis of [124] and also propose new observables and asymmetries which are theoretically clean and can be used with the limited data expected in the near future.

### 3.2.1 Angular distribution of $\Lambda_b \to \Lambda(\to N\pi)\ell^+\ell^-$

The four-body differential decay $\Lambda_b(p) \to \Lambda(k)[\to N(k_1)\pi(k_2)]\ell^+(q_1)\ell^-(q_2)$ can be conveniently written in terms of the variables: invariant mass squared of the lepton system $q^2 = (p-k)^2$, helicity angles $\theta_\Lambda$ and $\theta_\ell$ of the hadronic and leptonic subsystems respectively, and the azimuthal angle $\phi$ between the hadronic and leptonic planes. The four body differential decay rate can be written as

$$\frac{d^4\Gamma}{dq^2 d\cos\theta_\ell d\cos\theta_\Lambda d\phi} = \frac{3}{8\pi} K(q^2, \cos\theta_\ell, \cos\theta_\Lambda, \phi). \tag{3.2.8}$$

where

$$\begin{aligned} K(q^2, \cos\theta_\ell, \cos\theta_\Lambda, \phi) \;=\;& K_{1ss}\sin^2\theta_\ell + K_{1cc}\cos^2\theta_\ell + K_{1c}\cos\theta_\ell \\ &+ (K_{2ss}\sin^2\theta_\ell + K_{2cc}\cos^2\theta_\ell + K_{2c}\cos\theta_\ell)\cos\theta_\Lambda \\ &+ (K_{3sc}\sin\theta_\ell\cos\theta_\ell + K_{3s}\sin\theta_\ell)\sin\theta_\Lambda\cos\phi \\ &+ (K_{4sc}\sin\theta_\ell\cos\theta_\ell + K_{4s}\sin\theta_\ell)\sin\theta_\Lambda\sin\phi. \end{aligned} \tag{3.2.9}$$

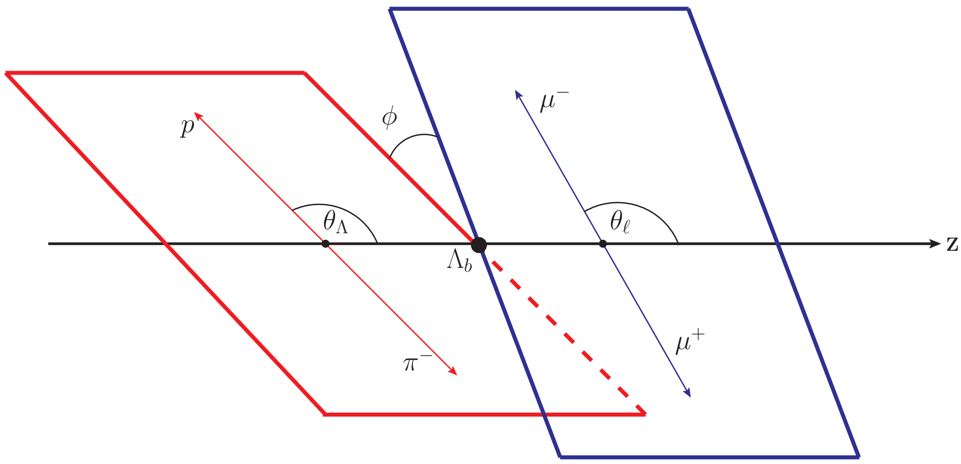


Figure 3.1: Schematic diagram showing the angular distribution of $\Lambda_b \to \Lambda(\to N\pi)\ell^+\ell^-$ decay with the description of the angles $\theta_\ell$, $\theta_\Lambda$ and $\phi$.

The angular coefficients $K_i$'s depend only on the dilepton invariant mass, $q^2$, and carry the hadronic information. They are in turn expressed in terms of the transversity amplitudes. These transversity amplitudes are written as combinations of Wilson coefficients and baryonic form factors in the helicity basis. A typical helicity amplitude, defined by the contraction of matrix elements with the virtual polarization vectors, is denoted as $H(s_{\Lambda_b}, s_\Lambda)$ where we have suppressed the indices $V$, $T$, $A$ signifying the type of operator sandwiched between the external hadronic states but have explicitly shown the two spin projection vectors which take values $\pm 1/2$. The explicit expressions of helicity amplitudes $H(s_{\Lambda_b}, s_\Lambda)$ in terms of $\Lambda_b \to \Lambda$ form factors $f^{V,A}_{t,0,\perp}$, $f^{T,T_5}_{0,\perp}$ are given in Ref. [124] and have been collected in Appendix C. The transversity amplitudes then in the SM are given by

$$A^{L(R)}_{\perp_1} = \sqrt{2}N\left(C^{L(R)}_{9,10} H^V_+(-1/2,1/2) - \frac{2m_b C_7}{q^2} H^T_+(-1/2,1/2)\right), \tag{3.2.10}$$

$$A^{L(R)}_{\parallel_1} = -\sqrt{2}N\left(C^{L(R)}_{9,10} H^A_+(-1/2,1/2) + \frac{2m_b C_7}{q^2} H^{T_5}_+(-1/2,1/2)\right), \tag{3.2.11}$$

$$A^{L(R)}_{\perp_0} = \sqrt{2}N\left(C^{L(R)}_{9,10} H^V_0(1/2,1/2) - \frac{2m_b C_7}{q^2} H^T_0(1/2,1/2)\right), \tag{3.2.12}$$

$$A^{L(R)}_{\parallel_0} = -\sqrt{2}N\left(C^{L(R)}_{9,10} H^A_0(1/2,1/2) + \frac{2m_b C_7}{q^2} H^{T_5}_0(1/2,1/2)\right), \tag{3.2.13}$$

where $C^{L(R)}_{9,10} = (C_9 \mp C_{10})$ and $N$ is the normalization factor given by

$$N = G_F V_{tb} V^*_{ts} \alpha_e \sqrt{\frac{q^2 \sqrt{\lambda(m^2_{\Lambda_b}, m^2_\Lambda, q^2)}}{3\,\pi^5 (2)^{11}\, m^3_{\Lambda_b}}} \tag{3.2.14}$$

with $\lambda(m^2_{\Lambda_b}, m^2_\Lambda, q^2) = m^4_{\Lambda_b} + m^4_\Lambda + q^4 - 2(m^2_{\Lambda_b} m^2_\Lambda + m^2_{\Lambda_b} q^2 + m^2_\Lambda q^2)$.

In terms of the transversity amplitudes, the angular coefficients appearing in the fully differential decay rate are defined as [124]

$$K_{1ss} = \frac{1}{4}\left[|A^R_{\perp_1}|^2 + |A^R_{\parallel_1}|^2 + 2|A^R_{\perp_0}|^2 + 2|A^R_{\parallel_0}|^2 + (R \leftrightarrow L)\right], \tag{3.2.15}$$

$$K_{1cc} = \frac{1}{2}\left[|A^R_{\perp_1}|^2 + |A^R_{\parallel_1}|^2 + (R \leftrightarrow L)\right], \tag{3.2.16}$$

$$K_{1c} = -\mathrm{Re}\left\{A^R_{\perp_1} A^{*R}_{\parallel_1} - (R \leftrightarrow L)\right\}, \tag{3.2.17}$$

$$K_{2ss} = \frac{\alpha}{2}\mathrm{Re}\left\{A^R_{\perp_1} A^{*R}_{\parallel_1} + 2A^R_{\perp_0} A^{*R}_{\parallel_0} + (R \leftrightarrow L)\right\}, \tag{3.2.18}$$

$$K_{2cc} = \alpha\mathrm{Re}\left\{A^R_{\perp_1} A^{*R}_{\parallel_1} + (R \leftrightarrow L)\right\}, \tag{3.2.19}$$

$$K_{2c} = -\frac{\alpha}{2}\left[|A^R_{\perp_1}|^2 + |A^R_{\parallel_1}|^2 - (R \leftrightarrow L)\right], \tag{3.2.20}$$

$$K_{3sc} = \frac{\alpha}{\sqrt{2}}\mathrm{Im}\left\{A^R_{\perp_1} A^{*R}_{\perp_0} - A^R_{\parallel_1} A^{*R}_{\parallel_0} + (R \leftrightarrow L)\right\}, \tag{3.2.21}$$

$$K_{3s} = \frac{\alpha}{\sqrt{2}}\mathrm{Im}\left\{A^R_{\perp_1} A^{*R}_{\parallel_0} - A^R_{\parallel_1} A^{*R}_{\perp_0} - (R \leftrightarrow L)\right\}, \tag{3.2.22}$$

$$K_{4sc} = \frac{\alpha}{\sqrt{2}}\mathrm{Re}\left\{A^R_{\perp_1} A^{*R}_{\parallel_0} - A^R_{\parallel_1} A^{*R}_{\perp_0} + (R \leftrightarrow L)\right\}, \tag{3.2.23}$$

$$K_{4s} = \frac{\alpha}{\sqrt{2}}\mathrm{Re}\left\{A^R_{\perp_1} A^{*R}_{\perp_0} - A^R_{\parallel_1} A^{*R}_{\parallel_0} - (R \leftrightarrow L)\right\}, \tag{3.2.24}$$

where the parameter $\alpha$ is the parity violating parameter in the $\Lambda \to N\pi$ decay. Experimentally, we have $\alpha(\Lambda \to p\pi^-) = 0.642 \pm 0.013$, $\alpha(\bar{\Lambda} \to \bar{p}\pi^+) = -0.71 \pm 0.08$, and $\alpha(\Lambda \to n\pi^0)/\alpha(\Lambda \to p\pi^-) = 1.01 \pm 0.07$ [9].

The task then is to experimentally determine these angular coefficients. In principle, once there is sufficient data, a full angular fit would end up determining these coefficients (up to discrete ambiguities). One could proceed by studying angular asymmetries allowing for the extraction of specific angular coefficients and/or some combinations of those. In [124], the authors considered the following observables which provide a handle on a select few angular coefficients:

(i) Decay rate as a function of $q^2$

$$\frac{d\Gamma}{dq^2} = 2K_{1ss} + K_{1cc}. \tag{3.2.25}$$

(ii) Transverse (and therefore longitudinal) polarization fraction

$$F_L = 1 - F_T = \frac{2K_{1ss} - K_{1cc}}{2K_{1ss} + K_{1cc}}. \tag{3.2.26}$$

(iii) Forward-backward asymmetries in the leptonic, hadronic and mixed sub-systems:

$$\begin{aligned} A^{\ell}_{FB} &= \frac{3}{2}\frac{K_{1c}}{2K_{1ss} + K_{1cc}}, \\ A^{\Lambda}_{FB} &= \frac{1}{2}\frac{2K_{2ss} + K_{2cc}}{2K_{1ss} + K_{1cc}}, \\ A^{\ell,\Lambda}_{FB} &= \frac{3}{4}\frac{K_{2c}}{2K_{1ss} + K_{1cc}}. \end{aligned} \tag{3.2.27}$$

Analogous to the lepton forward-backward asymmetry in $B \to K^*\ell^+\ell^-$, $A^{\ell}_{FB}$ and $A^{\ell,\Lambda}_{FB}$ have a zero crossing, which essentially depends on the short distance parameters only (in the approximation when the form factor dependence more or less cancels) and its value is the same as in the the mesonic case, scaled by the $\Lambda_b$ mass instead of the B-meson mass. Specifically, the zero of $A^{\ell}_{FB}$ [124]

$$s^{\ell}_0 = -2m_b m_{\Lambda_b}\frac{C_7}{C_9}. \tag{3.2.28}$$

## 3.3 More asymmetries and new observables

We extend the previous work by constructing asymmetries such that all the angular coefficients can be extracted. To this end, we construct the following observables:

$$
\begin{aligned}
Y_2 &= \frac{\int_0^{2\pi} d\phi \left[\int_0^1 - \int_{-1}^0\right] d\cos\theta_\Lambda \left[\int_{-1}^{-1/2} - \int_{-1/2}^0 - \int_0^{1/2} + \int_{1/2}^1\right] d\cos\theta_\ell K(q^2, \theta_\ell, \theta_\Lambda, \phi)}{\int_0^{2\pi} d\phi \int_{-1}^1 d\cos\theta_\Lambda \int_{-1}^1 d\cos\theta_\ell K(q^2, \theta_\ell, \theta_\Lambda, \phi)}, \\
&= \frac{3}{8}\frac{K_{2cc} - K_{2ss}}{2K_{1ss} + K_{1cc}}, \qquad (3.3.1)
\end{aligned}
$$

$$
\begin{aligned}
Y_{3s} &= \frac{\left[\int_0^{\pi/2} - \int_{\pi/2}^{\pi} - \int_{\pi}^{3\pi/2} + \int_{3\pi/2}^{2\pi}\right] d\phi \int_{-1}^1 d\cos\theta_\Lambda \int_{-1}^1 d\cos\theta_\ell K(q^2, \theta_\ell, \theta_\Lambda, \phi)}{\int_0^{2\pi} d\phi \int_{-1}^1 d\cos\theta_\Lambda \int_{-1}^1 d\cos\theta_\ell K(q^2, \theta_\ell, \theta_\Lambda, \phi)}, \\
&= \frac{3\pi}{8}\frac{K_{3s}}{2K_{1ss} + K_{1cc}}, \qquad (3.3.2)
\end{aligned}
$$

$$
\begin{aligned}
Y_{3sc} &= \frac{\left[\int_0^{\pi/2} - \int_{\pi/2}^{\pi} - \int_{\pi}^{3\pi/2} + \int_{3\pi/2}^{2\pi}\right] d\phi \int_{-1}^1 d\cos\theta_\Lambda \left[\int_0^1 - \int_{-1}^0\right] d\cos\theta_\ell K(q^2, \theta_\ell, \theta_\Lambda, \phi)}{\int_0^{2\pi} d\phi \int_{-1}^1 d\cos\theta_\Lambda \int_{-1}^1 d\cos\theta_\ell K(q^2, \theta_\ell, \theta_\Lambda, \phi)}, \\
&= \frac{1}{2}\frac{K_{3sc}}{2K_{1ss} + K_{1cc}}, \qquad (3.3.3)
\end{aligned}
$$

$$
\begin{aligned}
Y_{4s} &= \frac{\left[\int_0^{\pi} - \int_{\pi}^{2\pi}\right] d\phi \int_{-1}^1 d\cos\theta_\Lambda \int_{-1}^1 d\cos\theta_\ell K(q^2, \theta_\ell, \theta_\Lambda, \phi)}{\int_0^{2\pi} d\phi \int_{-1}^1 d\cos\theta_\Lambda \int_{-1}^1 d\cos\theta_\ell K(q^2, \theta_\ell, \theta_\Lambda, \phi)}, \\
&= \frac{3\pi}{8}\frac{K_{4s}}{2K_{1ss} + K_{1cc}}, \qquad (3.3.4)
\end{aligned}
$$

and

$$
\begin{aligned}
Y_{4sc} &= \frac{\left[\int_0^{\pi} - \int_{\pi}^{2\pi}\right] d\phi \int_{-1}^1 d\cos\theta_\Lambda \left[\int_0^1 - \int_{-1}^0\right] d\cos\theta_\ell K(q^2, \theta_\ell, \theta_\Lambda, \phi)}{\int_0^{2\pi} d\phi \int_{-1}^1 d\cos\theta_\Lambda \int_{-1}^1 d\cos\theta_\ell K(q^2, \theta_\ell, \theta_\Lambda, \phi)}, \\
&= \frac{1}{2}\frac{K_{4sc}}{2K_{1ss} + K_{1cc}}. \qquad (3.3.5)
\end{aligned}
$$

Clearly, Eq. (3.3.1)-Eq. (3.3.5) along with the other equations above determine all the angular coefficients. Although true in principle, in practice any such determination will be severely hampered by the uncertainties coming from transition form factors. In the baryonic case, the form factors are rather poorly known when one compares the situation with the mesonic counterparts. In the latter, there has been lot of progress in having a reliable set of form factors. But even there, hadronic uncertainties prevent one from making any sound claim of new physics when encountering deviations from the SM.

### 3.3.1 In large $q^2$ (low-recoil energy) approximation

The kinematic region can be divided into the large and small $q^2$ or equivalently the low and large recoil regions. In each of the regions, one can make suitable approximations which allow a smaller set of form factors to be employed, and there are certain relations that emerge between various form factors. A typical matrix element one is interested in is of the form: $\langle\Lambda(k, s_\Lambda|\bar{s}\Gamma b|\Lambda_b(p, s_{\Lambda_b}\rangle$, where $s_{\Lambda_{(b)}}$ are the spin vectors associated with the baryons. In full generality, there are a large number of form factors that would contribute to the physical decay rate. There exists several estimates of the form factors in the literature [128–137]. If, however, one makes use of the heavy quark symmetry (working systematically in heavy quark effective theory (HQET)), the number of independent form factors reduces to just two. Employing HQET, the two relevant form factors appear in the hadronic matrix elements as:

$$\langle\Lambda(k, s_\Lambda|\bar{s}\Gamma b|\Lambda_b(p, s_{\Lambda_b}\rangle = \bar{u}(k, s_\Lambda)\left[F_1(k.v) + \not{p}F_2(k.v)\right]\Gamma\,\mathcal{U}(v, s_{\Lambda_b}) \tag{3.3.6}$$

where $v$ is the velocity of $\Lambda_b$ and the two form factors depend only on the invariant $k.v$, the energy of $\Lambda$ in the rest frame of $\Lambda_b$. The spinors satisfy the relations

$$\sum_{s=1,2} u(p, s)\bar{u}(p, s) = m_\Lambda + \not{p}, \qquad \sum_{s=1,2} \mathcal{U}(v, s)\bar{\mathcal{U}}(v, s) = 1 + \not{v} \tag{3.3.7}$$

It turns out that the two linear combinations $F_\pm = F_1 \pm F_2$ are more useful and one therefore prefers to work with them. Therefore in low recoil region, we have the following form factor relations:

$$f_\perp^V = f_0^V = f_\perp^T = f_0^T = F_-, \tag{3.3.8}$$

$$f_\perp^A = f_0^A = f_\perp^{T_5} = f_0^{T_5} = F_+ \tag{3.3.9}$$

Using the form factor relations (3.3.8) and (3.3.9) valid in the large $q^2$ region, one can rewrite the transversity amplitudes defined in Eqs. (3.2.10-3.2.13). In this approximation, the transversity amplitudes simplify to the following expressions:

$$A_{\perp_1}^{L(R)} = -2N\left(C_{9,10}^{L(R)} + \frac{2m_b(m_{\Lambda_b}+m_\Lambda)}{q^2}C_7\right)\sqrt{s_-}\,F_-, \tag{3.3.10}$$

$$A_{\parallel_1}^{L(R)} = 2N\left(C_{9,10}^{L(R)} + \frac{2m_b(m_{\Lambda_b}-m_\Lambda)}{q^2}C_7\right)\sqrt{s_+}\,F_+, \tag{3.3.11}$$

$$A_{\perp_0}^{L(R)} = \sqrt{2}N\left(C_{9,10}^{L(R)}(m_{\Lambda_b}+m_\Lambda) + 2m_bC_7\right)\sqrt{\frac{s_-}{q^2}}\,F_-, \tag{3.3.12}$$

$$A_{\parallel_0}^{L(R)} = -\sqrt{2}N\left(C_{9,10}^{L(R)}(m_{\Lambda_b}-m_\Lambda) + 2m_bC_7\right)\sqrt{\frac{s_+}{q^2}}\,F_+, \tag{3.3.13}$$

Thus, in heavy quark and large $q^2$ approximation, each transversity amplitudes depend on single form factor (either $F_-$ or $F_+$).

The recent LHC$b$ measurements of the branching ratio and the simplest angular asymmetries are mostly in the large $q^2$ region. It is worthwhile and important to construct observables which are as free of the hadronic inputs as possible and therefore can be used to probe the short-distance physics. In this spirit we propose the following observables written in terms of angular coefficients $K_i(q^2)$

$$\mathcal{T}_1(q^2) = \frac{K_{2ss} - K_{2cc}/2 - \alpha K_{1c}}{2K_{1ss}+K_{1cc}}, \tag{3.3.14}$$

$$\mathcal{T}_2(q^2) = \frac{\alpha(K_{1ss}-K_{1cc}) - K_{2c}/2}{2K_{1ss}+K_{1cc}}, \tag{3.3.15}$$

and

$$\mathcal{T}_3(q^2) = \frac{\alpha(K_{1ss}/\sqrt{2} - K_{1cc}/2) - K_{2c}/\sqrt{2}}{2K_{1ss}+K_{1cc}}. \tag{3.3.16}$$

Since the proposed observables $\mathcal{T}_1(q^2)$, $\mathcal{T}_2(q^2)$, and $\mathcal{T}_3(q^2)$ are combinations of angular coefficients $K_i$'s, these are experimentally measurable observables.

It is interesting to note that all three observables $\mathcal{T}_1$, $\mathcal{T}_2$, and $\mathcal{T}_3$ have zero crossing points in their $q^2$ profile. The observables $\mathcal{T}_1$, $\mathcal{T}_2$, and $\mathcal{T}_3$ are designed such that their zero crossing point lie in the large $q^2$ region where at present there is more control theoretically. Working in the large $q^2$ and HQET limit, the zeros can be evaluated easily and turn out to be less sensitive to form factor uncertainties. Especially, the zero crossing of $\mathcal{T}_1$ is completely independent of form factors and has the following expression in the SM

$$\begin{aligned}\hat{s}_0(\mathcal{T}_1) &= \frac{-\left(C_{10}^2+C_9^2\right)\left(m_{\Lambda_b}^2-m_\Lambda^2\right)-4C_7 m_b m_{\Lambda_b}(2C_{10}+C_9)-4C_7^2 m_b^2}{4C_{10}C_9 m_{\Lambda_b}^2}, \\ &\simeq \left(\frac{\hat{s}_0^\ell}{2}\right)^2+\frac{\hat{s}_0^\ell}{2}+\frac{1-\hat{m}_\Lambda^2}{2} \end{aligned} \tag{3.3.17}$$

where the 'hat' notation is used for convenience and corresponds to quantity normalized by mass of $\Lambda_b$ to make it dimensionless. For example, $\hat{s} = s(\equiv q^2)/m_{\Lambda_b}^2$, $\hat{m}_\Lambda = m_\Lambda/m_{\Lambda_b}$ etc. In the penultimate step of last equation we used the approximate relation of the leptonic forward-backward zero crossing, $s_0^\ell \simeq -2m_b m_{\Lambda_b} C_7/C_9$, given in Eq. (3.2.28), and the approximation $C_{10} \simeq -C_9$ valid in the SM. However, it should be mentioned that even without making use of this relation, $s_0(\mathcal{T}_1)$ is a genuinely short distance quantity, and therefore, has a precise value within the SM that can be unambiguously compared with the experimental determination. Numerically, using $C_9 = 4.2297$, $C_{10} =$ -4.2068, $C_7 =$ -0.2974 [71] in the SM, we find: $s_0(\mathcal{T}_1) = 16.89$ GeV$^2$ for $m_{\Lambda_b} = 5.619$ GeV, $m_\Lambda = 1.115$ GeV, and $m_b = 4.18$ GeV. Similarly, zeros of the other two observables, $\mathcal{T}_2$, and $\mathcal{T}_3$,

$$\hat{s}_0(\mathcal{T}_2) \sim \frac{1}{8}\left((\hat{s}_0^\ell)^2+2\hat{s}_0^\ell+2+\sqrt{(\hat{s}_0^\ell)^4+4(\hat{s}_0^\ell)^3-8(\hat{s}_0^\ell)^2+8(\hat{s}_0^\ell)+4}\right), \tag{3.3.18}$$

$$\begin{aligned}\hat{s}_0(\mathcal{T}_3) \sim \frac{1}{4}\Bigg(&\sqrt{\left\{(\hat{s}_0^\ell)^2+2\right\}\left\{\hat{s}_0^\ell\left((3-2\sqrt{2})\hat{s}_0^\ell+12\sqrt{2}-16\right)+6-4\sqrt{2}\right\}} \\ &+(\sqrt{2}-1)(\hat{s}_0^\ell)^2+(4-2\sqrt{2})\hat{s}_0^\ell+2\sqrt{2}-2\Bigg).\end{aligned} \tag{3.3.19}$$

The above two expressions for zeros are obtained in the approximation $m_\Lambda \simeq 0$ and turn out to be free of form factors in this limit. We find rough estimates for zeros: $s_0(\mathcal{T}_2) \sim 17.3$ GeV$^2$ and $s_0(\mathcal{T}_3) \sim 15.0$ GeV$^2$ using the approximated relations given in Eq. (3.3.18) and (3.3.19), respectively.

As discussed in the previous chapter, recent LHC$b$ results on the angular analysis of $B \to K^*\ell^+\ell^-$ have shown deviations from the SM expectations, especially for the observable $P_5'$. Many possible solutions have been suggested, among which the minimal solution that gives a reasonably good fit is the solution where the SM operator basis is employed and the only deviation is in $C_9$: $\delta C_9 \sim -1$, while there are practically no deviations in the other two Wilson coefficients [39, 48–50, 72]. Assuming this scenario, it is clear that the above observables, in particular the zero crossings can, very effectively and in a robust manner, test this hypothesis. In fact, extension to an extended operator basis is straight forward. We thus immediately see the immense potential of these asymmetries and zero crossing points which are very clean. The other advantage of these zero crossing points lies in the fact that they lie in the high $q^2$ region, in sharp contrast to the zero crossings of the observables in $B \to K^*\ell^+\ell^-$. This additional feature will also help in understanding possible $q^2$ dependence and differentiate between possibly overlooked hadronic effect from genuine new physics contribution which by definition should be $q^2$ independent.

These zero crossing points, along with the zeros of the leptonic and hadronic forward-backward asymmetries can be simultaneously used to not only test the SM but also to infer more about the form factors. Without making any assumptions, these quantities are functions of various form factors (actually ratios of various form factors). Measurement of these quantities, along with the profiles of various observables will allow us to extract some of these ratios at specific points. This information can then be utilized to cross-check the consistency of the form factors that one has employed. At present, this may appear as a daunting task but with more data available and more observables measured precisely, a simultaneous fit will provide this valuable information.

## 3.4 Discussion and conclusions

Experimentally, several anomalies, though not conclusive at the moment, have been seen in the flavor sector. Most recent ones are related to $b \to s$ semileptonic decay modes. In this vein, it is important to study different modes and channels which are mediated by the same $b \to s$ fundamental interactions. Recent times have seen a lot of theoretical and experimental effort in exploiting $B \to K^{(*)}\ell^+\ell^-$ modes to their full potential. The corresponding baryonic mode $\Lambda_b \to \Lambda\ell^+\ell^-$ has started to be studied experimentally. Since the baryonic counterpart now involves a completely different set of hadronic inputs, this becomes a very useful playground to cross-check the anomalies seen in the mesonic channels. Only recently, a more systematic approach to fully exploit the host of angular observables this mode has to offer has been initiated. In the present chapter we have extended that effort and listed all the angular asymmetries that pin down the complete set of angular coefficients. We have also proposed several other angular observables which should be easy to access experimentally. At present, this theoretical effort is limited by our knowledge of the hadronic effects in this mode (in particular, the estimates of nonfactorizable hadronic corrections are not available). However, the zero crossing points of the observables suggested in the chapter are less sensitive to hadronic effects (especially, the zero of $\mathcal{T}_1(q^2)$ is completely free of form factors in HQET and large $q^2$ limit ) and can be used to probe the genuine short distance content of the underlying theory. Therefore, this baryonic decay has an immense potential to test the SM precisely and even with limited amount of data available in near future, there may be hope to have a good indication of any new physics, if it is really there at the TeV scale. One of the possible improvements and future directions in this context would be to include other operators beyond the SM and study the proposed observables within the extended operator basis. This would shed some light on the (ir)relevance of some operators. When combined with similar studies on the mesonic counterparts, this could limit the beyond the SM contributions significantly. In particular, a detailed numerical investigation of the baryonic mode with inputs and recent hints of possible new physics from $B \to K^{(*)}\ell^+\ell^-$ would be very useful.

# Chapter 4

# Explaining Anomalies in $R_{D^{(*)}}$ in Alternative Left-Right Symmetric Model

## 4.1 Introduction

Recently, the LHC$b$ collaboration has reported the ratio of branching fractions for the semileptonic decay of the $B$ meson,

$$R_{D^{(*)}} = \frac{\mathrm{BR}(\bar{B} \to D^{(*)}\tau\bar{\nu})}{\mathrm{BR}(\bar{B} \to D^{(*)}\ell\bar{\nu})}; \qquad \ell = e, \mu, \tag{4.1.1}$$

to be $R_{D^*} = 0.336 \pm 0.027(\text{stat.}) \pm 0.030(\text{syst.})$ with the SM expectation $0.252 \pm 0.005$ [138], amounting to a $2.1\sigma$ excess [33]. This measurement is in agreement with the measurements of $\bar{B} \to D^{(*)}\tau\bar{\nu}$ reported by the BaBar [30, 31] and Belle [139] collaborations* and with earlier measurements [140, 141] and when combined together show a substantial deviation from the SM. A summary of the measurements of $R_{D^{(*)}}$ done by different collaborations together with the SM predictions is given in Table 4.1.

Several NP scenarios accommodating semileptonic $b \to c$ decay have been proposed to explain these excesses. The two-Higgs Doublet Model (2HDM) of

*Recently, Belle collaboration has updated its results on $R_{D^*}$ which came after the publication of this work. The updated measurement gives $R_{D^*} = 0.302 \pm 0.030 \pm 0.011$ [32] which is within $1.6\sigma$ of the SM prediction.

| | $R_{D^*}$ | $R_D$ |
|---|---|---|
| LHC$b$ [33] | $0.336 \pm 0.027 \pm 0.030$ | - |
| BaBar [30] | $0.332 \pm 0.024 \pm 0.018$ | $0.440 \pm 0.058 \pm 0.042$ |
| BELLE [139] | $0.293 \pm 0.038 \pm 0.015$ | $0.375 \pm 0.064 \pm 0.026$ |
| SM Pred. [138, 142] | $0.252 \pm 0.003$ | $0.300 \pm 0.010$ |

Table 4.1: Summary of experimental measurement for the ratios $R_{D^{(*)}}$, and the expectation in the SM. Here the first (second) errors are statistical (systematic).

type II is one of the well studied candidates of NP which can affect the semi-tauonic $B$ decays significantly [143–149]. However, the BABAR collaboration has excluded the 2HDM of type II at 99.8% confidence level [30, 31]. Phenomenological studies of the four fermion operators that can explain the discrepancy have been carried out in Refs. [138, 150–157]. The excesses have been explained in a more generalized framework of 2HDM in Refs. [158–160] and in the framework of $R$-parity violating (RPV) Minimal Supersymmetric Standard Model (MSSM) in Ref. [161], while in Refs. [151, 155, 156, 162, 163] the excesses have been addressed in the context of leptoquark models. In Ref. [164], a dynamical model based on a $SU(2)_L$ triplet of massive vector bosons, with predominant coupling to third generation fermion was proposed to explain the excesses, while other alternative approaches have been taken in Refs. [165–167].

From a theoretical point of view, NP scenarios explaining the above discrepancies and addressing other direct or indirect collider searches for NP are particularly intriguing. To this end, we must mention the recently announced results for the right-handed gauge boson $W_R$ search at $\sqrt{s} = 8$ TeV and 19.7 fb$^{-1}$ of integrated luminosity by the CMS Collaboration at the LHC. They have reported 14 observed events with 4 expected SM background events, amounting to a $2.8\sigma$ local excess in the bin $1.8\,\text{TeV} < m_{eejj} < 2.2$ TeV, which cannot be explained in the standard framework of Left-Right Symmetric Model (LRSM) with the gauge couplings $g_L = g_R$ [168]. On the other hand, the CMS search for di-leptoquark production at $\sqrt{s} = 8$ TeV and 19.6 fb$^{-1}$ of integrated luminosity have been reported to show a $2.4\sigma$ in the $eejj$ channel and a $2.6\sigma$ local excess in the $e\not{p}_T jj$ channel corresponding to 36 observed events with $20.49 \pm 2.4 \pm 2.45$ (syst.) expected SM events in the $eejj$ channel and 18 observed events with $7.54\pm1.20\pm1.07$ (syst.) expected SM events in the $e\not{p}_T jj$ channel respectively [169]. These excesses have been explained as arising from $W_R$ decay in the framework of LRSM with $g_L \neq g_R$ embedded in the $SO(10)$ gauge group in Refs. [170–172] and in LRSM with $g_L = g_R$ by taking into account the CP phases and non-degenerate masses of heavy neutrinos in Ref. [173], while other NP scenarios have been proposed in Refs. [174–186]. Interestingly, in some of these NP scenarios attempts were made to explain the discrepancies in decays of $B$ meson in a unified framework [178] or separately [161].

In this chapter we study the flavor structure of the $E_6$ motivated Alternative Left-Right Symmetric Model (ALRSM) [187], which can explain the CMS excesses and accommodate high scale leptogenesis [†] [181], to explore if this framework can address the experimental data for $R_{D^{(*)}}$ explaining the discrepancy with the SM expectations. This scenario is particularly interesting because unlike the R-parity violating MSSM in Refs. [161,176,178], this model involves only R-parity conserving interactions. Furthermore, a careful analysis of the flavor physics constraints, such as the rare decays and the mixing of mesons can play a crucial role in determining the viability of any NP scenario. Therefore, we study the leptonic decays $D_s^+ \to \tau^+\bar{\nu}$, $B^+ \to \tau^+\bar{\nu}$, $D^+ \to \tau^+\bar{\nu}$ and $D^0$-$\bar{D}^0$ mixing to constrain the semileptonic $b \to c$ transition in ALRSM. We find that despite being constrained by the above processes ALRSM can explain the current experimental data on $R_{D^{(*)}}$ quite well.

The rest of this chapter is organized as follows. In section 4.2, we discuss the effective Hamiltonian and the general four-fermion operators that can explain the $R_{D^{(*)}}$ data. In section 4.3, we introduce ALRSM and present the viable interactions, followed by the evaluation of the Wilson coefficients in section 4.4.

[†] Note that in the conventional LRSM framework the canonical mechanism of leptogenesis is inconsistent with the range of $W_R$ mass ($\sim 2$ TeV) corresponding to the excess at CMS [188,189].

In section 4.5, we discuss the constrains from the leptonic decays $D_s^+ \to \tau^+\bar{\nu}$, $B^+ \to \tau^+\bar{\nu}$, $D^+ \to \tau^+\bar{\nu}$ and mixing between $D^0$-$\bar{D}^0$. In section 4.6, we summarize our results and conclude.

## 4.2 The effective Hamiltonian for the decay $\overline{B} \to D^{(*)}\ell\overline{\nu}$

To include the effects of NP, the SM effective Hamiltonian for the quark level transition $b \to c\ell\bar{\nu}_\ell$ can be augmented with a set of four-Fermi operators in the following form [150]

$$\mathcal{H}_{eff} = \frac{4G_F}{\sqrt{2}} V_{cb} \sum_{\ell=e,\mu,\tau} [(1 + C^\ell_{V_L}) O^\ell_{V_L} + C^\ell_{V_R} O^\ell_{V_R} + C^\ell_{S_L} O^\ell_{S_L} + C^\ell_{S_R} O^\ell_{S_R} + C^\ell_{T_L} O^\ell_{T_L}], \tag{4.2.1}$$

where $G_F$ is the Fermi constant, $V_{cb}$ is the appropriate CKM matrix element and $C^\ell_i$ (i = $V_{L/R}$, $S_{L/R}$, $T_L$) are the Wilson coefficients associated with the new effective vector, scalar and tensor interaction operators respectively. These new six dimensional four-Fermi operators are generated by NP at some energy higher than the electroweak scale and are defined as

$$O^\ell_{V_L} = (\bar{c}_L \gamma^\mu b_L)(\bar{\ell}_L \gamma_\mu \nu_{\ell L}), \tag{4.2.2}$$
$$O^\ell_{V_R} = (\bar{c}_R \gamma^\mu b_R)(\bar{\ell}_L \gamma_\mu \nu_{\ell L}), \tag{4.2.3}$$
$$O^\ell_{S_L} = (\bar{c}_R b_L)(\bar{\ell}_R \nu_{\ell L}), \tag{4.2.4}$$
$$O^\ell_{S_R} = (\bar{c}_L b_R)(\bar{\ell}_R \nu_{\ell L}), \tag{4.2.5}$$
$$O^\ell_{T_L} = (\bar{c}_R \sigma^{\mu\nu} b_L)(\bar{\ell}_R \sigma_{\mu\nu} \nu_{\ell L}), \tag{4.2.6}$$

where $\sigma^{\mu\nu} = (i/2)[\gamma^\mu, \gamma^\nu]$. The SM effective Hamiltonian corresponds to the case $C^\ell_i = 0$. Note that in writing the general $\mathcal{H}_{\rm eff}$, we have neglected the tiny contributions from the right-handed neutrinos, and therefore, we treat the neutrinos to be left-handed only.

In order to perform the numerical analysis of the transition $B \to D^{(*)}\tau\nu$, we need to have the knowledge of the hadronic form factors which parametrize the vector, scalar and tensor current matrix elements. The $B \to D^{(*)}\tau\nu$ matrix elements of the aforementioned effective operators depend on the momentum transfer between B and $D^{(*)}(q^\mu = p_B^\mu - k^\mu)$, and are generally parametrized in the following way [163, 190].

$$\langle D(k)|\bar{c}\gamma_\mu b|\bar{B}(p_B)\rangle = \left[(p_B+k)_\mu - \frac{m_B^2-m_D^2}{q^2}q_\mu\right]F_1(q^2) + q_\mu\frac{m_B^2-m_D^2}{q^2}F_0(q^2), \tag{4.2.7}$$

$$\langle D^*(k,\epsilon)|\bar{c}\gamma_\mu b|\bar{B}(p_B)\rangle = -i\epsilon_{\mu\nu\rho\sigma}\epsilon^{\nu*}p_B^\rho k^\sigma\frac{2V(q^2)}{m_B+m_{D^*}}, \tag{4.2.8}$$

$$\begin{aligned}\langle D^*(k,\epsilon)|\bar{c}\gamma_\mu\gamma_5 b|\bar{B}(p_B)\rangle &= \epsilon_\mu^*(m_B+m_{D^*})A_1(q^2) - (p_B+k)_\mu(\epsilon^*\cdot q)\\ &\times\frac{A_2(q^2)}{m_B+m_{D^{ast}}} - q_\mu(\epsilon^*\cdot q)\frac{2m_{D^*}}{q^2}\left(A_3(q^2)-A_0(q^2)\right),\end{aligned} \tag{4.2.9}$$

$$\begin{aligned}\langle D^*(k,\epsilon)|\bar{c}\sigma_{\mu\nu}b|\bar{B}(p_B)\rangle &= \epsilon_{\mu\nu\rho\sigma}\left\{-\epsilon^{*\rho}(p_B+k)^\sigma T_1(q^2)\right.\\ &+\epsilon^{*\rho}q^\sigma\frac{m_B^2-m_{D^*}}{q^2}(T_1(q^2)-T_2(q^2))\\ &\left.+2\frac{\epsilon^* q}{q^2}p_B^\rho k^\sigma\left(T_1(q^2)-T_2(q^2)-\frac{q^2}{m_{B^2}-m_{D^{*2}}}T_3(q^2)\right)\right\},\end{aligned} \tag{4.2.10}$$

where $F_1(0) = F_0(0)$, $A_3(0) = A_0(0)$, and

$$A_3(q^2) = \frac{m_B+m_{D^*}}{2m_{D^*}}A_1(q^2) - \frac{m_B-m_{D^*}}{2m_{D^*}}A_2(q^2). \tag{4.2.11}$$

Here, $\epsilon_\mu$ is the polarization vector of the $D^*$. Note that the hadronic matrix elements of the scalar and pseudoscalar operators can be conveniently derived from their vector counterparts by applying the equations of motion $-i\partial^\mu(\bar{q}_a\gamma_\mu q_b) = (m_a - m_b)\bar{q}_a q_b$ and $-i\partial^\mu(\bar{q}_a\gamma_\mu\gamma_5 q_b) = (m_a + m_b)\bar{q}_a\gamma_5 q_b$. However, in what follows, we choose to work with the following parametrization of the form factors which are more suitable for including the results of the heavy quark effective theory (HQET). The matrix elements of the vector and axial vector operators can be expressed as [146, 191]

$$\langle D(v')|\bar{c}\gamma_\mu b|\bar{B}(v)\rangle = \sqrt{m_B m_D}\,\{\xi_+(w)(v+v')_\mu + \xi_-(w)(v-v')_\mu\}\,, \tag{4.2.12}$$

$$\langle D^*(v',\epsilon)|\bar{c}\gamma_\mu b|\bar{B}(v)\rangle = i\sqrt{m_B m_{D^*}}\xi_V(w)\epsilon_{\mu\nu\rho\sigma}\epsilon^{*\nu}v'^\rho v^\sigma, \tag{4.2.13}$$

$$\langle D^*(v',\epsilon)|\bar{c}\gamma_\mu\gamma_5 b|\bar{B}(v)\rangle = \sqrt{m_B m_{D^*}}\,\{\xi_{A_1}(w)(w+1)\epsilon^*_\mu - (\epsilon^*\cdot v)\,(\xi_{A_2}(w)v_\mu + \xi_{A_3}(w)v'^\mu)\}\,. \tag{4.2.14}$$

The form factors of tensor operators are defined as [155]

$$\langle D(v')|\bar{c}\sigma_{\mu\nu}b|\bar{B}(v)\rangle = -i\sqrt{m_B m_D}\xi_T(w)\left(v_\mu v'_\nu - v_\nu v'_\mu\right), \tag{4.2.15}$$

$$\langle D^*(v')|\bar{c}\sigma_{\mu\nu}b|\bar{B}(v)\rangle = -i\sqrt{m_B m_{D^*}}\epsilon_{\mu\nu\rho\sigma}\,\{\xi_{T_1}(w)\epsilon^{*\rho}(v+v')^\rho + \xi_{T_2}(w)\epsilon^{*\rho}(v-v')^\sigma + \xi_{T_3}(w)(\epsilon^*\cdot v)(v+v')^\rho(v-v')^\sigma\}\,, \tag{4.2.16}$$

where $v = p_B/m_B$, and $v' = k/m_{D^{(*)}}$ are the four-velocities of the B and $D^{(*)}$ mesons, respectively, and the kinematic variable $w(q^2)$ is the product of the velocities of initial and final mesons $w(q^2) = (m_B^2 + m_{D^{(*)}} - q^2)\,/2m_B m_{D^*}$. The HQET and QCD dispersive techniques can be used to constrain the shapes of these form factors [192]. To this end, the HQET form factors are redefined as linear combinations of the different form factors $V_1(w)$, $S_1(w)$, $A_1(w)$ and $R_{1,2,3}(w)$ [155, 192], which reduce to the universal Isgur-Wise function [193] normalized to unity at $w = 1$ in the heavy quark limit. The form factors in the parameterization of Caprini *et al.* [192], which describes the shape and normalization in terms of the four quantities: the normalizations $V_1(1)$, $A_1(1)$, the slopes $\rho_D^2$, $\rho_{D^*}^2$ and the amplitude ratios $R_1(1)$ and $R_2(1)$ are determined by measuring the differential decay width as a function of $w$. The form factors $V_1(w)$ and $S_1(w)$ contribute to the decay $B \to D\ell\bar{\nu}_\ell$ ($\ell = e, \mu, \tau$), while the decay $B \to D^*\ell\bar{\nu}_\ell$ receives contributions from $A_1(w)$ and $R_{1,2,3}(w)$. However, the semileptonic decay into light charged leptons $B \to D\ell\bar{\nu}_\ell$ involves only $V_1(w)$ and therefore, $V_1(w)$ can be measured experimentally. The parametrization of the form factors in terms of the slope parameters $\rho_D^2$, $\rho_{D^*}^2$ and the value of the respective form factors at the kinematic end point $w = 1$ is given by [192, 194]

$$V_1(w) = V_1(1)\left\{1 - 8\rho_D^2 z + (51\rho_D^2 - 10)z^2 - (252\rho_D^2 - 84)z^3\right\}, \quad (4.2.17)$$

$$A_1(w) = A_1(1)\left\{1 - 8\rho_{D^*}^2 z + (53\rho_{D^*}^2 - 15)z^2 - (231\rho_{D^*}^2 - 91)z^3\right\}, \quad (4.2.18)$$

$$R_1(w) = R_1(1) - 0.12(w-1) + 0.05(w-1)^2, \quad (4.2.19)$$

$$R_2(w) = R_2(1) + 0.11(w-1) - 0.06(w-1)^2, \quad (4.2.20)$$

$$R_3(w) = 1.22 - 0.052(w-1) + 0.026(w-1)^2, \quad (4.2.21)$$

with $z = (\sqrt{w+1} - \sqrt{2})/(\sqrt{w+1} + \sqrt{2})$. For $S_1(w)$ we use the parametrization given in Ref. [149]

$$S_1(w) = V_1(w)\left\{1 + \Delta\left(-0.019 + 0.041(w-1) - 0.015(w-1)^2\right)\right\}, \quad (4.2.22)$$

with $\Delta = 1 \pm 1$. By fitting the measured quantity $|V_{cb}|V_1(w)$ to the two parameter ansatz as given in Eq. (4.2.17), the heavy flavor averaging group (HFAG) extracts the following parameters: $V_1(1)|V_{cb}| = (42.65 \pm 1.53) \times 10^{-3}$, $\rho_D^2 = 1.185 \pm 0.054$ [195]. In the case of $B \to D^*\ell\bar{\nu}_\ell$, HFAG determines $A_1(1)|V_{cb}| = (35.81 \pm 0.45) \times 10^{-3}$, $\rho_{D^*}^2 = 1.207 \pm 0.026$, $R_1(1) = 1.406 \pm 0.033$ and $R_2(1) = 0.853 \pm 0.020$ by performing a four-dimensional fit of the parameters [195]. However, since the fitted curves are plagued with large statistical and systematic uncertainties, for form factor normalizations, we use $V_1(1) = 1.081 \pm 0.024$ from the recent lattice QCD calculations [196] and for $A_1(1)$ we use the updated value $A_1(1) = 0.920 \pm 0.014$ from the FNAL/MILC group [197]. The amplitude ratios $R_1(1)$ and $R_2(1)$ are determined from the fit by HFAG $R_1(1) = 1.406 \pm 0.033$, $R_2(1) = 0.853 \pm 0.020$ [195].

## 4.3 Low-energy effective subgroups of $E_6$ and leptoquarks

One of the most intriguing feature of the SM is that quarks and leptons field appear as independent fields. This is puzzling since leptons and quarks exhibit symmetry in their organization in the SM: both leptons and quarks are grouped into three generations with each consisting of a pair of leptons and a pair of quarks, respectively; all three generation of quarks (as well as leptons) are replicas of each other except for the hierarchy in their masses. The first generation contains the lightest matter fields and the next generation contains more massive fields than the previous one. Furthermore, it is known that, for any quantum field theory to be consistent, the gauge anomalies associated with it must cancel. In the SM, these anomalies are associated with triangular fermion loops with gauge bosons at the vertices. In the SM, the leptons and quarks of each generation provide equal and opposite contributions to cancel the anomalies. This cancellation does not happen for the quarks or the leptons alone, rather it occurs for each generation. Therefore, it is natural to consider that in a more fundamental theory than SM the leptons and quarks can interact with each other directly. As a result, there are many extensions of the SM which predict new bosons, namely, leptoquarks, which can convert leptons into quarks and vice versa. The leptoquarks are color-triplets under $\mathrm{SU}(3)_{\mathrm{C}}$ ; they carry lepton as well as baryon quantum numbers; they have fractional electric charge; and can be scalars or vectors. The existence of leptoquarks, for the first time, was proposed in the SU(4) model of Pati and Salam [198]. The most obvious extensions of the SM which naturally accommodate leptoquarks are the grand unified theories (GUTs) which try to unify all the matter fields by including leptons and quarks in a single multiplet. For example, GUTs based on gauge groups SU(5) [199], $SO(10)$ [200, 201], superstring-inspired $E_6$ models naturally contain leptoquarks (for a review, see [202]). Extended technicolor models (see, for example, [203, 204]), and composite models (see, for example, [205, 206]) are also the examples of models which contain leptoquarks. Scalar partners of quarks in supersymmetric theories with R-parity violating interactions also have leptoquark-type Yukawa couplings [207]. A comprehensive recent review on leptoquarks in the context of flavor physics can be found in Refs. [208].

In the present and the next chapter, we study low-energy effective rank-5 subgroups $\mathrm{SU}(3)_{\mathrm{C}} \times \mathrm{SU}(2)_{\mathrm{L}} \times \mathrm{SU}(2) \times \mathrm{U}(1)$ of superstring-inspired $E_6$, naturally accommodating leptoquarks, in the context of anomalies seen in the flavor sector. Our primary interest in this analysis will be to study the set of interactions involving leptoquarks and their supersymmetric partners. $E_6$ is a rank-6 exceptional group which has 78 generators, and is a natural anomaly-free choice for the GUT group [209]. There are several maximal subgroups of $E_6$ which contain the group $\mathrm{SU(3)_C \times U(1)_{EM}}$. For example, some of the choices are $\mathrm{E_6 \supset SO(10) \times U(1)}$, $\supset \mathrm{SU(2) \times SU(6)}$. The subgroup which we are interested in is $\mathrm{E_6 \supset SU(3)_C \times SU(3)_L \times SU(3)_R}$; it is the only maximal subgroup of $E_6$ which contains QCD as an explicit factor. The fundamental 27 representation of $E_6$ can be decomposed under this subgroup as

$$27 = (3,3,1) + (3^*,1,3^*) + (1,3^*,3) \tag{4.3.1}$$

where the fields are assigned as follows. $(3,3,1)$ corresponds to $(u,d,h)$, $(3^*,1,3^*)$ corresponds to $(h^c,d^c,u^c)$ and the leptons are assigned to $(1,3^*,3)$. Here $h$ represents the exotic $-\frac{1}{3}$ charge quark which can carry lepton number depending on the assignments. The other exotic fields are $N^c$, $n$ and two isodoublets $(\nu_E,E)$ and $(E^c,N_E^c)$. Note that superstring-motivated $E_6$ models carry an $N=1$ supersymmetry. Therefore the particle spectrum of the $E_6$ subgroups also contain the scalar superpartners of all the fermions along with these exotic fields. The presence of these exotic fields makes the phenomenology of the low energy subgroups of $E_6$ very interesting. The superfields of the first family can be represented as

$$\begin{pmatrix} u \\ d \\ h \end{pmatrix} + \begin{pmatrix} u^c & d^c & h^c \end{pmatrix} + \begin{pmatrix} E^c & \nu & \nu_E \\ N_E^c & e & E \\ e^c & N^c & n \end{pmatrix}, \tag{4.3.2}$$

where $SU(3)_L$ operates along columns and $SU(3)_R$ operates along rows. The most general renormalizable superpotential describing interactions among matter fields and invariant under the SM group $\mathrm{SU(3)_c \times SU(2)_L \times U(1)_Y}$ is given by [202]

$$W = W_0 + W_1 + W_2 + W_3, \tag{4.3.3}$$

where

$$
\begin{aligned}
W_0 &= \lambda_1 X^c Q u^c + \lambda_2 X Q d^c + \lambda_3 X L e^c + \lambda_4 X^c X n + \lambda_5 h h^c n, && (4.3.4)\\
W_1 &= \lambda_6 h u^c e^c + \lambda_7 L h^c Q + \lambda_8 N^c h d^c, && (4.3.5)\\
W_2 &= \lambda_9 h Q Q + \lambda_{10} h^c u^c d^c, && (4.3.6)\\
W_3 &= \lambda_{11} X^c L N^c, && (4.3.7)
\end{aligned}
$$

where notations used for isodoublets are $Q = (u, d)_L$, $L = (\nu, e)$, $X = (\nu_E, E)$ and $X^c = (E^c, N_E^c)$. Few points are to be noted here. First is that assignment of quantum numbers to the exotic fields is not unique. While the color, charge and isospin quantum numbers can be fixed by the breaking of $E_6$ to the SM group $\mathrm{SU(3)_c \times SU(2)_L \times U(1)_Y}$, there are several choices for assigning the baryon ($B$), lepton ($L$) numbers and $R$-parity quantum numbers to the exotic fields which lead to different interactions among these fields. Second point is that all the terms in the superpotential $W$ cannot be present simultaneously which would otherwise lead to rapid proton decay. For example, if exotic quark field $h$ is assigned $L = 1$ (the case we will be considering in this work), the conservation of $B$ and $L$ numbers ensure that couplings $\lambda_9$ and $\lambda_{10}$ are zero. Different assignments of $B$ and $L$ number results in vanishing of different couplings [202]. In this and the following chapters we will consider the low-energy $E_6$ subgroups having an additional SU(2) symmetry compared to the SM group, which also induces the vanishing of various terms given in Eq. (4.3.3). We will discuss these details later in the text.

The $\mathrm{SU(3)_L}$ in the maximal subgroup $\mathrm{SU(3)_C \times SU(3)_L \times SU(3)_R}$ of $E_6$ further break into $\mathrm{SU(2)_L \times U(1)_L}$. Note that $\mathrm{U(1)_L}$ here cannot be identified with the $\mathrm{U(1)_Y}$ of the SM because if this were the case then it has to satisfy charge equation $Q = T_{3L} + Y/2$ which would imply $(h^c, d^c, u^c)$ to have electric charge zero. Therefore the group $\mathrm{SU(3)_R}$ must contribute to the charge equation. Regarding the choice of $\mathrm{SU(3)_R}$ decomposition into $\mathrm{SU(2)_R \times U(1)_R}$, there are three choices of assigning the isospin doublets corresponding to $T, U, V$ isospins (generators of SU(2)) of SU(3).

Case 1:

One of the choices have $(d^c, u^c)_L$ assigned to the $\mathrm{SU(2)_R}$ doublet giving rise to subgroup $\mathrm{SU(3)_c \times SU(2)_L \times SU(2)_R \times U(1)_{Y_L+Y_R}}$. This choice corresponds to the usual left-right symmetric extension of the standard model [210–215] including the exotic particles. The charge equation in this case is given by $Q = T_{3L} + T_{3R} + \frac{1}{2}(Y_L + Y_R)$.

Case 2:

The second possible choice where the $\mathrm{SU(2)_R}$ doublet is chosen to be $(h^c, u^c)$ gives the subgroup referred to as the Alternative Left-Right Symmetric Model (ALRSM) [187], and will be the topic of this chapter.

Case 3:

In another choice, the $\mathrm{SU(2)_R}$ doublet is chosen to be $(h^c, d^c)$ [216] with the charge equation given by $Q = T_{3L} + \frac{1}{2}Y_L + \frac{1}{2}Y_N$ , where the chosen $\mathrm{SU(2)_R}$ does not contribute to the electric charge equation and is often denoted by $\mathrm{SU(2)_N}$. The further details of this subgroup are given in Chapter 5 where we discuss this subgroup in the context of various flavor processes and anomalous magnetic moment of the muon.

### 4.3.1 Alternative Left Right Symmetric Model

In ALRSM, the superfields have the following transformations under the subgroup $G = SU(3)_c \times SU(2)_L \times SU(2)_{R'} \times U(1)_{Y'}$

$$
\begin{aligned}
(u, d)_L &: (3, 2, 1, \frac{1}{6}) \\
(h^c, u^c)_L &: (\bar{3}, 1, 2, -\frac{1}{6}) \\
(\nu_E, E)_L &: (1, 2, 1, -\frac{1}{2}) \\
(e^c, n)_L &: (1, 1, 2, \frac{1}{2}) \\
h_L &: (3, 1, 1, -\frac{1}{3})
\end{aligned}
$$

$$\begin{aligned} d_L^c &: (\bar{3}, 1, 1, \frac{1}{3}) \\ \begin{pmatrix} \nu_e & E^c \\ e & N_E^c \end{pmatrix}_L &: (1, 2, 2, 0) \\ N_L^c &: (1, 1, 1, 0), \end{aligned} \tag{4.3.8}$$

where $Y' = Y_L + Y'_R$. The charge equation is given by $Q = T_{3L} + \frac{1}{2}Y_L + T'_{3R} + \frac{1}{2}Y'_R$, where $T'_{3R} = \frac{1}{2}T_{3R} + \frac{3}{2}Y_R$, $Y'_R = \frac{1}{2}T_{3R} - \frac{1}{2}Y_R$. The superpotential governing interactions of the superfields in ALRSM is given by [202]

$$\begin{aligned} W &= \lambda_1 \left(uu^c N_E^c - du^c E^c - uh^c e + dh^c \nu_e\right) + \lambda_2 \left(ud^c E - dd^c \nu_E\right) \\ &\quad + \lambda_3 \left(hu^c e^c - hh^c n\right) + \lambda_4 hd^c N_L^c + \lambda_5 \left(ee^c \nu_E + EE^c n - Ee^c \nu_e - \nu_E N_E^c n\right) \\ &\quad + \lambda_6 \left(\nu_e N_L^c N_E^c - eE^c N_L^c\right). \end{aligned} \tag{4.3.9}$$

The superpotential given in Eq. (4.3.9) gives the following assignments of $R$-parity, baryon number ($B$) and lepton number ($L$) for the exotic fermions ensuring proton stability. $h$ is a leptoquark with $R = -1, B = \frac{1}{3}, L = 1$. $\nu_E, E$ and $n$ have the assignments $R = -1, B = L = 0$. $N^c$ has two possible assignments. If $N^c$ has the assignments $R = -1$ and $B = L = 0$ (in a $R$-parity conserving scenario demanding $\lambda_4 = \lambda_6 = 0$ in Eq. (4.3.9), $\nu_e$ becomes exactly massless. However if $N^c$ is assigned $R = +1$, $B = 0$, $L = -1$, then $\nu_e$ can acquire a tiny mass via the seesaw mechanism.

ALRSM can explain both $eejj$ and $e\not{p}_T jj$ signals from the decay of scalar superpartners of the exotic particles, for example, through (i) resonant production of the exotic slepton $\tilde{E}$, subsequently decaying into a charged lepton and a neutrino, followed by R-parity conserving interactions of the neutrino producing an excess of events in both $eejj$ and $e\not{p}_T jj$ channels [181], (ii) pair production of scalar leptoquarks $\tilde{h}$. On the other hand, high scale leptogenesis can be obtained via the decay of the heavy Majorana neutrino $N^c$ in ALRSM. From the interaction terms $\lambda_4$ and $\lambda_6$ in Eq. (4.3.9), it can be seen that the Majorana neutrino $N_k^c$ can decay into final states with $B - L = -1$ given by $\nu_{e_i}\tilde{N}^c_{E_j}, \tilde{\nu}_{e_i}N^c_{E_j}, e_i\tilde{E}^c_j, \tilde{e}_i, E^c_j$ and $d_i\tilde{h}_j, \tilde{d^c}_i\tilde{h}_j$ and to their conjugate states. Thus, ALRSM has the attractive feature that it can explain both the excess $eejj$ and $e\not{p}_T jj$ signals and also high-scale leptogenesis [181].

ATLAS and CMS have searched for pair-produced scalar leptoquarks in different final states. The current limits on leptoquark masses from CMS searches for scalar leptoquarks pair production (assuming decaying branching fraction $\beta = 1$ ) exclude leptoquarks with masses below 830, 840, and 525 GeV for first, second, and third generations, respectively, while the lower bounds from ATLAS (for $\beta = 1$) are 660, 422, and 534 GeV, respectively [9]. However, by choosing $\beta$ to be smaller than 1 the lower limits on leptoquarks masses can be reduced. From single production of scalar leptoquarks with charge $-1/3$, the current lower limit on the first generation is 304 GeV [9].

## 4.4 Analysis of operators mediating semileptonic decay $B \to D^{(*)}\ell\nu_\ell$

Having introduced ALRSM above we are now ready to analyze the semitauonic $B$ decay $\bar{B} \to D^{(*)}\tau\bar{\nu}$ based on the general framework introduced in section 4.2. From the superpotential given in Eq. (4.3.9) it follows that in ALRSM there are two possible diagrams, shown in Fig 4.1, which can contribute to the decay $\bar{B} \to D^{(*)}\tau\bar{\nu}$. The effective Lagrangian corresponding to these diagrams is given by

$$\mathcal{L}_{\text{eff}} = -\sum_{j,k=1}^{3} V_{2k}\left[\frac{\lambda^{5}_{33j}\lambda^{2*}_{3kj}}{m^2_{\tilde{E}^j}}\bar{c}_L b_R\,\bar{\tau}_R\nu_L + \frac{\lambda^{1}_{33j}\lambda^{1*}_{3kj}}{m^2_{\tilde{h}^{j*}}}\bar{c}_L\tau^c_R\,\bar{\nu}^c_R b_L\right], \tag{4.4.1}$$

where the superscript corresponds to the superpotential coupling index and the generation indices are explicitly written as subscripts. Here $m_{\tilde{E}}(m_{\tilde{h}})$ is the mass of slepton $\tilde{E}^j$ (scalar leptoquark $\tilde{h}^{j*}$) and $V_{ij}$ corresponds to the $ij$-th component of the CKM matrix. Using Fierz transformation the second term of Eq. (4.4.1) can be put in the form given by

$$\bar{c}_L\tau^c_R\,\bar{\nu}^c_R b_L = \frac{1}{2}\bar{c}_L\gamma^\mu b_L\,\bar{\tau}_L\gamma_\mu\nu_L. \tag{4.4.2}$$

We can now readily obtain the expressions for the Wilson coefficients of operators $O^{\tau}_{S_L}$ and $O^{\tau}_{V_L}$ defined in Eqs. (4.2.4) and (4.2.2), respectively, and are given by

$$\begin{aligned} C^{\tau}_{S_L} &= \frac{1}{2\sqrt{2}G_F V_{cb}} \sum_{j,k=1}^{3} V_{2k} \frac{\lambda^{5}_{33j}\lambda^{2*}_{3kj}}{m^2_{\tilde{E}^j}} , \\ C^{\tau}_{V_L} &= \frac{1}{2\sqrt{2}G_F V_{cb}} \sum_{j,k=1}^{3} V_{2k} \frac{\lambda^{1}_{33j}\lambda^{1*}_{3kj}}{2\, m^2_{\tilde{h}^{j*}}}, \end{aligned} \tag{4.4.3}$$

where the neutrinos are assumed to be predominantly of tau flavor.

To simplify further analysis, we invoke the assumption that except the SM contribution only one of the NP operators in Eqs. (4.2.2 - 4.2.6) contributes dominantly. This assumption helps us in determining the limits on the dominant Wilson coefficient from the experimental data for $R_{D^{(*)}}$ and the generalization of this situation to incorporate more than one NP operator contribution is straight forward.

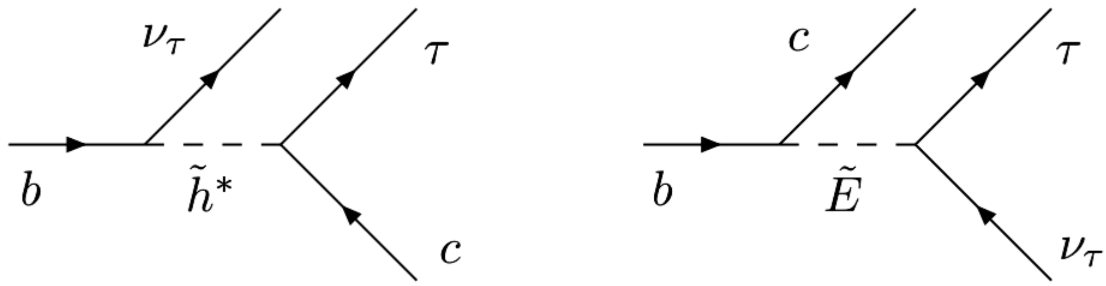


Figure 4.1: Feynman diagrams for the decays $\bar{B} \to D^{(*)}\tau\bar{\nu}$ induced by the exchange of scalar leptoquark ($\tilde{h}^*$) and $\tilde{E}$.

The case where $C^{\tau}_{S_L}$ is the dominant contribution, similar to 2HDM of type II or type III with minimal flavor violation, cannot explain both $R_D$ and $R_{D^*}$ data simultaneously [151, 160], as can be seen from Fig 4.2. However, $C^{\tau}_{V_L}$ has an allowed region which can explain both $R_D$ and $R_{D^*}$ data as shown in Fig 4.3. We find that for $\left|C^{\tau}_{V_L}\right| > 0.08$ the current experimental data can be explained. A comment regarding the RG running of these Wilson coefficients is in order. Wilson coefficients are computed at the matching scale (electroweak scale) by a matching between the full theory and the effective theory. With these Wilson coefficients at the electroweak scale as initial conditions, their evolution from the matching scale down to scale $\mathcal{O}(m_b)$ is governed by the RG equations. The charged (pseudo) vector currents do not renormalize and the anomalous dimension of corresponding operators ($O^{\ell}_{V_{L,R}}$) vanishes. Therefore, charged (pseudo) vector currents do not run. However, (pseudo) scalar and tensor current require renormalization and corresponding operators ($O^{\ell}_{V_{L,R}}$, $O^{\ell}_{T_L}$) have finite anomalous dimension. Therefore, (pseudo) scalar, and tensor current operators have QCD running. Owing to this reason, the Wilson coefficient $C^{\tau}_{S_L}$ of (pseudo) scalar operator has a non-trivial running while $C^{\tau}_{V_L}$ does not run. Since we focus on the case where only $C^{\tau}_{V_L}$ contribution is present, RG running does not affect the analysis of this work. Also note that we use the central values of the theoretical predictions because the theoretical uncertainties are sufficiently small compared to the experimental accuracy.

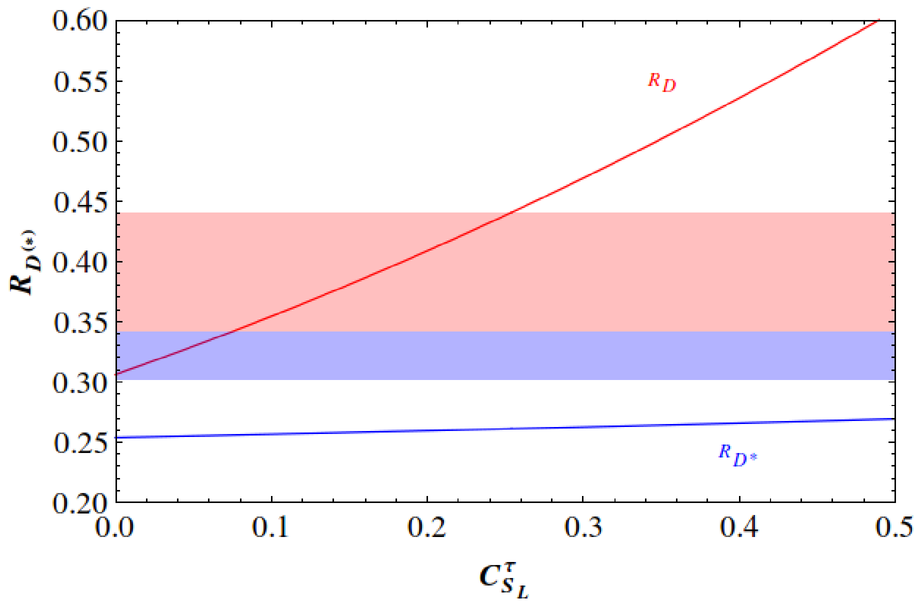


Figure 4.2: The dependence of the observables $R_{D^{(*)}}$ on $C^{\tau}_{S_L}$: red (blue) line corresponds to $R_D$ ($R_{D^*}$), and the horizontal light red (blue) band corresponds to the experimentally allowed $1\sigma$ values. No common region exists for $C^{\tau}_{S_L}$ which can simultaneously explain both $R_D$ and $R_{D^*}$.

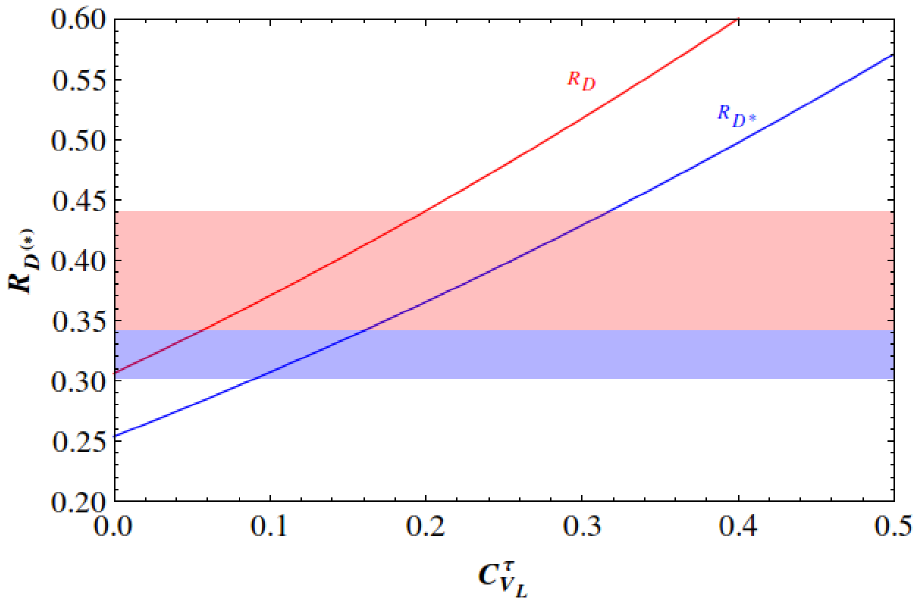


Figure 4.3: The dependence of the observables $R_{D^{(*)}}$ on $C^{\tau}_{V_L}$: red (blue) line corresponds to $R_D$ ($R_{D^*}$), and the horizontal light red (blue) band corresponds to the experimentally allowed $1\sigma$ values. $C^{\tau}_{V_L}$ can explain both $R_D$ and $R_{D^*}$ data.

## 4.5 Constraints from $B$, $D$ decays and oscillation $D^0 - \overline{D^0}$

### 4.5.1 Constraints from $B \to \tau\nu$

In this section we discuss the new contributions to purely leptonic decay mode $B \to \tau\nu$ due to scalar leptoquark $\tilde{h}^{j*}$ exchange and utilize the measured branching fractions of the decay to derive constraints on the product of couplings $\lambda^1_{33j}\lambda^{1*}_{31j}$. In the SM, the decay $B \to \tau\nu$ proceeds via annihilation to a $W$ boson. In the ALRSM, the exchange of the scalar leptoquark $\tilde{h}^{j*}$ leads to the additional diagrams shown in Fig 4.4. Since the mass scale of scalar leptoquark is far above the scale of the B meson, we can integrate out the heavy degree of freedom to generate new four-fermion interaction $\sim \bar{q}_L(\tau^c)_R\ (\bar{\nu}^c)_R b_L$, with the Wilson coefficients parameterizing the effects of the integrated out non-standard particles. The NP effective Hamiltonian is given by

$$\mathcal{H}^{\rm NP}_{\rm eff}(b\bar{q} \to \tau\bar{\nu}) = \frac{4G_F}{\sqrt{2}} V_{qb}\, C^{qb}_{V_L}(\bar{q}_L\gamma^\mu b_L)(\bar{\tau}_L\gamma_\mu\nu_L), \tag{4.5.1}$$

where $V_{qb}$ (here $q \equiv u$) is the relevant CKM matrix element. The Wilson coefficient $C^{ub}_{V_L}$ in terms of the couplings $\lambda'$s is given by

$$C^{ub}_{V_L} \;=\; \frac{1}{2\sqrt{2}G_F V_{ub}} \sum_{j,k=1}^{3} V_{1k} \frac{\lambda^1_{33j}\lambda^{1*}_{3kj}}{2\, m^2_{\tilde{h}^{j*}}}. \tag{4.5.2}$$

In our notation, the Wilson coefficient of the SM effective operator is set to unity.

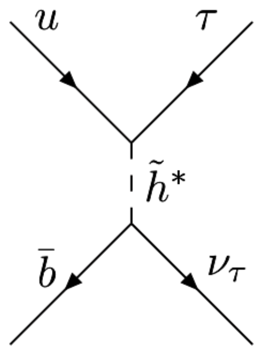


Figure 4.4: Feynman diagrams for the decay $B \to \tau\nu$ induced by the exchange of the scalar leptoquark $\tilde{h}^{j*}$.

In what follows, we will neglect the subleading $\mathcal{O}(\lambda)$ terms and retain only the leading CKM element $V_{11}$.

Note that the decay $B \to \tau\nu$ is the only experimentally measured purely leptonic mode of charged $B^{\pm}$. The current experimental value of the branching ratio of $B \to \tau\nu$ is $(1.14 \pm 0.27) \times 10^{-4}$ [9]. The presence of NP modifies the expression of the SM decay rate in the following way

$$\Gamma(B \to \tau\nu) = \frac{G_F^2 |V_{ub}|^2}{8\pi} m_B f_B^2 m_\tau^2 \times \left(1 - \frac{m_\tau^2}{m_B^2}\right)^2 |1 + C^{ub}_{V_L}|^2, \tag{4.5.3}$$

where $m_B$ is the mass of $B^{\pm}$ and $f_B$ is the decay constant which parametrize the matrix elements of the corresponding current as

$$\langle 0|\bar{b}\gamma^\mu\gamma_5 q|B_q(p_B)\rangle = i p_B^\mu f_B. \tag{4.5.4}$$

Here $p_B$ is the 4-momentum of the $B^{\pm}$ meson. We use the CKM matrix elements, the lifetimes, particle masses and decay constants $f_B$, $f_{D_s}$, $f_{D^+}$ from PDG [9] for numerical estimations throughout the chapter. Here, we assume that contribution from only one type of scalar leptoquarks is dominant and real. For simplicity, we will further assume the couplings to be real in the rest of this chapter. In Fig 4.5 we plot the BR($B \to \tau\nu$) as a function of the product of the couplings $\lambda_{33j}\lambda_{31j}$ for different values of $m_{\tilde{h}^{j*}}$. Numerically these constraints are given by

$$\lambda_{33j}\lambda_{31j} \leq 0.04 \left(\frac{m_{\tilde{h}^{j*}}}{1000\text{GeV}}\right)^2. \tag{4.5.5}$$

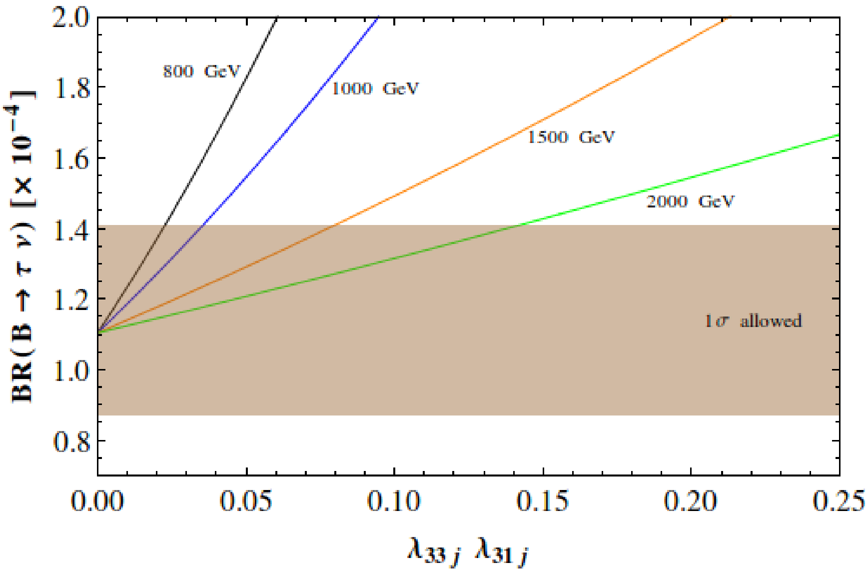


Figure 4.5: BR($B \to \tau\nu$) as a function of couplings $\lambda_{33j}\lambda_{31j}$ for $m_{\tilde{h}^{j*}} = 800$, 1000, 1500, 2000 GeV corresponding to black, blue, orange, and green lines respectively. The horizontal brown (light) band shows the $1\sigma$ experimentally favored values.

### 4.5.2 Constraints from $D_s^+ \to \tau\nu$ and $D^+ \to \tau\nu$

Along with rare B decays, the study of the decays of charmed mesons also offers attractive possibilities to test the predictions of extensions of the SM [217–219]. In fact, these processes are quite sensitive to the contributions of charged Higgs boson and scalar leptoquarks [220] and to the new contributions from squark exchange in the framework of R-parity violating SUSY as examined in Ref. [221]. In this section we consider the purely leptonic decays $D_s^+ \to \tau\nu$ and $D^+ \to \tau\nu$ in ALRSM and use their measured branching ratios to obtain constraints on the couplings $(\lambda_{32j})^2$ and $\lambda_{32j}\lambda_{31j}$ respectively. The relevant Feynman diagrams in

ALRSM for the decays $D_s^+ \to \tau\nu$ and $D^+ \to \tau\nu$ are shown in Fig 4.6. Integrating out the heavy energy scales yields the following non-standard effective Hamiltonian

$$\mathcal{H}_{\rm eff}^{\rm NP}(c\bar{q} \to \tau\bar{\nu}) = \frac{4G_F}{\sqrt{2}} V_{cq}\, C_{V_L}^{cq}(\bar{q}_L\gamma^\mu c_L)(\bar{\nu}_L\gamma_\mu\tau_L) \tag{4.5.6}$$

where $q = s, d$ for $D_s^+, D^+$ respectively. In the SM these processes occur (similar to $B \to \tau\nu$) via $W^\pm$ annihilation and the SM Wilson coefficient is given by unity in our notation. The corresponding Wilson coefficient $C_{V_L}^{cq}$ parameterizing the NP effects is given by

$$C_{V_L}^{cq} = \frac{1}{2\sqrt{2}G_F V_{cq}} \sum_{j,k=1}^{3} V_{kq} \frac{\lambda_{32j}^{1}\lambda_{3kj}^{1*}}{2\, m_{\tilde{h}^{j*}}^2}. \tag{4.5.7}$$

We will keep only the leading terms $V_{cs}$ for $D_s^+$ decay and $V_{ud}$ for $D^+$ case re-

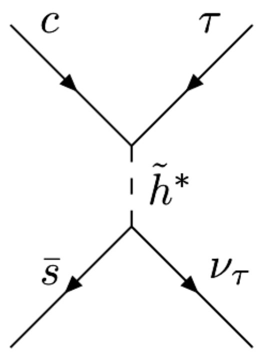


Figure 4.6: Feynman diagrams for the decay $D_s^+ \to \tau\nu$ induced by scalar leptoquarks. The corresponding diagram for the decay $D^+ \to \tau\nu$ can be obtained by replacing $s$ quark by $d$ quark.

spectively and neglect the subleading Cabibbo suppressed $\mathcal{O}(\lambda)$ terms. Although this process occurs in the SM at the tree level, the branching fraction is helicity-suppressed. For $\tau$, this suppression is less severe but phase-space suppression is larger compared to that for light leptons. In the presence of the scalar leptoquark contribution, the SM decay rate is affected in the following way [220, 222]

$$\Gamma(D_q^+ \to \tau\nu) = \frac{G_F^2|V_{cq}|^2}{8\pi} m_{D_q} f_{D_q}^2 m_\tau^2 \times \left(1 - \frac{m_\tau^2}{m_{D_q}^2}\right)^2 |1 + C_{V_L}^{cq}|^2. \tag{4.5.8}$$

Here $m_{D_q}$ is the mass of charm-mesons $D_s^+$ and $D^+$ for $q = s, d$ respectively and $V_{cq}$ is the relevant CKM element. The decay constant $f_{D_q}$ is defined by

$\langle 0|\bar{q}\gamma_\mu\gamma_5 c|D_q(p_{D_q})\rangle = i(p_{D_q})_\mu f_{D_q}$, where $(p_{D_q})_\mu$ is the 4-momentum of the $D_q$ meson.

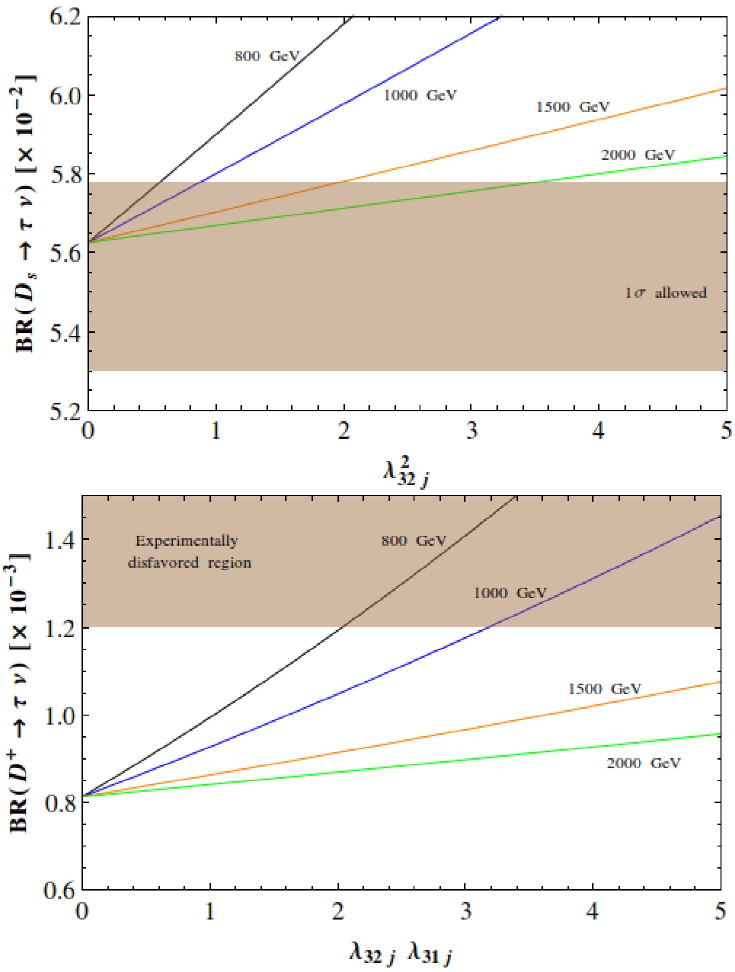


Figure 4.7: Dependence of (upper figure) $\mathrm{BR}(D_s^+ \to \tau\nu)$ on the coupling $\lambda_{32j}^2$ [(lower figure) $\mathrm{BR}(D^+ \to \tau\nu)$ on the coupling $\lambda_{32j}\lambda_{31j}$] for $m_{\tilde{h}^{j*}} = 800, 1000, 1500,$ 2000 GeV corresponding to black, blue, orange, and green lines respectively. In the upper (lower) figure the horizontal brown band shows the $1\sigma$ experimentally allowed (disfavored) region.

Assuming that only one combination of the product of scalar leptoquark couplings is nonzero, we get upper bounds on $(\lambda_{32j}^1)^2$ and $\lambda_{32j}^1\lambda_{31j}^{1*}$. In Fig 4.7, we plot the dependence of $\mathrm{BR}(B \to D_{(s)}^+\nu)$ on the coupling $\lambda_{32j}\lambda_{31j}(\lambda_{32j}^2)$ for different $m_{\tilde{h}^{j*}}$. Numerically the constraints are given by

$$\lambda_{32j}^2 \leq 0.85\left(\frac{m_{\tilde{h}^{j*}}}{1000\mathrm{GeV}}\right)^2, \tag{4.5.9}$$

$$\lambda_{32j}\lambda_{31j} \leq 3.12\left(\frac{m_{\tilde{h}^{j*}}}{1000\mathrm{GeV}}\right)^2. \tag{4.5.10}$$

### 4.5.3 Constraints from mixing $D^0 - \overline{D}^0$

The phenomenon of meson-antimeson oscillation, being a flavor changing neutral current (FCNC) process, is very sensitive to heavy particles propagating in the mixing amplitude and therefore, it provides a powerful tool to test the SM and a window to observe NP. In the $D^0 - \bar{D}^0$ system, the b-quark contribution to the fermion loop of the box diagram provides a $\Delta C = 2$ transition which is highly suppressed $\sim \mathcal{O}(\lambda^3)$ (by a tiny $V_{ub}$ CKM matrix element). Therefore, the large non-decoupling effect from a heavy fermion in the leading one-loop contribution is small. $D^0 - \bar{D}^0$ mixing involves the dynamical effects of rather light down-type particles and therefore it provides information complementary to the strange and bottom systems where the large effects of heavy top quark in the loops are quintessential. The $D^0 - \bar{D}^0$ mixing is described by $\Delta C = 2$ effective Hamiltonian which induces off-diagonal terms in the mass matrix for neutral D meson pair and typically parametrized in terms of following experimental observables

$$x_D \equiv \frac{\Delta M_D}{\Gamma_D}, \text{ and } \mathrm{y_D} \equiv \frac{\Gamma_\mathrm{D}}{2\Gamma_\mathrm{D}}, \tag{4.5.11}$$

where $\Delta M_D$ and $\Delta\Gamma_D$ are the mass and width splittings between mass eigenstates of $D^0 - \bar{D}^0$ systems respectively and $\Gamma_D$ is the average width. The parameters $x_D$ and $y_D$ can be written in terms of the mixing matrix as follows

$$x_D = \frac{1}{2M_D\Gamma_D}\mathrm{Re}\left[2\langle\bar{\mathrm{D}}^0|\mathrm{H}^{|\Delta\mathrm{C}|=2}|\mathrm{D}^0\rangle + \langle\bar{\mathrm{D}}^0|\mathrm{i}\int \mathrm{d}^4\mathrm{x}\mathrm{T}\{\mathcal{H}_\mathrm{w}^{|\Delta\mathrm{C}|=1}(\mathrm{x})\mathcal{H}_\mathrm{w}^{|\Delta\mathrm{C}|=1}(0)\}|\mathrm{D}^0\rangle\right], \tag{4.5.12}$$

$$y_D = \frac{1}{2M_D\Gamma_D}\mathrm{Im}\langle\bar{\mathrm{D}}^0|\mathrm{i}\int \mathrm{d}^4\mathrm{x} \times \mathrm{T}\{\mathcal{H}_\mathrm{w}^{|\Delta\mathrm{C}|=1}(\mathrm{x})\mathcal{H}_\mathrm{w}^{|\Delta\mathrm{C}|=1}(0)\}|\mathrm{D}^0\rangle, \tag{4.5.13}$$

with $\mathcal{H}_w^{|\Delta C|=1}(x)$ being the Hamiltonian density that describes $|\Delta C| = 1$ transitions at space-point $x$ and T denotes the time ordered product. Since the local $|\Delta C| = 2$ interaction does not contain an absorptive part, this term does not affect $y_D$ and contributes to $x_D$ only. The measured values of $x_D$ and $y_D$ as determined by HFAG are [223]

$$x_D = 0.49^{+0.14}_{-0.15} \times 10^{-2}, \tag{4.5.14}$$

$$y_D = (0.61 \pm 0.08) \times 10^{-2}, \tag{4.5.15}$$

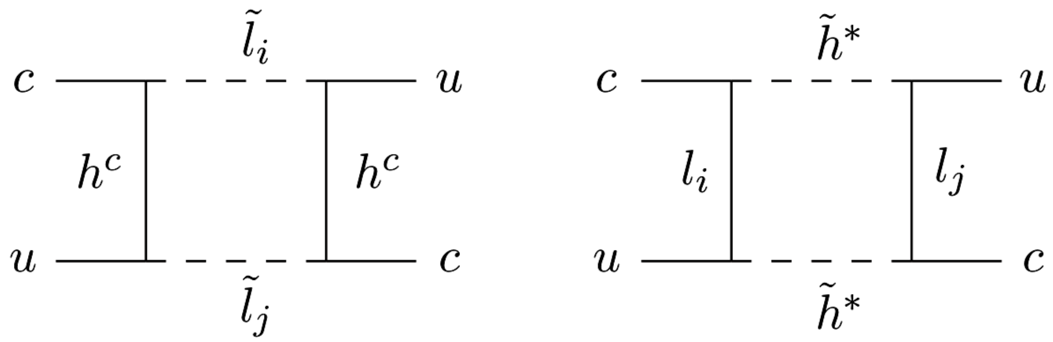


Figure 4.8: Feynman diagrams contributing to $D^0-\bar{D}^0$ mixing in ALRSM induced by scalar leptoquark and slepton.

Charm mixing in the SM is highly affected by contributions from intermediate hadronic states, and therefore the theoretical estimations in the SM suffer from large uncertainties and generally stretch over several orders of magnitude (for a review, see Ref. [224]). Like in the case of mixing in neutral K and B systems, $D^0-\bar{D}^0$ mixing is also sensitive to NP effects. Both $x_D$ and $y_D$ can receive large contributions from NP. The contribution to $y_D$ in several NP models including LR models, multi Higgs models, SUSY without R-parity violations and models with extra vector like quarks has been studied in Ref. [225], while in Ref. [224] the NP contributions to $x_D$ in 21 NP models have been discussed. In this section, we use the neutral D meson mixing to obtain constraints on $\lambda_{32j}\lambda_{31j}$. These bounds are tighter than those obtained in the previous section from measured BR of $D^+ \to \tau\nu$. The relevant Feynman diagrams which contribute to $D^0-\bar{D}^0$ mixing in the ALRSM are shown in Fig 4.8. These box diagrams are similar to the diagrams generated from internal line exchange of lepton-squark pair or slepton-quark pair in the case of R-parity violating models [224,226]. The mixing is described by the effective Hamiltonian

$$\mathcal{H}_{\rm eff} \;=\; \frac{1}{128\pi^2}(\lambda_{32j}\lambda_{31j})^2\left(\frac{1}{m^2_{\tilde{\tau}}}+\frac{1}{m^2_{\tilde{h}^{j*}}}\right)(\bar{c}_L\gamma^\mu u_L)(\bar{c}_L\gamma_\mu u_L), \quad (4.5.16)$$

where we assume that the box diagrams receive contributions from third generation of leptons only. Taking $m_{\tilde{h}^{j*}} \simeq m_{\tilde{\tau}}$, the constraints on the size of couplings is given by

$$\lambda_{32j}\lambda_{31j} \le 0.17\sqrt{x_D^{\rm expt}}\left(\frac{m_{\tilde{h}^{j*}}}{1000\text{GeV}}\right). \quad (4.5.17)$$

In Fig 4.9, we plot the dependence of $x_D^{ALRSM}$ on the product of the couplings $\lambda_{32j}\lambda_{31j}$ for different $m_{\tilde{h}^{j*}}$. As discussed in the subsection 4.5.3, the branching ratio of the decay $D^+ \to \tau\nu$ also constrain the same product of the couplings $\lambda_{32j}\lambda_{31j}$ (given in Eq. (4.5.9)) and for a 1 TeV leptoquark mass we find $\lambda_{32j}\lambda_{31j} \leq 3.12$. However, $D^0 - \bar{D}^0$ mixing rules out a large parameter space available for this coupling product as shown in Fig 4.9. For a 1 TeV leptoquark and taking the upper limit of the experimental value of $x_D^{\rm expt}$ given in Eq. (4.5.14) for a conservative estimate, we find the allowed size of product to be $\lambda_{32j}\lambda_{31j} \leq 1.3 \times 10^{-2}$ which is about two order of magnitude tighter compared to those from $D^+ \to \tau\nu$ .

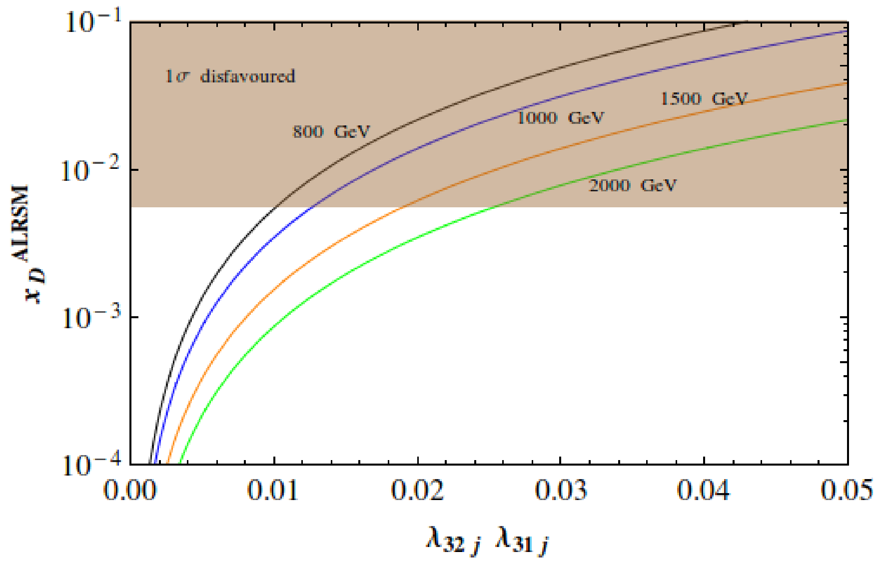


Figure 4.9: Dependence of $x_D^{ALRSM}$ on the coupling $\lambda_{32j}\lambda_{31j}$ for $m_{\tilde{h}^{j*}} = 800$, 1000, 1500, 2000 GeV corresponding to black, blue, orange, and green lines respectively. The horizontal brown (light) band shows the $1\sigma$ experimentally disfavored region.

## 4.6 Results and discussion

Having discussed the allowed region for $C_{V_L}^{\tau}$ which can explain both $R_D$ and $R_{D^*}$ data simultaneously in section 4.4 and the constraints on the couplings $\lambda_{33j}$ and $\lambda_{32j}$ involved in $C_{V_L}^{\tau}$ from the leptonic decays $D_s^+ \to \tau^+\bar{\nu}$, $B^+ \to \tau^+\bar{\nu}$, $D^+ \to \tau^+\bar{\nu}$ and $D^0$-$\bar{D}^0$ mixing in section 4.5, we are now ready to translate these analysis into a simple $\lambda_{33j}$-$\lambda_{32j}$ parameter space analysis. In Fig 4.10, we plot the range

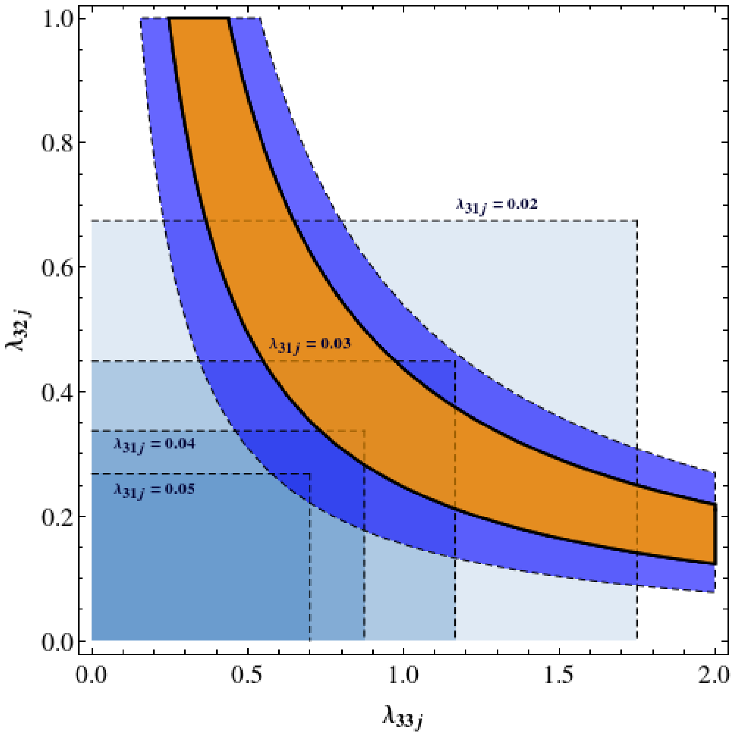


Figure 4.10: The region of $\lambda_{33j}$-$\lambda_{32j}$ parameter space compatible with the experimental data for $R_{D^{(*)}}$ and constraints from the leptonic decays $D_s^+ \to \tau^+\bar{\nu}$, $B^+ \to \tau^+\bar{\nu}$, $D^+ \to \tau^+\bar{\nu}$ and $D^0$-$\bar{D}^0$ mixing. We take $m_{\tilde{h}^{j*}} = 1000$ GeV for this plot. Blue band between dashed lines shows allowed values considering constraints from $R_D$ only, Orange band between bold black lines shows allowed region favored by experimental data for both $R_{D^*}$ and $R_D$. The shaded (light blue) rectangles correspond to the allowed regions of $\lambda_{33j}$-$\lambda_{32j}$ parameter space for different values of $\lambda_{31j}$ marked with the corresponding allowed upper boundary shown in dashed lines consistent with the present experimental data on $B \to \tau\nu$, $D_s \to \tau\nu$, $D^+ \to \tau\nu$ and $D - \bar{D}$ mixing.

of the couplings $\lambda_{33j}$ and $\lambda_{32j}$ (for $m_{\tilde{h}^{j*}} = 1000$ GeV) that can explain both $R_D$ and $R_{D^*}$ data over the parameter space allowed by the the leptonic decays and $D^0$-$\bar{D}^0$ mixing. From the decay $D_s^+ \to \tau^+\bar{\nu}$, we constrain the allowed upper limit of the coupling $\lambda_{32j}$. The decay $D^+ \to \tau^+\bar{\nu}$ and $D^0$-$\bar{D}^0$ mixing give constraints on the upper limit of the product of couplings $\lambda_{32j}\lambda_{31j}$. We find that among the two processes the latter gives more stringent constraints and therefore we use the constrains on the allowed upper limit of $\lambda_{32j}\lambda_{31j}$ coming from $D^0$-$\bar{D}^0$ mixing. Finally, we use the decay $B^+ \to \tau^+\bar{\nu}$ to constrain the upper limit of $\lambda_{33j}\lambda_{31j}$. The latter two constraints on the products of couplings have $\lambda_{31j}$ as a common free parameter and the shaded rectangles in Fig 4.10 correspond to the allowed regions of $\lambda_{33j}$-$\lambda_{32j}$ parameter space for different values of $\lambda_{31j}$ marked in the figure with the corresponding allowed upper boundary shown in dashed lines. The blue band corresponds to the allowed band of $\lambda_{33j}$-$\lambda_{32j}$ explaining the $R_D$ data and the orange band corresponds to the allowed band of $\lambda_{33j}$-$\lambda_{32j}$ explaining both $R_D$ and $R_{D^*}$ data simultaneously. We would like to note that the list of constraints mentioned above is far from exhaustive and many other possible leptonic and semileptonic decays can give independent constrains. For instance, the decay process $\tau^+ \to \pi^+\nu$ can give independent constraint on $\lambda_{31j}$, which we find to be consistent with the values extracted out of the above constraints and used for the parameter space analysis. On the other hand, the semileptonic decay $t \to b\tau\nu$ can give constraint on $\lambda_{33j}$ which we find to be again consistent with the values used in the above parameter space analysis. Also the effective NP operators under consideration may induce $B$-decays such as $b \to s\nu\bar{\nu}$ [227, 228], which can be an interesting channel for the future experiments.

In conclusion, we have studied the superstring inspired $E_6$ motivated Alternative Left-Right Symmetric model to explore if this model can explain the current experimental data for both $R_D$ and $R_{D^{(*)}}$ simultaneously addressing the excesses over the SM expectations. We use the leptonic decays $D_s^+ \to \tau^+\bar{\nu}$, $B^+ \to \tau^+\bar{\nu}$, $D^+ \to \tau^+\bar{\nu}$ and $D^0$-$\bar{D}^0$ mixing to constrain the couplings involved in the semileptonic $b \to c$ transition in ALRSM. We find that ALRSM can explain the current experimental data on $R_{D^{(*)}}$ quite well while satisfying the constraints from the rare $B$, $D$ decays $D^0$-$\bar{D}^0$ mixing. Furthermore, ALRSM can also explain both the $eejj$ and $e\not{p}_T jj$ signals recently reported by CMS and also accommodate successful leptogenesis. If these excess signals are confirmed in future B-physics experiments and at the LHC then ALRSM will be an interesting candidate for NP beyond the Standard Model.

# Chapter 5

# Explanation of Anomalies in $R_{D^{(*)}}$, $R_K$, and $(g-2)_\mu$ in $E_6$ Motivated Left-Right Model with Leptoquarks

Apart from the discrepancies seen in the measured decay rates of semileptonic decays $B \to D^{(*)}\tau\nu_\tau$, the LHC$b$ collaboration [34] has recently also reported another striking deviation from the SM prediction of the ratio of branching fractions of charged $\bar{B} \to \bar{K}\ell^+\ell^-$ decays

$$R_K = \frac{\mathrm{Br}(\bar{B} \to \bar{K}\mu^+\mu^-)}{\mathrm{Br}(\bar{B} \to \bar{K}e^+e^-)}. \tag{5.0.1}$$

The measured value of $R_K^{\mathrm{LHCb}} = 0.745 \pm^{0.090}_{0.074} \pm 0.036$, in the dilepton invariant mass squared bin $1\,\mathrm{GeV}^2 \leq q^2 \leq 6\,\mathrm{GeV}^2$ corresponds to a $2.6\sigma$ deviation from the SM prediction $R_K^{\mathrm{SM}} = 1.0003 \pm 0.0001$ [35]*.

On the other hand, currently the most precise measurement of the anomalous muon magnetic moment by E821 experiment at BNL has been reported to show a significant deviation from the SM prediction $\Delta a_\mu = a_\mu^{\mathrm{exp}} - a_\mu^{\mathrm{SM}} = (2.8 \pm 0.9) \times 10^{-9}$

*The updated SM estimate for $R_K$ using unquenched lattice QCD results for form factors involves somewhat larger errors than the quoted value here and is predicted to be $R_K = 1.00074 \pm 0.00035$ [36] in the low $q^2$ bin $1 < q^2 < 6$ GeV$^2$.

amounting to a $\sim 3\sigma$ level deviation [229, 230]. This discrepancy also points to the possible existence of NP beyond the SM.

Several attempts have been made in the literature to explain the above anomalies in $B$ decays by invoking NP models [66, 164, 231–237] and separately using a model independent approach [101, 138, 151, 152, 156, 163, 208, 238–240]. Among them, one of the extensively studied class of models relies on scalar or vector leptoquarks. However, in these models the leptoquark couplings are often taken at an effective level without any concrete framework. In this chapter we explain all three anomalies consistently within the framework of a left-right symmetric gauge theory naturally accommodating leptoquarks. This framework, motivated by one of the low energy subgroups of $E_6$, can naturally enhance both $\bar{B} \to D\tau\bar{\nu}$ and $\bar{B} \to D^*\tau\bar{\nu}$ via the exchange of scalar leptoquarks to explain the anomalies, while the $R_K$ data can be explained simultaneously through one loop diagrams induced by leptoquarks. The anomalous muon magnetic moment can also be explained in this model without utilizing a nonzero right handed coupling of leptoquarks. We also discuss various constraints from the current measurements of (semi-) leptonic decays and $B_s^0 - \bar{B}_s^0$, $D^0 - \bar{D}^0$ mixings.

## 5.1 $E_6$ motivated Neutral Left-Right Symmetric Model

In the previous chapter, we discussed that the breaking of $SU(3)_L$ to $SU(2)_L \times U(1)_L$ is fixed by the SM isodoublet structure, for example, $(u, d, h)_L : (3, 3, 1)$ must break to the usual SM isodoublet $(u, d)_L$ and an isosinglet $h_L$. However, there are three choices to break $SU(3)_R$ to $SU(2)_R \times U(1)_R$ depending on the three possible choices of the $SU(2)_R$ doublet corresponding to $T, U, V$ isospins of $SU(3)_R$. The three choices of the residual $SU(2)_R$ give three possible left-right symmetric frameworks. In this chapter, we are interested in the choice where $(h^c, d^c)_L$ is the residual $SU(2)_R$ isodoublet [216]. Interestingly, this choice results in a unique situation where the residual $SU(2)_R$ does not contribute to electric charge [216] and hence we call this model "Neutral" Left-Right Symmetric Model

(NLRSM). We will denote the residual $SU(2)_R$ by $SU(2)_N$. The corresponding charge equation is given by $Q = T_{3L} + \frac{1}{2}Y_L + \frac{1}{2}Y_N$. The fields have the following transformations under the NLRSM gauge group $G = SU(3)_c \times SU(2)_L \times SU(2)_N \times U(1)_Y$ [181]

$$\begin{aligned}
(u,d)_L &: (3,2,1,\frac{1}{6}), \quad (h^c,d^c)_L : (\bar{3},1,2,\frac{1}{3}),\\
(E^c,N_E^c)_L &: (1,2,1,\frac{1}{2}), \quad (N^c,n)_L : (1,1,2,0),\\
h_L &: (3,1,1,-\frac{1}{3}), \quad u_L^c : (\bar{3},1,1,-\frac{2}{3}),\\
e_L^c &: (1,1,1,1), \quad \begin{pmatrix} \nu_e & \nu_E \\ e & E \end{pmatrix}_L : (1,2,2,-\frac{1}{2}).
\end{aligned} \tag{5.1.1}$$

The gauge bosons corresponding to $SU(2)_N$ are electrically neutral and are denoted by $Z_N, W_N^{\pm}$, where the $\pm$ sign refers to the $SU(2)_N$ charge. The interactions of the new exotic fields with the SM sector are governed by the superpotential

$$\begin{aligned}
W &= \lambda^1 \left(\nu_e N_L^c N_E^c + eE^c N_L^c + \nu_E N_E^c n + EE^c n\right)\\
&+ \lambda^2 \left(d^c N_L^c h + hh^c n\right) + \lambda^3 u^c e^c h + \lambda^4 \left(uu^c N_E^c + u^c dE^c\right)\\
&+ \lambda^5 \left(\nu_e e^c E + ee^c \nu_E\right) + \lambda^6 \left(ud^c E + dd^c \nu_E + uh^c e + dh^c \nu_e\right).
\end{aligned} \tag{5.1.2}$$

From the superpotential it follows that the leptoquark $h$ has the assignment $B = 1/3$ and $L = 1$, while the exotic fields $\nu_E, E$ and $n$ have $B = L = 0$ and $N^c$ has $B = 0, L = -1$. In the gauge sector, $W_N$ carries a nonzero lepton number $B = 0, L = -1$.

In addition to the above superpotential couplings, the gauge couplings of $W_N$ and $Z_N$ to the fermions can also induce FCNC processes such as $B^0 - \bar{B}^0$, $K^0 - \bar{K}^0$ mixings and in the leptonic sector lepton flavor violating processes such as the decay $\mu \to e\gamma$, as well as can contribute to the anomalous muon magnetic moment in presence of mixing between new exotic fields [202]. To keep things minimal, in the following analysis we assume that the dominant FCNC and LFV contributions come from scalar leptoquark induced processes.

## 5.2 Explaining $R_{D^{(*)}}$ anomalies

In NLRSM the scalar leptoquark ($\tilde{h}^*$) and slepton ($\tilde{E}$) can mediate the semileptonic decays $\bar{B} \to D^{(*)}\tau\bar{\nu}$ at tree level. The effective Lagrangian is given by

$$\mathcal{L}_{\text{eff}} = \sum_{i,k=1}^{3} V_{2i} \left[ \frac{\lambda^5_{33k}\lambda^{6*}_{i3k}}{m^2_{\tilde{E}^k}} \bar{c}_L b_R \, \bar{\tau}_R \nu_L + \frac{\lambda^6_{33k}\lambda^{6*}_{i3k}}{m^2_{\tilde{h}^{k*}}} \bar{c}_L \tau^c_R \, \bar{\nu}^c_R b_L \right], \tag{5.2.1}$$

where the superscripts are superpotential coupling indices and the generation indices are written as subscripts. Here $m_{\tilde{h}}(m_{\tilde{E}})$ is the mass of scalar leptoquark $\tilde{h}^{k*}$ (slepton $\tilde{E}^k$) and $V_{ij}$ is the $ij$-th component of the CKM matrix. Adhering to the convention used in Chapter 4, the Wilson coefficients are given by

$$\begin{aligned} C^\tau_{S_L} &= -\frac{1}{2\sqrt{2}G_F V_{cb}} \sum_{i,k=1}^{3} V_{2i} \frac{\lambda^5_{33k}\lambda^{6*}_{i3k}}{m^2_{\tilde{E}^k}}\,, \\ C^\tau_{V_L} &= -\frac{1}{2\sqrt{2}G_F V_{cb}} \sum_{i,k=1}^{3} V_{2i} \frac{\lambda^6_{33k}\lambda^{6*}_{i3k}}{2\,m^2_{\tilde{h}^{k*}}}, \end{aligned} \tag{5.2.2}$$

where the neutrinos are assumed to be of tau flavor. To simplify further analysis, we assume that except the SM contribution only the scalar leptoquark NP operator contributes dominantly.

The leptonic decay modes $B \to \tau\nu$, $D^+_s \to \tau\nu$, $D^+ \to \tau\nu$ and $D^0 - \bar{D}^0$ mixing induced by scalar leptoquark $\tilde{h}^{k*}$ exchange can be utilized to derive constraints on the product of couplings $\lambda^6_{33k}\lambda^{6*}_{13k}$ using measured branching fractions for the decays and $D^0 - \bar{D}^0$ mixing parameters. In NLRSM, the exchange of the scalar leptoquark $\tilde{h}^{k*}$ leads to an additional tree level diagram for the decay $B \to \tau\nu$ in addition to the usual SM contribution. Assuming couplings to be real, the modified rate of the decay process $B \to \tau\nu$ gives constraint on the product of couplings $\lambda^6_{33k}\lambda^{6*}_{13k}$ given by

$$-0.04 \left(\frac{m_{\tilde{h}^{k*}}}{1000\text{GeV}}\right)^2 \le \lambda^6_{33k}\lambda^6_{13k} \le 0.03 \left(\frac{m_{\tilde{h}^{k*}}}{1000\text{GeV}}\right)^2. \tag{5.2.3}$$

The measured branching ratios of the decays $D^+_s \to \tau\nu$ and $D^+ \to \tau\nu$ can be used to obtain constraints on $(\lambda^6_{23k})^2$ and $\lambda^6_{23k}\lambda^6_{13k}$ respectively. The decay $D^+_s \to \tau\nu$ gives the constraint

$$(\lambda^6_{23k})^2 \le 1.9 \left(\frac{m_{\tilde{h}^{k*}}}{1000\text{GeV}}\right)^2, \tag{5.2.4}$$

and the decay process $D^+ \to \tau\nu$ gives a weaker constraint on $\lambda^6_{23k}\lambda^6_{13k}$ compared to $D^0 - \bar{D}^0$. The relevant box diagrams for $D^0 - \bar{D}^0$ are similar to the diagrams generated from internal line exchange of lepton-squark pair or slepton-quark pair in the case of R-parity violating models [224, 226]. The relevant constraint is given by

$$-0.012\left(\frac{m_{\tilde{h}^{k*}}}{1000\text{GeV}}\right) \leq \lambda^6_{23k}\lambda^6_{13k} \leq 0.012\left(\frac{m_{\tilde{h}^{k*}}}{1000\text{GeV}}\right). \quad (5.2.5)$$

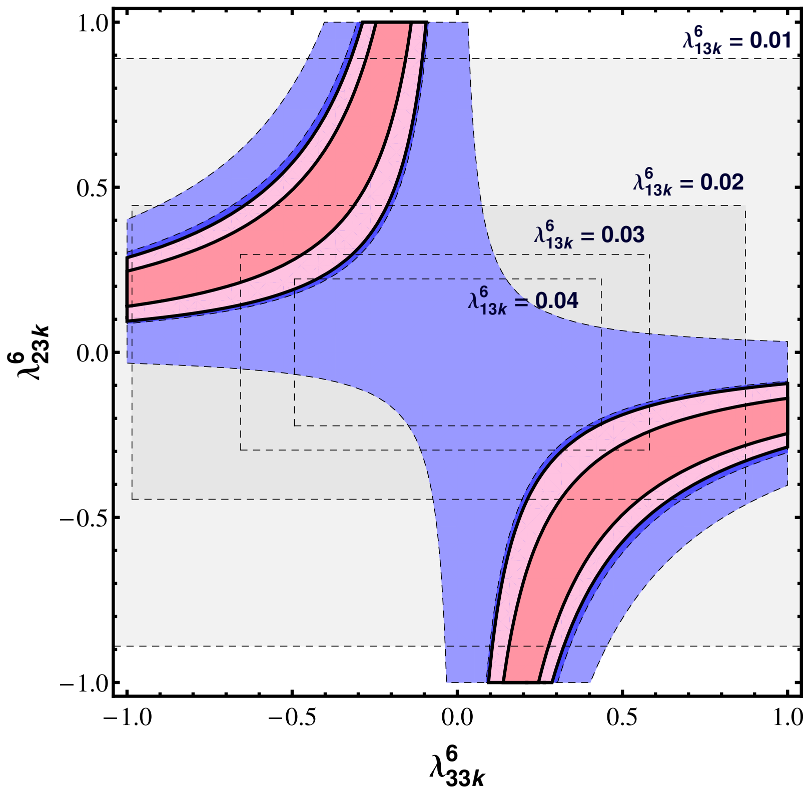


Figure 5.1: $R_{D^{(*)}}$ compatible $\lambda^6_{33k} - \lambda^6_{23k}$ parameter space constrained from $B \to \tau\nu$, $D_s^+ \to \tau\nu$ and $D^0 - \bar{D}^0$ mixing for $m_{\tilde{h}^{k}*} = 750\,\text{GeV}$. The (deep) blue bands show the region consistent with the $R_D$ experimental data at $(1\sigma)$ $2\sigma$ level and the (deep) pink bands show the region consistent with both $R_{D^*}$ [at $(1\sigma)$ $2\sigma$ level] and $R_D$ data simultaneously. See text for details on the constraints from the flavor processes.

In Fig 5.1, we plot the range of the couplings $\lambda^6_{33k}$ and $\lambda^6_{23k}$ (for $m_{\tilde{h}^{k}*} = 750\,\text{GeV}$) that can explain both $R_D$ and $R_{D^*}$ data over the parameter space allowed by the leptonic decays and $D^0$-$\bar{D}^0$ mixing. The shaded (light gray) rectangles with dashed boundaries correspond to regions of $\lambda^6_{33k}$-$\lambda^6_{23k}$ parameter space allowed by the constraints from the $B \to \tau\nu$, $D_s^+ \to \tau\nu$ decays and $D^0 - \bar{D}^0$ mixing for different values of $\lambda^6_{13k}$. The (deep) blue bands correspond to the ($1\sigma$) $2\sigma$ allowed band explaining the $R_D$ data and the (deep) pink bands correspond to the allowed band explaining both $R_D$ and $R_{D^*}$ data simultaneously. Finally, the effective NP operators under consideration also predict an enhanced decay rate for $b \to s\nu\bar{\nu}$ [227, 228], which can be an interesting channel for the future experiments and can be intriguing in the context of radiative neutrino masses.

## 5.3 Explaining $R_K$ anomaly

The lepton non-universality in the ratio $R_K$ has been analyzed in a model-independent fashion in Refs. [101, 238] suggesting that a good fit to the data is obtained for the constraints

$$\begin{aligned} -1.5 \lesssim \quad & C^\mu_{LL} \quad \lesssim -0.7\,, \\ -1.9 \lesssim \ & C^\mu_{LL} - C^\mu_{LR} \ \lesssim 0. \end{aligned} \tag{5.3.1}$$

The study [101] has also discussed leptoquark induced tree level contributions which require either very large leptoquark masses or small couplings in order to explain the data. In Ref. [234] it was explicitly pointed out that one loop box diagrams can also explain the departure from the SM prediction for $\mathcal{O}(1)$ left handed couplings and suppressed right handed couplings. In NLRSM also, the $b \to s\ell\ell$ flavor changing transition can occur at one-loop level via the scalar leptoquark and its supersymmetric partner induced box and penguin diagrams shown in Fig 5.2. We find that the $\gamma$- and $Z$-penguin diagrams (including their supersymmetric counterparts) give a vanishing contribution [†], which is in agreement with Ref. [234]. The contribution to $C^\mu_{LL}$ from scalar leptoquark and its supersymmetric partner induced box diagrams in the limit $m^2_{\tilde{h},h} \gg m^2_{W,t}$ is given

[†] Note that that a careful dimensional reduction ensures a vanishing contribution from Z-penguin diagrams Ref. [241–244]. Note that there are also diagrams involving charginos and neutralinos at one loop level independent of the leptoquarks giving a subdominant contribution.

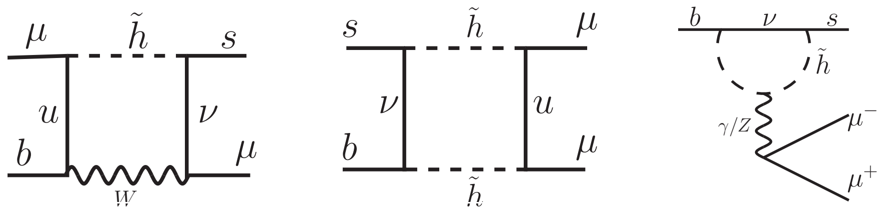


Figure 5.2: Representative diagrams for $b \to s\ell\ell$ transition. The supersymmetric counterparts of these diagrams are also present.

by

$$C^{\mu}_{LL} = \frac{\lambda^{6}_{32k}\lambda^{6*}_{32k}}{8\pi\alpha_e}\left(\frac{m_t}{m_{\tilde{h}_j}}\right)^2 - \frac{\lambda^{6}_{3jk}\lambda^{6*}_{2jl}\lambda^{6}_{i2k}\lambda^{6*}_{i2l}}{32\sqrt{2}\,G_F\,V_{tb}V^{*}_{ts}\pi\alpha_e m^2_{\tilde{h}}} - \frac{\lambda^{6}_{3jk}\lambda^{6*}_{2jl}\lambda^{6}_{i2k}\lambda^{6*}_{i2l}}{32\sqrt{2}\,G_F\,V_{tb}V^{*}_{ts}\pi\alpha_e m^2_{h}}\, g\left(\frac{m^2_{\tilde{u}_i}}{m^2_{\tilde{h}}}, 1, \frac{m^2_{\tilde{\nu}_j}}{m^2_{h}}\right), \tag{5.3.2}$$

where repeated indices are summed over and the loop function $g(x, y, z)$ is defined by

$$g(x, y, z) = \frac{x^2 \log x}{(x-1)(x-y)(x-z)} + (\text{cycl. perm.}).$$

Note that $C^{\mu}_{LL}$ depends on the product of couplings $\lambda^{6}_{3jk}\lambda^{6*}_{2jk}$ with the $j = 3$ set of couplings appearing in the Wilson coefficient $C^{\tau}_{V_L}$ in Eq. (5.2.2). The contribution from the box diagrams also involves one additional set of couplings $\lambda^{6*}_{i2k}\lambda^{6}_{i2l}$ which can be constrained from the measurement of $Z \to \mu\bar{\mu}$ decay rate. In Ref. [234], it was found that for a TeV scale leptoquark, the size of such couplings can be as large as $\sim \mathcal{O}(1)$. Processes such as $t \to b\mu\bar{\nu}_{\mu}$, $D_s \to \mu\bar{\nu}_{\mu}$ etc give similar constraints on individual couplings $\lambda^{6*}_{i2k}\lambda^{6}_{i2l}$. The product of couplings $\lambda^{6}_{3jk}\lambda^{6*}_{2jk}$ contributes to $B_s - \bar{B}_s$ mixing amplitude. Following the suggestion of the UT$fit$ collaboration [245] we define the ratio $C_{B_s}e^{2i\phi_{B_s}} = \langle B_s|H^{\text{full}}_{\text{eff}}|\bar{B}_s\rangle / \langle B_s|H^{\text{SM}}_{\text{eff}}|\bar{B}_s\rangle$ to obtain

$$C_{B_s}e^{2i\phi_{B_s}} = 1 + \frac{m^2_W}{g^4 S_0(x_t)}\left(\frac{1}{m^2_{\tilde{h}}} + \frac{1}{m^2_{h}}\right)\frac{\lambda^{6}_{3jk}\lambda^{6}_{3lm}\lambda^{6*}_{2jm}\lambda^{6*}_{2lk}}{(V_{tv}V^{*}_{ts})^2}, \tag{5.3.3}$$

which gives an allowed range consistent with the value of $\lambda^{6}_{3jk}\lambda^{6*}_{2jk}$ required to explain the $R_K$ data using the latest UT$fit$ values of the $B_s - \bar{B}_s$ mixing parameters. As a benchmark point taking $\lambda^{6}_{3jk}\lambda^{6*}_{2jk} \simeq 0.07$ for $m_{\tilde{h}} \sim 750$ GeV, $m_h \sim 600$ GeV and taking $\lambda^{6*}_{i2k} \sim \mathcal{O}(1)$, we obtain the standard benchmark solution $C^\mu_{LL} = -1$ and $C^\mu_{LR} = 0$ which satisfies the conditions given in Eq. (5.3.1). Note that in this model the leptoquark induced additional contribution to $C_{7\gamma}$ turns out to be too small to have any perceptible effects.

## 5.4 Explaining anomalous muon magnetic moment

In the SM the muon anomalous magnetic moment is chirally suppressed due to the small muon mass, $a_\mu \sim m_\mu^2/m_W^2$. In NLRSM, leptoquarks can induce an additional contribution to the anomalous magnetic moment of the muon through one-loop vertex diagrams. However, the sole contribution from leptoquark induced diagrams cannot explain the experimental deviation from the SM. One way out is to follow the approach taken in Ref. [234], where a nonzero right handed coupling of leptoquark is utilized. Interestingly, in NLRSM it is possible to explain the experimental data through a dominant contribution from $\lambda^5$ terms in Eq. (5.1.2). The new contribution from $\lambda^6_{ijk}$ terms in Eq. (5.1.2) is given by

$$a_\mu(\lambda^6) = \frac{m_\mu^2}{32\pi^2}\left[\frac{1}{m^2_{\tilde{h}^*_{jR}} - m_t^2}|\lambda^6_{32j}|^2\left(1+\frac{2x_t}{1-x_t}\right)\left(\frac{1}{2}+\frac{3}{1-x_t}+\frac{2+x_t}{(1-x_t)^2}\ln x_t\right)\right], \tag{5.4.1}$$

where $x_t = m_t^2/m_{\tilde{h}}^2$. The $\lambda^5_{ijk}$ terms in Eq. (5.1.2) give the following contribution induced by sleptons

$$\begin{aligned}\delta a_\mu(\lambda^5) = \frac{m_\mu^2}{16\pi^2}\Big[&|\lambda_{i2k}|^2F(e_k,\tilde{\nu}_{Ei}) - |\lambda_{i2k}|^2F(\tilde{e}_k,\nu_{Ei}) + |\lambda_{ij2}|^2F(e_j,\tilde{\nu}_{Ei}) \\ &-|\lambda_{ij2}|^2F(\tilde{e}_j,\nu_{Ei}) + |\lambda_{ij2}|^2F(E_j,\tilde{\nu}_{ei}) - |\lambda_{ij2}|^2F(\tilde{E}_j,\nu_{ei})\Big],\end{aligned} \tag{5.4.2}$$

where $F(a,b)$ is defined as

$$F(a,b) = \int_0^1 dx \frac{x^2-x^3}{m_\mu^2x^2+(m_a^2-m_\mu^2)x+m_b^2(1-x)}. \tag{5.4.3}$$

The existing measurements of the decay rates like $\tau \to \mu\gamma$, $\tau \to 3l$, and $\tau \to \mu\nu\bar{\nu}$ can give constraints on $\lambda^5_{i2k}$ and $\lambda^5_{ij2}$ separately in combination with some other independent couplings [246]. Assuming a hierarchy between $m_{\tilde{E},\tilde{e}}$ and $m_{\tilde{\nu}_E,\tilde{\nu}_e}$, and taking $m_{\tilde{E},\tilde{e}} \sim 700$ GeV and $m_{\tilde{\nu}_E,\tilde{\nu}_e} \sim 250$ GeV as a benchmark point, we find that the current experimental data can be explained with less than order unity values of the couplings. Interestingly, in the presence of a mixing between left and right handed leptoquarks ($\tilde{h}_{L,R}$) it is possible to enhance the leptoquark contribution significantly to explain the data even without the slepton induced contributions.

## 5.5 Conclusions

We have presented a minimal framework of a left-right symmetric gauge theory naturally accommodating leptoquarks which can provide a unified explanation of the $B$-decay anomalies in $R_{D^{(*)}}$ and $R_K$ together with the anomalous muon magnetic moment, while being consistent with the constraints from the current measurements of (semi-)leptonic decays and $B_s^0 - \bar{B}_s^0$, $D^0 - \bar{D}^0$ mixings. In this model both $R_D$ and $R_{D^*}$ anomalies can be explained via the exchange of scalar leptoquarks at tree level, while the $R_K$ data can be explained simultaneously using one loop diagrams induced by leptoquarks. The anomalous muon magnetic moment can also be addressed in this model without utilizing a nonzero right handed coupling of leptoquark.

# Chapter 6

# Constraining Scalar Leptoquark from the Kaon Sector

## 6.1 Introduction

In view of recently observed anomalies in the flavor sector, we are motivated to study a TeV-scale leptoquark model in this chapter, and analyze NP effects on the kaon sector. It is known that the studies of kaon decays have played a vital role in retrieving information on the flavor structure of the SM. In particular, neutral kaon mixing and rare decays of the kaon have been analyzed in various extensions of the SM and are known to provide some of the most stringent constraints on NP [247–256]. The NP model we consider in this chapter is a simple extension of the SM by a single scalar leptoquark. The leptoquark $\phi$ with mass $M_\phi$ has ($\mathrm{SU(3)_C}$, $\mathrm{SU(2)_L}$) quantum numbers $(3, 1)$ and is of charge $-1/3$. This model is interesting considering that it has all the necessary ingredients accommodating semileptonic $b \to c$ and $b \to s$ decays [101, 234] to explain the anomalies in the lepton flavor universality ratios discussed in the previous chapter. To this end, we must mention that along with anomalies observed in the flavor sector, the leptoquark model under study is also capable of explaining the new diphoton excess recently reported by the ATLAS and CMS collaborations in their analysis of $\sqrt{s} = 13\,\mathrm{TeV}$ $pp$ collision [257].

Following the conventions of Ref. [234], the Lagrangian governing the leptoquark interaction with first-family fermions is given by

$$\mathcal{L}^{(\phi)} \ni \lambda^L_{ue} \bar{u}^c_L e_L \phi^* + \lambda^R_{ue} \bar{u}^c_R e_R \phi^* - \lambda^L_{d\nu} \bar{d}^c_L \nu_L \phi^* + \text{h.c.}\,, \tag{6.1.1}$$

where L/R are the left/right projection operators $(1 \mp \gamma_5)/2$. The couplings $\lambda$'s are family dependent, and $u^c{=}C\bar{u}^T$ are the charge-conjugated spinors. Similar interaction terms for the second and third families can also be written down. In this model, $B \to D^{(*)}\tau\bar{\nu}$ proceeds at tree level through the exchange of leptoquark ($\phi$). Integrating out the heavy particles gives rise to low-energy dimension-6 effective operators, which can produce the required effects to satisfy the experimental data. In Ref. [234] it was shown that with $O(1)$ left-handed and relatively suppressed right-handed couplings, one can explain the observed excesses in the rate of $B \to D^{(*)}\tau\bar{\nu}$ decays. The authors of Ref. [234] were also able to simultaneously explain the observed anomalies in $R_K$ with large [$\sim O(1)$] left-handed couplings for a TeV scale leptoquark. In this model, such large couplings are possible because the leading contribution to $\bar{B} \to \bar{K}\mu^+\mu^-$ comes from one-loop diagrams and therefore additional GIM and CKM suppression compensates for the "largeness" of the couplings. This is in contrast to NP models [101, 258, 259] in which $R_K$ arises at tree level, which renders the couplings very small in order to have leptoquarks within the reach of the LHC. Apart from B system, this model has also been explored in the context of FCNC decays of D-meson. In Refs. [260–262] impact of scalar (as well as vector) leptoquarks on the FCNC processes $D^0 \to \mu^+\mu^-$ and $D^+ \to \pi^+\mu^+\mu^-$ have been studied, and using the existing experimental results, strong bounds on the leptoquark coupling have been derived. However, to the best of our knowledge, the effects of new physics on the kaon sector have not been investigated before in the scalar leptoquark $(3, 1)_{-1/3}$ model. We start by writing the effective Hamiltonian relevant for each case and discuss the effective operators and corresponding coupling strengths (Wilson coefficients) generated in the model. The explicit expressions of new contributions in terms of parameters of the model are derived. We then discuss NP affecting the various kaon processes such as $K^+ \to \pi^+\nu\bar{\nu}$, $K_L \to \pi^0\nu\bar{\nu}$, $K_L \to \mu^+\mu^-$, and the LFV decay $K_L \to \mu^\pm e^\mp$. Using the existing experimental information on these processes, constraints on the leptoquark couplings are obtained.

The rest of the chapter is organized in the following way. In section 6.2 we study $K^0 - \bar{K}^0$ mixing in this model and obtain constraints on the couplings. In section 6.3 and 6.4 we constrain the parameter space using information on BR$(K^+ \to \pi^+\nu\bar{\nu})$ and CP-violating BR$(K_L \to \pi^0\nu\bar{\nu})$ respectively. In section 6.5 we discuss the new contribution to the short-distance part of the rare decay $K_L \to \mu^+\mu^-$ in this model and obtain constraints on the generation-diagonal leptoquark couplings using the bounds on BR$(K_L \to \mu^+\mu^-)_{\rm SD}$. In section 6.6, we discuss the LFV process $K_L \to \mu^\mp e^\pm$ and constrain the off-diagonal couplings of the leptoquark contributing to NP Wilson coefficients. Finally, we summarize our results in the last section.

## 6.2 Constraints From $K^0 - \overline{K}^0$ Mixing

The phenomenon of meson-antimeson oscillation, being a FCNC process, is very sensitive to heavy particles propagating in the mixing amplitude, and therefore, it provides a powerful tool to test the SM and a window to observe NP. In this section, we focus on the mixing of the neutral kaon meson. The experimental measurement of the $K^0 - \bar{K}^0$ mass difference $\Delta m_K$ and of CP-violating parameter $\epsilon_K$ has been instrumental in not only constraining the parameters of the unitarity triangle but also providing stringent constraints on NP. The theoretical calculations for $K^0 - \bar{K}^0$ mixing are done in the framework of effective field theories (EFT), which allow one to separate long- and short-distance contributions. The leading contribution to $K^0 - \bar{K}^0$ oscillations in the SM comes from the so-called box diagrams generated through internal line exchange of the $W$ boson and up-type quark pair. The effective SM Hamiltonian for $|\Delta S| = 2$ resulting from the evaluation of box diagrams is written as [263, 264]

$$\mathcal{H}_{\rm eff}^{|\Delta S|=2} = \frac{G_F^2 M_W^2}{4\pi^2}\left[\lambda_c^2\eta_{cc}S_0(x_c) + \lambda_t^2\eta_{tt}S_0(x_t) + 2\ \lambda_t\lambda_c\eta_{ct}S_0(x_c, x_t)\right] K(\mu)Q_s(\mu), \tag{6.2.1}$$

where $x_i = m_i^2/M_W^2$, $G_F$ is the Fermi constant, and $\lambda_i = V_{is}^* V_{id}$ contains CKM matrix elements. $Q_s(\mu)$ is the dimension-6, four-fermion local operator $(\bar{s}\gamma_\mu {\rm L} d)(\bar{s}\gamma^\mu {\rm L} d)$, and $K(\mu)$ is the relevant short-distance factor which makes product $K(\mu)Q_s(\mu)$ independent of $\mu$. The Inami-Lim functions $S_0(x)$ and $S_0(x_i, x_j)$ [265] contain contributions of loop diagrams and are given by [266]

$$\begin{aligned} S(x_c, x_t) &= x_c x_t \left[ -\frac{3}{4(1-x_c)(1-x_t)} + \frac{\mathrm{Ln}\, x_t}{(x_t - x_c)(1-x_t)^2} \left(1 - 2x_t + \frac{x_t^2}{4}\right) \right. \\ & \left. + \frac{\mathrm{Ln}\, x_c}{(x_c - x_t)(1-x_c)^2} \left(1 - 2x_c + \frac{x_c^2}{4}\right) \right], \end{aligned} \tag{6.2.2}$$

and the function $S_0(x)$ is the limit of $S_0(x, y)$ when $y \to x$, while $\eta_i$ in Eq. (6.2.1) are the short-distance QCD correction factors $\eta_{cc} = 1.87$, $\eta_{tt} = 0.57$, and $\eta_{ct} = 0.49$ [267–269]. The hadronic matrix element $\langle \bar{K}^0 | Q_s | K^0 \rangle$ is parametrized in terms of decay constant $f_K$ and kaon bag parameter $B_K$ in the following way:

$$B_K = \frac{3}{2} K(\mu) \frac{\langle \bar{K}^0 | Q_s | K^0 \rangle}{f_K^2 m_K^2}. \tag{6.2.3}$$

The contribution of NP to $|\Delta S| = 2$ transition can be parametrized as the ratio of the full amplitude to the SM one as follows [245]:

$$C_{\Delta m_K} = \frac{\mathrm{Re}\langle\, K | H_{\rm eff}^{\rm Full} | \bar{K} \rangle}{\mathrm{Re}\langle K | H_{\rm eff}^{\rm SM} | \bar{K} \rangle}, \tag{6.2.4}$$

$$C_{\varepsilon_K} = \frac{\mathrm{Im}\langle K | H_{\rm eff}^{\rm Full} | \bar{K} \rangle}{\mathrm{Im}\langle K | H_{\rm eff}^{\rm SM} | \bar{K} \rangle}. \tag{6.2.5}$$

In the SM, $C_{\Delta m_K}$ and $C_{\varepsilon_K}$ are unity. The effective Hamiltonian $\langle \bar{K}^0 | H_{\rm eff} | K^0 \rangle$ can be related to the off-diagonal element $M_{12}$ through the relation *

$$\langle \bar{K}^0 | H_{\rm eff}^{\rm Full} | K^0 \rangle = 2 m_K M_{12}^*, \tag{6.2.6}$$

with $M_{12} = (M_{12})_{SM} + (M_{12})_{NP}$. In the SM, the theoretical expression of $(M_{12})_{SM}$ reads [247]

$$(M_{12})_{SM} = \frac{G_F^2}{12\pi^2} f_K^2 B_K m_K M_W^2 F^*(\lambda_c, \lambda_t, x_c, x_t), \tag{6.2.7}$$

*The observables mass difference $\Delta m_K$ and CP-violating parameter $\varepsilon_K$ are related to off-diagonal element $M_{12}$ through the following relations: $\Delta m_K = 2[\mathrm{Re}(M_{12})_{SM} + \mathrm{Re}(M_{12})_{NP}]$, and $\varepsilon_K = \frac{k_\varepsilon \exp^{i\phi_\varepsilon}}{\sqrt{2}(\Delta m_K)_{\rm exp}}[\mathrm{Im}(M_{12})_{SM} + \mathrm{Im}(M_{12})_{NP}]$, where $\phi_\varepsilon \simeq 43^o$ and $k_\varepsilon \simeq 0.94$ [270–272].

where the function $F(\lambda_c, \lambda_t, x_c, x_t)$ stands for

$$F(\lambda_c, \lambda_t, x_c, x_t) = \lambda_c^2 \eta_{cc} S_0(x_c) + \lambda_t^2 \eta_{tt} S_0(x_t) + 2\,\lambda_t \lambda_c \eta_{ct} S_0(x_c, x_t), \tag{6.2.8}$$

with $x_i = m_i^2/M_W^2$.

In the leptoquark model considered, the internal line exchange of the neutrino-leptoquark pair induces new Feynman diagram shown in Fig 6.1, which contributes to $K^0 - \bar{K}^0$ mixing. The new effects modify the observables $C_{\Delta m_K}$ and

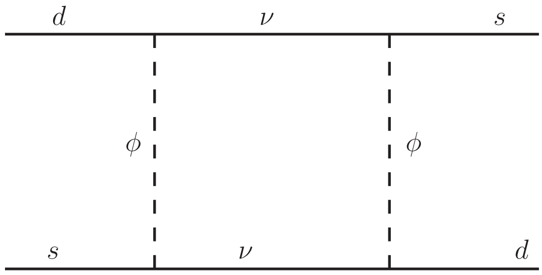


Figure 6.1: New contribution to $K - \bar{K}$ mixing induced by the scalar leptoquark ($\phi$).

$C_{\varepsilon_K}$, and in the approximation $M_\phi^2 \gg m_{t,W}^2$, their expressions are given by

$$C_{\Delta m_K} = 1 + \frac{1}{g_2^4} \frac{M_W^2}{M_\phi^2} \frac{\eta_{tt}}{\mathrm{Re}(F^*)} \mathrm{Re}\,(\xi_{ds})^2\,, \tag{6.2.9}$$

$$C_{\varepsilon_K} = 1 + \frac{1}{g_2^4} \frac{M_W^2}{M_\phi^2} \frac{\eta_{tt}}{\mathrm{Im}(F^*)} \mathrm{Im}\,(\xi_{ds})^2\,, \tag{6.2.10}$$

where we have used notation $F$ for $F(\lambda_c, \lambda_t, x_c, x_t)$ for simplicity. $g_2$ is the SU(2) gauge coupling and we define

$$\xi_{ds} \equiv (\lambda^L \lambda^{L\dagger})_{ds} = \sum_i \lambda^L_{d\nu_i} \lambda^{L*}_{s\nu_i}. \tag{6.2.11}$$

Solving Eqs. (6.2.9) and (6.2.10) for real and imaginary parts of $\xi_{ds}$ in terms of the experimental observables $C_{\Delta m_K}$, and $C_{\varepsilon_K}$, we obtain the following expressions:

$$(\mathrm{Re}\,\xi_{ds})^2 = \left(\frac{g_2^4}{2} \frac{M_\phi^2}{M_W^2}\right) \left(\frac{\mathrm{Re}(F^*)}{\eta_{tt}} \left(-1 + C_{\Delta m_K}\right)\right) \left(1 + \sqrt{1 + \left(\frac{\mathrm{Im}F^*}{\mathrm{Re}F^*} \cdot \frac{C_{\varepsilon_K} - 1}{C_{\Delta m_K} - 1}\right)^2}\,\right), \tag{6.2.12}$$

$$(\mathrm{Im}\,\xi_{ds})^2 = \left(\frac{g_2^4}{2}\frac{M_\phi^2}{M_W^2}\right)\left(\frac{\mathrm{Re}(F^*)}{\eta_{tt}}\left(-1+C_{\Delta m_K}\right)\right)\left(-1+\sqrt{1+\left(\frac{\mathrm{Im}F^*}{\mathrm{Re}F^*}\cdot\frac{C_{\varepsilon_K}-1}{C_{\Delta m_K}-1}\right)^2}\,\right). \tag{6.2.13}$$

To constrain the leptoquark couplings $\mathrm{Re}\,\xi_{\mathrm{ds}}$ and $\mathrm{Im}\,\xi_{\mathrm{ds}}$, we use the latest global fit results provided by the UTfit collaboration and to be conservative evaluate the constraints at the $2\sigma$ level: $C_{\Delta m_K} = 1.10 \pm 0.44$ and $C_{\varepsilon_K} = 1.05 \pm 0.32$ [245]. Here, to account for the significant uncertainties from poorly known long-distance effects [273], we allow for a $\pm 40\%$ uncertainty in the case of $\Delta M_K$. For $\mathrm{Re}\,\xi_{ds}$ and $\mathrm{Im}\,\xi_{ds}$, we obtain the following upper bounds:

$$(\mathrm{Re}\,\xi_{ds})^2 \leq 6.0\times 10^{-4}\left(\frac{M_\phi}{1000\,\mathrm{GeV}}\right)^2, \tag{6.2.14}$$

$$(\mathrm{Im}\,\xi_{ds})^2 \leq 3.8\times 10^{-4}\left(\frac{M_\phi}{1000\,\mathrm{GeV}}\right)^2. \tag{6.2.15}$$

As discussed in the next section, we find that a more constraining bound on the product of the couplings $\mathrm{Re}(\xi_{ds})$ and $\mathrm{Im}(\xi_{ds})$ can be obtained from the theoretically rather clean rare processes $K^+ \to \pi^+\nu\bar{\nu}$ and $K_L \to \pi^0\nu\bar{\nu}$ as compared to $K-\bar{K}$ mixing.

## 6.3 Constraints from rare decay $K^+ \to \pi^+\nu\overline{\nu}$

The charged and neutral $K \to \pi\nu\bar{\nu}$ are in many ways interesting FCNC processes and considered as *golden* modes. Both the decays can play an important role in indirect searches for NP because these decays are theoretically very clean and their branching ratio can be computed with an exceptionally high level of precision (for a review, see Ref. [274]). In the SM these decays are dominated by Z-penguin and box diagrams, which exhibit hard, power-like GIM suppression as compared to logarithmic GIM suppression generally seen in other loop-induced meson decays. At the leading order, both modes are induced by a single dimension-6 local operator $(\bar{s}d)_{\mathrm{V-A}}(\bar{\nu}\nu)_{\mathrm{V-A}}$. The hadronic matrix element of this operator can be measured precisely in $K^+ \to \pi^0 e^+\nu$ decays, including isospin breaking corrections [275, 276]. The principal contribution to the error in theoretical predictions originates from the uncertainties on the current values of $\lambda_t$ and $m_c$. The long-distance effects are rather suppressed and have been found to be small [277–279].

In the SM, the effective Hamiltonian for $K \to \pi\nu\bar{\nu}$ decays is written as [280]

$$\mathcal{H}_{\rm eff}^{\rm SM} = \frac{G_F}{\sqrt{2}} \frac{2\alpha}{\pi \sin^2\theta_W} \sum_{\ell=e,\mu,\tau} \left(\lambda_c X_{\rm NNL}^{\ell} + \lambda_t X(x_t)\right) (\bar{s}_L\gamma_\mu d_L)(\bar{\nu}_{\ell L}\gamma^\mu \nu_{\ell L}), \quad (6.3.1)$$

The index $\ell = e, \mu, \tau$ denotes the lepton flavor. The short-distance function $X(x_t)$ corresponds to the loop-function containing top contribution and is given by

$$X(x_t) = \eta_X \cdot \frac{x_t}{8}\left[\frac{x_t+2}{x_t-1} + \frac{3x_t-6}{(x_t-1)^2}{\rm Ln}\, x_t\right], \quad (6.3.2)$$

where the factor $\eta_X$ includes the next-to-leading-order (NLO) correction and is close to unity ($\eta_X = 0.995$) while the remaining part describes the contribution of the top quark without QCD correction. The NLO QCD corrections have been computed in Refs. [281–283], while two-loop electroweak corrections have been studied in Ref. [284]. The loop-function $X_{\rm NNL}$ summarizes the contribution from the charm quark and can be written as [249]

$$X_{NNL} = \frac{2}{3}X_{NNL}^{e} + \frac{1}{3}X_{NNL}^{\tau} \equiv \lambda^4 P_c^{SD}(X), \quad (6.3.3)$$

where $\lambda = |V_{us}|$. The NLO results for the function $X_{\rm NNL}$ can be found in [280,283] while next-to-next-leading-order (NNLO) calculations are done in Refs. [285,286].

In the model considered, leptoquark $\phi$ mediates $K^+ \to \pi^+\nu\bar{\nu}$ at tree level. The corresponding Feynman diagram is shown in Fig 6.2. The NP effective Hamiltonian relevant for $K^+ \to \pi^+\nu\bar{\nu}$ decay is given by

$$\mathcal{H}_{\rm eff}^{\rm NP} = -\frac{\lambda^{L*}_{s\nu_\ell}\lambda^{L}_{d\nu_\ell}}{2M_\phi^2}(\bar{s}\gamma_\mu L d)(\bar{s}\gamma^\mu L d). \quad (6.3.4)$$

The new contribution alters the SM branching ratio of $K^+ \to \pi^+\nu\bar{\nu}$ [287] as

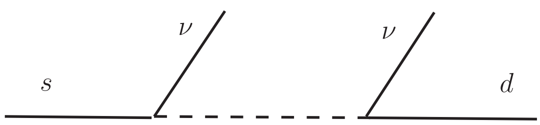


Figure 6.2: Feynman diagram for the decay $K \to \pi\nu\bar{\nu}$ induced by the exchange of the scalar leptoquark $\phi$.

$$\mathrm{BR}(K^+ \to \pi^+ \nu\bar{\nu}) = \kappa_+(1+\Delta_{\mathrm{EM}}) \left[ \left( \frac{\mathrm{Im}\,\lambda_t}{\lambda^5} X_{\mathrm{new}} \right)^2 + \left( \frac{\mathrm{Re}\,\lambda_c}{\lambda} P_c(X) + \frac{\mathrm{Re}\,\lambda_t}{\lambda^5} X_{\mathrm{new}} \right)^2 \right], \tag{6.3.5}$$

where $\kappa_+$ contains relevant hadronic matrix elements extracted from the decay rate of $K^+ \to \pi^0 e^+ \nu$ along with an isospin-breaking correction factor and is given by [287]

$$\kappa_+ = (5.173 \pm 0.025) \cdot 10^{-11} \left( \frac{\lambda}{0.225} \right)^8 . \tag{6.3.6}$$

In Eq. (6.3.5), $\Delta_{\mathrm{EM}}$ describes the electromagnetic radiative correction from photon exchanges and amounts to -0.3%. The charm contribution $P_c(X)$ includes the short-distance part $P_c^{\mathrm{SD}}(X)$ plus the long-distance contribution $\delta P_c$ (calculated in Ref. [276]). We use $P_c(X) = 0.404$ given in [287]. The function $X_{\mathrm{new}}$ contains a new short-distance contribution from the leptoquark-mediated diagram and modifies the SM contribution through

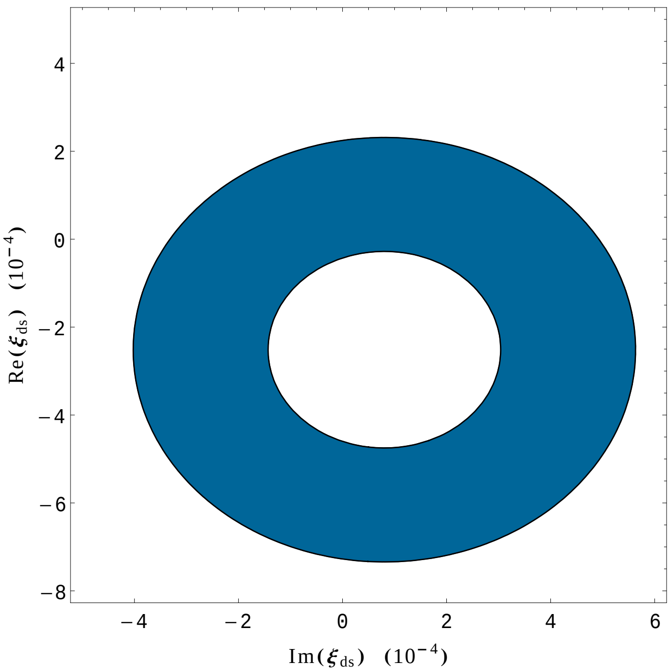


Figure 6.3: The constraints on $\mathrm{Re}(\xi_{ds}) - \mathrm{Im}(\xi_{ds})$ parameter space from the measured value of $\mathrm{BR}(K^+ \to \pi^+ \nu\bar{\nu})$. The blue colored region shows experimentally allowed values at the $1\sigma$ level.

$$X_{new} = X(x_t) + \frac{X_\phi}{\lambda_t}, \tag{6.3.7}$$

where $X(x_t)$ is the top contribution in the SM already defined in Eq. (6.3.2) and $X_\phi$ is the contribution due to leptoquark exchange. In terms of the model parameters, $X_\phi$ is given by

$$X_\phi = -\frac{\sqrt{2}}{4G_F}\frac{\pi \sin^2\theta_W}{\alpha}\frac{\xi_{ds}}{M_\phi^2}, \tag{6.3.8}$$

where $\alpha(M_Z) = 1/127.9$ is the electromagnetic coupling constant and $\sin^2\theta_W = 0.23$ is the weak mixing angle. Using the experimental value of the branching ratio provided by BNL-E949 experiment, $\mathrm{BR}(K^+ \to \pi^+\nu\bar{\nu}) = (1.7 \pm 1.1) \times 10^{-10}$ [288], we obtain the constraint on $\mathrm{Re}\,\xi_{ds}$ and $\mathrm{Im}\,\xi_{ds}$, shown in Fig 6.3. A most conservative bound on individual couplings $\mathrm{Re}\,\xi_{ds}$ and $\mathrm{Im}\,\xi_{ds}$ can be obtained by taking only one set to be nonzero at a time. We find that for a leptoquark of 1 TeV mass the constraints are given by $-7.2 \times 10^{-4} < \mathrm{Re}\,\xi_{ds} < 2.2 \times 10^{-4}$ and $-3.3 \times 10^{-4} < \mathrm{Im}\,\xi_{ds} < 4.9 \times 10^{-4}$. As pointed out before, these bounds rule out a large parameter space allowed from $K^0 - \bar{K}^0$ mixing. The coupling $\mathrm{Im}\,\xi_{ds}$ can also be probed independently through the decay $K_L \to \pi^0\nu\bar{\nu}$, which is the subject of our next section.

## 6.4 Constraints from $K_L \to \pi^0 \nu\overline{\nu}$

The neutral decay mode $K_L \to \pi^0\nu\bar{\nu}$ is CP-violating. In contrast to the decay rate of $K^+ \to \pi^+\nu\bar{\nu}$ which depends on the real and imaginary parts of $\lambda_t$, with a small contribution from the real part of $\lambda_c$, the rate of $K_L \to \pi^0\nu\bar{\nu}$ depends only on $\mathrm{Im}\lambda_t$. Because of the absence of the charm contribution, the prediction for $\mathrm{BR}(K_L \to \pi^0\nu\bar{\nu})$ is theoretically cleaner. The principal sources of error are the uncertainties on $\mathrm{Im}\lambda_t$ and $m_t$. In the SM, the branching ratio is given by [274]

$$\mathrm{BR}(K_L \to \pi\nu\bar{\nu}) \quad = \quad \kappa_L \left(\frac{\mathrm{Im}\lambda_t}{\lambda^5} X(x_t)\right)^2, \tag{6.4.1}$$

with [287]

$$\kappa_L = 2.231 \times 10^{-10} \left(\frac{\lambda}{0.225}\right)^8. \tag{6.4.2}$$

The exchange of leptoquark $\phi$ induces a new contribution to the rate which can be accommodated in the expression for the branching ratio by replacing $X(x_t)$ by $X_{\rm new}$ given in Eq. (6.3.7). KEK-E391a experiment has searched for $K_L \to \pi^0\nu\bar{\nu}$ and set an upper limit on $\mathrm{BR}(K_L \to \pi^0\nu\bar{\nu}) < 2.6\times 10^{-8}$ at 90% C.L. [289]. In Fig 6.4, we plot the dependence of the $K_L \to \pi\nu\bar{\nu}$ branching ratio on the imaginary part of the effective couplings $\xi_{ds}$. Numerically, the constraints are given by

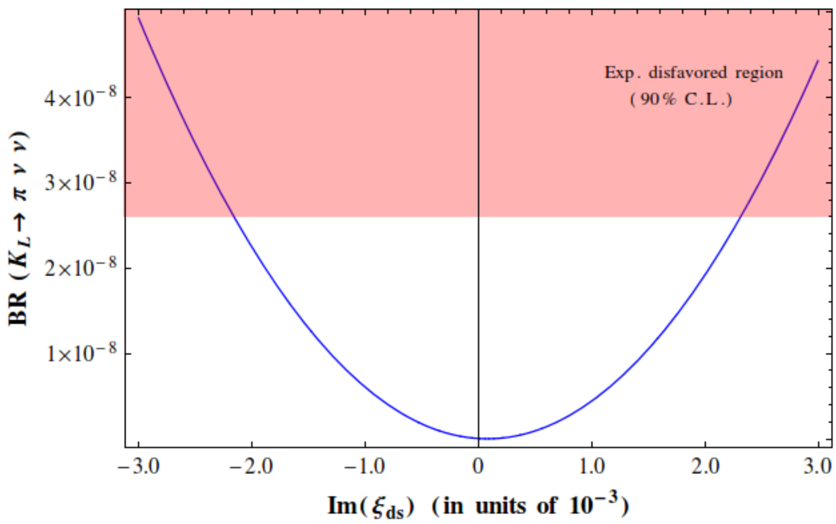


Figure 6.4: The dependence of $\mathrm{BR}(K_L \to \pi^0\nu\bar{\nu})$ on $\mathrm{Im}\,\xi_{ds}$. The red shaded region is currently disfavored by the experimental data at 90% C.L.

$$-0.0021 < \frac{\mathrm{Im}\,\xi_{ds}}{\left(\frac{M_\phi}{1000\,\mathrm{GeV}}\right)^2} < 0.0023, \tag{6.4.3}$$

Since the decay has not been observed so far and the present experimental limits are 3 orders of magnitude above the SM predictions [287], we find that constraints from $K_L \to \pi^0\nu\bar{\nu}$ are weaker compared to those obtained in the case of $K^+ \to \pi^+\nu\bar{\nu}$.

Before proceeding further, we summarize the analysis done so far and present combined constraints on $\mathrm{Re}\,(\xi_{ds})$ - $\mathrm{Im}\,(\xi_{ds})$ parameter space from $K^0-\bar{K}^0$ mixing, rare decays $K^+ \to \pi^+\nu\bar{\nu}$ and $K_L \to \pi^0\nu\bar{\nu}$ in Fig 6.5 for a scalar leptoquark $(\phi)$ of 1 TeV mass. The real and imaginary part of NP amplitude for neutral kaon mixing give individual bound on $\mathrm{Re}\,(\xi_{ds})$ and $\mathrm{Im}\,(\xi_{ds})$, respectively and are

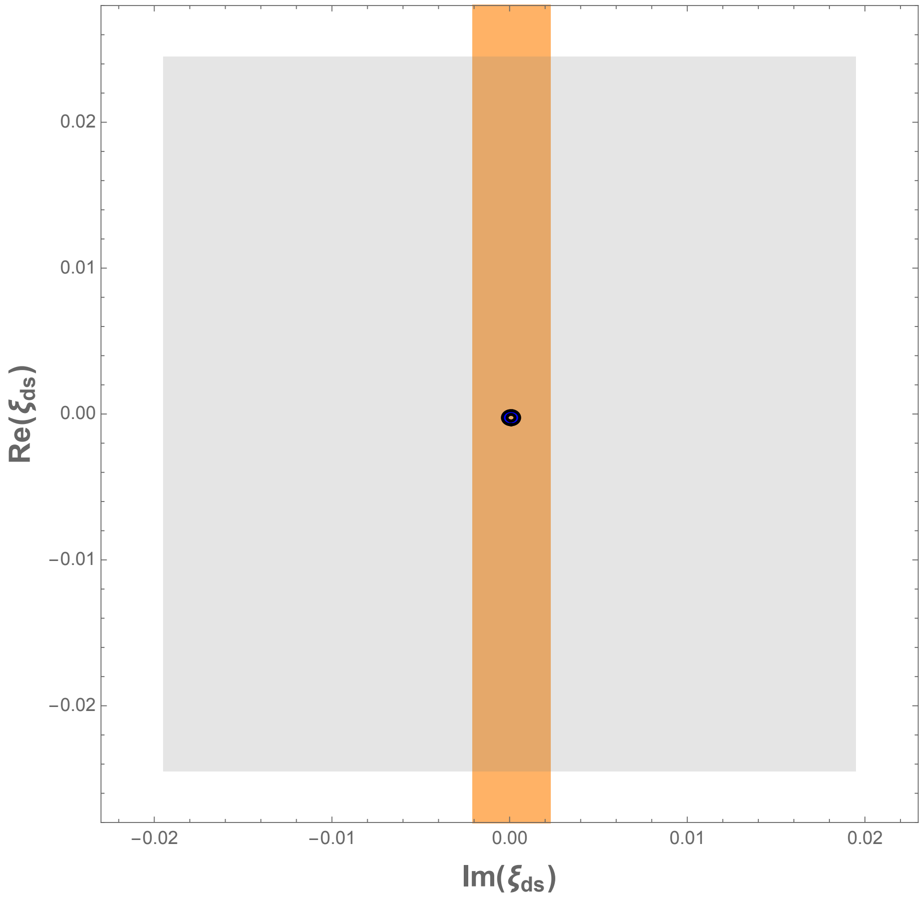


Figure 6.5: Re$(\xi_{ds})$ - Im$(\xi_{ds})$ parameter space allowed by neutral kaon mixing (gray), rare decays $K_L \to \pi^0\nu\bar{\nu}$ (orange) and $K^+ \to \pi^+\nu\bar{\nu}$ (dark blue) for a 1 TeV leptoquark ($\phi$) mass. For details see text.

the weakest among processes considered in this work. The CP violating process $K_L \to \pi^0\nu\bar{\nu}$ gives bounds on Im$(\xi_{ds})$ only and is relatively tighter than those from neutral kaon mixing. But the most stringent constraints come from $K^+ \to \pi^+\nu\bar{\nu}$ and allows only a very small parameter space as discussed in section 6.3.

## 6.5 Constraints from $K_L \to \mu^+\mu^-$

The decay $K_L \to \mu^+\mu^-$ is sensitive to much of the same short-distance physics (i.e., $\lambda_t$ and $m_t$) as $K \to \pi\nu\bar{\nu}$ and therefore provides complementary information on the structure of FCNC $|\Delta S| = 1$ transitions. This is important because experimentally a much more precise measurement compared to $K \to \pi\nu\bar{\nu}$ is available: BR$(K_L \to \mu\mu) = (6.84 \pm 0.11) \times 10^{-9}$ [9]. However, the theoretical situation is far more complex (for a review, see Refs. [290, 291]). The amplitude for $K_L \to \mu^+\mu^-$ can be decomposed into a dispersive (real) and an absorptive (imaginary) part. The dominant contribution to the absorptive part [as well as to total decay rate $(K_L \to \mu^+\mu^-)$] comes from the real two-photon intermediate state. The dispersive amplitude is the sum of the so-called long-distance and the short-distance contributions. Only the short-distance (SD) part can be reliably calculated. The most recent estimates of the SD part from the data give $\mathrm{BR}(K_L \to \mu^+\mu^-)_{\mathrm{SD}} \leq 2.5 \times 10^{-9}$ [292]. The effective Hamiltonian relevant for the decay $K_L \to \mu^+\mu^-$ is given by [280]

$$\begin{aligned}\mathcal{H}_{\rm eff}(K_L \to \mu^+\mu^-) &= \frac{G_F}{\sqrt{2}}\frac{\alpha}{2\pi \sin^2\theta_W}[\lambda_c Y_{NL} + \lambda_t Y(x_t)]\; (\bar{s}\gamma^\mu(1-\gamma_5)d)(\bar{\mu}\gamma_\mu\gamma_5\mu),\\ &= \frac{G_F}{\sqrt{2}} V_{us}^* V_{ud}\; \Delta^K_{SM}\; (\bar{s}\gamma^\mu(1-\gamma_5)d)(\bar{\mu}\gamma_\mu\gamma_5\mu),\end{aligned} \tag{6.5.1}$$

where $\Delta^K_{SM}$ describes the Wilson coefficient of the effective local operator $[\bar{s}\gamma^\mu(1-\gamma_5)d][\bar{\mu}\gamma_\mu\gamma_5\mu]$ and is given as

$$\Delta^K_{SM} = \frac{\alpha(\lambda_c Y_{NL} + \lambda_t Y(x_t))}{2\pi \sin^2\theta_w\, V_{us}^* V_{ud}}, \tag{6.5.2}$$

The short-distance function $Y(x_t)$ describes contribution from Z-penguin and box diagrams with an internal top quark with QCD corrections. Its expression at NLO can be written as [282, 283]

$$Y(x_t) = \eta_Y \cdot \frac{x_t}{8}\left(\frac{4-x_t}{1-x_t} + \frac{3x_t}{(1-x_t)^2}\mathrm{Ln}\, x_t\right), \tag{6.5.3}$$

where the factor $\eta_Y$ summarizes the QCD corrections ($\eta_Y = 1.012$). The function $Y_{\rm NL}$ represents the contribution of loop-diagrams involving internal charm-quark exchange and is known to NLO [280, 283] and recently to NNLO [293]. The charm contribution is also often denoted by $P_c(Y)$ and is related to $Y_{NL}$ analogous to the relation in Eq. (6.3.3). In the SM, the branching ratio for the SD part is written as [293, 294]

$$\mathrm{BR}(K_L \to \mu^+\mu^-)_{SM}(\mathrm{SD}) = \frac{N_K^2}{2\pi\,\Gamma_{K_L}}\left(\frac{m_\mu}{m_K}\right)^2\sqrt{1-\frac{4\,m_\mu^2}{m_K^2}}\, f_K^2 m_K^3 (\mathrm{Re}\,\Delta^K_{SM})^2, \tag{6.5.4}$$

where $N_K = G_F V_{us}^* V_{ud}$ and $\Gamma_{K_L}$ is the decay width of $K_L$. Before proceeding

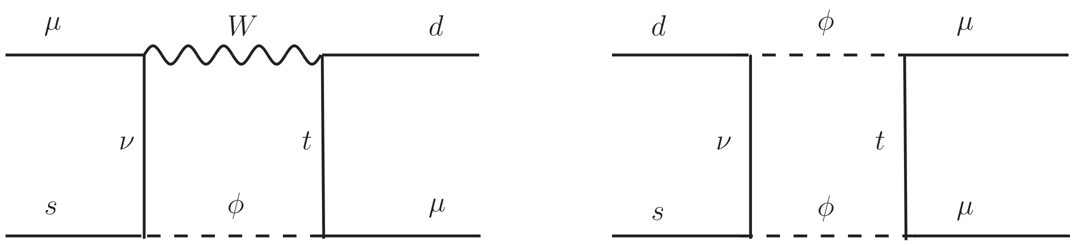


Figure 6.6: Feynman diagrams relevant for the decay $K_L \to \mu^+\mu^-$ induced by the scalar leptoquark $\phi$.

to discuss the constraints on leptoquark couplings from $K_L \to \mu^+\mu^-$, we give a description of the "operator basis" we use in the present and the next sections. The effective Hamiltonian for $K_L \to \mu^+\mu^-$ in Eq. (6.5.1) is written in the operator basis of $\{Q_{7V}, Q_{7A}\}$ following [294]. In what follows, we will switch to the $\{Q^K_{VLL}, Q^K_{VLR}\}$ operator basis. The operators in the two bases are written as

$$
\begin{aligned}
Q_{7V} &= (\bar{s}\gamma_\alpha(1-\gamma_5)d)(\bar{\mu}\gamma^\alpha\mu), \\
Q_{7A} &= (\bar{s}\gamma_\alpha(1-\gamma_5)d)(\bar{\mu}\gamma^\alpha\gamma_5\mu),
\end{aligned}
\tag{6.5.5}
$$

and

$$
\begin{aligned}
Q^K_{VLL} &= (\bar{s}\gamma_\alpha L d)(\bar{\mu}\gamma^\alpha L\mu), \\
Q^K_{VLR} &= (\bar{s}\gamma_\alpha L d)(\bar{\mu}\gamma^\alpha R\mu).
\end{aligned}
\tag{6.5.6}
$$

To change from the basis $\{Q_{7V}, Q_{7A}\}$ to the basis $\{Q^K_{VLL}, Q^K_{VLR}\}$, the following transformation rules hold:

$$
Q^K_{VLL} = \frac{1}{4}\left(Q_{7V} - Q_{7A}\right), \quad Q^K_{VLR} = \frac{1}{4}\left(Q_{7V} + Q_{7A}\right).
\tag{6.5.7}
$$

The scalar leptoquark $\phi$ contributes to the quark-level transition $\bar{s} \to \bar{d}\mu^+\mu^-$ at the leading order through loop diagrams. The Feynman diagrams relevant for $K_L \to \mu^+\mu^-$ are shown in Fig 6.6. These diagrams are similar to the ones calculated in the case of $b \to s\mu\mu$ in Ref. [234]. Correcting for the different quark content and coupling, and taking into account the prefactors in the definitions of the effective Hamiltonian for K and B system, we obtain the following NP Wilson coefficients of effective operators $Q^K_{VLL}$ and $Q^K_{VLR}$:

$$C^{K(new)}_{VLL} = -\frac{1}{8\pi^2}\frac{\lambda_t}{\lambda_u}\frac{m_t^2}{M_\phi^2}|\lambda^L_{t\mu}|^2 + \frac{\sqrt{2}}{64 G_F \pi^2 M_\phi^2}\frac{\xi_{ds}\,\xi^L_{\mu\mu}}{\lambda_u}, \tag{6.5.8}$$

$$C^{K(new)}_{VLR} = -\frac{1}{16\pi^2}\frac{\lambda_t}{\lambda_u}\frac{m_t^2}{M_\phi^2}|\lambda^R_{t\mu}|^2\left(\mathrm{Ln}\frac{M_\phi^2}{m_t^2} - f(x_t)\right) + \frac{\sqrt{2}}{64 G_F \pi^2 M_\phi^2}\frac{\xi_{ds}\,\xi^R_{\mu\mu}}{\lambda_u}, \tag{6.5.9}$$

where the function $f(x_t)$ depends on the top-quark mass and is given in Ref. [234] and we define

$$\xi^{L(R)}_{\ell\ell'} = \sum_i \lambda^{L(R)*}_{u_i\ell}\lambda^{L(R)}_{u_i\ell'}. \tag{6.5.10}$$

The one advantage we get by the change of basis is that the contribution of

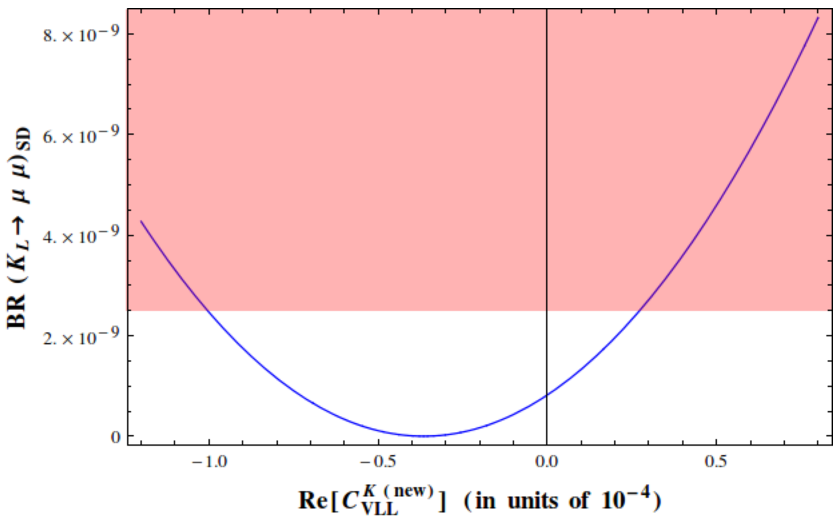


Figure 6.7: The dependence of BR($K_L \to \mu^+\mu^-$) on the Wilson coefficient $C^{K(new)}_{VLL}$. We have assumed one-operator dominance as discussed in the text. The red shaded area shows the disallowed values satisfying the conservative upper bound on BR$(K_L \to \mu^+\mu^-)_{\rm SD} \leq 2.5 \times 10^{-9}$.

right-handed interaction terms in the Lagrangian [Eq. (6.1.1)] is contained only in $C^{K(new)}_{VLR}$. After adding the leptoquark contribution to the SM value, the total SD branching ratio for the decay $K_L \to \mu^+\mu^-$ is given by

$$\begin{aligned}\mathrm{BR}(K_L \to \mu^+\mu^-)_{\mathrm{SD}} &= \frac{N_K^2}{2\pi\,\Gamma_{K_L}}\left(\frac{m_\mu}{m_K}\right)^2\sqrt{1-\frac{4\,m_\mu^2}{m_K^2}}f_K^2 m_K^3\lambda^{10}\left\{\frac{\mathrm{Re}\lambda_c}{\lambda}\frac{\alpha\,P_c(Y)}{2\pi\sin^2\theta_W\lambda_u}\right.\\ &\left.+\frac{1}{\lambda^5}\left(\mathrm{Re}\lambda_t\frac{\alpha\,Y(x_t)}{2\pi\sin^2\theta_W\lambda_u}+\frac{1}{4}\mathrm{Re}(C_{VLR}^{K(new)}-C_{VLL}^{K(new)})\right)\right\}^2,\end{aligned} \tag{6.5.11}$$

To simplify further analysis, we invoke the assumption that, except the SM contribution, only one of the NP operators contributes dominantly. This assumption helps us in determining the limits on the dominant Wilson coefficient from $\mathrm{BR}\,(K_L \to \mu^+\mu^-)_{\mathrm{SD}}$, and the generalization of this situation to incorporate more than one NP operator contribution is straight forward. Therefore, in what follows, we will ignore the contribution of the right-handed operator in further analysis. In Fig 6.7, we show the dependence of the SD part of $\mathrm{BR}(K_L \to \mu^+\mu^-)$ on $\mathrm{Re}\,C_{VLL}^{K(new)}$. Numerically, the bound on the Wilson coefficient reads $-1.00\times 10^{-4} < \mathrm{Re}\,C_{VLL}^{K(new)} < 0.27\times 10^{-4}$. We use the upper bound to constrain the generation-diagonal leptoquark couplings in the following way. Employing Eq. (6.5.8), the upper bound on the Wilson coefficient can be written in terms of model parameters as

$$\left(-\frac{1}{8\pi^2}\frac{\mathrm{Re}\,\lambda_{\mathrm{t}}}{\lambda_u}\frac{m_t^2}{M_\phi^2}|\lambda_{t\mu}^L|^2+\frac{\sqrt{2}}{64G_F\pi^2M_\phi^2}\frac{\mathrm{Re}\,\xi_{\mathrm{ds}}}{\lambda_u}\,\xi_{\mu\mu}^L\right) < 0.27\times 10^{-4}, \tag{6.5.12}$$

Assuming the worst possible case in which the bound on $\mathrm{Re}\,\xi_{\mathrm{ds}}$ from $K^+ \to \pi^+\nu\bar{\nu}$ (as obtained in section 6.3) is saturated, i.e., using $\mathrm{Re}\,\xi_{\mathrm{ds}} = 2.2\times 10^{-4}$ in the above equation, we get

$$\sqrt{|\lambda_{u\mu}^L|^2+|\lambda_{c\mu}^L|^2+\left(1+\frac{2.52}{(\frac{M_\phi}{1000\,\mathrm{GeV}})^2}\right)|\lambda_{t\mu}^L|^2} < 11.83, \tag{6.5.13}$$

We find that constraints from the SD branching ratio of $K_L \to \mu^+\mu^-$ are not severe and large $\sim O(1)$ generation-diagonal leptoquark couplings are allowed. In this context, we must mention that the above bound is in agreement with the constraint obtained in Ref. [234] while explaining the anomaly in $R_K$ in this model. We also note from Eq. (6.5.13) that the top contribution to $\bar{s} \to \bar{d}\mu^+\mu^-$

for the considered masses of the leptoquark ($\sim 1\,\text{TeV}$) is enhanced in contrast to the effects found in the case of $b \to s\mu^+\mu^-$ processes [234] where the top contribution is suppressed for the same choice of the leptoquark masses.

## 6.6 Constraints from LFV decay $K_L \to \mu^\mp e^\pm$

In this section, we discuss the effects of the leptoquark $\phi$ on the LFV process $K \to \mu^\mp e^\pm$. BNL E871 experiment has searched for this decay and provided an upper limit on $\text{BR}(K_L \to \mu^\mp e^\pm) < 4.7 \times 10^{-12}$ at 90% C.L. [295]. LFV processes are interesting because in the SM they are forbidden. Therefore any observation of such a process immediately indicates the presence of NP. The leptoquark $\phi$ can mediate $K_L \to \mu e$ decay through diagrams similar to those shown in Fig 6.6 with one of the $\mu$ lines replaced by $e$. After integrating out heavy particles, new effective operators relevant for $K_L \to \mu e$ are generated. The operators are similar to those in Eq. (6.5.6) but with one of the $\mu$ changed to $e$. The branching ratio in terms of the new Wilson coefficients $C^{\mu e}_{VLL}$ and $C^{\mu e}_{VLR}$ is given by [294]

$$\text{BR}(K_L \to \mu e) = \frac{N_K^2 f_K^2}{64\pi\Gamma_{K_L}} \left(\frac{m_\mu}{m_K}\right)^2 \left(1 - \frac{m_\mu^2}{m_K^2}\right)^2 \left(|C^{\mu e}_{VLL}|^2 + |C^{\mu e}_{VLR}|^2\right). \quad (6.6.1)$$

Adapting the results of Eq. (6.5.8) to the LFV case, we find

$$\begin{aligned} C^{\mu e}_{VLL} &= -\frac{1}{8\pi^2}\frac{\lambda_t}{\lambda_u}\frac{m_t^2}{M_\phi^2}(\lambda^L_{te}\lambda^{L*}_{t\mu}) + \frac{\sqrt{2}}{64 G_F \pi^2 M_\phi^2}\frac{\xi_{ds}\,\xi^L_{\mu e}}{\lambda_u}, && (6.6.2)\\ C^{\mu e}_{VLR} &= -\frac{1}{16\pi^2}\frac{\lambda_t}{\lambda_u}\frac{m_t^2}{M_\phi^2}(\lambda^R_{t\mu}\lambda^R_{te})\left(\text{Ln}\frac{M_\phi^2}{m_t^2} - f(x_t)\right) \\ &\quad + \frac{\sqrt{2}}{64 G_F \pi^2 M_\phi^2}\frac{\xi_{ds}\,\xi^R_{\mu e}}{\lambda_u}. && (6.6.3)\end{aligned}$$

Using the current experimental bound on $K_L \to \mu e$, we get $[|C^{\mu e}_{VLL}|^2 + |C^{\mu e}_{VLR}|^2]^{1/2} < 3.9 \times 10^{-6}$. Following a similar analysis as done in section 6.5 for the case of $K_L \to \mu\mu$, we obtain the constraints on the leptoquark couplings,

$$\sqrt{(\lambda^L_{u\mu}\lambda^L_{ue}) + (\lambda^L_{c\mu}\lambda^L_{ce}) + \left(1 + \frac{2.52}{(\frac{M_\phi}{1000\,\text{GeV}})^2}\right)(\lambda^L_{t\mu}\lambda^L_{te})} \;<\; 4.49, \quad (6.6.4)$$

where the top contribution is again enhanced. For simplicity, we assumed the couplings to be real. Here, we would like to mention that the same Wilson coefficients also contribute to other LFV processes such as $K \to \pi\mu e$. However, as pointed out in Ref. [294], the constraints on Wilson coefficients $(|C^{\mu e}_{VLL}|^2 + |C^{\mu e}_{VLR}|^2)^{1/2}$ are about an order of magnitude weaker than the one from $K_L \to \mu^{\mp} e^{\pm}$. Therefore, experimental data on $K \to \pi\mu e$ do not improve the constraints obtained in Eq. (6.6.4).

## 6.7 Results and Discussion

In light of several anomalies observed in semileptonic B decays, often explained by invoking leptoquark NP models, we have studied a scalar leptoquark model in the context of rare decays of kaons and neutral kaon mixing in this chapter. The model is interesting because it can provide one of the possible explanations for the observed discrepancies in semileptonic B decays. We examined the effects of leptoquark contributions to several kaon processes involving $K^0 - \bar{K^0}$ mixing, $K^+ \to \pi^+ \nu\bar{\nu}$, $K_L \to \pi^0 \nu\bar{\nu}$, $K_L \to \mu^+\mu^-$, and LFV decay $K_L \to \mu^{\mp} e^{\pm}$. Working in the framework of effective field theory, we have discussed the effective operators generated, and written down the explicit expressions for the corresponding Wilson coefficient in terms of the leptoquark couplings. Using the present experimental information on these decays, we derived bounds on the couplings relevant for kaon processes. We found that the constraints from $K^0 - \bar{K^0}$ on the real and imaginary parts of left-handed coupling $\xi_{ds}$ are $\sim O(10^{-2})$. However, the same set of couplings can also be constrained from BR($K^+ \to \pi^+ \nu\bar{\nu}$), BR($K_L \to \pi^0 \nu\bar{\nu}$), and it was found that constraints from the rare process BR($K^+ \to \pi^+ \nu\bar{\nu}$) are about 2 orders of magnitude more severe than those obtained from the mixing of neutral kaons. In fact, the decay BR($K^+ \to \pi^+ \nu\bar{\nu}$) gives the most stringent constraints on the leptoquark couplings among all the processes studied in this chapter and therefore is the most interesting observable to test the NP effects of the scalar leptoquark in the kaon sector. Assuming a one-operator dominance scenario, we constrained the NP Wilson coefficient contributing to the rate of

$K_L \to \mu^+\mu^-$. We further used the bounds on the NP Wilson coefficient to obtain the constraints on generation-diagonal leptoquark couplings. We found that the present measured value of BR$(K_L \to \mu^+\mu^-)$ allows generation-diagonal coupling of the leptoquark to be $\sim O(1)$. The constraint on the combination of generation-diagonal couplings from $K_L \to \mu^+\mu^-$ is in agreement with the one obtained in Ref. [234] for explaining experimental data on $R_K$. However, whereas the top contribution to $b \to s\mu^+\mu^-$ is suppressed, we found that in the case of $\bar{s} \to \bar{d}\mu^+\mu^-$ the top contribution is enhanced for the considered range of leptoquark masses. We also did a similar analysis for the case of the LFV decay $K_L \to \mu^\mp e^\pm$, which involves generation-diagonal as well as off-diagonal couplings. We found that present experimental limits on BR$\,(K_L \to \mu^\mp e^\pm)$ do not provide very strong constraints and involved couplings can be as large as $\sim O(1)$.

# Chapter 7

# Summary

In recent years, a great amount of experimental data on flavor physics has been accumulated which has contributed to a better understanding of flavor structure of the SM and beyond it. A more precise study of rare FCNC decays of hadrons is now possible at collider experiments such as the LHC, which are capable of providing sufficient luminosity to overcome the problem of low statistics. Interestingly, the recent measurements reported on flavor changing decays of b quark show several deviations from the SM predictions, which have received a lot of attention theoretically. In particular, a significant deviation has been reported for the observable $R_K$, which, if true, signals the violation of lepton universality. Another set of remarkable deviations has been seen in the decay rates of $B \to D^{(*)}\tau\nu$, which is more interesting considering that these decays proceeds at the tree level in the SM, and the observation of deviation is against the general expectation that the first sign of NP in flavor physics is most likely to come from the loop induced processes. The full angular analysis of $B \to K^*\ell^+\ell^-$ performed by the LHC$b$ collaboration also indicates deviations from the SM expectations.

In this thesis, in Chapter 2, we have studied the four-body angular distribution of the rare decay $B \to K^*\ell^+\ell^-$, which is one of the most promising candidates to search for NP due to multiple observables it offers. In order to predict the theoretical value of the observables, the knowledge of hadronic form factors is required. The estimates of hadronic effects involve sizeable uncertainties, thereby inducing the errors in the theoretical predictions. This issue calls for measuring observables which are more or less free from such hadronic effects. We have shown that similar to the celebrated zero crossing of the forward-backward asymmetry of the lepton pair, $A_{\rm FB}$, the zero crossings of the observables $P_4'$ and $P_5'$ are also free from form factors in the large recoil region and heavy quark limit. We also proposed a new observable, $O_T^{\rm L,R}$, which has a unique property that its zero crossing, in the SM-like operator basis, coincides with the zero of $A_{\rm FB}$. But, in the presence of NP (for example, finite contribution of right-handed operators), the zero crossings of $O_T^{\rm L,R}$ and $A_{\rm FB}$ shift differently. This feature can be useful to probe NP once the precise measurements on the value of zero crossings are available. All the zero crossings of the considered observables depend on the Wilson coefficients and the mass of the B meson, and therefore are sensitive to NP and theoretically cleaner observables to measure experimentally. We have pointed out that in the heavy quark and large recoil limit, the zero crossings of $A_{\rm FB}$, $P_5'$, $P_4'$, and $O_T^{\rm L,R}$ are correlated in the SM. The relations, in the considered approximation, are also independent of form factors. Since the zeros and the relation among them are functions of the Wilson coefficients only, their measurement can be used to constrain the NP contribution present in the Wilson coefficients. We have discussed the constraints on the $C_7^{\rm NP} - C_9^{\rm NP}$ plane, stemming from the zeros of these observables. We considered multiple BSM scenarios, which are favoured over the SM by the present global fits to present data on $b \to s\ell^+\ell^-$, and showed that precise measurements of the zero crossings have the potential of differentiating between different BSM cases. Interestingly, the LHC$b$ collaboration has started measuring the zero crossing of these observables. Current measurements still have large uncertainties to have any conclusive result on the presence of NP. But, high precision data on these zeros in the future can certainly provide crucial information in this regard.

In Chapter 3, we have studied the semileptonic $b \to s$ baryonic decay $\Lambda_b \to \Lambda\ell^+\ell^-$. The angular distribution of the final state, similar to mesonic counterpart $B \to K^*\ell^+\ell^-$, gives access to many observables. The analysis of these observables can offer information which can complement the current search of NP in $b \to s$ transition. We have listed the angular observables and asymmetries which can be used to extract all the angular coefficients independently. In order to probe the short-distance NP, it is necessary to focus on observables which do not depend on hadronic form factors or are largely insensitive to them. With this in mind, we have presented three new observables [$\mathcal{T}_1(q^2)$, $\mathcal{T}_2(q^2)$, and $\mathcal{T}_3(q^2)$], which can be experimentally probed. The new observables are constructed such that the zero crossings of these observables lie in the large $q^2$ region. In the HQET and large $q^2$ approximation, these zeros turn out to be less sensitive to the form factors (especially the zero of $\mathcal{T}_1(q^2)$), and therefore their measurement holds a better chance of probing the NP effects in $b \to s$ transitions.

In Chapter 4 and 5, we have presented an NP explanation of the flavor anomalies seen in $B$ decays in the framework of $E_6$ motivated left-right symmetric gauge theories. $E_6$ provides one of the natural, anomaly free choices for grand unified theories which have a unique virtue of unifying matter–leptons and quarks. Due to the presence of new particles in the theory, the phenomenology of low energy subgroups is quite rich and interesting. We have considered the maximal subgroup, $\mathrm{SU(3)_C}\times \mathrm{SU(3)_L} \times \mathrm{SU(3)_R}$, of $E_6$. The $SU(3)_{(L,R)}$ in the maximal subgroup can further break into $SU(2)_{(L,R)} \times U(1)_{(L,R)}$. Among the three possible options for choosing $SU(2)_R$, in Chapter 4, we have considered the choice where $(h^c, u^c)$ is assigned to the $SU(2)_R$ doublet. This subgroup is referred to as the Alternative Left-Right Symmetric Model (ALRSM). We have studied ALRSM in the context of charged decay modes $B \to D^{(*)}\tau\nu$, and have shown that the enhanced decay rates reported by the Belle, BaBar and LHC$b$ collaborations can be explained with new contributions involving the tree level exchange of scalar leptoquark. We have discussed the constraints on the NP couplings coming from $B \to \tau\nu$, $D_{(s)} \to \tau\nu$ and $D^0 - \bar{D}^0$ in detail. The constraints are compatible with the size of the couplings required to explain the data. In Chapter 5, we have studied $E_6$ motivated Neutral Left-Right Symmetric Model (NLRSM), which corresponds to the choice where $(h^c, d^c)_L$ is chosen as the $SU(2)_R$ doublet. Working in this framework, we have shown that anomalies observed in $R_K$ and $R_{D^{(*)}}$ can be simultaneously explained. In this model, $R_{D^{(*)}}$ can be explained via new contribution from tree level Feynman diagrams involving exchange of scalar leptoquarks, while $R_K$ can be explained by the one loop diagrams involving leptoquarks. We have also shown that the anomalous magnetic moment of the muon can also be explained simultaneously. The analysis is compatible with present measurements of other flavor observables like $B^0 - \bar{B}^0$ and $D^0 - \bar{D}^0$ mixings, and (semi) leptonic decays of $B$ and $D$.

In Chapter 6, noticing that NP models having a scalar leptoquark $\phi$ of charge $-1/3$ with $(\mathrm{SU}(3)_\mathrm{C}, \mathrm{SU}(2)_\mathrm{L})$ quantum numbers $(3, 1)$ are capable of explaining the flavor anomalies in semileptonic B decays, we have investigated the constraints from the kaon sector. This study provides the information on the allowed size of the couplings of the scalar leptoquark, and helps in shedding light on the kaon observables where promising signals of the considered leptoquark can be expected. We have analysed the effects of the leptoquark on the neutral kaon mixing, rare decays $K^+ \to \pi^+\nu\bar{\nu}$, $K_L \to \pi^0\nu\bar{\nu}$, $K_L \to \mu^+\mu^-$, and lepton flavor violating decay $K_L \to \mu^\mp e^\pm$. The scalar leptoquark $\phi$ contributes to $K^0 - \bar{K}^0$ via new box diagrams involving internal exchange of leptoquark and neutrinos. We noticed that constraints from $K^0 - \bar{K}^0$ on the left-handed coupling $\xi_{ds}$ are $\sim O(10^{-2})$. On the other hand, scalar leptoquark $\phi$ contributes to rare decays $K^+ \to \pi^+\nu\bar{\nu}$ and $K_L \to \pi^0\nu\bar{\nu}$ via tree level exchange. We found that the constraints from $\mathrm{BR}(K^+ \to \pi^+\nu\bar{\nu})$ turn out be about 2 orders of magnitude tighter. We then discussed the effects of leptoquark $\phi$ on the decay $K_L \to \mu^+\mu^-$. The leptoquark $\phi$ contributes to $K_L \to \mu^+\mu^-$ via box diagrams. We have found that present measurement of $\mathrm{BR}(K_L \to \mu^+\mu^-)$ allows generation-diagonal coupling of the leptoquark to be $\sim O(1)$, which is compatible with the required size of the relevant couplings needed to explain the B decay anomalies. We also studied the leptoquark effects on the LFV decay $K_L \to \mu^\mp e^\pm$, which allows to constrain the off-diagonal couplings as well. We found that the present experimental data on $K_L \to \mu^\mp e^\pm$ allows the involved coupling to be $\sim O(1)$. Therefore, at present, the tightest bounds on the leptoquark couplings in kaon-related observables are from the decay $\mathrm{BR}(K^+ \to \pi^+\nu\bar{\nu})$, and therefore appears to be the most interesting observable to test the NP effects of scalar leptoquark in the kaon sector.

In the end, we would like to conclude with the following remarks. At present, in the face of non-observation of new particles at direct collider searches, and with the lack of any unambiguous signal of NP in flavor precision data, the task of uncovering NP seems to be challenging. However, there are some tantalizing hints of NP in the flavor sector, as discussed in this thesis, which demand for a more careful scrutiny of these signals in order to probe NP. The advancement of flavor physics has always banked on close interplay and cooperation between experiment and theory. On the theory side, there has been immense progress in calculating the low-energy observables with high precision. The theoretical uncertainties in the estimation of several observables have reduced significantly, and the current values are sufficiently accurate to be compared with the high-precision experimental data to detect any discrepancy between the SM and experiment. On the other hand, very high-luminosity particle physics experiments are now able to measure the flavor-precision observables with great accuracy and large statistics. With the upgraded LHC, and the possible future experimental facilities such as super B-factories, capable of providing higher luminosity, the level of precision in the measurements of low-energy observables is certainly going to improve. Hopefully, with these improvements, flavor physics will be able to either provide unambiguous signs of NP or give us a clear direction towards this goal.

# Appendix

## A A compendium of effective operators

Here, we present a partial list of the effective operators relevant for weak decays of hadrons given in Refs. [264] (for a recent review, see [296] ).

### A.1 The effective $\Delta F = 1$ nonleptonic operators

**Current-Current operators**

$$O_1(\Delta S = 1) = (\bar{s}_i \gamma^\mu \mathrm{L} u_j)\,(\bar{u}_j \gamma_\mu \mathrm{L} d_i), \tag{A.1}$$
$$O_2(\Delta S = 1) = (\bar{s}_i \gamma^\mu \mathrm{L} u_i)\,(\bar{u}_j \gamma_\mu \mathrm{L} d_j), \tag{A.2}$$

$$O_1(\Delta C = 1) = (\bar{s}_i \gamma^\mu \mathrm{L} c_j)\,(\bar{u}_j \gamma_\mu \mathrm{L} d_i), \tag{A.3}$$
$$O_2(\Delta C = 1) = (\bar{s}_i \gamma^\mu \mathrm{L} c_i)\,(\bar{u}_j \gamma_\mu \mathrm{L} d_j), \tag{A.4}$$

$$O_1(\Delta B = 1) = (\bar{b}_i \gamma^\mu \mathrm{L} c_j)\,(\bar{u}_j \gamma_\mu \mathrm{L} d_i), \tag{A.5}$$
$$O_2(\Delta B = 1) = (\bar{b}_i \gamma^\mu \mathrm{L} c_i)\,(\bar{u}_j \gamma_\mu \mathrm{L} d_j). \tag{A.6}$$

**QCD-Penguin operators**

$$O_3 = (\bar{s}_i \gamma^\mu \mathrm{L} b_i) \sum_q (\bar{q}_j \gamma_\mu \mathrm{L} q_j), \tag{A.7}$$
$$O_4 = (\bar{s}_i \gamma^\mu \mathrm{L} b_j) \sum_q (\bar{q}_j \gamma_\mu \mathrm{L} q_i), \tag{A.8}$$

$$O_5 = (\bar{s}_i\gamma^\mu \mathrm{L} b_i)\sum_q(\bar{q}_j\gamma_\mu \mathrm{R} q_j), \tag{A.9}$$

$$O_6 = (\bar{s}_i\gamma^\mu \mathrm{L} b_j)\sum_q(\bar{q}_j\gamma_\mu \mathrm{R} q_i). \tag{A.10}$$

**Electroweak-Penguin operators**

$$O_7^{\mathrm{EW}} = \frac{3}{2}(\bar{s}_i\gamma^\mu \mathrm{L} b_i)\sum_q e_q(\bar{q}_j\gamma_\mu \mathrm{R} q_j), \tag{A.11}$$

$$O_8^{\mathrm{EW}} = \frac{3}{2}(\bar{s}_i\gamma^\mu \mathrm{L} b_j)\sum_q e_q(\bar{q}_j\gamma_\mu \mathrm{R} q_i), \tag{A.12}$$

$$O_9^{\mathrm{EW}} = \frac{3}{2}(\bar{s}_i\gamma^\mu \mathrm{L} b_i)\sum_q e_q(\bar{q}_j\gamma_\mu \mathrm{L} q_j), \tag{A.13}$$

$$O_{10}^{\mathrm{EW}} = \frac{3}{2}(\bar{s}_i\gamma^\mu \mathrm{L} b_j)\sum_q e_q(\bar{q}_j\gamma_\mu \mathrm{L} q_i). \tag{A.14}$$

**Magnetic-Penguin operators**

$$O_7 = \frac{e}{16\pi^2}m_b(\bar{s}_i\sigma^{\mu\nu}\mathrm{R} b_i)F_{\mu\nu}, \tag{A.15}$$

$$O_8 = \frac{g_s}{16\pi^2}m_b(\bar{s}_i T^a_{ij}\sigma^{\mu\nu}\mathrm{R} b_j)G^a_{\mu\nu}. \tag{A.16}$$

## A.2 $\Delta S = 2$ and $\Delta B = 2$ operators

$$O(\Delta S = 2) = (\bar{s}_i\gamma^\mu \mathrm{L} d_i)(\bar{s}_j\gamma_\mu \mathrm{L} d_j), \tag{A.17}$$

$$O(\Delta B = 2) = (\bar{b}_i\gamma^\mu \mathrm{L} d_i)(\bar{b}_j\gamma_\mu \mathrm{L} d_j). \tag{A.18}$$

## A.3 Semileptonic operators

$$O_{9V}^{\ell} = (\bar{s}_i\gamma^\mu \mathrm{L} b_i)(\bar{\ell}\gamma_\mu\ell), \tag{A.19}$$

$$O_{10A}^{\ell} = (\bar{s}_i\gamma^\mu \mathrm{L} b_i)(\bar{\ell}\gamma_\mu\gamma_5\ell), \tag{A.20}$$

$$O(\bar{\nu}\nu) = (\bar{s}_i\gamma^\mu \mathrm{L} b_i)\,(\bar{\nu}\gamma_\mu \mathrm{L}\nu). \tag{A.21}$$

where $i, j$ are the color indices and $\mathrm{L/R} = (1 \mp \gamma_5)/2$.

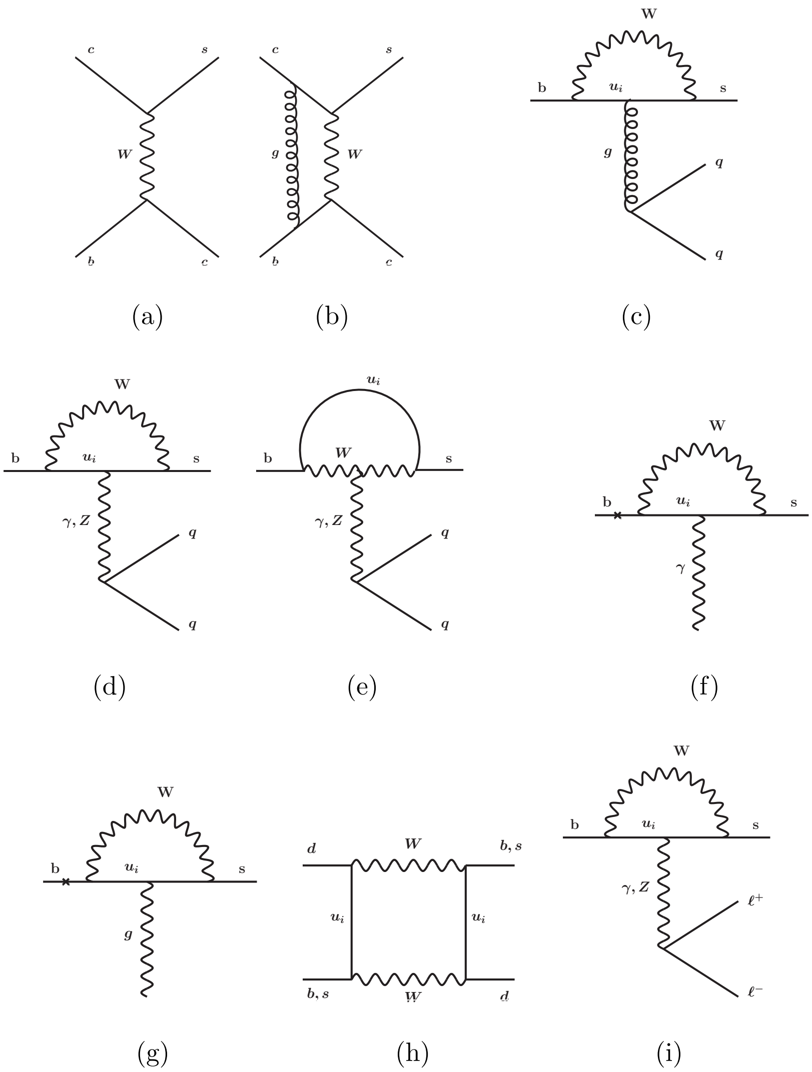


Figure A: Representative Feynman diagrams in the full theory. (a), (b) the current-current diagrams, (c) QCD-penguin diagram, (d), (e) electroweak penguin diagram, (f) QED magnetic penguin diagram, (g) QCD magnetic penguin diagram, (h) $\Delta F = 2$ box diagram, and (i) semileptonic penguin diagram.

# B Form Factors for $B \to K^*$

Here, we give $q^2$ dependence of the form factors for the process $B \to K^*$. We have employed two sets of form factors ($V$, $A_{0,1,2}$, $T_{1,2,3}$) [75] and ($\xi_\perp$, $\xi_\parallel$) [79] for numerical evaluation of the zeroes of the angular observables in chapter 2. The form factors ($V$, $A_{0,1,2}$, $T_{1,2,3}$) are valid in full kinematical range of $q^2$, while the form factors ($\xi_\perp$, $\xi_\parallel$) are applicable in the large recoil (low-$q^2$) region. The parametrization of $q^2$ dependence of $V$, $A_{0,1,2}$, $T_{1,2,3}$ is given by [75]

$$V(q^2) = \frac{r_1}{1-q^2/m_R^2} + \frac{r_2}{1-q^2/m_{\rm fit}^2}, \tag{B.1}$$
$$A_0(q^2) = \frac{r_1}{1-q^2/m_R^2} + \frac{r_2}{1-q^2/m_{\rm fit}^2}, \tag{B.2}$$
$$A_1(q^2) = \frac{r_2}{1-q^2/m_{\rm fit}^2}, \tag{B.3}$$
$$A_2(q^2) = \frac{r_1}{1-q^2/m_{\rm fit}^2} + \frac{r_2}{(1-q^2/m_{\rm fit}^2)^2}, \tag{B.4}$$
$$T_1(q^2) = \frac{r_1}{1-q^2/m_R^2} + \frac{r_2}{1-q^2/m_{\rm fit}^2}, \tag{B.5}$$
$$T_2(q^2) = \frac{r_2}{1-q^2/m_{\rm fit}^2}, \tag{B.6}$$
$$\tilde{T}_3(q^2) = \frac{r_1}{1-q^2/m_{\rm fit}^2} + \frac{r_2}{(1-q^2/m_{\rm fit}^2)^2}, \tag{B.7}$$

where form factor $T_3$ is related to $\tilde{T}_3$ through the following relation

$$T_3(q^2) = \frac{m_B^2 - m_{K^*}^2}{q^2}[\tilde{T}_3(q^2) - T_2(q^2)]. \tag{B.8}$$

The values of the parameters $r_1$, $r_2$, $m_R^2$, and $m_{\rm fit}^2$ are given in Ref. [75], and are listed in the Table below.

| | $r_1$ | $m_R^2$ | $r_2$ | $m_{\rm fit}^2$ |
|---|---|---|---|---|
| $V(q^2)$ | 0.923 | 28.30 | -0.511 | 49.40 |
| $A_0(q^2)$ | 1.364 | 27.88 | -0.990 | 36.78 |
| $A_1(q^2)$ | | | 0.290 | 40.38 |
| $A_2(q^2)$ | -0.084 | | 0.342 | 52.00 |
| $T_1(q^2)$ | 0.823 | 28.30 | -0.491 | 46.31 |
| $T_2(q^2)$ | | | 0.333 | 41.41 |
| $\tilde{T}_3(q^2)$ | -0.036 | | 0.368 | 48.10 |

Table A: Values of the fit parameters for $B \to K^*$ form factors.

On the other hand, for the form factors $\xi_\perp$, $\xi_\parallel$, we use the following parametrization [78]

$$\xi_\perp(q^2) = \xi_\perp(0)\left(\frac{1}{1-q^2/m_B^2}\right)^2, \tag{B.9}$$

$$\xi_\parallel(q^2) = \xi_\parallel(0)\left(\frac{1}{1-q^2/m_B^2}\right)^3, \tag{B.10}$$

where $\xi_\perp(0) = 0.266 \pm 0.032$ and $\xi_\parallel(0) = 0.118 \pm 0.008$ [74].

# C $\Lambda_b \to \Lambda$ Helicity Form Factors

Here we provide the relations of helicity amplitudes and $\Lambda_b \to \Lambda$ form factors for a particular Dirac spinor $[u\left(p(k), s_{\Lambda_b(\Lambda)}\right)]$ representation as obtained in Ref. [124]. The helicity amplitudes $H_\lambda^{V,A,T,T5}$ are defined by

$$H_\lambda^\kappa(s_{\Lambda_b}, s_\Lambda) \equiv \epsilon^*(\lambda) \cdot \langle \Lambda(k, s_\Lambda|\bar{s}\Gamma^\kappa b|\Lambda_b(p, s_{\Lambda_b}\rangle, \tag{C.1}$$

where $s_{\Lambda_{(b)}}$ are the spin vectors associated with the baryons; $\epsilon^*(\lambda = t, +, -, 0)$ are virtual polarization vectors with $q.\epsilon(\pm) = 0 = q.\epsilon(0)$; and $\Gamma^\kappa = \gamma^\mu$, $\gamma^\mu\gamma_5$, $i\sigma^{\mu\nu}q_\nu$, and $i\sigma^{\mu\nu}q_\nu\gamma_5$ correspond to helicity amplitudes $H_\lambda^V$, $H_\lambda^{A,}$, $H_\lambda^T$, and $H_\lambda^{T5}$, respectively.

For the vector current, the corresponding helicity amplitudes $H_i^V(s_{\Lambda_b}, s_\Lambda)$ in terms of helicity form factors $f_t^V$, $f_0^V$, $f_\perp^V$ are given by

$$H_t^V(1/2,1/2) = H_t^V(-1/2,-1/2) = f_t^V(q^2)\frac{m_{\Lambda_b} - m_\Lambda}{\sqrt{q^2}}\sqrt{s_+}\,, \tag{C.2}$$

$$H_0^V(1/2,1/2) = H_0^V(-1/2,-1/2) = f_0^V(q^2)\frac{m_{\Lambda_b} + m_\Lambda}{\sqrt{q^2}}\sqrt{s_-}\,, \tag{C.3}$$

$$H_+^V(-1/2,1/2) = H_-^V(1/2,-1/2) = -\,f_\perp^V(q^2)\sqrt{2s_-}\,. \tag{C.4}$$

For the axial-vector current, the analogous expressions for the corresponding helicity amplitudes $H_\lambda^A(s_{\Lambda_b}, s_\Lambda)$ are given by

$$H_t^A(1/2,1/2) = -H_t^A(-1/2,-1/2) = f_t^A(q^2)\frac{m_{\Lambda_b} + m_\Lambda}{\sqrt{q^2}}\sqrt{s_-}\,, \tag{C.5}$$

$$H_0^A(1/2,1/2) = -H_0^A(-1/2,-1/2) = f_0^A(q^2)\frac{m_{\Lambda_b} - m_\Lambda}{\sqrt{q^2}}\sqrt{s_+}\,, \tag{C.6}$$

$$H_+^A(-1/2,1/2) = -H_-^A(1/2,-1/2) = -\,f_\perp^A(q^2)\sqrt{2s_+}\,. \tag{C.7}$$

For the tensor current, the corresponding nonzero helicity amplitudes $H_\lambda^T(s_{\Lambda_b}, s_\Lambda)$ involve two form factors $f_0^T$ and $f_\perp^T$ only

$$H_0^T(1/2,1/2) = H_0^T(-1/2,-1/2) = -f_0^T(q^2)\sqrt{q^2}\sqrt{s_-}\,, \tag{C.8}$$

$$H_+^T(-1/2,1/2) = H_-^T(1/2,-1/2) = f_\perp^T(q^2)(m_{\Lambda_b}+m_\Lambda)\sqrt{2s_-}\,. \tag{C.9}$$

The expressions for nonzero $H_\lambda^{T_5}(s_{\Lambda_b}, s_\Lambda)$ corresponding to pseudo-tensor current involve two more form factors $f_0^{T_5}$ and $f_\perp^{T_5}$

$$H_0^{T_5}(1/2,1/2) = -H_0^{T_5}(-1/2,-1/2) = f_0^{T_5}(q^2)\sqrt{q^2}\sqrt{s_+}\,, \tag{C.10}$$

$$H_+^{T_5}(-1/2,1/2) = -H_-^{T_5}(1/2,-1/2) = -f_\perp^{T_5}(q^2)(m_{\Lambda_b}-m_\Lambda)\sqrt{2s_+}\,. \tag{C.11}$$

# Bibliography


[1] S. L. Glashow, "*Partial Symmetries of Weak Interactions*," Nucl. Phys. **22** (1961) 579–588.

[2] S. Weinberg, "*A Model of Leptons*," Phys. Rev. Lett. **19** (1967) 1264–1266.

[3] A. Salam, "*Weak and Electromagnetic Interactions*," Conf. Proc. **C680519** (1968) 367–377.

[4] **ATLAS**, G. Aad *et al.*, "*Observation of a new particle in the search for the Standard Model Higgs boson with the ATLAS detector at the LHC*," Phys. Lett. **B716** (2012) 1–29, `arXiv:1207.7214`.

[5] **CMS**, S. Chatrchyan *et al.*, "*Observation of a new boson at a mass of 125 GeV with the CMS experiment at the LHC*," Phys. Lett. **B716** (2012) 30–61, `arXiv:1207.7235`.

[6] P. W. Higgs, "*Broken Symmetries and the Masses of Gauge Bosons*," Phys. Rev. Lett. **13** (1964) 508–509.

[7] N. Cabibbo, "*Unitary Symmetry and Leptonic Decays*," Phys. Rev. Lett. **10** (1963) 531–533.

[8] M. Kobayashi and T. Maskawa, "*CP Violation in the Renormalizable Theory of Weak Interaction*," Prog. Theor. Phys. **49** (1973) 652–657.

[9] **Particle Data Group**, K. A. Olive *et al.*, "*Review of Particle Physics*," Chin. Phys. **C38** (2014) 090001.

[10] L. Wolfenstein, "*Parametrization of the Kobayashi-Maskawa Matrix*," Phys. Rev. Lett. **51** (1983) 1945.

[11] C. Jarlskog, "*Commutator of the Quark Mass Matrices in the Standard Electroweak Model and a Measure of Maximal CP Violation*," Phys. Rev. Lett. **55** (1985) 1039.

[12] K. G. Wilson, "*Nonlagrangian models of current algebra*," Phys. Rev. **179** (1969) 1499–1512.

[13] K. G. Wilson and W. Zimmermann, "*Operator product expansions and composite field operators in the general framework of quantum field theory*," Commun. Math. Phys. **24** (1972) 87–106.

[14] W. Zimmermann, "*Normal products and the short distance expansion in the perturbation theory of renormalizable interactions*," Annals Phys. **77** (1973) 570–601. [Lect. Notes Phys.558,278(2000)].

[15] D. J. Gross and F. Wilczek, "*Ultraviolet Behavior of Nonabelian Gauge Theories*," Phys. Rev. Lett. **30** (1973) 1343–1346.

[16] H. D. Politzer, "*Reliable Perturbative Results for Strong Interactions?*," Phys. Rev. Lett. **30** (1973) 1346–1349.

[17] T. Mannel, "*Effective Field Theories in Flavor Physics*," Springer Tracts Mod. Phys. **203** (2004) 1–175.

[18] A. G. Grozin, "*Introduction to the heavy quark effective theory. part 1*," `arXiv:hep-ph/9908366`.

[19] T. Mannel, "*Review of heavy quark effective theory*," in *Heavy quarks at fixed target. Proceedings, Workshop, St. Goar, Germany, October 3-6, 1996*, pp. 107–129. 1996. `arXiv:hep-ph/9611411`.

[20] M. B. Wise, "*Heavy quark physics: Course*," in *Probing the standard model of particle interactions. Proceedings, Summer School in Theoretical Physics, NATO Advanced Study Institute, 68th session, Les Houches, France, July 28-September 5, 1997. Pt. 1, 2*, pp. 1051–1089. 1997. `arXiv:hep-ph/9805468`.

[21] G. 't Hooft, "*A Planar Diagram Theory for Strong Interactions*," Nucl. Phys. **B72** (1974) 461.

[22] E. Witten, "*Baryons in the 1/n Expansion*," Nucl. Phys. **B160** (1979) 57–115.

[23] E. E. Jenkins, "*Large N(c) baryons*," Ann. Rev. Nucl. Part. Sci. **48** (1998) 81–119, arXiv:hep-ph/9803349.

[24] V. A. Novikov, L. B. Okun, M. A. Shifman, A. I. Vainshtein, M. B. Voloshin, and V. I. Zakharov, "*Charmonium and Gluons: Basic Experimental Facts and Theoretical Introduction*," Phys. Rept. **41** (1978) 1–133.

[25] E. de Rafael, "*An Introduction to sum rules in QCD: Course*," in *Probing the standard model of particle interactions. Proceedings, Summer School in Theoretical Physics, NATO Advanced Study Institute, 68th session, Les Houches, France, July 28-September 5, 1997. Pt. 1, 2*, pp. 1171–1218. 1997. arXiv:hep-ph/9802448.

[26] P. Colangelo and A. Khodjamirian, "*QCD sum rules, a modern perspective*," arXiv:hep-ph/0010175.

[27] A. J. Buras, "*Weak Hamiltonian, CP violation and rare decays*," in *Probing the standard model of particle interactions. Proceedings, Summer School in Theoretical Physics, NATO Advanced Study Institute, 68th session, Les Houches, France, July 28-September 5, 1997. Pt. 1, 2*, pp. 281–539. 1998. arXiv:hep-ph/9806471. http://alice.cern.ch/format/showfull?sysnb=0282793.

[28] J. H. Christenson, J. W. Cronin, V. L. Fitch, and R. Turlay, "*Evidence for the 2 pi Decay of the k(2)0 Meson*," Phys. Rev. Lett. **13** (1964) 138–140.

[29] S. L. Glashow, J. Iliopoulos, and L. Maiani, "*Weak Interactions with Lepton-Hadron Symmetry*," Phys. Rev. **D2** (1970) 1285–1292.

[30] **BaBar**, J. P. Lees *et al.*, "*Evidence for an excess of $\bar{B} \to D^{(*)}\tau^-\bar{\nu}_\tau$ decays*," Phys. Rev. Lett. **109** (2012) 101802, arXiv:1205.5442.

[31] **BaBar**, J. P. Lees *et al.*, "*Measurement of an Excess of $\bar{B} \to D^{(*)}\tau^-\bar{\nu}_\tau$ Decays and Implications for Charged Higgs Bosons*," Phys. Rev. **D88** (2013) no. 7, 072012, arXiv:1303.0571.

[32] **Belle**, Y. Sato *et al.*, "*Measurement of the branching ratio of $\bar{B}^0 \to D^{*+}\tau^-\bar{\nu}_\tau$ relative to $\bar{B}^0 \to D^{*+}\ell^-\bar{\nu}_\ell$ decays with a semileptonic tagging method*," Phys. Rev. **D94** (2016) no. 7, 072007, arXiv:1607.07923.

[33] **LHCb**, R. Aaij *et al.*, "*Measurement of the ratio of branching fractions $\mathcal{B}(\bar{B}^0 \to D^{*+}\tau^-\bar{\nu}_\tau)/\mathcal{B}(\bar{B}^0 \to D^{*+}\mu^-\bar{\nu}_\mu)$*," Phys. Rev. Lett. **115** (2015) no. 11, 111803, arXiv:1506.08614. [Addendum: Phys. Rev. Lett.115,no.15,159901(2015)].

[34] **LHCb**, R. Aaij *et al.*, "*Test of lepton universality using $B^+ \to K^+\ell^+\ell^-$ decays*," Phys. Rev. Lett. **113** (2014) 151601, arXiv:1406.6482.

[35] C. Bobeth, G. Hiller, and G. Piranishvili, "*Angular distributions of $\bar{B} \to \bar{K}\ell^+\ell^-$ decays*," JHEP **12** (2007) 040, arXiv:0709.4174.

[36] **HPQCD**, C. Bouchard, G. P. Lepage, C. Monahan, H. Na, and J. Shigemitsu, "*Standard Model Predictions for $B \to K\ell^+\ell^-$ with Form Factors from Lattice QCD*," Phys. Rev. Lett. **111** (2013) no. 16, 162002, arXiv:1306.0434. [Erratum: Phys. Rev. Lett.112,no.14,149902(2014)].

[37] **LHCb**, R. Aaij *et al.*, "*Measurement of Form-Factor-Independent Observables in the Decay $B^0 \to K^{*0}\mu^+\mu^-$*," Phys. Rev. Lett. **111** (2013) 191801, arXiv:1308.1707.

[38] **LHCb**, R. Aaij *et al.*, "*Angular analysis of the $B^0 \to K^{*0}\mu^+\mu^-$ decay using 3 fb$^{-1}$ of integrated luminosity*," JHEP **02** (2016) 104, arXiv:1512.04442.

[39] W. Altmannshofer and D. M. Straub, "*Implications of $b \to s$ measurements*," in *Proceedings, 50th Rencontres de Moriond Electroweak interactions and unified theories*, pp. 333–338. 2015. arXiv:1503.06199. http://inspirehep.net/record/1353682/files/arXiv:1503.06199.pdf.

[40] **LHCb**, R. Aaij *et al.*, "*Angular analysis and differential branching fraction of the decay $B_s^0 \to \phi\mu^+\mu^-$*," JHEP **09** (2015) 179, arXiv:1506.08777.

[41] **Belle**, A. Abdesselam *et al.*, "*Angular analysis of $B^0 \to K^*(892)^0\ell^+\ell^-$*," in *Proceedings, LHCSki 2016 - A First Discussion of 13 TeV Results: Obergurgl, Austria, April 10-15, 2016*. 2016. arXiv:1604.04042. https://inspirehep.net/record/1446979/files/arXiv:1604.04042.pdf.

[42] D. Das and R. Sinha, "*New Physics Effects and Hadronic Form Factor Uncertainties in $B \to K^*\ell^+\ell^-$*," Phys. Rev. **D86** (2012) 056006, arXiv:1205.1438.

[43] S. Jager and J. Martin Camalich, "*On $B \to V\ell\ell$ at small dilepton invariant mass, power corrections, and new physics*," JHEP **05** (2013) 043, arXiv:1212.2263.

[44] C. Hambrock, G. Hiller, S. Schacht, and R. Zwicky, "*$B \to K^\star$ form factors from flavor data to QCD and back*," Phys. Rev. **D89** (2014) no. 7, 074014, arXiv:1308.4379.

[45] J. Lyon and R. Zwicky, "*Resonances gone topsy turvy - the charm of QCD or new physics in $b \to s\ell^+\ell^-$?*," arXiv:1406.0566.

[46] S. Descotes-Genon, L. Hofer, J. Matias, and J. Virto, "*On the impact of power corrections in the prediction of $B \to K^*\mu^+\mu^-$ observables*," JHEP **12** (2014) 125, arXiv:1407.8526.

[47] R. Mandal, R. Sinha, and D. Das, "*Testing New Physics Effects in $B \to K^*\ell^+\ell^-$*," Phys. Rev. **D90** (2014) no. 9, 096006, arXiv:1409.3088.

[48] S. Descotes-Genon, J. Matias, and J. Virto, "*Understanding the $B \to K^* \mu^+ \mu^-$ Anomaly*," Phys. Rev. **D88** (2013) 074002, arXiv:1307.5683.

[49] W. Altmannshofer and D. M. Straub, "*New physics in $B \to K^* \mu\mu$?*," Eur. Phys. J. **C73** (2013) 2646, arXiv:1308.1501.

[50] R. Gauld, F. Goertz, and U. Haisch, "*On minimal $Z'$ explanations of the $B \to K^* \mu^+ \mu^-$ anomaly*," Phys. Rev. **D89** (2014) 015005, arXiv:1308.1959.

[51] A. J. Buras and J. Girrbach, "*Left-handed $Z'$ and $Z$ FCNC quark couplings facing new $b \to s\mu^+ \mu^-$ data*," JHEP **12** (2013) 009, arXiv:1309.2466.

[52] A. Datta, M. Duraisamy, and D. Ghosh, "*Explaining the $B \to K^* \mu^+ \mu^-$ data with scalar interactions*," Phys. Rev. **D89** (2014) no. 7, 071501, arXiv:1310.1937.

[53] W. Altmannshofer and D. M. Straub, "*New physics in $b \to s$ transitions after LHC run 1*," Eur. Phys. J. **C75** (2015) no. 8, 382, arXiv:1411.3161.

[54] S. Jager and J. Martin Camalich, "*Reassessing the discovery potential of the $B \to K^* \ell^+ \ell^-$ decays in the large-recoil region: SM challenges and BSM opportunities*," Phys. Rev. **D93** (2016) no. 1, 014028, arXiv:1412.3183.

[55] S. Descotes-Genon, L. Hofer, J. Matias, and J. Virto, "*Theoretical status of $B \to K^* \mu^+ \mu^-$: The path towards New Physics*," J. Phys. Conf. Ser. **631** (2015) no. 1, 012027, arXiv:1503.03328.

[56] A. J. Buras, F. De Fazio, and J. Girrbach, "*331 models facing new $b \to s\mu^+ \mu^-$ data*," JHEP **02** (2014) 112, arXiv:1311.6729.

[57] W. Altmannshofer, S. Gori, M. Pospelov, and I. Yavin, "*Quark flavor transitions in $L_\mu - L_\tau$ models*," Phys. Rev. **D89** (2014) 095033, arXiv:1403.1269.

[58] A. Crivellin, G. D'Ambrosio, and J. Heeck, "*Explaining* $h \to \mu^{\pm}\tau^{\mp}$, $B \to K^*\mu^+\mu^-$ *and* $B \to K\mu^+\mu^-/B \to Ke^+e^-$ *in a two-Higgs-doublet model with gauged* $L_\mu - L_\tau$," Phys. Rev. Lett. **114** (2015) 151801, arXiv:1501.00993.

[59] A. Crivellin, G. D'Ambrosio, and J. Heeck, "*Addressing the LHC flavor anomalies with horizontal gauge symmetries*," Phys. Rev. **D91** (2015) no. 7, 075006, arXiv:1503.03477.

[60] D. Aristizabal Sierra, F. Staub, and A. Vicente, "*Shedding light on the* $b \to s$ *anomalies with a dark sector*," Phys. Rev. **D92** (2015) no. 1, 015001, arXiv:1503.06077.

[61] F. Mahmoudi, S. Neshatpour, and J. Virto, "$B \to K^*\mu^+\mu^-$ *optimised observables in the MSSM*," Eur. Phys. J. **C74** (2014) no. 6, 2927, arXiv:1401.2145.

[62] A. Celis, W.-Z. Feng, and M. Vollmann, "*Dirac Dark Matter and* $b \to s\ell^+\ell^-$ *with* $\mathbf{U(1)}$ *gauge symmetry*," arXiv:1608.03894.

[63] A. Celis, J. Fuentes-Martin, M. Jung, and H. Serodio, "*Family nonuniversal* $Z'$ *models with protected flavor-changing interactions*," Phys. Rev. **D92** (2015) no. 1, 015007, arXiv:1505.03079.

[64] E. Megias, G. Panico, O. Pujolas, and M. Quiros, "*A Natural origin for the LHCb anomalies*," JHEP **09** (2016) 118, arXiv:1608.02362.

[65] B. Gripaios, M. Nardecchia, and S. A. Renner, "*Composite leptoquarks and anomalies in* $B$*-meson decays*," JHEP **05** (2015) 006, arXiv:1412.1791.

[66] L. Calibbi, A. Crivellin, and T. Ota, "*Effective Field Theory Approach to* $b \to s\ell\ell'$, $B \to K^*\nu\bar{\nu}$ *and* $B \to D^{(*)}\tau\nu$ *with Third Generation Couplings*," Phys. Rev. Lett. **115** (2015) 181801, arXiv:1506.02661.

[67] B. Allanach, F. S. Queiroz, A. Strumia, and S. Sun, "$Z'$ *models for the LHCb and* $g-2$ *muon anomalies*," Phys. Rev. **D93** (2016) no. 5, 055045, arXiv:1511.07447.

[68] A. Celis, W.-Z. Feng, and D. Lust, "*Stringy explanation of $b \to s\ell^+\ell^-$ anomalies*," JHEP **02** (2016) 007, arXiv:1512.02218.

[69] C.-W. Chiang, X.-G. He, and G. Valencia, "*$Z'$ model for $b \to s\ell\ell$ flavor anomalies*," Phys. Rev. **D93** (2016) no. 7, 074003, arXiv:1601.07328.

[70] P. Arnan, L. Hofer, F. Mescia, and A. Crivellin, "*Loop effects of heavy new scalars and fermions in $b \to s\mu^+\mu^-$*," arXiv:1608.07832.

[71] T. Hurth and F. Mahmoudi, "*On the LHCb anomaly in $B \to K^*\ell^+\ell^-$*," JHEP **04** (2014) 097, arXiv:1312.5267.

[72] S. Descotes-Genon, L. Hofer, J. Matias, and J. Virto, "*Global analysis of $b \to s\ell\ell$ anomalies*," JHEP **06** (2016) 092, arXiv:1510.04239.

[73] H. M. Asatrian, K. Bieri, C. Greub, and A. Hovhannisyan, "*NNLL corrections to the angular distribution and to the forward backward asymmetries in $B \to X_s\ell^+\ell^-$*," Phys. Rev. **D66** (2002) 094013, arXiv:hep-ph/0209006.

[74] W. Altmannshofer, P. Ball, A. Bharucha, A. J. Buras, D. M. Straub, and M. Wick, "*Symmetries and Asymmetries of $B \to K^*\mu^+\mu^-$ Decays in the Standard Model and Beyond*," JHEP **01** (2009) 019, arXiv:0811.1214.

[75] P. Ball and R. Zwicky, "*$B_{d,s} \to \rho, \omega, K^*, \phi$ decay form-factors from light-cone sum rules revisited*," Phys. Rev. **D71** (2005) 014029, arXiv:hep-ph/0412079.

[76] J. Charles, A. Le Yaouanc, L. Oliver, O. Pene, and J. C. Raynal, "*Heavy to light form-factors in the heavy mass to large energy limit of QCD*," Phys. Rev. **D60** (1999) 014001, arXiv:hep-ph/9812358.

[77] M. Beneke and T. Feldmann, "*Symmetry breaking corrections to heavy to light B meson form-factors at large recoil*," Nucl. Phys. **B592** (2001) 3–34, arXiv:hep-ph/0008255.

[78] M. Beneke, T. Feldmann, and D. Seidel, "*Systematic approach to exclusive $B \to V\ell^+\ell^-$, $V\gamma$ decays*," Nucl. Phys. **B612** (2001) 25–58, arXiv:hep-ph/0106067.

[79] M. Beneke, T. Feldmann, and D. Seidel, "*Exclusive radiative and electroweak $b \to d$ and $b \to s$ penguin decays at NLO*," Eur. Phys. J. **C41** (2005) 173–188, arXiv:hep-ph/0412400.

[80] F. Kruger, L. M. Sehgal, N. Sinha, and R. Sinha, "*Angular distribution and CP asymmetries in the decays $\bar{B} \longrightarrow K^-\pi^+e^-e^+$ and $\bar{B} \longrightarrow \pi^-\pi^+e^-e^+$*," Phys. Rev. **D61** (2000) 114028, arXiv:hep-ph/9907386. [Erratum: Phys. Rev.D63,019901(2001)].

[81] J. Matias, F. Mescia, M. Ramon, and J. Virto, "*Complete Anatomy of $\bar{B}_d->\bar{K}^{*0}(->K\pi)l^+l^-$ and its angular distribution*," JHEP **04** (2012) 104, arXiv:1202.4266.

[82] U. Egede, T. Hurth, J. Matias, M. Ramon, and W. Reece, "*New observables in the decay mode $\bar{B} \to \bar{K}^*\ell^+\ell^-$*," JHEP **11** (2008) 032, arXiv:0807.2589.

[83] F. Kruger and J. Matias, "*Probing new physics via the transverse amplitudes of B0 —¿ K*0 (—¿ K- pi+) l+l- at large recoil*," Phys. Rev. **D71** (2005) 094009, arXiv:hep-ph/0502060.

[84] S. Descotes-Genon, J. Matias, M. Ramon, and J. Virto, "*Implications from clean observables for the binned analysis of $B->K*\mu^+\mu^-$ at large recoil*," JHEP **01** (2013) 048, arXiv:1207.2753.

[85] S. Descotes-Genon, T. Hurth, J. Matias, and J. Virto, "*Optimizing the basis of B-¿K*ll observables in the full kinematic range*," JHEP **05** (2013) 137, arXiv:1303.5794.

[86] G. Burdman, "*Short distance coefficients and the vanishing of the lepton asymmetry in $B \to V\ \ell^+$ lepton-*," Phys. Rev. **D57** (1998) 4254–4257, arXiv:hep-ph/9710550.

[87] A. Ali, P. Ball, L. T. Handoko, and G. Hiller, "*A Comparative study of the decays $B \to (K, K^{*)} \ell^+ \ell^-$ in standard model and supersymmetric theories*," Phys. Rev. **D61** (2000) 074024, `arXiv:hep-ph/9910221`.

[88] **LHCb Collaboration**, "*Angular analysis of the $B^0 \to K^{*0} \mu^+ \mu^-$ decay*,". `https://cds.cern.ch/record/2002772`.

[89] **LHCb**, R. Aaij *et al.*, "*Differential branching fraction and angular analysis of the decay $B^0 \to K^{*0} \mu^+ \mu^-$*," JHEP **08** (2013) 131, `arXiv:1304.6325`.

[90] C. Bobeth, G. Hiller, D. van Dyk, and C. Wacker, "*The Decay $B \to K \ell^+ \ell^-$ at Low Hadronic Recoil and Model-Independent $\Delta B = 1$ Constraints*," JHEP **01** (2012) 107, `arXiv:1111.2558`.

[91] A. Ali, G. Kramer, and G.-h. Zhu, "*$B \to K^+ l^+ l^-$ decay in soft-collinear effective theory*," Eur. Phys. J. **C47** (2006) 625–641, `arXiv:hep-ph/0601034`.

[92] P. Gambino and M. Misiak, "*Quark mass effects in anti-B —¿ X(s gamma)*," Nucl. Phys. **B611** (2001) 338–366, `arXiv:hep-ph/0104034`.

[93] C. W. Bauer, Z. Ligeti, M. Luke, A. V. Manohar, and M. Trott, "*Global analysis of inclusive B decays*," Phys. Rev. **D70** (2004) 094017, `arXiv:hep-ph/0408002`.

[94] M. Benzke, S. J. Lee, M. Neubert, and G. Paz, "*Factorization at Subleading Power and Irreducible Uncertainties in $\bar{B} \to X_s \gamma$ Decay*," JHEP **08** (2010) 099, `arXiv:1003.5012`.

[95] M. Misiak *et al.*, "*Estimate of $\mathcal{B}(\bar{B} \to X_s \gamma)$ at $O(\alpha_s^2)$*," Phys. Rev. Lett. **98** (2007) 022002, `arXiv:hep-ph/0609232`.

[96] M. Misiak and M. Steinhauser, "*NNLO QCD corrections to the anti-B —¿ X(s) gamma matrix elements using interpolation in m(c)*," Nucl. Phys. **B764** (2007) 62–82, `arXiv:hep-ph/0609241`.

[97] M. Misiak *et al.*, "*Updated NNLO QCD predictions for the weak radiative B-meson decays*," Phys. Rev. Lett. **114** (2015) no. 22, 221801, arXiv:1503.01789.

[98] A. Paul and D. M. Straub, "*Constraints on new physics from radiative B decays*," arXiv:1608.02556.

[99] A. Bharucha, D. M. Straub, and R. Zwicky, "*$B \to V\ell^+\ell^-$ in the Standard Model from light-cone sum rules*," JHEP **08** (2016) 098, arXiv:1503.05534.

[100] R. R. Horgan, Z. Liu, S. Meinel, and M. Wingate, "*Rare B decays using lattice QCD form factors*," PoS **LATTICE2014** (2015) 372, arXiv:1501.00367.

[101] G. Hiller and M. Schmaltz, "*$R_K$ and future $b \to s\ell\ell$ physics beyond the standard model opportunities*," Phys. Rev. **D90** (2014) 054014, arXiv:1408.1627.

[102] C.-S. Huang and H.-G. Yan, "*Exclusive rare decays of heavy baryons to light baryons: $\Lambda_b \to \Lambda\gamma$ and $\Lambda_b \to \Lambda\ell^+\ell^-$*," Phys. Rev. **D59** (1999) 114022, arXiv:hep-ph/9811303. [Erratum: Phys. Rev.D61,039901(2000)].

[103] T. M. Aliev and M. Savci, "*Exclusive $\Lambda_b \to \Lambda\ell^+\ell^-$ decay in two Higgs doublet model*," J. Phys. **G26** (2000) 997–1010, arXiv:hep-ph/9906473.

[104] C.-H. Chen and C. Q. Geng, "*Rare $\Lambda_b \to \Lambda\ell^+\ell^-$ decays with polarized $\Lambda$*," Phys. Rev. **D63** (2001) 114024, arXiv:hep-ph/0101171.

[105] C.-H. Chen and C. Q. Geng, "*Lepton asymmetries in heavy baryon decays of $\Lambda_b \to \Lambda\ell^+\ell^-$*," Phys. Lett. **B516** (2001) 327–336, arXiv:hep-ph/0101201.

[106] T. M. Aliev, A. Ozpineci, and M. Savci, "*New physics effects in $\Lambda_b \to \Lambda\ell^+\ell^-$ decay with lepton polarizations*," Phys. Rev. **D65** (2002) 115002, arXiv:hep-ph/0203045.

[107] T. M. Aliev, A. Ozpineci, M. Savci, and C. Yuce, "*$T$ violation in $\Lambda_b \to \Lambda \ell^+ \ell^-$ decay beyond standard model*," Phys. Lett. **B542** (2002) 229–238, `arXiv:hep-ph/0206014`.

[108] T. M. Aliev, A. Ozpineci, and M. Savci, "*Model independent analysis of Lambda baryon polarizations in $\Lambda_b \to \Lambda \ell^+ \ell^-$ decay*," Phys. Rev. **D67** (2003) 035007, `arXiv:hep-ph/0211447`.

[109] T. M. Aliev, V. Bashiry, and M. Savci, "*Forward-backward asymmetries in $\Lambda_b \to \Lambda \ell^+ \ell^-$ decay beyond the standard model*," Nucl. Phys. **B709** (2005) 115–140, `arXiv:hep-ph/0407217`.

[110] T. M. Aliev, V. Bashiry, and M. Savci, "*Double-lepton polarization asymmetries in $\Lambda_b \to \Lambda \ell^+ \ell^-$ decay*," Eur. Phys. J. **C38** (2004) 283–295, `arXiv:hep-ph/0409275`.

[111] A. K. Giri and R. Mohanta, "*Effect of R-parity violation on the rare decay $\Lambda_b \to \Lambda \mu^+ \mu^-$*," J. Phys. **G31** (2005) 1559–1569.

[112] T. M. Aliev and M. Savci, "*$\Lambda_b \to \Lambda \ell^+ \ell^-$ decay in universal extra dimensions*," Eur. Phys. J. **C50** (2007) 91–99, `arXiv:hep-ph/0606225`.

[113] T. M. Aliev, M. Savci, and B. B. Sirvanli, "*Double-lepton polarization asymmetries in $\Lambda_b \to \Lambda \ell^+ \ell^-$ decay in universal extra dimension model*," Eur. Phys. J. **C52** (2007) 375–382, `arXiv:hep-ph/0608143`.

[114] F. Zolfagharpour and V. Bashiry, "*Double Lepton Polarization in $\Lambda_b \to \Lambda \ell^+ \ell^-$ Decay in the Standard Model with Fourth Generations Scenario*," Nucl. Phys. **B796** (2008) 294–319, `arXiv:0707.4337`.

[115] Y.-m. Wang, Y. Li, and C.-D. Lu, "*Rare Decays of $\Lambda_b \to \Lambda \gamma^-$ and $\Lambda_b \to \Lambda \ell^+ \ell^-$ in the Light-cone Sum Rules*," Eur. Phys. J. **C59** (2009) 861–882, `arXiv:0804.0648`.

[116] M. J. Aslam, Y.-M. Wang, and C.-D. Lu, "*Exclusive semileptonic decays of $\Lambda_b \to \Lambda \ell^+ \ell^-$ in supersymmetric theories*," Phys. Rev. **D78** (2008) 114032, `arXiv:0808.2113`.

[117] T. M. Aliev, K. Azizi, and M. Savci, "*Analysis of the Lambda*$_b \to \Lambda\ell^+\ell^-$ *decay in QCD*," Phys. Rev. **D81** (2010) 056006, arXiv:1001.0227.

[118] S. Sahoo, C. K. Das, and L. Maharana, "*Effect of both Z and Z-prime mediated flavor-changing neutral currents on the baryonic rare decay* $\Lambda_b \to \Lambda\ell^+\ell^-$," Int. J. Mod. Phys. **A24** (2009) 6223–6235, arXiv:1112.4563.

[119] L. Mott and W. Roberts, "*Rare dileptonic decays of* $\Lambda_b$ *in a quark model*," Int. J. Mod. Phys. **A27** (2012) 1250016, arXiv:1108.6129.

[120] T. Gutsche, M. A. Ivanov, J. G. Korner, V. E. Lyubovitskij, and P. Santorelli, "*Rare baryon decays* $\Lambda_b \to \Lambda l^+l^-(l = e, \mu, \tau)$ *and* $\Lambda_b \to \Lambda\gamma$ *: differential and total rates, lepton- and hadron-side forward-backward asymmetries*," Phys. Rev. **D87** (2013) 074031, arXiv:1301.3737.

[121] R. N. Faustov and V. O. Galkin, "*Semileptonic decays of* $\Lambda_b$ *baryons in the relativistic quark model*," Phys. Rev. **D94** (2016) no. 7, 073008, arXiv:1609.00199.

[122] S.-W. Wang and Y.-D. Yang, "*Analysis of* $\Lambda_b \to \Lambda\mu^+\mu^-$ *decay in scalar leptoquark model*," Adv. High Energy Phys. **2016** (2016) 5796131, arXiv:1608.03662.

[123] S. Sahoo and R. Mohanta, "*Effects of scalar leptoquark on semileptonic* $\Lambda_b$ *decays*," New J. Phys. **18** (2016) no. 9, 093051, arXiv:1607.04449.

[124] P. Böer, T. Feldmann, and D. van Dyk, "*Angular Analysis of the Decay* $\Lambda_b \to \Lambda(\to N\pi)\ell^+\ell^-$," JHEP **01** (2015) 155, arXiv:1410.2115.

[125] **CDF**, T. Aaltonen *et al.*, "*Observation of the Baryonic Flavor-Changing Neutral Current Decay* $\Lambda_b \to \Lambda\mu^+\mu^-$," Phys. Rev. Lett. **107** (2011) 201802, arXiv:1107.3753.

[126] **LHCb**, R. Aaij *et al.*, "*Measurement of the differential branching fraction of the decay* $\Lambda_b^0 \to \Lambda\mu^+\mu^-$," Phys. Lett. **B725** (2013) 25–35, arXiv:1306.2577.

[127] **LHCb**, R. Aaij *et al.*, "*Differential branching fraction and angular analysis of $\Lambda_b^0 \to \Lambda\mu^+\mu^-$ decays*," JHEP **06** (2015) 115, arXiv:1503.07138.

[128] T. Feldmann and M. W. Y. Yip, "*Form Factors for Lambda$_b \to \Lambda$ Transitions in SCET*," Phys. Rev. **D85** (2012) 014035, arXiv:1111.1844. [Erratum: Phys. Rev.D86,079901(2012)].

[129] T. Mannel, W. Roberts, and Z. Ryzak, "*Baryons in the heavy quark effective theory*," Nucl. Phys. **B355** (1991) 38–53.

[130] F. Hussain, J. G. Korner, M. Kramer, and G. Thompson, "*On heavy baryon decay form-factors*," Z. Phys. **C51** (1991) 321–328.

[131] F. Hussain, D.-S. Liu, M. Kramer, J. G. Korner, and S. Tawfiq, "*General analysis of weak decay form-factors in heavy to heavy and heavy to light baryon transitions*," Nucl. Phys. **B370** (1992) 259–277.

[132] H.-Y. Cheng and B. Tseng, "*1/M corrections to baryonic form-factors in the quark model*," Phys. Rev. **D53** (1996) 1457, arXiv:hep-ph/9502391. [Erratum: Phys. Rev.D55,1697(1997)].

[133] Y.-M. Wang, Y.-L. Shen, and C.-D. Lu, "*$\Lambda_b \to p, \Lambda$ transition form factors from QCD light-cone sum rules*," Phys. Rev. **D80** (2009) 074012, arXiv:0907.4008.

[134] T. Mannel and Y.-M. Wang, "*Heavy-to-light baryonic form factors at large recoil*," JHEP **12** (2011) 067, arXiv:1111.1849.

[135] W. Wang, "*Factorization of Heavy-to-Light Baryonic Transitions in SCET*," Phys. Lett. **B708** (2012) 119–126, arXiv:1112.0237.

[136] W. Detmold, C. J. D. Lin, S. Meinel, and M. Wingate, "*$\Lambda_b \to \Lambda\ell^+\ell^-$ form factors and differential branching fraction from lattice QCD*," Phys. Rev. **D87** (2013) no. 7, 074502, arXiv:1212.4827.

[137] W. Detmold and S. Meinel, "*$\Lambda_b \to \Lambda \ell^+ \ell^-$ form factors, differential branching fraction, and angular observables from lattice QCD with relativistic b quarks*," Phys. Rev. **D93** (2016) no. 7, 074501, arXiv:1602.01399.

[138] S. Fajfer, J. F. Kamenik, and I. Nisandzic, "*On the $B \to D^* \tau \bar{\nu}_\tau$ Sensitivity to New Physics*," Phys. Rev. **D85** (2012) 094025, arXiv:1203.2654.

[139] **Belle**, M. Huschle *et al.*, "*Measurement of the branching ratio of $\bar{B} \to D^{(*)} \tau^- \bar{\nu}_\tau$ relative to $\bar{B} \to D^{(*)} \ell^- \bar{\nu}_\ell$ decays with hadronic tagging at Belle*," Phys. Rev. **D92** (2015) no. 7, 072014, arXiv:1507.03233.

[140] **BaBar**, B. Aubert *et al.*, "*Observation of the semileptonic decays $B \to D^* \tau^- \bar{\nu}(\tau)$ and evidence for $B \to D \tau^- \bar{\nu}(\tau)$*," Phys. Rev. Lett. **100** (2008) 021801, arXiv:0709.1698.

[141] **Belle**, A. Bozek *et al.*, "*Observation of $B^+ \to \bar{D}^{*0} \tau^+ \nu_\tau$ and Evidence for $B^+ \to \bar{D}^0 \tau^+ \nu_\tau$ at Belle*," Phys. Rev. **D82** (2010) 072005, arXiv:1005.2302.

[142] **HPQCD**, H. Na, C. M. Bouchard, G. P. Lepage, C. Monahan, and J. Shigemitsu, "*$B \to Dl\nu$ form factors at nonzero recoil and extraction of $|V_{cb}|$*," Phys. Rev. **D92** (2015) no. 5, 054510, arXiv:1505.03925. [Erratum: Phys. Rev.D93,no.11,119906(2016)].

[143] P. Krawczyk and S. Pokorski, "*Strongly Coupled Charged Scalar in B and t Decays*," Phys. Rev. Lett. **60** (1988) 182.

[144] J. Kalinowski, "*Semileptonic Decays of B Mesons into $\tau \nu_\tau$ in a Two Higgs Doublet Model*," Phys. Lett. **B245** (1990) 201–206.

[145] W.-S. Hou, "*Enhanced charged Higgs boson effects in $B^- \to \tau \bar{\nu}$, $\mu \bar{\nu}$ and $b \to \tau \bar{\nu} + X$*," Phys. Rev. **D48** (1993) 2342–2344.

[146] M. Tanaka, "*Charged Higgs effects on exclusive semitauonic B decays*," Z. Phys. **C67** (1995) 321–326, arXiv:hep-ph/9411405.

[147] J. F. Kamenik and F. Mescia, "*$B \to D\tau\nu$ Branching Ratios: Opportunity for Lattice QCD and Hadron Colliders*," Phys. Rev. **D78** (2008) 014003, arXiv:0802.3790.

[148] U. Nierste, S. Trine, and S. Westhoff, "*Charged-Higgs effects in a new $B \to D\tau\nu$ differential decay distribution*," Phys. Rev. **D78** (2008) 015006, arXiv:0801.4938.

[149] M. Tanaka and R. Watanabe, "*Tau longitudinal polarization in $B \to D\tau\nu$ and its role in the search for charged Higgs boson*," Phys. Rev. **D82** (2010) 034027, arXiv:1005.4306.

[150] Y. Sakaki and H. Tanaka, "*Constraints on the charged scalar effects using the forward-backward asymmetry on $B^- \to D^{(*)}\tau\bar{\nu}_\tau$*," Phys. Rev. **D87** (2013) no. 5, 054002, arXiv:1205.4908.

[151] S. Fajfer, J. F. Kamenik, I. Nisandzic, and J. Zupan, "*Implications of Lepton Flavor Universality Violations in B Decays*," Phys. Rev. Lett. **109** (2012) 161801, arXiv:1206.1872.

[152] A. Datta, M. Duraisamy, and D. Ghosh, "*Diagnosing New Physics in $b \to c\,\tau\,\nu_\tau$ decays in the light of the recent BaBar result*," Phys. Rev. **D86** (2012) 034027, arXiv:1206.3760.

[153] J. A. Bailey *et al.*, "*Refining new-physics searches in $B- > D\tau\nu$ decay with lattice QCD*," Phys. Rev. Lett. **109** (2012) 071802, arXiv:1206.4992.

[154] D. Becirevic, N. Kosnik, and A. Tayduganov, "*$\bar{B} \to D\tau\bar{\nu}_\tau$ vs. $\bar{B} \to D\mu\bar{\nu}_\mu$*," Phys. Lett. **B716** (2012) 208–213, arXiv:1206.4977.

[155] M. Tanaka and R. Watanabe, "*New physics in the weak interaction of $\bar{B} \to D^{(*)}\tau\bar{\nu}$*," Phys. Rev. **D87** (2013) no. 3, 034028, arXiv:1212.1878.

[156] M. Freytsis, Z. Ligeti, and J. T. Ruderman, "*Flavor models for $\bar{B} \to D^{(*)}\tau\bar{\nu}$*," Phys. Rev. **D92** (2015) no. 5, 054018, arXiv:1506.08896.

[157] S. Bhattacharya, S. Nandi, and S. K. Patra, "*Optimal-observable analysis of possible new physics in $B \to D^{(*)}\tau\nu_\tau$*," Phys. Rev. **D93** (2016) no. 3, 034011, arXiv:1509.07259.

[158] A. Celis, M. Jung, X.-Q. Li, and A. Pich, "*Sensitivity to charged scalars in $\boldsymbol{B \to D^{(*)}\tau\nu_\tau}$ and $\boldsymbol{B \to \tau\nu_\tau}$ decays*," JHEP **01** (2013) 054, arXiv:1210.8443.

[159] P. Ko, Y. Omura, and C. Yu, "*$B \to D^{(*)}\tau\nu$ and $B \to \tau\nu$ in chiral $U(1)'$ models with flavored multi Higgs doublets*," JHEP **03** (2013) 151, arXiv:1212.4607.

[160] A. Crivellin, C. Greub, and A. Kokulu, "*Explaining $B \to D\tau\nu$, $B \to D^*\tau\nu$ and $B \to \tau\nu$ in a 2HDM of type III*," Phys. Rev. **D86** (2012) 054014, arXiv:1206.2634.

[161] N. G. Deshpande and A. Menon, "*Hints of R-parity violation in B decays into $\tau\nu$*," JHEP **01** (2013) 025, arXiv:1208.4134.

[162] I. Dorsner, S. Fajfer, J. F. Kamenik, and N. Kosnik, "*Can scalar leptoquarks explain the f(D(s)) puzzle?*," Phys. Lett. **B682** (2009) 67–73, arXiv:0906.5585.

[163] Y. Sakaki, M. Tanaka, A. Tayduganov, and R. Watanabe, "*Testing leptoquark models in $\bar{B} \to D^{(*)}\tau\bar{\nu}$*," Phys. Rev. **D88** (2013) no. 9, 094012, arXiv:1309.0301.

[164] A. Greljo, G. Isidori, and D. Marzocca, "*On the breaking of Lepton Flavor Universality in B decays*," JHEP **07** (2015) 142, arXiv:1506.01705.

[165] I. Dorsner, S. Fajfer, N. Kosnik, and I. Nisandzic, "*Minimally flavored colored scalar in $\bar{B} \to D^{(*)}\tau\bar{\nu}$ and the mass matrices constraints*," JHEP **11** (2013) 084, arXiv:1306.6493.

[166] P. Biancofiore, P. Colangelo, and F. De Fazio, "*On the anomalous enhancement observed in $B \to D^{(*)}\tau\bar{\nu}_\tau$ decays*," Phys. Rev. **D87** (2013) no. 7, 074010, arXiv:1302.1042.

[167] Y.-Y. Fan, Z.-J. Xiao, R.-M. Wang, and B.-Z. Li, "*The $B \to D^{(*)} l \nu_l$ decays in the pQCD approach with the Lattice QCD input*," arXiv:1505.07169.

[168] **CMS**, V. Khachatryan *et al.*, "*Search for heavy neutrinos and* W *bosons with right-handed couplings in proton-proton collisions at $\sqrt{s} = 8$ TeV*," Eur. Phys. J. **C74** (2014) no. 11, 3149, arXiv:1407.3683.

[169] **CMS**, C. Collaboration, "*Search for Pair-production of First Generation Scalar Leptoquarks in pp Collisions at sqrt s = 8 TeV*,".

[170] F. F. Deppisch, T. E. Gonzalo, S. Patra, N. Sahu, and U. Sarkar, "*Signal of Right-Handed Charged Gauge Bosons at the LHC?*," Phys. Rev. **D90** (2014) no. 5, 053014, arXiv:1407.5384.

[171] F. F. Deppisch, T. E. Gonzalo, S. Patra, N. Sahu, and U. Sarkar, "*Double beta decay, lepton flavor violation, and collider signatures of left-right symmetric models with spontaneous D-parity breaking*," Phys. Rev. **D91** (2015) no. 1, 015018, arXiv:1410.6427.

[172] P. S. Bhupal Dev and R. N. Mohapatra, "*Unified explanation of the eejj, diboson and dijet resonances at the LHC*," Phys. Rev. Lett. **115** (2015) no. 18, 181803, arXiv:1508.02277.

[173] J. Gluza and T. Jelinski, "*Heavy neutrinos and the pp?lljj CMS data*," Phys. Lett. **B748** (2015) 125–131, arXiv:1504.05568.

[174] B. A. Dobrescu and A. Martin, "*Interpretations of anomalous LHC events with electrons and jets*," Phys. Rev. **D91** (2015) no. 3, 035019, arXiv:1408.1082.

[175] J. A. Aguilar-Saavedra and F. R. Joaquim, "*Closer look at the possible CMS signal of a new gauge boson*," Phys. Rev. **D90** (2014) no. 11, 115010, arXiv:1408.2456.

[176] B. Allanach, S. Biswas, S. Mondal, and M. Mitra, "*Explaining a CMS eejj Excess With $\mathcal{R}-$parity Violating Supersymmetry and Implications for*

*Neutrinoless Double Beta Decay*," Phys. Rev. **D91** (2015) no. 1, 011702, arXiv:1408.5439.

[177] F. S. Queiroz, K. Sinha, and A. Strumia, "*Leptoquarks, Dark Matter, and Anomalous LHC Events*," Phys. Rev. **D91** (2015) no. 3, 035006, arXiv:1409.6301.

[178] S. Biswas, D. Chowdhury, S. Han, and S. J. Lee, "*Explaining the lepton non-universality at the LHCb and CMS within a unified framework*," JHEP **02** (2015) 142, arXiv:1409.0882.

[179] B. C. Allanach, S. Biswas, S. Mondal, and M. Mitra, "*Resonant slepton production yields CMS $eejj$ and $ep_T jj$ excesses*," Phys. Rev. **D91** (2015) no. 1, 015011, arXiv:1410.5947.

[180] B. Allanach, A. Alves, F. S. Queiroz, K. Sinha, and A. Strumia, "*Interpreting the CMS $\ell^+\ell^- jj\not{E}_{\mathrm{T}}$ Excess with a Leptoquark Model*," Phys. Rev. **D92** (2015) no. 5, 055023, arXiv:1501.03494.

[181] M. Dhuria, C. Hati, R. Rangarajan, and U. Sarkar, "*Explaining the CMS $eejj$ and $e$ missing $\mathrm{p_T}$ jj excess and leptogenesis in superstring inspired $E_6$ models*," Phys. Rev. **D91** (2015) no. 5, 055010, arXiv:1501.04815.

[182] B. Dutta, Y. Gao, T. Ghosh, T. Kamon, and N. Kolev, "*Explaining the CMS dilepton mass endpoint in the NMSSM*," Phys. Lett. **B749** (2015) 326–330, arXiv:1506.04336.

[183] B. A. Dobrescu, "*Leptophobic Boson Signals with Leptons, Jets and Missing Energy*," arXiv:1506.04435.

[184] J. Berger, J. A. Dror, and W. H. Ng, "*Sneutrino Higgs models explain lepton non-universality in $eejj, e\nu jj$ excesses*," JHEP **09** (2015) 156, arXiv:1506.08213.

[185] M. E. Krauss and W. Porod, "*Is the CMS eejj excess a hint for light supersymmetry?*," Phys. Rev. **D92** (2015) no. 5, 055019, arXiv:1507.04349.

[186] M. Dhuria, C. Hati, and U. Sarkar, "*Explaining the CMS excesses, baryogenesis and neutrino masses in $E_6$ motivated $U(1)_N$ model*," Phys. Rev. **D93** (2016) no. 1, 015001, arXiv:1507.08297.

[187] E. Ma, "*Particle Dichotomy and Left-Right Decomposition of E(6) Superstring Models*," Phys. Rev. **D36** (1987) 274.

[188] M. Dhuria, C. Hati, R. Rangarajan, and U. Sarkar, "*The $eejj$ Excess Signal at the LHC and Constraints on Leptogenesis*," JCAP **1509** (2015) no. 09, 035, arXiv:1502.01695.

[189] M. Dhuria, C. Hati, R. Rangarajan, and U. Sarkar, "*Falsifying leptogenesis for a TeV scale $W_R^\pm$ at the LHC*," Phys. Rev. **D92** (2015) no. 3, 031701, arXiv:1503.07198.

[190] K. Hagiwara, A. D. Martin, and M. F. Wade, "*EXCLUSIVE SEMILEPTONIC B MESON DECAYS*," Nucl. Phys. **B327** (1989) 569–594.

[191] M. Neubert, "*Model independent extraction of V(cb) from semileptonic decays*," Phys. Lett. **B264** (1991) 455–461.

[192] I. Caprini, L. Lellouch, and M. Neubert, "*Dispersive bounds on the shape of $\bar{B} \to D^{(*)}\ell\bar{\nu}$ form-factors*," Nucl. Phys. **B530** (1998) 153–181, arXiv:hep-ph/9712417.

[193] N. Isgur and M. B. Wise, "*Weak Decays of Heavy Mesons in the Static Quark Approximation*," Phys. Lett. **B232** (1989) 113–117.

[194] M. Neubert, "*Heavy quark symmetry*," Phys. Rept. **245** (1994) 259–396, arXiv:hep-ph/9306320.

[195] **Heavy Flavor Averaging Group (HFAG)**, Y. Amhis *et al.*, "*Averages of b-hadron, c-hadron, and $\tau$-lepton properties as of summer 2014*," arXiv:1412.7515.

[196] M. Okamoto *et al.*, "*Semileptonic $D \to \pi/K$ and $B \to \pi/D$ decays in 2+1 flavor lattice QCD*," Nucl. Phys. Proc. Suppl. **140** (2005) 461–463, arXiv:hep-lat/0409116. [,461(2004)].

[197] **Fermilab Lattice, MILC**, J. A. Bailey *et al.*, "*Update of $|V_{cb}|$ from the $\bar{B} \to D^* \ell \bar{\nu}$ form factor at zero recoil with three-flavor lattice QCD*," Phys. Rev. **D89** (2014) no. 11, 114504, arXiv:1403.0635.

[198] J. C. Pati and A. Salam, "*Lepton Number as the Fourth Color*," Phys. Rev. **D10** (1974) 275–289. [Erratum: Phys. Rev.D11,703(1975)].

[199] H. Georgi and S. L. Glashow, "*Unity of All Elementary Particle Forces*," Phys. Rev. Lett. **32** (1974) 438–441.

[200] H. Georgi, "*The State of the Art-Gauge Theories*," AIP Conf. Proc. **23** (1975) 575–582.

[201] H. Fritzsch and P. Minkowski, "*Unified Interactions of Leptons and Hadrons*," Annals Phys. **93** (1975) 193–266.

[202] J. L. Hewett and T. G. Rizzo, "*Low-Energy Phenomenology of Superstring Inspired E(6) Models*," Phys. Rept. **183** (1989) 193.

[203] E. Farhi and L. Susskind, "*Technicolor*," Phys. Rept. **74** (1981) 277.

[204] K. D. Lane and M. V. Ramana, "*Walking technicolor signatures at hadron colliders*," Phys. Rev. **D44** (1991) 2678–2700.

[205] B. Schrempp and F. Schrempp, "*LIGHT LEPTOQUARKS*," Phys. Lett. **B153** (1985) 101–107.

[206] J. Wudka, "*COMPOSITE LEPTOQUARKS*," Phys. Lett. **B167** (1986) 337–342.

[207] R. Barbier *et al.*, "*R-parity violating supersymmetry*," Phys. Rept. **420** (2005) 1–202, arXiv:hep-ph/0406039.

[208] I. Dorsner, S. Fajfer, A. Greljo, J. F. Kamenik, and N. Kosnik, "*Physics of leptoquarks in precision experiments and at particle colliders*," arXiv:1603.04993.

[209] R. Slansky, "*Group Theory for Unified Model Building*," Phys. Rept. **79** (1981) 1–128.

[210] R. N. Mohapatra and J. C. Pati, "*A Natural Left-Right Symmetry*," Phys. Rev. **D11** (1975) 2558.

[211] G. Senjanovic and R. N. Mohapatra, "*Exact Left-Right Symmetry and Spontaneous Violation of Parity*," Phys. Rev. **D12** (1975) 1502.

[212] R. N. Mohapatra and J. C. Pati, "*Left-Right Gauge Symmetry and an Isoconjugate Model of CP Violation*," Phys. Rev. **D11** (1975) 566–571.

[213] V. Elias, J. C. Pati, and A. Salam, "*Light Neutral Z0 Boson in the PETRA and PEP Energy Range Within the Unifying Symmetry SU(4)**4*," Phys. Lett. **B73** (1978) 451–456.

[214] Q. Shafi and C. Wetterich, "*Left-Right Symmetric Gauge Models and Possible Existence of a Neutral Gauge Boson with Mass in the PETRA-PEP Energy Range*," Phys. Lett. **B73** (1978) 65–70.

[215] R. N. Mohapatra, *UNIFICATION AND SUPERSYMMETRY. THE FRONTIERS OF QUARK - LEPTON PHYSICS*. Springer, Berlin, 1986.

[216] D. London and J. L. Rosner, "*Extra Gauge Bosons in E(6)*," Phys. Rev. **D34** (1986) 1530.

[217] M. Artuso *et al.*, "*B, D and K decays*," Eur. Phys. J. **C57** (2008) 309–492, arXiv:0801.1833.

[218] G. Burdman, E. Golowich, J. L. Hewett, and S. Pakvasa, "*Rare charm decays in the standard model and beyond*," Phys. Rev. **D66** (2002) 014009, arXiv:hep-ph/0112235.

[219] A. G. Akeroyd and F. Mahmoudi, "*Constraints on charged Higgs bosons from D(s)+- —¿ mu+- nu and D(s)+- —¿ tau+- nu*," JHEP **04** (2009) 121, arXiv:0902.2393.

[220] B. A. Dobrescu and A. S. Kronfeld, "*Accumulating evidence for nonstandard leptonic decays of $D_s$ mesons*," Phys. Rev. Lett. **100** (2008) 241802, arXiv:0803.0512.

[221] Y. Kao and T. Takeuchi, "*Single-Coupling Bounds on R-parity violating Supersymmetry, an update*," arXiv:0910.4980.

[222] J. Barranco, D. Delepine, V. Gonzalez Macias, and L. Lopez-Lozano, "*Constraining New Physics with D meson decays*," Phys. Lett. **B731** (2014) 36–42, arXiv:1303.3896.

[223] "*Heavy Flavor Averaging Group*,". http://www.slac.stanford.edu/xorg/hfag/charm/CHARM15/results_mix_cpv.html.

[224] E. Golowich, J. Hewett, S. Pakvasa, and A. A. Petrov, "*Implications of $D^0$ - $\bar{D}^0$ Mixing for New Physics*," Phys. Rev. **D76** (2007) 095009, arXiv:0705.3650.

[225] E. Golowich, S. Pakvasa, and A. A. Petrov, "*New Physics contributions to the lifetime difference in D0-anti-D0 mixing*," Phys. Rev. Lett. **98** (2007) 181801, arXiv:hep-ph/0610039.

[226] K. Agashe and M. Graesser, "*R-parity violation in flavor changing neutral current processes and top quark decays*," Phys. Rev. **D54** (1996) 4445–4452, arXiv:hep-ph/9510439.

[227] Y. Grossman, Z. Ligeti, and E. Nardi, "*New limit on inclusive $B \to X_s$ anti-neutrino neutrino decay and constraints on new physics*," Nucl. Phys. **B465** (1996) 369–398, arXiv:hep-ph/9510378. [Erratum: Nucl. Phys.B480,753(1996)].

[228] A. J. Buras, J. Girrbach-Noe, C. Niehoff, and D. M. Straub, "*$B \to K^{(*)}\nu\overline{\nu}$ decays in the Standard Model and beyond*," JHEP **02** (2015) 184, arXiv:1409.4557.

[229] **Muon g-2**, G. W. Bennett *et al.*, "*Measurement of the negative muon anomalous magnetic moment to 0.7 ppm*," Phys. Rev. Lett. **92** (2004) 161802, arXiv:hep-ex/0401008.

[230] **Muon g-2**, G. W. Bennett *et al.*, "*Final Report of the Muon E821 Anomalous Magnetic Moment Measurement at BNL*," Phys. Rev. **D73** (2006) 072003, arXiv:hep-ex/0602035.

[231] B. Bhattacharya, A. Datta, D. London, and S. Shivashankara, "*Simultaneous Explanation of the $R_K$ and $R(D^{(*)})$ Puzzles*," Phys. Lett. **B742** (2015) 370–374, arXiv:1412.7164.

[232] S. L. Glashow, D. Guadagnoli, and K. Lane, "*Lepton Flavor Violation in $B$ Decays?*," Phys. Rev. Lett. **114** (2015) 091801, arXiv:1411.0565.

[233] R. Alonso, B. Grinstein, and J. Martin Camalich, "*Lepton universality violation and lepton flavor conservation in $B$-meson decays*," JHEP **10** (2015) 184, arXiv:1505.05164.

[234] M. Bauer and M. Neubert, "*Minimal Leptoquark Explanation for the $R_{D^{(*)}}$, $R_K$, and $(g-2)_g$ Anomalies*," Phys. Rev. Lett. **116** (2016) no. 14, 141802, arXiv:1511.01900.

[235] S. Fajfer and N. Kosnik, "*Vector leptoquark resolution of $R_K$ and $R_{D^{(*)}}$ puzzles*," Phys. Lett. **B755** (2016) 270–274, arXiv:1511.06024.

[236] S. M. Boucenna, A. Celis, J. Fuentes-Martin, A. Vicente, and J. Virto, "*Non-abelian gauge extensions for B-decay anomalies*," Phys. Lett. **B760** (2016) 214–219, arXiv:1604.03088.

[237] G. Belanger, C. Delaunay, and S. Westhoff, "*A Dark Matter Relic From Muon Anomalies*," Phys. Rev. **D92** (2015) 055021, arXiv:1507.06660.

[238] R. Alonso, B. Grinstein, and J. Martin Camalich, "*$SU(2) \times U(1)$ gauge invariance and the shape of new physics in rare $B$ decays*," Phys. Rev. Lett. **113** (2014) 241802, arXiv:1407.7044.

[239] T. Hurth, F. Mahmoudi, and S. Neshatpour, "*Global fits to $b \to s\ell\ell$ data and signs for lepton non-universality*," JHEP **12** (2014) 053, arXiv:1410.4545.

[240] G. Couture and H. Konig, "*Bounds on second generation scalar leptoquarks from the anomalous magnetic moment of the muon*," Phys. Rev. **D53** (1996) 555–557, arXiv:hep-ph/9507263.

[241] E. Lunghi, A. Masiero, I. Scimemi, and L. Silvestrini, "*$B \to X_s \ell^+ \ell^-$ decays in supersymmetry*," Nucl. Phys. **B568** (2000) 120–144, arXiv:hep-ph/9906286.

[242] A. Abada, D. Das, A. Vicente, and C. Weiland, "*Enhancing lepton flavour violation in the supersymmetric inverse seesaw beyond the dipole contribution*," JHEP **09** (2012) 015, arXiv:1206.6497.

[243] M. E. Krauss, W. Porod, F. Staub, A. Abada, A. Vicente, and C. Weiland, "*Decoupling of heavy sneutrinos in low-scale seesaw models*," Phys. Rev. **D90** (2014) no. 1, 013008, arXiv:1312.5318.

[244] A. Abada, M. E. Krauss, W. Porod, F. Staub, A. Vicente, and C. Weiland, "*Lepton flavor violation in low-scale seesaw models: SUSY and non-SUSY contributions*," JHEP **11** (2014) 048, arXiv:1408.0138.

[245] **UTfit**, M. Bona *et al.*, "*Model-independent constraints on $\Delta F = 2$ operators and the scale of new physics*," JHEP **03** (2008) 049, arXiv:0707.0636.

[246] J. E. Kim, B. Kyae, and H. M. Lee, "*Effective supersymmetric theory and (g-2)(muon with R-parity violation*," Phys. Lett. **B520** (2001) 298–306, arXiv:hep-ph/0103054.

[247] A. J. Buras and J. Girrbach, "*Towards the Identification of New Physics through Quark Flavour Violating Processes*," Rept. Prog. Phys. **77** (2014) 086201, arXiv:1306.3775.

[248] M. Blanke, "*New Physics Signatures in Kaon Decays*," PoS **KAON13** (2013) 010, arXiv:1305.5671.

[249] A. J. Buras, A. Romanino, and L. Silvestrini, "*$K \to \pi\nu\bar{\nu}$ : A Model independent analysis and supersymmetry*," Nucl. Phys. **B520** (1998) 3–30, arXiv:hep-ph/9712398.

[250] A. J. Buras and J. Girrbach, "*BSM models facing the recent LHCb data: A First look*," Acta Phys. Polon. **B43** (2012) 1427–1472, arXiv:1204.5064.

[251] A. J. Buras, T. Ewerth, S. Jager, and J. Rosiek, "*$K^+ \to \pi^+\nu\bar{\nu}$ and $K_L \to \pi\nu\bar{\nu}$ decays in the general MSSM*," Nucl. Phys. **B714** (2005) 103–136, arXiv:hep-ph/0408142.

[252] M. Blanke, A. J. Buras, B. Duling, S. Recksiegel, and C. Tarantino, "*FCNC Processes in the Littlest Higgs Model with T-Parity: a 2009 Look*," Acta Phys. Polon. **B41** (2010) 657–683, arXiv:0906.5454.

[253] M. Blanke, A. J. Buras, B. Duling, K. Gemmler, and S. Gori, "*Rare K and B Decays in a Warped Extra Dimension with Custodial Protection*," JHEP **03** (2009) 108, arXiv:0812.3803.

[254] M. Bauer, S. Casagrande, U. Haisch, and M. Neubert, "*Flavor Physics in the Randall-Sundrum Model: II. Tree-Level Weak-Interaction Processes*," JHEP **09** (2010) 017, arXiv:0912.1625.

[255] A. J. Buras, F. De Fazio, J. Girrbach, and M. V. Carlucci, "*The Anatomy of Quark Flavour Observables in 331 Models in the Flavour Precision Era*," JHEP **02** (2013) 023, arXiv:1211.1237.

[256] A. J. Buras, F. De Fazio, and J. Girrbach-Noe, "*$Z$-$Z'$ mixing and $Z$-mediated FCNCs in $SU(3)_C \times SU(3)_L \times U(1)_X$ models*," JHEP **08** (2014) 039, arXiv:1405.3850.

[257] "*ATLAS and CMS physics results from Run-II, see:*". http://indico.cern.ch/event/442432/.

[258] S. Sahoo and R. Mohanta, "*Scalar leptoquarks and the rare B meson decays*," Phys. Rev. **D91** (2015) no. 9, 094019, arXiv:1501.05193.

[259] D. Becirevic, S. Fajfer, and N. Kosnik, "*Lepton flavor nonuniversality in $b \to s\ell^+\ell^-$ processes*," Phys. Rev. **D92** (2015) no. 1, 014016, arXiv:1503.09024.

[260] S. Fajfer and N. Kosnik, "*Leptoquarks in FCNC charm decays*," Phys. Rev. **D79** (2009) 017502, arXiv:0810.4858.

[261] S. de Boer and G. Hiller, "*Flavor and new physics opportunities with rare charm decays into leptons*," Phys. Rev. **D93** (2016) no. 7, 074001, arXiv:1510.00311.

[262] S. Fajfer and N. Kosnik, "*Prospects of discovering new physics in rare charm decays*," Eur. Phys. J. **C75** (2015) no. 12, 567, arXiv:1510.00965.

[263] M. Antonelli *et al.*, "*Flavor Physics in the Quark Sector*," Phys. Rept. **494** (2010) 197–414, arXiv:0907.5386.

[264] G. Buchalla, A. J. Buras, and M. E. Lautenbacher, "*Weak decays beyond leading logarithms*," Rev. Mod. Phys. **68** (1996) 1125–1144, arXiv:hep-ph/9512380.

[265] T. Inami and C. S. Lim, "*Effects of Superheavy Quarks and Leptons in Low-Energy Weak Processes $K_L \to \mu^+\mu^-$, $K^+ \to \pi^+\nu\bar{\nu}$ and $K^0 \leftrightarrow \bar{K}^0$*," Prog. Theor. Phys. **65** (1981) 297. [Erratum: Prog. Theor. Phys.65,1772(1981)].

[266] G. C. Branco, L. Lavoura, and J. P. Silva, "*CP Violation*," Int. Ser. Monogr. Phys. **103** (1999) 1–536.

[267] A. J. Buras, M. Jamin, and P. H. Weisz, "*Leading and Next-to-leading QCD Corrections to $\epsilon$ Parameter and $B^0 - \bar{B}^0$ Mixing in the Presence of a Heavy Top Quark*," Nucl. Phys. **B347** (1990) 491–536.

[268] J. Brod and M. Gorbahn, "*Next-to-Next-to-Leading-Order Charm-Quark Contribution to the CP Violation Parameter $\epsilon_K$ and $\Delta M_K$*," Phys. Rev. Lett. **108** (2012) 121801, arXiv:1108.2036.

[269] J. Brod and M. Gorbahn, "*$\epsilon_K$ at Next-to-Next-to-Leading Order: The Charm-Top-Quark Contribution*," Phys. Rev. **D82** (2010) 094026, arXiv:1007.0684.

[270] A. J. Buras and D. Guadagnoli, "*Correlations among new CP violating effects in $\Delta$ $F = 2$ observables*," Phys. Rev. **D78** (2008) 033005, arXiv:0805.3887.

[271] A. J. Buras, D. Guadagnoli, and G. Isidori, "*On $\epsilon_K$ Beyond Lowest Order in the Operator Product Expansion*," Phys. Lett. **B688** (2010) 309–313, arXiv:1002.3612.

[272] Z. Ligeti and F. Sala, "*A new look at the theory uncertainty of $\epsilon_K$*," arXiv:1602.08494.

[273] A. J. Buras, J.-M. Gerard, and W. A. Bardeen, "*Large $N$ Approach to Kaon Decays and Mixing 28 Years Later: $\Delta I = 1/2$ Rule, $\hat{B}_K$ and $\Delta M_K$*," Eur. Phys. J. **C74** (2014) 2871, arXiv:1401.1385.

[274] A. J. Buras, F. Schwab, and S. Uhlig, "*Waiting for precise measurements of $K^+ \to \pi^+ \nu\bar{\nu}$ and $K_L \to \pi^0 \nu\bar{\nu}$*," Rev. Mod. Phys. **80** (2008) 965–1007, arXiv:hep-ph/0405132.

[275] F. Mescia and C. Smith, "*Improved estimates of rare K decay matrix-elements from Kl3 decays*," Phys. Rev. **D76** (2007) 034017, arXiv:0705.2025.

[276] G. Isidori, F. Mescia, and C. Smith, "*Light-quark loops in $K \to \pi\nu\bar{\nu}$*," Nucl. Phys. **B718** (2005) 319–338, arXiv:hep-ph/0503107.

[277] G. Buchalla and G. Isidori, "*The CP conserving contribution to $K_L \to \pi^0 \nu\bar{\nu}$ in the standard model*," Phys. Lett. **B440** (1998) 170–178, arXiv:hep-ph/9806501.

[278] C. Q. Geng, I. J. Hsu, and Y. C. Lin, "*Study of long distance contributions to* $K \to n\pi\nu\bar{\nu}$," Phys. Rev. **D54** (1996) 877–881, arXiv:hep-ph/9604228.

[279] G. Buchalla and A. J. Buras, "*Two loop large* $m_t$ *electroweak corrections to* $K \to \pi\nu\bar{\nu}$ *for arbitrary Higgs boson mass*," Phys. Rev. **D57** (1998) 216–223, arXiv:hep-ph/9707243.

[280] G. Buchalla and A. J. Buras, "*The rare decays* $K^+ \to \pi^+\nu\bar{\nu}$ *and* $K_L \to \mu^+\mu^-$ *beyond leading logarithms*," Nucl. Phys. **B412** (1994) 106–142, arXiv:hep-ph/9308272.

[281] G. Buchalla and A. J. Buras, "*QCD corrections to rare K and B decays for arbitrary top quark mass*," Nucl. Phys. **B400** (1993) 225–239.

[282] M. Misiak and J. Urban, "*QCD corrections to FCNC decays mediated by Z penguins and W boxes*," Phys. Lett. **B451** (1999) 161–169, arXiv:hep-ph/9901278.

[283] G. Buchalla and A. J. Buras, "*The rare decays* $K \to \pi\nu\bar{\nu}$, $B \to X\nu\bar{\nu}$ *and* $B \to l^+l^-$*: An Update*," Nucl. Phys. **B548** (1999) 309–327, arXiv:hep-ph/9901288.

[284] J. Brod, M. Gorbahn, and E. Stamou, "*Two-Loop Electroweak Corrections for the* $K \to \pi\nu\bar{\nu}$ *Decays*," Phys. Rev. **D83** (2011) 034030, arXiv:1009.0947.

[285] A. J. Buras, M. Gorbahn, U. Haisch, and U. Nierste, "*The Rare decay K+ —¿ pi+ nu anti-nu at the next-to-next-to-leading order in QCD*," Phys. Rev. Lett. **95** (2005) 261805, arXiv:hep-ph/0508165.

[286] A. J. Buras, M. Gorbahn, U. Haisch, and U. Nierste, "*Charm quark contribution to K+ —¿ pi+ nu anti-nu at next-to-next-to-leading order*," JHEP **11** (2006) 002, arXiv:hep-ph/0603079. [Erratum: JHEP11,167(2012)].

[287] A. J. Buras, D. Buttazzo, J. Girrbach-Noe, and R. Knegjens, "*$K^+ \to \pi^+ \nu\bar{\nu}$ and $K_L \to \pi^0 \nu\bar{\nu}$ in the Standard Model: status and perspectives*," JHEP **11** (2015) 033, arXiv:1503.02693.

[288] **BNL-E949**, A. V. Artamonov *et al.*, "*Study of the decay $K^+ \to \pi^+ \nu\bar{\nu}$ in the momentum region $140 < P_\pi < 199$ $MeV/c$*," Phys. Rev. **D79** (2009) 092004, arXiv:0903.0030.

[289] **E391a**, J. K. Ahn *et al.*, "*Experimental study of the decay K0(L) —¿ pi0 nu nu-bar*," Phys. Rev. **D81** (2010) 072004, arXiv:0911.4789.

[290] J. L. Ritchie and S. G. Wojcicki, "*Rare $K$ decays*," Rev. Mod. Phys. **65** (1993) 1149–1198.

[291] V. Cirigliano, G. Ecker, H. Neufeld, A. Pich, and J. Portoles, "*Kaon Decays in the Standard Model*," Rev. Mod. Phys. **84** (2012) 399, arXiv:1107.6001.

[292] G. Isidori and R. Unterdorfer, "*On the short distance constraints from $K_{L,S} \to \mu^+\mu^-$*," JHEP **01** (2004) 009, arXiv:hep-ph/0311084.

[293] M. Gorbahn and U. Haisch, "*Charm Quark Contribution to $K_L \to \mu^+\mu^-$ at Next-to-Next-to-Leading*," Phys. Rev. Lett. **97** (2006) 122002, arXiv:hep-ph/0605203.

[294] A. Crivellin, G. D'Ambrosio, M. Hoferichter, and L. C. Tunstall, "*Violation of lepton flavor and lepton flavor universality in rare kaon decays*," Phys. Rev. **D93** (2016) no. 7, 074038, arXiv:1601.00970.

[295] **BNL**, D. Ambrose *et al.*, "*New limit on muon and electron lepton number violation from K0(L) —¿ mu+- e-+ decay*," Phys. Rev. Lett. **81** (1998) 5734–5737, arXiv:hep-ex/9811038.

[296] A. J. Buras, "*Climbing NLO and NNLO Summits of Weak Decays*," arXiv:1102.5650.

# List of Publications

## Publications in Journals

1. **Girish Kumar**, Namit Mahajan, *$B \to K^* l^+ l^-$: Zeros of angular observables as test of standard model*, Phys. Rev. D **93**, (2016) no.5, 054041, doi: 10.1103/PhysRevD.93.054041.

2. Chandan Hati, **Girish Kumar**, Namit Mahajan, *$\bar{B} \to D^{(*)} \tau \bar{\nu}$ excesses in ALRSM constrained from $B$, $D$ decays and $D^0 - \bar{D}^0$ mixing*, JHEP 1601 (2016) 117, doi: 10.1007/JHEP01(2016)117.

3. **Girish Kumar**, *Constraints on a scalar leptoquark from the kaon sector*, Phys. Rev. D **94**, (2016) no.1, 014022, doi: 10.1103/PhysRevD.94.014022.

4. Diganta Das, Chandan Hati, **Girish Kumar**, Namit Mahajan, *Towards a unified explanation of $R_{D^{(*)}}$, $R_K$ and $(g-2)_\mu$ anomalies in a left-right model with leptoquarks*, Phys. Rev. D **94**, (2016), 055034, doi: 10.1103/PhysRevD.94.055034.

## Preprints

1. **Girish Kumar**, Namit Mahajan, *Asymmetries and observables for $\Lambda_b \to \Lambda \ell^+ \ell^-$*, arXiv:1511.00935.

# Publications attached with thesis

1. **Girish Kumar**, Namit Mahajan, *$B \to K^* l^+ l^-$: Zeros of angular observables as test of standard model*, Phys. Rev. D **93**, (2016) no.5, 054041, doi: 10.1103/PhysRevD.93.054041.

2. Chandan Hati, **Girish Kumar**, Namit Mahajan, *$\bar{B} \to D^{(*)} \tau \bar{\nu}$ excesses in ALRSM constrained from $B$, $D$ decays and $D^0 - \bar{D}^0$ mixing*, JHEP 1601 (2016) 117, doi: 10.1007/JHEP01(2016)117.

3. **Girish Kumar**, *Constraints on a scalar leptoquark from the kaon sector*, Phys. Rev. D **94**, (2016) no.1, 014022, doi: 10.1103/PhysRevD.94.014022.

PHYSICAL REVIEW D **93,** 054041 (2016)

# $B \to K^* l^+ l^-$: Zeros of angular observables as test of standard model

Girish Kumar[1,2,*] and Namit Mahajan[1,†]

[1]*Theoretical Physics Division, Physical Research Laboratory, Navrangpura, Ahmedabad 380 009, India*
[2]*Department of Physics, Indian Institute of Technology, Gandhinagar, Ahmedabad 382 424, India*
(Received 17 December 2014; revised manuscript received 17 April 2015; published 28 March 2016)

We calculate the zeros of angular observables $P_4'$ and $P_5'$ of the angular distribution of 4-body decay $B \to K^*(\to K\pi)l^+l^-$ where LHCb, in its analysis of form-factor independent angular observables, has found deviations from the standard model predictions. In the large recoil region, we obtain relations between the zeros of $P_4'$, $P_5'$ and the zero ($\hat{s}_0$) of forward-backward asymmetry of lepton pair, $A_{FB}$. These relations are independent of hadronic uncertainties and depend only on the Wilson coefficients. We also construct a new observable, $\mathcal{O}_T^{L,R}$, whose zero in the standard model coincides with $\hat{s}_0$, but in the presence of new physics contributions will show different behavior. Moreover, the profile of the new observable, even within the standard model, is very different from $A_{FB}$. We point out that precise measurements of these zeros in the near future would provide a crucial test of the standard model and would be useful in distinguishing between different possible new physics contributions to the Wilson coefficients.

DOI: 10.1103/PhysRevD.93.054041

## I. INTRODUCTION

Rare B decays are mediated by flavor changing neutral current (FCNC) transitions (e.g. $b \to s$) which are absent in the standard model (SM) at tree level. The leading contributions come from one-loop diagrams. Being suppressed by Glashow-Iliopoulos-Maiani mechanism (GIM) and Cabibbo-Kobayashi-Maskawa (CKM) factors, their predictions in SM are very tiny. As these processes are very sensitive to heavy particles in the loops, any effect of new physics (NP) will show significant deviation from SM predictions. This makes these decays assets in probing NP. So far data collected on rare B-decays by dedicated experiments (LHCb, B-factories) are in excellent agreement with the predictions of SM. The data have been used to retrieve information on flavor structure of possible new physics and to put stringent constraints on beyond Standard Model (BSM) scenarios, but expectations of looking for any definitive hints of NP have not met with success. The results seem to be consistent with the Cabibbo-Kobayashi-Maskawa mechanism of the SM [1]. However, recent data on angular observables of 4-body distribution in the process $[B \to K^*(\to K\pi)l^+l^-]$ indicate a plausible change in this situation. LHCb has measured several angular observables as a binned function of the dilepton invariant mass squared ($q^2$). The data indicate some tension with the SM [2]. These discrepancies might be a result of statistical fluctuations or inevitable theoretical uncertainties inherent to the calculation of these observables [3]. One has to wait for more experimental data and a more careful analysis of theoretical uncertainties to clear the smoke. Assuming that these discrepancies are solely due to NP effects, there have been attempts in the literature to resolve this tension between theory and the experimental side (see for example [4]).

In this paper, we study some of the angular observables $P_4'$, $P_5'$, $A_{FB}$ and a new observable, which we call $\mathcal{O}_T^{L,R}$, with a different approach. We look at the zeros of these observables. The expressions, under certain reasonable assumptions, are more or less independent of theoretical uncertainties, and depend solely on the short distance Wilson coefficients, and thus have very clean predictions in SM. Precise measurement of these quantities gives certain relations (experimentally testable) among the Wilson coefficients and therefore provides tests of short-distance physics. The most favored solutions to the present data explaining these deviations generally indicate towards new physics in the Wilson coefficient ($C_9^{\rm eff}$) of the semileptonic operator $O_9$ [5]. Since these zeros essentially probe new contributions to the Wilson coefficients, their experimental measurement in the near future can be worthwhile.

We proceed as follows. In the next section, we recall the effective Hamiltonian for $b \to sl^+l^-$. We discuss the 4-body angular distribution of $B \to K^*(\to K\pi)l^+l^-$ and various observables in the large energy recoil limit. In Sec. III, we calculate zeros of the observables $P_4'$, $P_5'$, $\mathcal{O}_T^{L,R}$ and obtain correlations among them. In Sec. IV, we give SM predictions for the zeros of the considered observables and discuss the implications of the zeros and their correlations in providing the new constraints on the BSM scenarios. The NP sensitivity of these zeros is discussed in detail. Finally, we summarize the results of this paper in Sec. V.

## II. ANGULAR OBSERVABLES OF $B \to K^* l^+ l^-$ IN THE LARGE RECOIL LIMIT

The basic framework to study rare FCNC decays is that of the effective Hamiltonian which is obtained after

*girishk@prl.res.in
†nmahajan@prl.res.in

 

integrating out the heavy degrees of freedom. The rare decay $B \to K^* l^+ l^-$ is governed by the effective Hamiltonian,

$$\mathcal{H}_{\text{eff}} = -\frac{4G_F}{\sqrt{2}} V_{ts}^* V_{tb} \sum_i (C_i(\mu) O_i + C_i'(\mu) O_i') + \text{H.c.}, \quad (1)$$

where contribution of the term $\propto \frac{V_{ub} V_{us}^*}{V_{tb} V_{ts}^*}$ is neglected. $O_i$ are the effective local operators and $C_i(\mu)$ are called Wilson coefficients evaluated at scale $\mu$. The factorization scale $\mu$ distinguishes between short distance physics (above scale $\mu$) and long distance physics (below scale $\mu$). The Wilson coefficients encode information about heavy degrees of freedom which have been integrated out while matrix elements of local operators $O_i$ dictate the low energy dynamics (for a review, see [6]). The operators contributing significantly to the process $B \to K^* l^+ l^-$ in SM are

$$\begin{aligned}
O_7 &= \frac{e}{16\pi^2} m_b (\bar{s}_\alpha \sigma_{\mu\nu} R b_\alpha) F^{\mu\nu}, \\
O_9 &= \frac{e^2}{16\pi^2} (\bar{s}_\alpha \gamma^\mu L b_\alpha)(\bar{l} \gamma_\mu l), \\
O_{10} &= \frac{e^2}{16\pi^2} (\bar{s}_\alpha \gamma^\mu L b_\alpha)(\bar{l} \gamma_\mu \gamma_5 l). \quad (2)
\end{aligned}$$

Here, $\alpha$, $\beta$ are the color indices, $L$, $R = \frac{(1 \mp \gamma_5)}{2}$ represent chiral projections and $m_b$ is the $b$-quark mass. The primed operators come with flipped helicity. Their contribution within SM is either severely suppressed or not present. The effective coefficient of operator $O_9$ is given by $C_9^{\text{eff}} = C_9 + Y(\hat{s})$. Here $s$ is lepton invariant mass ($q^2$) and $\hat{s} = s/m_B^2$. $Y(\hat{s})$ contains contributions from one-loop matrix elements of operators $O_{1,2,3,4,5,6}$. The functional form of $Y(\hat{s})$ can be found in [7]. Due to $Y(\hat{s})$, $C_9^{\text{eff}}$ is not real but has a small imaginary part. In the analytic relations below, $Y(\hat{s})$ is neglected and all the Wilson coefficients are assumed real, but for numerical calculations we include $Y(\hat{s})$ in $C_9^{\text{eff}}$. As we will see, this turns out to be a good working approximation.

To calculate observables for the $B \to K^*$ process, one needs to calculate matrix elements of the local operators $O_i$'s. These matrix elements are generally expressed in terms of seven form factors $V$, $A_0$, $A_1$, $A_2$, $T_1$, $T_2$ and $T_3$. These form factors are calculated via nonperturbative methods like QCD sum rules on the light cone [8]. Working in the QCD factorization framework and heavy quark and large recoil limit, all seven form factors can be written in terms of only two independent universal factors: $\xi_\perp$ and $\xi_\parallel$ [9]. The two sets of form factors are related to each other as (see for example [10])

$$\begin{aligned}
\xi_\perp &= \frac{m_B}{m_B + m_{K^*}} V(q^2), \\
\xi_\parallel &= \frac{m_B + m_{K^*}}{2E} A_1(q^2) - \frac{m_B - m_{K^*}}{m_B} A_2(q^2). \quad (3)
\end{aligned}$$

The angular distribution of $B \to K^*(\to K\pi) l^+ l^-$ offers experimentally accessible observables which are independent of form factors and hence theoretically cleaner. The fully differential decay distribution is given by [11]

$$\begin{aligned}
\frac{d^4\Gamma(b \to K^*(\to K\pi) l^+ l^-)}{\mathrm{d}q^2 \mathrm{d}\cos\theta_{K^*} \mathrm{d}\cos\theta_l \mathrm{d}\phi} &= \frac{9}{32\pi} J(q^2, \theta_l, \theta_{K^*}, \phi) \\
&= J_1^s \sin^2\theta_{K^*} + J_1^c \cos^2\theta_{K^*} + (J_2^s \sin^2\theta_{K^*} + J_2^c \cos^2\theta_{K^*}) \cos 2\theta_l \\
&\quad + J_3 \sin^2\theta_{K^*} \sin^2\theta_l \cos 2\phi + J_4 \sin 2\theta_{K^*} \sin 2\theta_l \cos\phi + J_5 \sin 2\theta_{K^*} \sin\theta_l \cos\phi \\
&\quad + (J_6^s \sin^2\theta_{K^*} + J_6^c \cos^2\theta_{K^*}) \cos\theta_l + J_7 \sin 2\theta_{K^*} \sin\theta_l \sin\phi \\
&\quad + J_8 \sin 2\theta_{K^*} \sin 2\theta_l \sin\phi + J_9 \sin^2\theta_{K^*} \sin^2\theta_l \sin 2\phi, \\
&= \sum_i J_i(q^2) f(\theta_l, \theta_{K^*}, \phi) \quad (4)
\end{aligned}$$

The angular coefficients $J_i(q^2)$ are expressed in terms of complex transversity amplitudes $A_{\perp,0,\parallel}^{L,R}$, $A_t$ and $A_s$. For $m_l \neq 0$, we have [11]

$$\begin{aligned}
J_1^s &= \frac{(2 + \beta_l^2)}{4} [|A_\perp^L|^2 + |A_\parallel^L|^2 + (L \to R)] + \frac{4m_l^2}{q^2} \mathrm{Re}(A_\perp^L A_\perp^{R*} + A_\parallel^L A_\parallel^{R*}), \\
J_1^c &= |A_0^L|^2 + |A_0^R|^2 + \frac{4m_l^2}{q^2} [|A_t|^2 + 2\mathrm{Re}(A_0^L A_0^{R*})] + \beta_l^2 |A_s|^2, \\
J_2^s &= \frac{\beta_l^2}{4} [|A_\perp^L|^2 + |A_\parallel^L|^2 + (L \to R)], \\
J_2^c &= -\beta_l^2 [|A_0^L|^2 + (L \to R),
\end{aligned}$$

$$
\begin{aligned}
J_3 &= \frac{1}{2}\beta_l^2[|A_\perp^L|^2 - |A_\parallel^L|^2 + (L \to R)],\\
J_4 &= \frac{\beta_l^2}{\sqrt{2}}[\mathrm{Re}(A_0^L A_\parallel^{L*}) + (L \to R)],\\
J_5 &= \sqrt{2}\beta_l\left[\mathrm{Re}(A_0^L A_\perp^{L*}) - (L \to R) - \frac{m_l}{\sqrt{q^2}}\mathrm{Re}(A_\parallel^L A_s^* + A_\parallel^R A_s^*)\right],\\
J_6^s &= 2\beta_l[\mathrm{Re}(A_\parallel^L A_\perp^{L*}) - (L \to R)],\\
J_6^c &= 4\beta_l\frac{m_l}{\sqrt{q^2}}\mathrm{Re}[A_0^L A_s^* + (L \to R)],\\
J_7 &= \sqrt{2}\beta_l\left[\mathrm{Im}\left(A_0^L A_\parallel^{L*} - (L \to R) + \frac{m_l}{\sqrt{q^2}}\mathrm{Im}(A_\perp^L A_s^* + A_\perp^R A_s^*\right)\right],\\
J_8 &= \frac{1}{\sqrt{2}}\beta_l^2[\mathrm{Im}(A_0^L A_\perp^{L*}) + (L \to R)],\\
J_9 &= \beta_l^2[\mathrm{Im}A_\parallel^{L*} A_\perp^L) + (L \to R)],
\end{aligned} \tag{5}
$$

where

$$\beta_l = \sqrt{1 - \frac{4m_l^2}{q^2}}. \tag{6}$$

Note that $A_s$ contributes only when scalar operators are taken into account. In this paper, we do not consider contributions from scalar operators. However, for the sake of generality, we have included $A_s$ in the expressions of $J_i(q^2)$. Also, we have dropped the explicit $q^2$ dependence of the transversity amplitudes for notational simplicity. At the leading order in $1/m_b$ and $\alpha_s$, the transversity amplitudes read

$$A_\perp^{L,R} = \sqrt{2}Nm_B(1-\hat{s})\left[(C_9^{\mathrm{eff}} + C_9^{\prime\mathrm{eff}}) \mp (C_{10} + C_{10}^\prime) + 2\frac{\hat{m}_b}{\hat{s}}(C_7^{\mathrm{eff}} + C_7^{\prime\mathrm{eff}})\right]\xi_\perp(E_{K^*}), \tag{7}$$

$$A_\parallel^{L,R} = -\sqrt{2}Nm_B(1-\hat{s})\left[(C_9^{\mathrm{eff}} - C_9^{\prime\mathrm{eff}}) \mp (C_{10} - C_{10}^\prime) + 2\frac{\hat{m}_b}{\hat{s}}(C_7^{\mathrm{eff}} - C_7^{\prime\mathrm{eff}})\right]\xi_\perp(E_{K^*}), \tag{8}$$

$$A_0^{L,R} = -\frac{Nm_b}{2\hat{m}_{K^*}\sqrt{\hat{s}}}(1-\hat{s})^2[(C_9^{\mathrm{eff}} - C_9^{\prime\mathrm{eff}}) \mp (C_{10} - C_{10}^\prime) + 2\hat{m}_b(C_7^{\mathrm{eff}} - C_7^{\prime\mathrm{eff}})]\xi_\parallel(E_{K^*}), \tag{9}$$

$$A_t = \frac{Nm_b}{\hat{m}_{K^*}\sqrt{\hat{s}}}(1-\hat{s})^2[C_{10} - C_{10}^\prime]\xi_\parallel(E_{K^*}). \tag{10}$$

In the above expressions,

$$N = \left[\frac{G_F^2\alpha^2}{3\times 2^{10}\pi^5 m_B^3}|V_{tb}V_{ts}^*|^2 q^2 \lambda^{1/2}\beta_l\right]^{1/2}. \tag{11}$$

Here, $\lambda = m_B^4 + m_{K^*}^4 + q^4 - 2(m_B^2 m_{K^*}^2 + m_{K^*}^2 q^2 + m_B^2 q^2)$, $\hat{m}_b = m_b/m_B$, and $E_{K^*}$ is the energy of $K^*$ meson. Terms of $\mathcal{O}(\hat{m}_{K^*}^2)$ have been neglected. However, it is worth mentioning that these relations hold only in the kinematic region $1 < q^2$ ($\mathrm{GeV}^2$) $< 6$, which is precisely the region of interest. There are in total 24 angular coefficients [$J_i(q^2)$ and $\bar{J}_i(q^2)$]. The charge-parity (CP) conjugated coefficients $\bar{J}_i$ [corresponding to CP conjugate mode of $B \to K^*(\to K\pi)l^+l^-$] are given by $J_i$ with the weak phases conjugated. The full angular analysis of $B \to K^*(\to K\pi)l^+l^-$ offers opportunities to construct observables which are insensitive to form factors as much as possible and therefore are theoretically cleaner and have high sensitivity to NP effects [11,12].

## III. ZEROS OF ANGULAR OBSERVABLES AND RELATIONS IN SM

The zero crossing of the forward backward asymmetry of the lepton pair ($\hat{s}_0$) is known to be highly insensitive to form factors. This was first pointed out in [13] where a number of form-factor models were considered and was noted that the value of $\hat{s}_0$ is practically independent of hadronic form factors. Later Ali *et al.* [14] in their analysis showed that $\hat{s}_0$ depends on the Wilson coefficients and ratios of form factors and in the heavy quark limit and large $E_{K^*} \sim \mathcal{O}(m_B/2)$, the hadronic uncertainties in ratios of form factors drop out, and $\hat{s}_0$ essentially depends on a combination of short distance parameters only. This leads to a nearly model-independent relation between the Wilson coefficients. The position of the zero crossing is thus heralded as a test of SM.

In SM, $\hat{s}_0$ is given by [14]

$$\mathrm{Re}(C_9^{\mathrm{eff}}(\hat{s}_0)) = -2\frac{\hat{m}_b}{\hat{s}_0}C_7^{\mathrm{eff}}\frac{1-\hat{s}_0}{1+\hat{m}_{K^*}^2-\hat{s}_0} \sim -2\frac{\hat{m}_b}{\hat{s}_0}C_7^{\mathrm{eff}}. \tag{12}$$

Note that existence of zero from the above Eq. (12) necessarily requires the condition $\mathrm{Sign}[\mathrm{Re}(C_9^{\mathrm{eff}})C_7^{\mathrm{eff}}] = -1$ to be satisfied. For NP models where $C_7^{\mathrm{eff}}$ has the same sign as $C_9^{\mathrm{eff}}$, there will then be no zero crossing. The LHCb collaboration [15][1] has measured the zero of forward-backward asymmetry of the lepton pair to be $q_0^2 = 4.9 \pm 0.9\ \mathrm{GeV}^2$ which, within errors, is consistent with SM predictions. The SM predictions for $\hat{s}_0$ typically lie in the range (3.7–4.3) $\mathrm{GeV}^2$ which in units normalized by mass of $B$-meson ($\hat{s}=q^2/m_B^2$) translates to range (0.13–0.16) and have relative uncertainties below 10% level [10,17,18].

The value of zero $\hat{s}_0$ can be easily obtained from integrated $q^2$ angular observable, $A_{FB}$. In terms of the angular coefficients $(J_i(q^2))$, $A_{FB}$ is defined as

$$A_{FB} = -\frac{3}{4}\frac{\int dq^2(J_{6s}+\bar{J}_{6s})}{\int dq^2(d\Gamma/dq^2+d\bar{\Gamma}/dq^2)}. \tag{13}$$

To calculate $\hat{s}_0$, we use the expressions of the transversity amplitudes given in Eqs. (7)–(10), which are valid in the large recoil region. We retain contributions of helicity-flipped Wilson coefficients so that analysis done includes a subset of NP models involving primed Wilson coefficients.[2] We now discuss the angular variables of interest and work in the basis where SM operators are augmented with their helicity flipped counterparts. The expressions below clearly show the power of the zero-crossing point of these angular observables to probe different NP scenarios. The zero crossing of any observable is easily obtained by equating the numerator to zero. From Eq. (13), we obtain

$$\hat{s}_0 = -2\frac{(C_{10}C_7^{\mathrm{eff}} - C'_{10}C'_7)}{(C_{10}C_9^{\mathrm{eff}} - C'_{10}C'_9)}\hat{m}_b. \tag{14}$$

Within SM ($C'_i \to 0$), dependence on $C_{10}$ cancels out and the expression reduces to Eq. (12), sensitive to the ratio of $C_7^{\mathrm{eff}}$ and $C_9^{\mathrm{eff}}$.

The angular observables $P'_5$ and $P'_4$ both have zero-crossing point in their mass spectrum. The value of zero crossing for both lies in the "theoretically clean" low-$q^2$ region; interestingly the same region where LHCb has measured deviation from SM prediction for angular observables $P'_5$.

Observable $P'_5$ is related to angular coefficients $J_5$ through the following relation:

$$P'_5 = \frac{\int dq^2(J_5+\bar{J}_5)}{2\sqrt{-\int dq^2(J_{2s}+\bar{J}_{2s})\int dq^2(J_{2c}+\bar{J}_{2c})}}. \tag{15}$$

The numerator of $P'_5$ in the massless lepton limit is proportional to $[\mathrm{Re}(A_0^L A_\perp^{L*}) - (L\leftrightarrow R)]$. Then the zero of $P'_5$, in the low-recoil region, is given by the following combination of short-distance parameters:

$$\hat{s}_0^{P_5} = \frac{(C_7^{\mathrm{eff}}+C'_7)(C'_{10}-C_{10})}{[C_{10}C_9^{\mathrm{eff}} - C'_{10}C'_9 + (C_7^{\mathrm{eff}}-C'_7)(C_{10}+C'_{10})\hat{m}_b]}\hat{m}_b. \tag{16}$$

The zero of $P'_5$ turns out to be insensitive to hadronic form factors similar to the zero of $A_{FB}$. In the SM limit, $C_{10}$ dependence disappears and the expression reduces to a very simple relation between the value of zero and the Wilson coefficient $C_7^{\mathrm{eff}}$ and $C_9^{\mathrm{eff}}$,

$$\hat{s}_0^{P_5,\mathrm{SM}} = -\frac{C_7^{\mathrm{eff}}}{C_9^{\mathrm{eff}}+C_7^{\mathrm{eff}}\hat{m}_b}\hat{m}_b. \tag{17}$$

Interestingly enough, we find that within SM, the zero of $P'_5$ can be written solely in terms of $\hat{s}_0$: zero of $A_{FB}$

$$\hat{s}_0^{P_5,\mathrm{SM}} = \frac{\hat{s}_0^{\mathrm{SM}}/2}{1-\hat{s}_0^{\mathrm{SM}}/2}. \tag{18}$$

We find this correlation between zero of $A_{FB}$ and that of $P'_5$ an important result. Equation (18) can be expanded in a Taylor series and dropping out terms of order $\mathcal{O}((\hat{s}_0^{\mathrm{SM}}/2)^2)$ and higher, the relation predicts that zero of $P'_5$ is approximately half of the value of $\hat{s}_0$ in SM.

A similar analysis can also be done for observable $P'_4$. In terms of angular coefficients $J_i's$, observable $P'_4$ is written as

$$P'_4 = \frac{\int dq^2(J_4+\bar{J}_4)}{\sqrt{-\int dq^2(J_{2s}+\bar{J}_{2s})\int dq^2(J_{2c}+\bar{J}_{2c})}}. \tag{19}$$

The numerator of $P'_4$ is $\propto [\mathrm{Re}(A_0^L A_\parallel^{L*}) + (L\leftrightarrow R)]$. Using expressions (8) and (9) for transversity amplitudes $A_0^L$ and $A_\parallel^L$, we find zero of $P'_4$ to be

[1]The LHCb collaboration has recently updated its measured value: $q_0^2 = 3.7^{+0.8}_{-1.1}$ [16].

[2]We reiterate that in the analytic relations, we assume $C_i$'s to be real but retain the complex nature in numerical analysis.

$$\hat{s}_0^{P_4} = -2\frac{(C_7^{\rm eff} - C_7')[C_9^{\rm eff} - C_9' + 2(C_7^{\rm eff} - C_7')\hat{m}_b]}{[(C_9^{\rm eff} - C_9')^2 + (C_{10} - C_{10}')^2 + 2(C_7^{\rm eff} - C_7')(C_9^{\rm eff} - C_9')\hat{m}_b]}\hat{m}_b. \tag{20}$$

The expression is again very "clean" and has a nontrivial dependence on short-distance parameters in the large recoil region. In the SM limit, this relation yields

$$\hat{s}_0^{P_4,\rm SM} = -2\frac{C_7^{\rm eff}C_9^{\rm eff} + 2(C_7^{\rm eff})^2\hat{m}_b}{C_{10}^2 + (C_9^{\rm eff})^2 + 2C_7^{\rm eff}C_9^{\rm eff}\hat{m}_b}\hat{m}_b. \tag{21}$$

The zero of $P_4'$ can also be written in terms of $\hat{s}_0$ only as

$$\hat{s}_0^{P_4,\rm SM} = \frac{\hat{s}_0^{\rm SM}(1-\hat{s}_0^{\rm SM})}{(2-\hat{s}_0^{\rm SM})}. \tag{22}$$

Again using the fact that the value of $\hat{s}_0$ is very small compared to unity, we find the value of zero of $P_4'$ to be approximately half of $\hat{s}_0$, similar to the case of $P_5'$. However, if we keep effects of higher order terms in $\hat{s}_0$, the value of zero of $P_5'$ and that of $P_4'$ turns out be a bit larger and smaller than $\hat{s}_0^{\rm SM}/2$ respectively and the leading effect is of order $(\hat{s}_0)^2$. From the experimental point of view, this accuracy is currently not there and therefore the effect can be safely neglected. The correlation between zeros of $A_{FB}$, $P_4'$, $P_5'$ is quite intriguing since in a chosen optimal basis of observables, $A_{FB}$, $P_5{}'$ and $P_4'$ are independent observables and there is no *a priori* reason for their zero-crossing points to develop this dependence on each other.

With enough data available, one would be able to perform a full angular analysis of the final state distribution in the decay $B \to K^*(\to K\pi)l^+l^-$ and this would allow complete determination of the $K^*$ spin amplitudes. Therefore one can use the spin amplitudes to design observables which are sensitive to specific NP and have relatively controlled theoretical uncertainties. With this in mind, we propose a new CP conserving observable which we call $\mathcal{O}_T^{L,R}$. It has the following form:

$$\mathcal{O}_T^{L,R} = \frac{|A_\perp^L|^2 + |A_\parallel^L|^2 - (L\leftrightarrow R)}{8(J_{2s}+\bar{J}_{2s})}. \tag{23}$$

This new observable is constructed out of both parallel and perpendicular spin amplitudes of $K^*$ and has not been explored before in the literature. The ratio of amplitudes is chosen such that theoretical uncertainties due to the hadronic form factors cancel at the leading order. The profile of $\mathcal{O}_T^{L,R}$ also has a zero in the low-$q^2$ region. In a basis where SM operator structure is augmented with right-handed currents, the zero of $\mathcal{O}_T^{L,R}$ has NP sensitivity differently from that of $A_{FB}$. Its zero-crossing point occurs at

$$\hat{s}_0^{\mathcal{O}_T^{L,R}} = -2\frac{(C_{10}C_7^{\rm eff} + C_{10}'C_7')}{(C_{10}C_9^{\rm eff} + C_{10}'C_9')}\hat{m}_b. \tag{24}$$

The expressions $\hat{s}_0$ [Eq. (14)] and $\hat{s}_0^{\mathcal{O}_T^{L,R}}$ [Eq. (24)] have some interesting features. By definition, observables $A_{FB}$ and $\mathcal{O}_T^{L,R}$ have nonidentical dependence on invariant mass $\hat{s}$ and therefore vary differently as a function of $\hat{s}$. But within SM, in spite of the different profiles, the values of zero crossings, $\hat{s}_0^{\rm SM}$ and $\hat{s}_0^{\mathcal{O}_T^{L,R},\rm SM}$, are degenerate. However, in the presence of helicity flipped operators, the positions of zero-crossing shift in a dissimilar fashion and the degeneracy gets lifted. This rather utilitarian feature can be used to probe contributions from helicity flipped operators once the values of $\hat{s}_0$ and $\hat{s}_0^{\mathcal{O}_T^{L,R}}$ are known experimentally with good precision.

Let us remark that all the expressions and relations obtained above have been worked out under the hypothesis of no scalar and tensor contributions. Observables $A_{FB}$, $P_4'$ and the proposed new observable $\hat{s}_0^{\mathcal{O}_T^{L,R}}$ are blind to the presence of scalar/tensor contributions. Therefore, the expressions for zeros will remain unaltered even in the presence of these new contributions. Observable $P_5'$, however, does receive contributions from the scalar component of $K^*$-spin amplitudes. But the sensitivity to this contribution is highly suppressed ($m_\mu^2/q^2$ is the suppression factor) and in the limit of massless leptons limit, which we have entertained in this paper, these contributions vanish.

## IV. CONSTRAINING NEW PHYSICS

All the Wilson coefficients are real in this analysis, i.e., NP does not introduce any new weak phase in the Wilson coefficients and we assume that the sign of $C_7$ is as in the SM. We will ignore NP scenarios where $C_7$ and $C_9$ have the same sign. The expressions of zeros of these observables depend only on the Wilson coefficients, practically independent of form factors, thereby leading to theoretically clean predictions. To calculate these zeros, we use $C_9 = 4.2297$, $C_{10} = -4.2068$, $C_7^{\rm eff} = -0.2974$ [19] at scale $m_b$. Other input parameters are $m_b^{\rm pole} = 4.80\,\text{GeV}$, $G_F = 1.166\times10^{-5}$, $m_B = 5.280\,\text{GeV}$, $m_{K^*} = 0.895$ GeV, $m_\mu = 0.106$ GeV, $\alpha = 1/129$, and $\alpha_s = 0.21$.

In Table I, we give the numerical values of zeros of the observables in the SM. The values in the second column are obtained using the relations in Eqs. (14), (18), (22), and (24). To compare with the exact predictions in the SM and to have a consistency check of these relations, we also calculate values of these zeros in the SM using the form factors and retaining $Y(\hat{s})$ in $C_9^{\rm eff}$, which we had ignored for obtaining analytic relations among the zeros. We use the form factors calculated in [8] using the light-cone sum rule and tabulate the results in the third column of Table I whereas in the last column we tabulate the same results

TABLE I. Zeros in the SM. In the second column, we quote the values calculated using Eqs. (14), (18), (22), and (24), while the third and fourth columns have entries predicted in the SM using form factors from [8,9], respectively.

| | Value of zero | Exact values of zero crossings | |
|---|---|---|---|
| Observable | Using analytic relations | Using FFs from [8] | Using FFs from [9] |
| $A_{FB}$ | 0.128 | 0.122 | 0.125 |
| $P'_5$ | 0.068 | 0.069 | 0.069 |
| $P'_4$ | 0.059 | 0.054 | 0.056 |
| $\mathcal{O}_T^{L,R}$ | 0.128 | 0.122 | 0.125 |

using form factors as in Beneke *et al.* [9]. As is evident, the two sets of form factors yield very similar values, thereby confirming that these zeros are (almost) independent of form factors. Clearly, the employed analytic relations yield values close to those when no approximations are made, showing the robustness of these relations. All the zeros lie in the low-$q^2$ region, where form factors are known with relatively greater precision. At leading order, soft form factors cancel precisely and predictions of zeros are clean. Largest corrections to the values of zeros come from form-factor uncertainties when next-to-leading order effects are included (as noted in [20] for the case of $\hat{s}_0$). The typical error on form factors is ∼10%–12% (see [8]). Assuming the size of errors in all the form factors of the same order, we find the relative uncertainties in our estimates of these zeros to be of order ∼30%. So far experimentally as well as theoretically only $\hat{s}_0$ has received attention. The experimental value of $\hat{s}_0$ has large relative uncertainties (of order 35%) [15,16]. Though we have ignored $\mathcal{O}(\alpha_s)$ contributions in favor of obtaining form-factor insensitive correlations among the zeros, our theoretical estimate of $\hat{s}_0$ is still competitive with the experimental value with current precision as discussed above. The zeros and the relations among them can be used to constrain the Wilson coefficients in the following ways:

(i) Under the hypothesis of no NP-induced right-handed currents and real Wilson coefficients, all the zeros including that of the new observable $\mathcal{O}_T^{L,R}$ are functions of $C_7^{\rm eff}$ and $C_9^{\rm eff}$ only. With the magnitude of $C_7^{\rm eff}$ stringently constrained from branching ratio of decay $B \to K^*\gamma$ (and $B \to X_s\gamma$), the zeros provides new information on $C_9^{\rm eff}$.

(ii) Some of the zero-crossing points are sensitive to the right-handed currents (more details below). These contributions can be probed once the precise measurements of zero crossings are made.

Global fits to recently updated data on angular analysis of the $B \to K^*\mu\mu$ indicate significant tension with the SM [5]. It has been suggested that solutions having a destructive NP contribution to $C_9$ or with $C_9^{\rm NP} = -C_{10}^{\rm NP} < 0$ are in very good agreement with the data. From this perspective, the measurement of these zero-crossing points would provide a very clean and good test of the hypothesis of the NP contribution to $C_9$. In Fig. 1, we show the constrained region in $C_7$ and $C_9$ plane in the SM-like operator basis. The most stringent bounds on $C_7$ come from decay $B \to X_s\gamma$. Then the precise measurement of $\hat{s}_0$ essentially determines the effective coefficient $C_9^{\rm eff}$. The recently measured value of $\hat{s}_0$ currently involves large errors (∼35%) [16]. Therefore, bounds on $C_9^{\rm eff}$ are not as stringent. But a qualitative analysis shows that $\hat{s}_0$ is compatible with models having NP contribution to $C_9$. We also provide a constrained region in the $C_7$–$C_9$ plane using bounds from the zero of $P'_4$ and $P'_5$. To this end, we employ derived relations between $\hat{s}_0$ and zeros of $P'_4$ and $P'_5$. Further, we use the experimentally measured value of $\hat{s}_0$ as an input to get constraints from zeros of $P'_4$ and $P'_5$. We find that the measurement of these zeros will provide equally efficient constraints on $C_9$ as drawn from $\hat{s}_0$. We

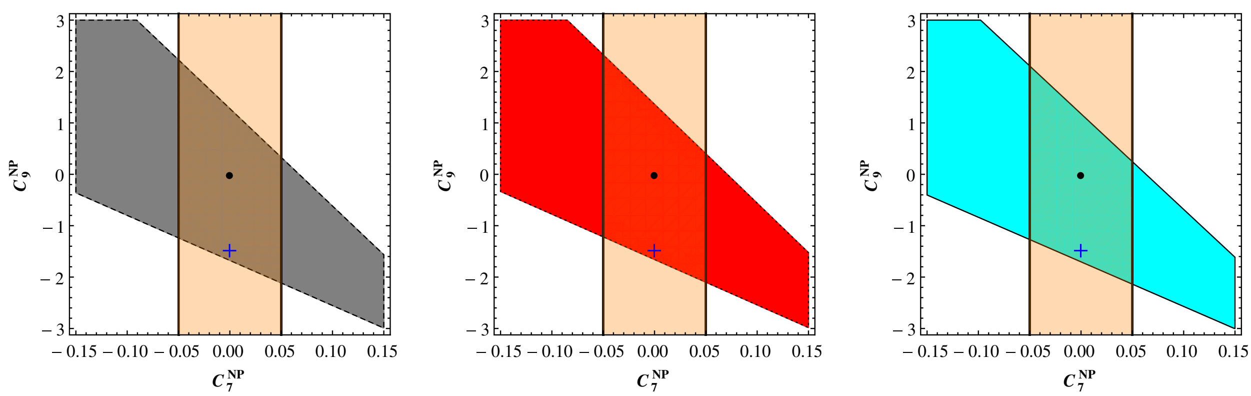


FIG. 1. Constraints on $C_7^{\rm NP} - C_9^{\rm NP}$ from zeros of observables $A_{FB}$ (gray), $P'_5$ (red) and $P'_4$ (cyan) using analytic relations [Eqs. (14), (18), (22), and (24)]. The light orange band shows the constraints on the values of $C_7$ from $B \to X_s\gamma$. The black filled circle shows the SM point whereas the blue colored "+" in the plots corresponds to the simplest possible NP solution $C_9^{NP} = -1.5$ to explain the observed tension in the experimental data on $b \to s\mu^+\mu^-$. The NP solution $C_9^{NP} = -1.5$ corresponds to the "BSM1" scenario and has been discussed in detail later in the text.

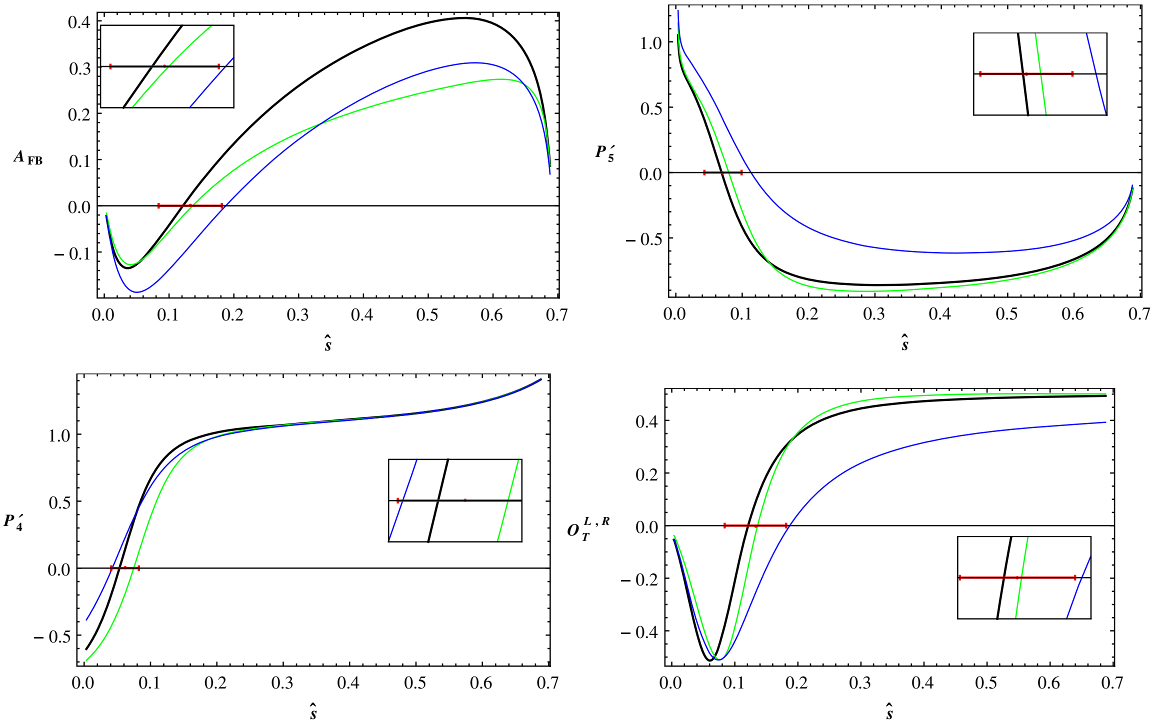


FIG. 2. The $q^2$ spectrum of observables $A_{FB}$, $P_5'$, $P_4'$ and $\mathcal{O}_T^{L,R}$ in SM (black curve) and two BSM scenarios: $Z'$ motivated models (blue curve) and SUSY models (green curve). The $Z'$ model [21,22] corresponds to $C_9^{NP} \sim -1.5$. The SUSY model (green curve) corresponds to large $\tan\beta$ with superpartners being heavy [23]. The red interval on the x-axis shows the experimentally allowed $1\sigma$ region. We use $\hat{s} = q^2/m_B^2$.

also note that zero-crossing points of these observables are rather sensitive to a slight change in the Wilson coefficient $C_7$ compared to a change in $C_9$ and $C_{10}$ in the SM-like basis. For illustrative purposes, we individually varied $C_7$, $C_9$, and $C_{10}$ by 15% with respect to their SM value. We find that the change in $C_7$ causes central values of $\hat{s}_0$, $\hat{s}_0^{P_5'}$, $\hat{s}_0^{P_4'}$ and $\hat{s}_0^{\mathcal{O}_T^{L,R}}$ to shift by about 15% with respect to the SM value on the negative side, the change in $C_9$ causes relatively less shift (about 13%) in $\hat{s}_0$, $\hat{s}_0^{P_5'}$, $\hat{s}_0^{P_4'}$ and $\hat{s}_0^{\mathcal{O}_T^{L,R}}$ and no shift in $\hat{s}_0^{P_4'}$ while the change in the Wilson coefficient $C_{10}$ does not cause any modification in the SM value of the $\hat{s}_0$, $\hat{s}_0^{P_5'}$ and $\hat{s}_0^{\mathcal{O}_T^{L,R}}$ but shifts the SM value of $\hat{s}_0^{P_4'}$ by a positive 15%.

In Fig. 2, we plot the $q^2$ spectrum of all four observables ($A_{FB}$, $P_5'$, $P_4'$ and $\mathcal{O}_T^{L,R}$) in different NP models along with SM. On the x-axis, the red interval shows the $1\sigma$ allowed region currently supported by experimental data on $\hat{s}_0$. In the plot $A_{FB}$ vs $\hat{s}$, the red interval corresponds to experimental value $q_0^2 = 3.7^{+0.8}_{-1.1}$ GeV$^2$ [16]. Since at present measurements of zeros except $A_{FB}$ are not available, we employ the correlations in Eqs. (14), (18), (22) and (24) and use the experimental value of $\hat{s}_0$ with associated errors to obtain the values and corresponding errors in the values of other zeros. As an illustration of how much these zeros can constrain the NP models, we include two scenarios of new physics in our analysis. First is the often discussed NP scenario which postulates a new $U(1)'$ gauge boson. These models, typically known as $Z'$ models, have been shown to explain the observed anomalies in $B \to K^*\mu\mu$ [21,22]. We find that such models, which have NP contribution to $C_9^{NP} \sim -1.5$, are at $1.1\sigma$ tension with the current data on $\hat{s}_0$. The same tension translates to the zero of $P_4'$ as well. The theoretical value of $\hat{s}_0^{P_5'}$ in this model is at $1.5\sigma$ tension with the data while the value of $\hat{s}_0^{\mathcal{O}_T^{L,R}}$ has $1.3\sigma$ tension with experimental data.[3] We also show the $q^2$ profile of all four observables with their zeros in the supersymmetric models (SUSY). The decays $B \to (K, K^*)ll$ are sensitive to the new contributions in these models and the invariant mass spectrum, forward-backward asymmetry, and lepton polarizations of these modes can constrain these models [23]. The variant of SUSY we have considered corresponds to large $\tan\beta$ with the masses of superpartners being relatively large. The details of the model can be found in [23]. Here we only show that zeros of all four observables in this model are consistent with the

[3]Let us remind again that since no actual data is available for the zeros if $P_4'$, $P_5'$, and $O_T^{L,R}$, what is meant by data in this specific context is the values obtained using correlations [Eqs. (18), (22) and (24)] with $\hat{s}_0$ as measured by LHCb as an input.

experimental data within $1\sigma$. This good agreement between predictions in the discussed models and the measurement can be expected given the fact that substantial uncertainties are affecting the present experimental measurement of these zeros. Let us remark that the analysis in Fig. 2 for the cases of $P'_5$, $P'_4$, $\mathcal{O}_T^{L,R}$ is of qualitative nature since the zeros of these observables have not been measured so far (we again reiterate that we have used the experimental value of $\hat{s}_0$ to obtain the "experimentally allowed" red interval for these observables in Fig. 2). Our purpose here is just to illustrate that not only the $q^2$ profile, but the precise measurement of the zero-crossing points can also be used to discriminate various NP models. Once precise measurements of the zeros are available, the analysis can be done more precisely and the relations can certainly provide improved constraints on NP, especially on the $C_9^{\rm eff}$.

Finally, we investigate the BSM reach of these zeros by carrying out a numerical study of $\hat{s}_0^{P'_5}$, $\hat{s}_0^{P'_4}$ and $\hat{s}_0^{\mathcal{O}_T^{L,R}}$ in Table II. In the SM, their values lie in the large recoil region and therefore these observables, like zero of $A_{FB}$, are expected to be very clean. These zeros also have sensitivity to BSM effects induced by right-handed currents. The BSM scenarios we have chosen in Table II are motivated from the analysis [5] of the updated data on $B \to K^*\mu\mu$ and are obtained by allowing variation in a single Wilson coefficient at a time. The case BSM1 is most favored while the cases BSM2 and BSM3 are less favorable. The three columns in Table II correspond to these scenarios as follows:

(i) The scenario BSM1 corresponds to a negative contribution of $-1.5$ to the SM value of $C_9$ (shown in Fig. 1 by the symbol "+"). This kind of scenario could, for example, be generated by a $Z'$ boson which has vectorlike coupling to muons [24], where $C_9$ has a nonzero contribution while the NP contribution to the Wilson coefficient $C_{10}$ vanishes.

(ii) The other two columns correspond to cases where NP enters in a correlated way in two Wilson coefficients. The second scenario, BSM2, has new physics in the $SU(2)_L$ invariant direction $C_9^{NP} = -C_{10}^{NP}$ and can be realized in $Z'$ models with the $Z'$ boson having coupling to left-handed muons [24]. A scalar leptoquark $\phi$ transforming as $(3,3)_{-1/3}$ under $(SU(3), SU(2))_{U(1)}$ with couplings to left-handed muons can also generate this scenario [25].

(iii) The third scenario stems from new contributions from helicity-flipped semileptonic operators $O'_9$ and $O'_{10}$. This case was specifically chosen to show the distinguishing features of these zeros when only right-handed currents have new physics contributions.

In each of the BSM scenarios, estimates of uncertainties are the same as discussed for the SM case. Our numerical analysis explicitly shows that the observables $\hat{s}_0^{P'_5}$, $\hat{s}_0^{P'_4}$ and $\hat{s}_0^{\mathcal{O}_T^{L,R}}$ along with $\hat{s}_0$ can certainly distinguish between the SM case (SM predictions for zeros are given in Table I) and different BSM hypotheses. An important point we would like to make here is that from Table II, it is clear that $\hat{s}_0$ has very similar values as $\hat{s}_0^{\mathcal{O}_T^{L,R}}$ in all scenarios. This is true only when there is no contribution from right-handed currents (like the cases BSM1 and BSM2). The values of zero-crossing points would not be identical when right-handed currents are invoked (like in the case BSM3). However, the difference between $\hat{s}_0$ and $\hat{s}_0^{\mathcal{O}_T^{L,R}}$ in the case BSM3 is arising only beyond the third decimal place and therefore, at present, can be neglected in favor of experimental errors. We would like to draw attention to the fact, as emphasized above also, that not just the position of the zero of an angular observable but also the complete profile as a function of $\hat{s}_0$ is a powerful tool at hand. This is illustrated in Fig. 2 where one can clearly see that, though the value of $\hat{s}_0^{\rm SM}$ coincides with $\hat{s}_0^{\mathcal{O}_T^{L,R}}$ in the SM, the $q^2$ spectrums of $A_{FB}$ and $\mathcal{O}_T^{L,R}$ are quite different.

We would be able to identify distinctions among different NP scenarios more accurately once these zeros are precisely measured. Experimentally, only $\hat{s}_0$ has received attention. We stress that the other zeros are equally important and should be measured or extracted experimentally, since this could already yield crucial information about NP, if present. Further, it may happen that some of the observable profiles (i.e. values in experimentally measured bins) turn out to be different from SM, as is the case say with $P'_5$. In such a situation, a further check would be the position of the zero. These two pieces of information put together will clearly point out to any NP present.

TABLE II. Values of zeros compared between different BSM scenarios. Only nonzero NP Wilson coefficients are shown in each scenario. The values in the parentheses correspond to beyond the third decimal place. See Table I for values in the SM.

| | BSM1 | BSM2 | BSM3 |
|---|---|---|---|
| Observable | $C_9^{NP} = -1.5$ | $C_9^{NP} = -C_{10}^{NP} = -0.53$ | $C'_9 = C'_{10} = -0.10$ |
| $\hat{s}_0$ | 0.198 | 0.146 | 0.127(76) |
| $\hat{s}_0^{P'_5}$ | 0.109 | 0.078 | 0.067 |
| $\hat{s}_0^{P'_4}$ | 0.050 | 0.067 | 0.061 |
| $\hat{s}_0^{\mathcal{O}_T^{L,R}}$ | 0.198 | 0.146 | 0.127(91) |

## V. SUMMARY AND CONCLUSIONS

The radiative and semileptonic $b \to s$ decays have a potential sensitivity to effects beyond the SM. With LHCb's dedicated efforts to measure the decay $B \to K^* ll$ and associated angular observables extensively, the decay $B \to K^* ll$ seems to be a promising field to identify patterns of NP which can be provided by experimental data. Recent data shows some discrepancies in comparison to SM predictions but due to uncertainties inherent in the theoretical calculations of such processes, at present, it is difficult to infer the same in affirmation. Precise measurements of theoretically clean observables hold the best chance of unambiguously revealing the presence of physics beyond the SM, if any. The zero of forward-backward asymmetry ($\hat{s}_0$) is known to fall under this category of observables. But the current measurement is not precise enough to say anything definitive and is totally consistent with the SM. It may be useful to have more such observables measured with precision. In this paper, we point out that along with $\hat{s}_0$, the zeros of observables $P'_5$, $P'_4$ and $\mathcal{O}_T^{L,R}$ (a new angular observable proposed in this paper) are suitable candidates in this regard. The zeros of these observables, like the case of $\hat{s}_0$, have good theoretical control over hadronic uncertainties and can provide crucial tests of the SM. We note that there exist correlations among zeros of different observables within the SM and the position of all the zeros is essentially fixed by $\hat{s}_0$, up to small corrections. We further use these relations to model-independently constrain the $C_7^{NP} - C_9^{NP}$ plane. To this end, we define our framework by considering that NP enters in electromagnetic ($O_7$) and semileptonic operators ($O_9$, $O_{10}$), together with their chirally flipped counterparts. We have assumed the Wilson coefficients to be real, but generalization to complex coefficients is straightforward.

We studied the implications of these zeros on $C_7^{NP} - C_9^{NP}$ plane in the SM-like operator basis. The conservative bounds on $C_7^{NP}$ are taken from $B \to X_s \gamma$ experimental data. Owing to the rather large uncertainties in the current measured value of $\hat{s}_0$, the constraints on the Wilson coefficient $C_9$ are rather weak and the deviations of up to $\sim -1.5$ in $C_9$ are compatible with experimental data within the $1\sigma$ range. Using relations between $\hat{s}_0$ and zeros of $P'_5$ and $P'_4$, we show that observables $\hat{s}_0^{P'_5}$, $\hat{s}_0^{P'_4}$ have equally good sensitivity to $C_9$ and $C_7$ as present in $\hat{s}_0$. In addition to the SM-like basis scenario, we further investigated the cases where operator basis is augmented by helicity-flipped operators. We note that these observables are quite sensitive to the effects stemming from BSM models. This can be observed from the numerical analysis we performed in Table II and Fig. 2. The analysis clearly shows that these observables have the capability to discriminate between different BSM models. Especially, the new proposed observable $\mathcal{O}_T^{L,R}$ and its zero are relatively more sensitive to the scenarios where one only includes the NP contribution to semileptonic vector operator $O_9$ (e.g. $Z'$-model). These scenarios are currently favored by data over SM (by $3.7\sigma$ for $C_9^{NP} \sim -1.1$) as noted in [5]. This sensitivity can be further exploited to test such scenarios once more precise data on this new observable as well as on the zeros of aforementioned observables become available. To date, only $\hat{s}_0$ has received attention but we have shown that zeros of other angular observables also carry important and complementary information on short-distance parameters. We thus hope that these observables will be measured precisely by the LHCb collaboration and data on these observables can certainly be used to put stern constraints on NP. The relations are obtained in the large recoil region in the large energy limit where theoretical uncertainties are supposed to be minimal. To the best of our knowledge, this is the first attempt to use such correlations as a stringent test of SM itself. A simultaneous accurate determination of these zeros will surely provide conclusive evidence of any NP present. Moreover, in a general setting, the zeros by themselves carry complementary information about the Wilson coefficients and their measurement together with the existing data can be used to pinpoint the class of NP scenarios which can give rise to such predictions. This is clearly evident from the position of $\hat{s}_0^{\mathcal{O}_T^{L,R}}$ which in the standard model limit yields the same value as $\hat{s}_0$ but when the helicity flipped operators are included, leads to complementary information on the Wilson coefficients compared to what was inferred from $\hat{s}_0$. We also hope that with more data, not just the position of various zeros, but also the complete profiles of angular observables will be known with high precision, which can be used further as a crucial test of the standard model.


[1] M. Kobayashi and T. Maskawa, *CP* violation in the renormalizable theory of weak interaction, Prog. Theor. Phys. **49**, 652 (1973).

[2] R. Aaij *et al.* (LHCb Collaboration), Measurement of Form-Factor-Independent Observables in the Decay $B^0 \to K^{*0}\mu^+\mu^-$, Phys. Rev. Lett. **111**, 191801 (2013).

[3] D. Das and R. Sinha, New physics effects and hadronic form-factor uncertainties in $B \to K^* \ell^+ \ell^-$, Phys. Rev. D **86**, 056006 (2012); S. Jäger and J. Martin Camalich, On $B \to V$ l l at small dilepton invariant mass, power corrections, and new physics, J. High Energy Phys. 05 (2013) 043; C. Hambrock, G. Hiller, S. Schacht, and R. Zwicky, $B \to K^*$

form factors from flavor data to QCD and back, Phys. Rev. D **89**, 074014 (2014); J. Lyon and R. Zwicky, Resonances gone topsy turvy—the charm of QCD or new physics in $b \to s\ell^+\ell^-$?, arXiv:1406.0566; S. Descotes-Genon, L. Hofer, J. Matias, and J. Virto, On the impact of power corrections in the prediction of $B \to K*mu+mu-$ observables, J. High Energy Phys. 12 (2014) 125; R. Mandal, R. Sinha, and D. Das, Testing new physics effects in $B \to K^*\ell^+\ell^-$, Phys. Rev. D **90**, 096006 (2014).

[4] S. Descotes-Genon, J. Matias, and J. Virto, Understanding the $B \to K^*\mu^+\mu^-$ anomaly, Phys. Rev. D **88**, 074002 (2013); W. Altmannshofer and D. M. Straub, New physics in $B \to K^*\mu\mu$?, Eur. Phys. J. C **73**, 2646 (2013); R. Gauld, F. Goertz, and U. Haisch, On minimal Z' explanations of the $B \to K*mu+mu-$ anomaly, Phys. Rev. D **89**, 015005 (2014); A. J. Buras and J. Girrbach, Left-handed Z' and Z FCNC quark couplings facing new $b \to s\mu^+\mu^-$ data, J. High Energy Phys. 12 (2013) 009; A. Datta, M. Duraisamy, and D. Ghosh, Explaining the $B \to K^*\mu^+\mu^-$ data with scalar interactions, Phys. Rev. D **89**, 071501 (2014); W. Altmannshofer and D. M. Straub, New physics in $b \to s$ transitions after LHC run 1, arXiv:1411.3161; S. Jäger and J. Martin Camalich, Reassessing the discovery potential of the $B \to K^*\ell^+\ell^-$ decays in the large-recoil region: SM challenges and BSM opportunities, Phys. Rev. D **93**, 014028 (2016); L. Hofer and J. Matias, Exploiting the symmetries of P and S wave for $B \to K^*mu^+mu^-$, J. High Energy Phys. 09 (2015) 104; S. Descotes-Genon, L. Hofer, J. Matias, and J. Virto, Theoretical status of $B \to K^*\mu^+\mu^-$: The path towards new physics, J. Phys. Conf. Ser. **631**, 012027 (2015).

[5] W. Altmannshofer and D. M. Straub, Implications of $b \to s$ measurements, arXiv:1503.06199.

[6] G. Buchalla, A. J. Buras, and M. E. Lautenbacher, Weak decays beyond leading logarithms, Rev. Mod. Phys. **68**, 1125 (1996).

[7] H. M. Asatrian, K. Bieri, C. Greub, and A. Hovhannisyan, NNLL corrections to the angular distribution and to the forward backward asymmetries in $b \to X(s)l+l-$, Phys. Rev. D **66**, 094013 (2002).

[8] P. Ball and R. Zwicky, $B(D,S) \to \rho$, $\omega$, $K*$, $\phi$ decay form factors from light-cone sum rules revisited, Phys. Rev. D **71**, 014029 (2005).

[9] J. Charles, A. Le Yaouanc, L. Oliver, O. Pene, and J. C. Raynal, Heavy to light form factors in the heavy mass to large energy limit of QCD, Phys. Rev. D **60**, 014001 (1999); M. Beneke and T. Feldmann, Symmetry breaking corrections to heavy to light B meson form-factors at large recoil, Nucl. Phys. **B592**, 3 (2001); M. Beneke, T. Feldmann, and D. Seidel, Systematic approach to exclusive $B \to Vl+l-$, $V\gamma$ decays, Nucl. Phys. **B612**, 25 (2001).

[10] M. Beneke, T. Feldmann, and D. Seidel, Exclusive radiative and electroweak $b \to d$ and $b \to s$ penguin decays at NLO, Eur. Phys. J. C **41**, 173 (2005).

[11] F. Kruger, L. M. Sehgal, N. Sinha, and R. Sinha, Angular distribution and CP asymmetries in the decays anti-$B \to K-\pi+e-e+$ and anti-$B \to \pi-\pi+e-e+$, Phys. Rev. D **61**, 114028 (2000); Phys. Rev. D **63**, 019901(E) (2000); W. Altmannshofer, P. Ball, A. Bharucha, A. J. Buras, D. M. Straub, and M. Wick, Symmetries and asymmetries of $B \to K^*\mu^+\mu^-$ decays in the standard model and beyond, J. High Energy Phys. 01 (2009) 019; J. Matias, F. Mescia, M. Ramon, and J. Virto, Complete Anatomy of $\bar{B}_d \to \bar{K}^{*0}(\to K\pi)l^+l^-$ and its angular distribution, J. High Energy Phys. 04 (2012) 104.

[12] F. Kruger and J. Matias, Probing new physics via the transverse amplitudes of $B0 \to K*0(\to K-pi+)l+l-$ at large recoil, Phys. Rev. D **71**, 094009 (2005); U. Egede, T. Hurth, J. Matias, M. Ramon, and W. Reece, New observables in the decay mode anti-$B(d) \to$ anti $-K*0l+l-$, J. High Energy Phys. 11 (2008) 032.

[13] G. Burdman, Short distance coefficients and the vanishing of the lepton asymmetry in $B \to$ V $\ell^+$lepton−, Phys. Rev. D **57**, 4254 (1998).

[14] A. Ali, P. Ball, L. T. Handoko, and G. Hiller, A comparative study of the decays $B \to (K, K^{*)}\ell^+\ell^-$ in standard model and supersymmetric theories, Phys. Rev. D **61**, 074024 (2000).

[15] R. Aaij *et al.* (LHCb Collaboration), Differential branching fraction and angular analysis of the decay $B^0 \to K^{*0}\mu^+\mu^-$, J. High Energy Phys. 08 (2013) 131.

[16] LHCb Collaboration, Angular analysis of the $B^0 \to K^{*0}\mu^+\mu^-$ decay, Reports No. LHCb-CONF-2015-002 and No. CERN-LHCb-CONF-2015-002.

[17] C. Bobeth, G. Hiller, D. van Dyk, and C. Wacker, The decay $B \to K\ell^+\ell^-$ at low hadronic recoil and model-independent $\Delta B = 1$ constraints, J. High Energy Phys. 01 (2012) 107.

[18] A. Ali, G. Kramer, and G. h. Zhu, $B \to K+l+l-$ decay in soft-collinear effective theory, Eur. Phys. J. C **47**, 625 (2006).

[19] T. Hurth and F. Mahmoudi, On the LHCb anomaly in $B \to K^*\ell^+\ell^-$, J. High Energy Phys. 04 (2014) 097.

[20] M. Beneke, T. Feldmann, and D. Seidel, Systematic approach to exclusive $B \to Vl+l-$, $V\gamma$ decays, Nucl. Phys. **B612**, 25 (2001).

[21] R. Gauld, F. Goertz, and U. Haisch, On minimal $Z'$ explanations of the $B \to K^*\mu^+\mu^-$ anomaly, Phys. Rev. D **89**, 015005 (2014).

[22] R. Gauld, F. Goertz, and U. Haisch, An explicit Z'-boson explanation of the $B \to K^*\mu^+\mu^-$ anomaly, J. High Energy Phys. 01 (2014) 069.

[23] Q. S. Yan, C. S. Huang, W. Liao, and S. H. Zhu, Exclusive semileptonic rare decays $B \to (K, K^{*)}\ell^+\ell^-$ in supersymmetric theories, Phys. Rev. D **62**, 094023 (2000).

[24] W. Altmannshofer and D. M. Straub, New physics in $b \to s$ transitions after LHC run 1, Eur. Phys. J. C **75**, 382 (2015).

[25] G. Hiller and M. Schmaltz, $R_K$ and future $b \to s\ell\ell$ physics beyond the standard model opportunities, Phys. Rev. D **90**, 054014 (2014).

Published for SISSA by Springer

Received: November 23, 2015
Accepted: January 4, 2016
Published: January 19, 2016

JHEP01(2016)117

# $\bar{B} \to D^{(*)}\tau\bar{\nu}$ excesses in ALRSM constrained from $B$, $D$ decays and $D^0 - \bar{D}^0$ mixing

**Chandan Hati,**[a,b] **Girish Kumar**[a,b] **and Namit Mahajan**[a]

[a] *Physical Research Laboratory, Navrangpura, Ahmedabad 380 009, India*
[b] *Indian Institute of Technology Gandhinagar, Chandkheda, Ahmedabad 382 424, India*

*E-mail:* chandan@prl.res.in, girishk@prl.res.in, nmahajan@prl.res.in

Abstract: Recent experimental results from the LHCb, BaBar and Belle collaborations on the semitauonic decays of $B$ meson, $\bar{B} \to D^{(*)}\tau\bar{\nu}$, showing a significant deviation from the Standard Model (SM), hint towards a new physics scenario beyond the SM. In this work, we show that these enhanced decay rates can be explained within the framework of $E_6$ motivated Alternative Left-Right Symmetric Model (ALRSM), which has been successful in explaining the recent CMS excesses and has the feature of accommodating high scale leptogenesis. The R-parity conserving couplings in ALRSM can contribute universally to both $\bar{B} \to D\tau\bar{\nu}$ and $\bar{B} \to D^*\tau\bar{\nu}$ via the exchange of scalar leptoquarks. We study the leptonic decays $D_s^+ \to \tau^+\bar{\nu}$, $B^+ \to \tau^+\bar{\nu}$, $D^+ \to \tau^+\bar{\nu}$ and $D^0 - \bar{D}^0$ mixing to constrain the couplings involved in explaining the enhanced $B$ decay rates and we find that ALRSM can explain the current experimental data on $\mathcal{R}(D^{(*)})$ quite well while satisfying these constraints.

Keywords: Rare Decays, Beyond Standard Model, B-Physics

ArXiv ePrint: 1511.03290



doi:10.1007/JHEP01(2016)117

## Contents



## 1 Introduction

Recently the LHCb collaboration has reported the ratio of branching fractions for the semitauonic decay of $B$ meson, $\bar{B} \to D^*\tau\bar{\nu}$, to be $\mathcal{R}(D^*) = 0.336 \pm 0.027(\text{stat.}) \pm 0.030(\text{syst.})$ with the Standard Model (SM) expectation $0.252 \pm 0.005$, amounting to a $2.1\sigma$ excess [1]. In general, the observables are introduced as ratios to reduce theoretical uncertainties

$$\mathcal{R}(X) = \frac{\mathcal{B}(\bar{B} \to X\tau\bar{\nu})}{\mathcal{B}(\bar{B} \to Xl\bar{\nu})}, \tag{1.1}$$

where $l = e, \mu$. This measurement is in agreement with the measurements of $\bar{B} \to D^{(*)}\tau\bar{\nu}$ reported by the BaBar [2, 3] and Belle [4] collaborations. The results reported by BaBar and Belle are given by $\mathcal{R}(D)^{\text{BaBar}} = 0.440 \pm 0.058 \pm 0.042$, $\mathcal{R}(D)^{\text{Belle}} = 0.375 \pm 0.064 \pm 0.026$ and $\mathcal{R}(D^*)^{\text{BaBar}} = 0.332 \pm 0.024 \pm 0.018$, $\mathcal{R}(D^*)^{\text{Belle}} = 0.293 \pm 0.038 \pm 0.015$, with the SM expectations given by $\mathcal{R}(D)^{\text{SM}} = 0.300 \pm 0.010$ and $\mathcal{R}(D^*)^{\text{SM}} = 0.252 \pm 0.005$. These results are consistent with earlier measurements [5, 6] and when combined together show a significant deviation from the SM.

Several new physics (NP) scenarios accommodating semileptonic $b \to c$ decay have been proposed to explain these excesses. The two-Higgs Doublet Model (2HDM) of type II is one of the well studied candidates of NP which can affect the semitauonic $B$ decays significantly [7–13]. However, the BABAR collaboration has excluded the 2HDM of type II at 99.8 % confidence level [2, 3]. Phenomenological studies of the four fermion operators that can explain the discrepancy have been addressed in refs. [14–22]. The excesses have been explained in a more generalized framework of 2HDM in refs. [23–25] and in the framework of $R$-parity violating (RPV) Minimal Supersymmetric Standard Model (MSSM)



JHEP01(2016)117

in ref. [26]. While in refs. [16, 20, 21, 27, 28] the excesses have been addressed in the context of leptoquark models. In ref. [29], a dynamical model based on a $\mathrm{SU}(2)_L$ triplet of massive vector bosons, with predominant coupling to third generation fermion was proposed to explain the excesses, while other alternative approaches have been taken in refs. [30–32].

From a theoretical point of view, NP scenarios explaining the above discrepancies and addressing other direct or indirect collider searches for NP are particularly intriguing. To this end, we must mention the recently announced results for the right-handed gauge boson $W_R$ search at $\sqrt{s} = 8$TeV and 19.7fb$^{-1}$ of integrated luminosity by the CMS Collaboration at the LHC. They have reported 14 observed events with 4 expected SM background events, amounting to a $2.8\sigma$ local excess in the bin $1.8\,\mathrm{TeV} < m_{eejj} < 2.2\,\mathrm{TeV}$, which cannot be explained in the standard framework of Left-Right Symmetric Model (LRSM) with the gauge couplings $g_L = g_R$ [33]. On the other hand, the CMS search for di-leptoquark production at $\sqrt{s} = 8$TeV and 19.6fb$^{-1}$ of integrated luminosity have been reported to show a $2.4\sigma$ in the $eejj$ channel and a $2.6\sigma$ local excess in the $e\not{p}_T jj$ channel corresponding to 36 observed events with $20.49 \pm 2.4 \pm 2.45(\mathrm{syst.})$ expected SM events in the $eejj$ channel and 18 observed events with $7.54 \pm 1.20 \pm 1.07(\mathrm{syst.})$ expected SM events in the $e\not{p}_T jj$ channel respectively [34]. These excesses has been explained from $W_R$ decay in the framework of LRSM with $g_L \neq g_R$ embedded in the SO(10) gauge group in refs. [35–37] and in LRSM with $g_L = g_R$ by taking into account the CP phases and non-degenerate masses of heavy neutrinos in ref. [38], while other NP scenarios have been proposed in refs. [39–51]. Interestingly, in some of these NP scenarios attempts were made to explain the discrepancies in decays of $B$ meson in an unified framework [43] or separately [26].

In this paper we study the flavor structure of the $E_6$ motivated Alternative Left-Right Symmetric Model (ALRSM) [52], which can explain the CMS excesses and accommodate high scale leptogenesis[1] [46], to explore if this framework can address the experimental data for $\mathcal{R}(D^{(*)})$ explaining the discrepancy with the SM expectations. This scenario is particularly interesting because unlike the R-parity violating MSSM in refs. [26, 41, 43], this model involves only R-parity conserving interactions. Furthermore, a careful analysis of the flavor physics constraints, such as the rare decays and the mixing of mesons can play a crucial role in determining the viability of any NP scenario. Therefore, we study the leptonic decays $D_s^+ \to \tau^+\bar{\nu}$, $B^+ \to \tau^+\bar{\nu}$, $D^+ \to \tau^+\bar{\nu}$ and $D^0$-$\bar{D}^0$ mixing to constrain the semileptonic $b \to c$ transition in ALRSM. We find that despite being constrained by the above processes ALRSM can explain the current experimental data on $\mathcal{R}(D^{(*)})$ quite well.

The rest of this article is organized as follows. In section 2, we discuss the effective Hamiltonian and the general four-fermion operators that can explain the $\mathcal{R}(D^{(*)})$ data. In section 3, we introduce ALRSM and present the viable interactions, followed by the evaluation of the Wilson coefficients. In section 4, we discuss the constrains from the leptonic decays $D_s^+ \to \tau^+\bar{\nu}$, $B^+ \to \tau^+\bar{\nu}$, $D^+ \to \tau^+\bar{\nu}$ and mixing between $D^0$-$\bar{D}^0$. In section 5, we summarize our results and conclude.

[1]Note that in the conventional LRSM framework the canonical mechanism of leptogenesis is inconsistent with the range of $W_R$ mass ($\sim 2\,\mathrm{TeV}$) corresponding to the excess at CMS [53, 54].

## 2 The effective Hamilonian for $\bar{B} \to D^{(*)}\tau\bar{\nu}$ decay

To include the effects of NP, the SM effective Hamiltonian for the quark level transition $b \to c l \bar{\nu}_l$ can be augmented with a set of four-Fermi operators in the following form [15]

$$\mathcal{H}_{\text{eff}} = \frac{4G_F}{\sqrt{2}} V_{cb} \sum_{l=e,\mu,\tau} [(1 + C^l_{V_L}) O^l_{V_L} + C^l_{V_R} O^l_{V_R} + C^l_{S_L} O^l_{S_L} + C^l_{S_R} O^l_{S_R} + C^l_{T_L} O^l_{T_L}], \quad (2.1)$$

where $G_F$ is the Fermi constant, $V_{cb}$ is the appropriate CKM matrix element and $C^l_i$ (i = $V_{L/R}$, $S_{L/R}$, $T_L$) are the Wilson coefficients associated with the new effective vector, scalar and tensor interaction operators respectively. These new six dimensional four-Fermi operators are generated by NP at some energy higher than the electroweak scale and are defined as

$$\begin{aligned}
O^l_{V_L} &= (\bar{c}_L \gamma^\mu b_L)(\bar{l}_L \gamma_\mu \nu_{lL}), \\
O^l_{V_R} &= (\bar{c}_R \gamma^\mu b_R)(\bar{l}_L \gamma_\mu \nu_{lL}), \\
O^l_{S_L} &= (\bar{c}_L b_R)(\bar{l}_R \nu_{lL}), \\
O^l_{S_R} &= (\bar{c}_R b_L)(\bar{l}_R \nu_{lL}), \\
O^l_{T_L} &= (\bar{c}_R \sigma^{\mu\nu} b_L)(\bar{l}_R \sigma_{\mu\nu} \nu_{lL}), \qquad (2.2)
\end{aligned}$$

where $\sigma^{\mu\nu} = (i/2)[\gamma^\mu, \gamma^\nu]$. The SM effective Hamiltonian corresponds to the case $C^l_i = 0$. Note that in writing the general $\mathcal{H}_{\text{eff}}$, we have neglected the tiny contributions from the right-handed neutrinos and therefore, we treat the neutrinos to be left-handed only.
In order to perform the numerical analysis of the transition $B \to D^{(*)}\tau\nu$, we need to have the knowledge of the hadronic form factors which parametrize the vector, scalar and tensor current matrix elements. The $B \to D^{(*)}\tau\nu$ matrix elements of the aforementioned effective operators depend on the momentum transfer between B and $D^{(*)}(q^\mu = p^\mu_B - k^\mu)$ and are generally parametrized in the following way [15, 55]

$$\begin{aligned}
\langle D(k)|\bar{c}\gamma_\mu b|\bar{B}(p_B)\rangle &= \left[(p_B + k)_\mu - \frac{m_B^2 - m_D^2}{q^2} q_\mu\right] F_1(q^2) + q_\mu \frac{m_B^2 - m_D^2}{q^2} F_0(q^2), \quad (2.3) \\
\langle D^*(k,\epsilon)|\bar{c}\gamma_\mu b|\bar{B}(p_B)\rangle &= -i\epsilon_{\mu\nu\rho\sigma}\epsilon^{\nu *} p_B^\rho k^\sigma \frac{2V(q^2)}{m_B + m_{D^*}}, \qquad (2.4) \\
\langle D^*(k,\epsilon)|\bar{c}\gamma_\mu\gamma_5 b|\bar{B}(p_B)\rangle &= \epsilon^{\mu *}(m_B + m_{D^*}) A_1(q^2) - (p_B + k)_\mu (\epsilon^* \cdot q) \frac{A_2(q^2)}{m_B + m_{D^*}} \\
&\quad - q_\mu (\epsilon^* \cdot q) \frac{2 m_{D^*}}{q^2} \left(A_3(q^2) - A_0(q^2)\right), \qquad (2.5) \\
\langle D^*(k,\epsilon)|\bar{c}\sigma_{\mu\nu} b|\bar{B}(p_B)\rangle &= \epsilon_{\mu\nu\rho\sigma} \Bigg\{ -\epsilon^{*\rho}(p_B + k)^\sigma T_1(q^2) \\
&\quad + \epsilon^{*\rho} q^\sigma \frac{m_B^2 - m_{D^*}^2}{q^2} (T_1(q^2) - T_2(q^2)) \qquad (2.6) \\
&\quad + 2\frac{\epsilon^* q}{q^2} p_B^\rho k^\sigma \left(T_1(q^2) - T_2(q^2) - \frac{q^2}{m_B^2 - m_{D^*}^2} T_3(q^2)\right) \Bigg\},
\end{aligned}$$



JHEP01(2016)117

where $F_1(0) = F_0(0)$, $A_3(0) = A_0(0)$ and

$$A_3(q^2) = \frac{m_B + m_{D^*}}{2m_{D^*}} A_1(q^2) - \frac{m_B - m_{D^*}}{2m_{D^*}} A_2(q^2). \tag{2.7}$$

$\epsilon_\mu$ is the polarization vector of the $D^*$. Note that the hadronic matrix elements of the scalar and pseudoscalar operators can be conveniently derived from their vector counterpart by applying the equations of motion $-i\partial^\mu(\bar{q}_a\gamma_\mu q_b) = (m_a - m_b)\bar{q}_a q_b$ and $-i\partial^\mu(\bar{q}_a\gamma_\mu\gamma_5 q_b) = (m_a + m_b)\bar{q}_a\gamma_5 q_b$. However, in what follows, we choose to work with the following parametrization of the form factors which are more suitable for including the results of the heavy quark effective theory (HQET). The matrix elements of the vector and axial vector operators can be expressed as [10, 56]

$$\begin{aligned}
\langle D(v')|\bar{c}\gamma_\mu b|\bar{B}(v)\rangle &= \sqrt{m_B m_D}\left\{\xi_+(w)(v+v')_\mu + \xi_-(w)(v-v')_\mu\right\} \\
\langle D^*(v',\epsilon)|\bar{c}\gamma_\mu b|\bar{B}(v)\rangle &= i\sqrt{m_B m_{D^*}}\xi_V(w)\epsilon_{\mu\nu\rho\sigma}\epsilon^{*\nu}v'^\rho v^\sigma, \qquad (2.8)\\
\langle D^*(v',\epsilon)|\bar{c}\gamma_\mu\gamma_5 b|\bar{B}(v)\rangle &= \sqrt{m_B m_{D^*}}\left\{\xi_{A_1}(w)(w+1)\epsilon^*_\mu - (\epsilon^*\cdot v)\left(\xi_{A_2}(w)v_\mu + \xi_{A_3}(w)v'^\mu\right)\right\}.
\end{aligned}$$

The form factors of tensor operators are defined as [20]

$$\begin{aligned}
\langle D(v')|\bar{c}\sigma_{\mu\nu}b|\bar{B}(v)\rangle &= -i\sqrt{m_B m_D}\xi_T(w)\left(v_\mu v'_\nu - v_\nu v'_\mu\right), \\
\langle D^*(v')|\bar{c}\sigma_{\mu\nu}b|\bar{B}(v)\rangle &= -i\sqrt{m_B m_{D^*}}\epsilon_{\mu\nu\rho\sigma}\left\{\xi_{T_1}(w)\epsilon^{*\rho}(v+v')^\rho + \xi_{T_2}(w)\epsilon^{*\rho}(v-v')^\sigma\right. \\
&\qquad \left. + \xi_{T_3}(w)(\epsilon^*\cdot v)(v+v')^\rho(v-v')^\sigma\right\}, \qquad (2.9)
\end{aligned}$$

where $v = p_B/m_B$ and $v' = k/m_{D^{(*)}}$ are the four-velocities of the B and $D^{(*)}$ mesons respectively, and the kinematic variable $w(q^2)$ is the product of the velocities of initial and final mesons $w(q^2) = \left(m_B^2 + m_{D^{(*)}} - q^2\right)/2m_B m_{D^{(*)}}$. The HQET and QCD dispersive techniques can be used to constrain the shapes of these form factors [57]. To this end, the HQET form factors are redefined as linear combinations of the different form factors $V_1(w)$, $S_1(w)$, $A_1(w)$ and $R_{1,2,3}(w)$ [20, 57], which reduces to the universal Isgur-Wise function [58, 59] normalized to unity at $w = 1$ in the heavy quark limit. The form factors in the parameterization of Caprini et al. [57], which describes the shape and normalization in terms of the four quantities: the normalizations $V_1(1)$, $A_1(1)$, the slopes $\rho_D^2$, $\rho_{D^*}^2$ and the amplitude ratios $R_1(1)$ and $R_2(1)$ are determined by measuring the differential decay width as a function of $w$. The form factors $V_1(w)$ and $S_1(w)$ contribute to the decay $B \to D l\bar{\nu}_l$ ($l = e, \mu, \tau$), while the decay $B \to D^* l\bar{\nu}_l$ receives contributions from $A_1(w)$ and $R_{1,2,3}(w)$. However, the semileptonic decay into light charged leptons $B \to D l\bar{\nu}_l$ involves only $V_1(w)$ and therefore, $V_1(w)$ can be measured experimentally. The parametrization of the form factors in terms of the slope parameters $\rho_D^2$, $\rho_{D^*}^2$ and the value of the respective form factors at the kinematic end point $w = 1$ is given by [57, 60]

$$V_1(w) = V_1(1)\left\{1 - 8\rho_D^2 z + (51\rho_D^2 - 10)z^2 - (252\rho_D^2 - 84)z^3\right\}, \tag{2.10}$$

$$A_1(w) = A_1(1)\left\{1 - 8\rho_{D^*}^2 z + (53\rho_{D^*}^2 - 15)z^2 - (231\rho_{D^*}^2 - 91)z^3\right\}, \tag{2.11}$$

$$\begin{aligned}
R_1(w) &= R_1(1) - 0.12(w-1) + 0.05(w-1)^2, \\
R_2(w) &= R_2(1) + 0.11(w-1) - 0.06(w-1)^2, \\
R_3(w) &= 1.22 - 0.052(w-1) + 0.026(w-1)^2, \qquad (2.12)
\end{aligned}$$



JHEP01(2016)117

with $z = (\sqrt{w+1} - \sqrt{2})/(\sqrt{w+1} + \sqrt{2})$. For $S_1(w)$ we use the parametrization given in ref. [13]

$$S_1(w) = V_1(w) \left\{1 + \Delta \left(-0.019 + 0.041(w-1) \;\; -0.015(w-1)^2\right)\right\}, \tag{2.13}$$

with $\Delta = 1 \pm 1$. By fitting the measured quantity $|V_{cb}|V_1(w)$ to the two parameter ansatz as given in eq.(2.10), the heavy flavor averaging group (HFAG) extracts the following parameters: $V_1(1)|V_{cb}| = (42.65 \pm 1.53) \times 10^{-3}$, $\rho_D^2 = 1.185 \pm 0.054$ [61]. In the case of $B \to D^* l \bar{\nu}_l$, HFAG determines $A_1(1)|V_{cb}| = (35.81 \pm 0.45) \times 10^{-3}$, $\rho_{D^*}^2 = 1.207 \pm 0.026$, $R_1(1) = 1.406 \pm 0.033$ and $R_2(1) = 0.853 \pm 0.020$ by performing a four-dimensional fit of the parameters [61]. However, since the fitted curve are plagued with large statistical and systematic uncertainties, for form factor normalizations, we use $V_1(1) = 1.081 \pm 0.024$ from the recent lattice QCD calculations [62] and for $A_1(1)$ we use the updated value $A_1(1) = 0.920 \pm 0.014$ from the FNAL/MILC group [63]. The amplitude ratios $R_1(1)$ and $R_2(1)$ are determined from the fit by HFAG $R_1(1) = 1.406 \pm 0.033$, $R_2(1) = 0.853 \pm 0.020$ [61].

## 3 Alternative Left-Right Symmetric Model and analysis of operators mediating $\bar{B} \to D^{(*)} \tau \bar{\nu}$

One of the maximal subgroups of superstring inspired $E_6$ group is given by $\mathrm{SU}(3)_C \times \mathrm{SU}(3)_L \times \mathrm{SU}(3)_R$. The fundamental 27 representation of $E_6$ can be decomposed under this subgroup as

$$27 = (3,3,1) + (3^*,1,3^*) + (1,3^*,3) \tag{3.1}$$

where the fields are assigned as follows. $(3,3,1)$ corresponds to $(u,d,h)$, $(3^*,1,3^*)$ corresponds to $(h^c, d^c, u^c)$ and the leptons are assigned to $(1,3^*,3)$. Here $h$ represents the exotic $-\frac{1}{3}$ charge quark which can carry lepton number depending on the assignments. The other exotic fields are $N^c$ and two isodoublets $(\nu_E, E)$ and $(E^c, N_E^c)$. The presence of these exotic fields makes the phenomenology of the low energy subgroups of $E_6$ very interesting. The superfields of the first family can be represented as

$$\begin{pmatrix} u \\ d \\ h \end{pmatrix} + \begin{pmatrix} u^c & d^c & h^c \end{pmatrix} + \begin{pmatrix} E^c & \nu & \nu_E \\ N_E^c & e & E \\ e^c & N^c & n \end{pmatrix}, \tag{3.2}$$

where $\mathrm{SU}(3)_L$ operates along columns and $\mathrm{SU}(3)_{(R)}$ operates along rows. The $\mathrm{SU}(3)_{(L,R)}$ in the maximal subgroup of $E_6$ can further break into $\mathrm{SU}(2)_{(L,R)} \times \mathrm{U}(1)_{(L,R)}$ and there are three choices of assigning the isospin doublets corresponding to $T, U, V$ isospins (generators of SU(2)) of SU(3). One of the choices have $(d^c, u^c)_L$ assigned to the $\mathrm{SU}(2)_R$ doublet giving rise to the usual left-right symmetric extension of the standard model including the exotic particles. In another choice, the $\mathrm{SU}(2)_R$ doublet is chosen to be $(h^c, d^c)$ [64] with the charge equation given by $Q = T_{3L} + \frac{1}{2}Y_L + \frac{1}{2}Y_N$ , where the chosen $\mathrm{SU}(2)_R$ does not contribute to the electric charge equation and is often denoted by $\mathrm{SU}(2)_N$. While these two subgroups are quite interesting from a phenomenological point of view, the superpotential couplings in these two subgroups can not explain the $\mathcal{R}(D^{(*)})$ data. The third possible choice where the



JHEP01(2016)117

$\mathrm{SU}(2)_R$ doublet is chosen to be $(h^c, u^c)$ gives the subgroup referred to as the Alternative Left-Right Symmetric Model (ALRSM) [52] and it has the right ingredients to address $\mathcal{R}(D^{(*)})$ excesses.

In ALRSM, the superfields have the following transformations under the subgroup $G = \mathrm{SU}(3)_c \times \mathrm{SU}(2)_L \times \mathrm{SU}(2)_{R'} \times \mathrm{U}(1)_{Y'}$

$$\begin{aligned}
(u,d)_L &: \left(3,2,1,\frac{1}{6}\right) \\
(h^c,u^c)_L &: \left(\bar{3},1,2,-\frac{1}{6}\right) \\
(\nu_E,E)_L &: \left(1,2,1,-\frac{1}{2}\right) \\
(e^c,n)_L &: \left(1,1,2,\frac{1}{2}\right) \\
h_L &: \left(3,1,1,-\frac{1}{3}\right) \\
d^c_L &: \left(\bar{3},1,1,\frac{1}{3}\right) \\
\begin{pmatrix} \nu_e & E^c \\ e & N^c_E \end{pmatrix}_L &: (1,2,2,0) \\
N^c_L &: (1,1,1,0),
\end{aligned} \tag{3.3}$$

where $Y' = Y_L + Y'_R$. The charge equation is given by $Q = T_{3L} + \frac{1}{2}Y_L + T'_{3R} + \frac{1}{2}Y'_R$, where $T'_{3R} = \frac{1}{2}T_{3R} + \frac{3}{2}Y_R$, $Y'_R = \frac{1}{2}T_{3R} - \frac{1}{2}Y_R$. The superpotential governing interactions of the superfields in ALRSM is given by [65]

$$\begin{aligned}
W =& \lambda_1\left(uu^cN^c_E - du^cE^c - uh^ce + dh^c\nu_e\right) + \lambda_2\left(ud^cE - dd^c\nu_E\right) + \lambda_3\left(hu^ce^c - hh^cn\right) \\
&+\lambda_4 hd^cN^c_L + \lambda_5\left(ee^c\nu_E + EE^cn - Ee^c\nu_e - \nu_E N^c_E n\right) + \lambda_6\left(\nu_e N^c_L N^c_E - eE^cN^c_L\right).
\end{aligned} \tag{3.4}$$

The superpotential given in eq. (3.4) gives the following assignments of $R$-parity, baryon number ($B$) and lepton number ($L$) for the exotic fermions ensuring proton stability. $h$ is a leptoquark with $R = -1, B = \frac{1}{3}, L = 1$. $\nu_E, E$ and $n$ have the assignments $R = -1, B = L = 0$. $N^c$ has two possible assignments. If $N^c$ has the assignments $R = -1$ and $B = L = 0$ (in a $R$-parity conserving scenario demanding $\lambda_4 = \lambda_6 = 0$ in eq. (3.4)), $\nu_e$ becomes exactly massless. However if $N^c$ is assigned $R = +1$, $B = 0$, $L = -1$, then $\nu_e$ can acquire a tiny mass via the seesaw mechanism.

ALRSM can explain both $eejj$ and $e\not{p}_Tjj$ signals from the decay of scalar superpartners of the exotic particles, for example, through (i) resonant production of the exotic slepton $\tilde{E}$, subsequently decaying into a charged lepton and a neutrino, followed by R-parity conserving interactions of the neutrino producing an excess of events in both $eejj$ and $e\not{p}_Tjj$ channels [46] (ii) pair production of scalar leptoquarks $\tilde{h}$. On the other hand, high scale leptogenesis can be obtained via the decay of the heavy Majorana neutrino $N^c$ in ALRSM.

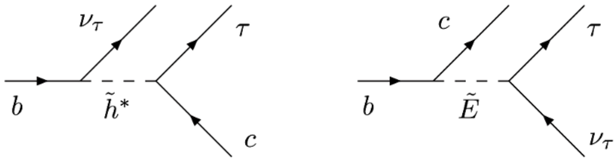


**Figure 1**. Feynman diagrams for the decays $\bar{B} \to D^{(*)}\tau\bar{\nu}$ induced by the exchange of scalar leptoquark ($\tilde{h}^*$) and $\tilde{E}$.

From the interaction terms $\lambda_4$ and $\lambda_6$ in eq. (3.4), it can be seen that the Majorana neutrino $N_k^c$ can decay into final states with $B-L=-1$ given by $\nu_{e_i}\tilde{N}^c_{E_j}, \tilde{\nu}_{e_i}N^c_{E_j}, e_i\tilde{E}^c_j, \tilde{e}_i, E^c_j$ and $d_i\tilde{h}_j, \tilde{d}^c_i\tilde{h}_j$ and to their conjugate states. Thus, ALRSM has the attractive feature that it can explain both the excess $eejj$ and $e\not{p}_Tjj$ signals and also high-scale leptogenesis [46].

Having introduced ALRSM above now we are ready to analyze the semitauonic $B$ decay $\bar{B} \to D^{(*)}\tau\bar{\nu}$ based on the general framework introduced in section 2. From the superpotential given in eq. (3.4) it follows that in ALRSM there are two possible diagrams shown in figure 1. which can contribute to the decay $\bar{B} \to D^{(*)}\tau\bar{\nu}$. The effective Lagrangian corresponding to these diagrams is given by

$$\mathcal{L}_{\rm eff} = -\sum_{j,k=1}^{3} V_{2k}\left[\frac{\lambda^5_{33j}\lambda^{2*}_{3kj}}{m^2_{\tilde{E}^j}}\bar{c}_L b_R\,\bar{\tau}_R\nu_L + \frac{\lambda^1_{33j}\lambda^{1*}_{3kj}}{m^2_{\tilde{h}^{j*}}}\bar{c}_L(\tau^c)_R\,(\bar{\nu}^c)_R b_L\right], \tag{3.5}$$

where the superscript corresponds to the superpotential coupling index and the generation indices are explicitly written as subscripts. Here $m_{\tilde{E}}(m_{\tilde{h}})$ is the mass of slepton $\tilde{E}^j$ (scalar leptoquark $\tilde{h}^{j*}$) and $V_{ij}$ corresponds to the $ij$-th component of the CKM matrix. Using Fiertz transformation the second term of eq. (3.5) can be put in the form given by

$$\bar{c}_L(\tau^c)_R\,(\bar{\nu}^c)_R b_L = \frac{1}{2}\bar{c}_L\gamma^\mu b_L\,\bar{\tau}_L\gamma_\mu\nu_L. \tag{3.6}$$

We can now readily obtain the expressions for the corresponding Wilson coefficients, defined in eq. (2.2), given by

$$\begin{aligned} C^\tau_{S_L} &= \frac{1}{2\sqrt{2}G_F V_{cb}}\sum_{j,k=1}^{3} V_{2k}\frac{\lambda^5_{33j}\lambda^{2*}_{3kj}}{m^2_{\tilde{E}^j}}\,, \\ C^\tau_{V_L} &= \frac{1}{2\sqrt{2}G_F V_{cb}}\sum_{j,k=1}^{3} V_{2k}\frac{\lambda^1_{33j}\lambda^{1*}_{3kj}}{2\,m^2_{\tilde{h}^{j*}}}, \end{aligned} \tag{3.7}$$

where the neutrinos are assumed to be predominantly of tau flavor.

To simplify further analysis, we invoke the assumption that except the SM contribution only one of the NP operators in eq. (2.2) contributes dominantly. This assumption helps us in determining the limits on the dominant Wilson coefficient from the experimental data for $\mathcal{R}(D^{(*)})$ and the generalization of this situation to incorporate more than one NP operator contribution is straight forward.

The case where $C^\tau_{S_L}$ is the dominant contribution, similar to 2HDM of type II or type III with minimal flavor violation, can not explain both $\mathcal{R}(D)$ and $\mathcal{R}(D^*)$ data simultaneously [16, 25], as can be seen from figure 2. However, $C^\tau_{V_L}$ has an allowed region which can

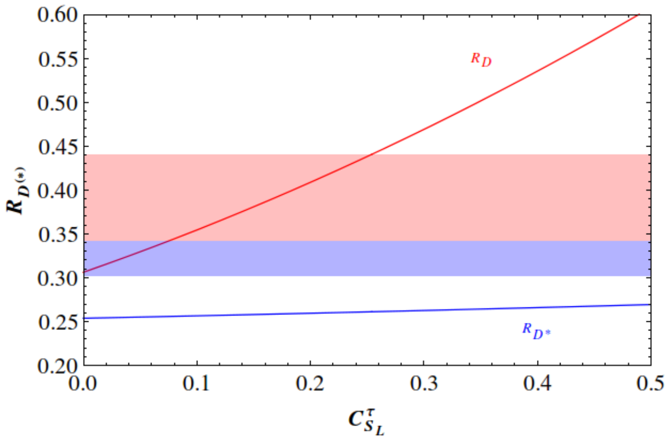


**Figure 2**. The dependence of the observables $R_{D^{(*)}}$ on $C^\tau_{S_L}$: red (blue) line corresponds to $R_D$ ($R_{D^*}$), and the horizontal light red (blue) band corresponds to the experimentally allowed $1\sigma$ values. No common region exists for $C^\tau_{S_L}$ which can simultaneously explain both $R_D$ and $R_{D^*}$.

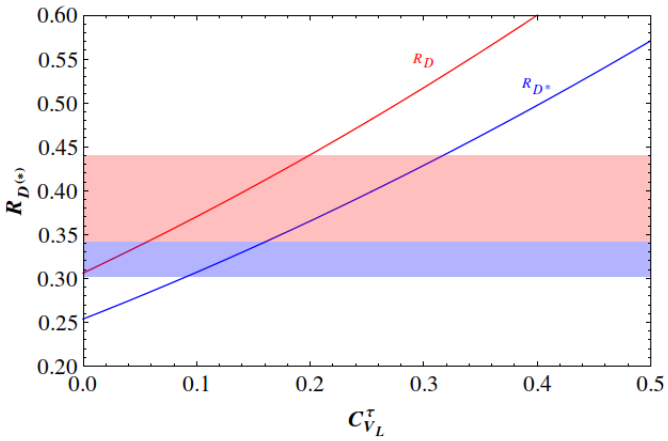


**Figure 3**. The dependence of the observables $R_{D^{(*)}}$ on $C^\tau_{V_L}$: red (blue) line corresponds to $R_D$ ($R_{D^*}$), and the horizontal light red (blue) band corresponds to the experimentally allowed $1\sigma$ values. $C^\tau_{V_L}$ can explain both $R_D$ and $R_{D^*}$ data.

explain both $\mathcal{R}(D)$ and $\mathcal{R}(D^*)$ data as shown in figure 3. We find that for $\left|C^\tau_{V_L}\right| > 0.08$ the current experimental data can be explained. A comment regarding the renormalization group (RG) running of these Wilson coefficients is in order. Wilson coefficients are computed at the matching scale (electroweak scale) by a matching between the full theory and effective theory. With these Wilson coefficients at electroweak scale as initial conditions, their evolution from matching scale down to scale $\mathcal{O}(m_b)$ is governed by the RG equations. Note that, the Wilson coefficient $C^\tau_{S_L}$ has a non-trivial running while $C^\tau_{V_L}$ does not run. Since we focus on the case where only $C^\tau_{V_L}$ contribution is present, RG running does not affect the analysis of this work. Also note that, we use the central values of the theoretical predictions because the theoretical uncertainties are sufficiently small compared to the experimental accuracy.



JHEP01(2016)117

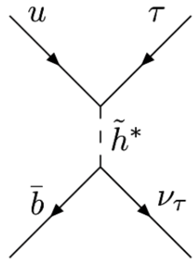


**Figure 4**. Feynman diagrams for the decay $B \to \tau\nu$ induced by the exchange of the scalar leptoquark $\tilde{h}^{j*}$.



## 4 Constraints from $B$, $D$ decays and $D^0 - \bar{D}^0$ oscillation

### 4.1 Constraints from $B \to \tau\nu$

In this section we discuss the new contributions to purely leptonic decay mode $B \to \tau\nu$ due to scalar leptoquark $\tilde{h}^{j*}$ exchange and utilize the measured branching fractions of the decay to derive constraints on the product of couplings $\lambda^1_{33j}\lambda^{1\,*}_{31j}$. In the SM, the decay $B \to \tau\nu$ proceeds via annihilation to a W boson in the s-channel. In the ALRSM, the exchange of the scalar leptoquark $\tilde{h}^{j*}$ leads to the additional diagrams shown in figure 4. Since the mass scale of scalar leptoquark is far above the scale of the B meson, we can integrate out the heavy degree of freedom to generate new four-fermion interaction $\sim \bar{q}_L(\tau^c)_R\,(\bar{\nu}^c)_R b_L$, with the Wilson coefficients parameterizing the effects of the integrated out non-standard particles. The NP effective Hamiltonian is given by

$$\mathcal{H}^{\rm NP}_{\rm eff}(b\bar{q} \to \tau\bar{\nu}) = \frac{4G_F}{\sqrt{2}} V_{qb}\, C^{qb}_{V_L}(\bar{q}_L\gamma^\mu b_L)(\bar{\tau}_L\gamma_\mu\nu_L), \tag{4.1}$$

where $V_{qb}$ (here $q \equiv u$) is the relevant CKM matrix element. The Wilson coefficient $C^{ub}_{V_L}$ in terms of the couplings $\lambda'$s is given by

$$C^{ub}_{V_L} = \frac{1}{2\sqrt{2}G_F V_{ub}} \sum_{j,k=1}^{3} V_{1k}\frac{\lambda^1_{33j}\lambda^{1*}_{3kj}}{2\,m^2_{\tilde{h}^{j*}}}. \tag{4.2}$$

In our notation, the Wilson coefficient of the SM effective operator is set to unity. In what follows, we will neglect the subleading $\mathcal{O}(\lambda)$ terms and retain only the leading CKM element $V_{11}$.

Note that, the decay $B \to \tau\nu$ is the only experimentally measured purely leptonic mode of charged $B^\pm$. The current experimental value of the branching ratio of $B \to \tau\nu$ is $(1.14 \pm 0.27) \times 10^{-4}$ [66]. The presence of NP modifies the expression of the SM decay rate in the following way

$$\frac{d\Gamma}{dq^2}(B \to \tau\nu) = \frac{G_F^2|V_{ub}|^2}{8\pi} m_B f_B^2 m_\tau^2 \times \left(1 - \frac{m_\tau^2}{m_B^2}\right)^2 |1 + C^{ub}_{V_L}|^2, \tag{4.3}$$

where $m_B$ is the mass of $B^\pm$ and $f_B$ is the decay constant which parametrize the matrix elements of the corresponding current as

$$\langle 0|\bar{b}_L\gamma^\mu q_L|B_q(p_B)\rangle = p^\mu_B f_B. \tag{4.4}$$

Here $p_B$ is the 4-momentum of the $B^\pm$ meson.

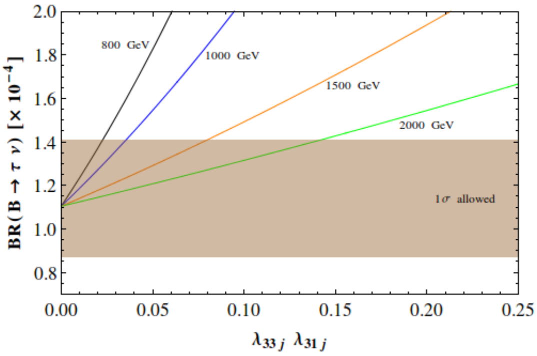


**Figure 5**. $\mathrm{BR}(B \to \tau\nu)$ as a function of couplings $\lambda_{33j}\lambda_{31j}$ for $m_{\tilde{h}^{j*}} = 800, 1000, 1500, 2000\,\mathrm{GeV}$ corresponding to black, blue, orange, and green lines respectively. The horizontal brown (light) band shows the $1\sigma$ experimentally favored values.

We use the CKM matrix elements, the lifetimes, particle masses and decay constants $f_B$, $f_{D_s}$, $f_{D^+}$ from PDG [66] for numerical estimations throughout the paper. There have been attempts to account for flavour symmetry breaking in pseudoscalar meson decay constants in literature [67, 68]. Here, we assume that contribution from only one type of scalar leptoquarks is dominant and real. For simplicity, we will further assume the couplings to be real in the rest of this paper. In figure 5 we plot the $\mathrm{BR}(B \to \tau\nu)$ as a function of the product of the couplings $\lambda_{33j}\lambda_{31j}$ for different values of $m_{\tilde{h}^{j*}}$. Numerically these constraints are given by

$$\lambda_{33j}\lambda_{31j} \leq 0.04 \left(\frac{m_{\tilde{h}^{j*}}}{1000\mathrm{GeV}}\right)^2 . \tag{4.5}$$

### 4.2 Constraints from $D_s^+ \to \tau\nu$ and $D^+ \to \tau\nu$

Along with rare B decays, the study of the decays of charmed mesons also offer attractive possibilities to test the predictions of extensions of the SM [69, 70]. In fact, these processes are quite sensitive to the contributions of charged Higgs boson and scalar leptoquarks [71] and to the new contributions from squark exchange in the framework of R-parity violating SUSY as examined in ref. [72]. In this section we consider the purely leptonic decays $D_s^+ \to \tau\nu$ and $D^+ \to \tau\nu$ in ALRSM and use their measured branching ratios to obtain constraints on the couplings $(\lambda_{32j})^2$ and $\lambda_{32j}\lambda_{31j}$ respectively. The relevant Feynman diagrams in ALRSM for the decays $D_s^+ \to \tau\nu$ and $D^+ \to \tau\nu$ are shown in figure 6. Integrating out the heavy energy scales yields the following non-standard effective Hamiltonian

$$\mathcal{H}_{\mathrm{eff}}^{\mathrm{NP}}(c\bar{q} \to \tau\bar{\nu}) = \frac{4G_F}{\sqrt{2}} V_{cq}\, C_{V_L}^{cq} (\bar{q}_L\gamma^\mu c_L)(\bar{\nu}_L\gamma_\mu\tau_L) \tag{4.6}$$

where $q = s, d$ for $D_s^+, D^+$ respectively. In the SM these processes occur (similar to $B \to \tau\nu$) via $W^\pm$ annihilation in the s-channel and the SM Wilson coefficient is given by unity in our notation. The corresponding Wilson coefficient $C_{V_L}^{cq}$ parameterizing the NP effects is given by

$$C_{V_L}^{cq} = \frac{1}{2\sqrt{2}G_F V_{cq}} \sum_{j,k=1}^{3} V_{kq} \frac{\lambda_{32j}^1 \lambda_{3kj}^{1*}}{2\, m_{\tilde{h}^{j*}}^2}. \tag{4.7}$$

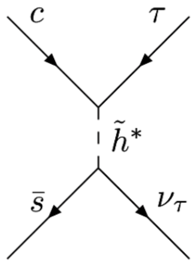


**Figure 6**. Feynman diagrams for the decay $D_s^+ \to \tau\nu$ induced by scalar leptoquarks. The corresponding diagram for the decay $D^+ \to \tau\nu$ can be obtained by replacing $s$ quark by $d$ quark.

We will keep only the leading terms $V_{cs}$ for $D_s^+$ decay and $V_{ud}$ for $D^+$ case respectively and neglect the subleadiing Cabibbo suppressed $\mathcal{O}(\lambda)$ terms. Although this process occurs in the SM at the tree level, the branching fraction is helicity-suppressed. For $\tau$, this suppression is less severe but phase-space suppression is larger compared to light leptons. In the presence of scalar leptoquark contribution, the SM decay rate is affected in the following way [71, 73]

$$\frac{d\Gamma}{dq^2}(D_q^+ \to \tau\nu) = \frac{G_F^2|V_{cq}|^2}{8\pi} m_{D_q} f_{D_q}^2 m_\tau^2 \times \left(1 - \frac{m_\tau^2}{m_{D_q}^2}\right)^2 |1 + C_{V_L}^{cq}|^2. \tag{4.8}$$

Here $m_{D_q}$ is the mass of charm-mesons $D_s^+$ and $D^+$ for $q = s, d$ respectively and $V_{cq}$ is the relevant CKM element. The decay constant $f_{D_q}$ is defined by $\langle 0|\bar{c}_L\gamma^\mu q_L|D_q(p_{D_q})\rangle = p_{D_q}^\mu f_{D_q}$, where $p_{D_q}$ is the 4-momentum of the $D_q$ meson.

Assuming that only one product combination of the scalar leptoquark couplings is nonzero, we get upper bounds on $(\lambda_{32j}^1)^2$ and $\lambda_{32j}^1\lambda_{31j}^{1*}$. In figure 7, we plot the dependence of BR$(B \to D_(s)^+\nu)$ on the coupling $\lambda_{32j}\lambda_{31j}(\lambda_{32j}^2)$ for different $m_{\tilde{h}^{j*}}$. Numerically the constrains are given by

$$\begin{aligned} \lambda_{32j}^2 &\leq 0.85 \left(\frac{m_{\tilde{h}^{j*}}}{1000\text{GeV}}\right)^2, \\ \lambda_{32j}\lambda_{31j} &\leq 3.12 \left(\frac{m_{\tilde{h}^{j*}}}{1000\text{GeV}}\right)^2. \end{aligned} \tag{4.9}$$

As discussed in the next subsection, we find that a more constraining bound on the product of the couplings $\lambda_{32j}\lambda_{31j}$ can be obtained from $D^0 - \bar{D}^0$ mixing as compared to those obtained from $D^+ \to \tau\nu$.

### 4.3 Constraints from $D^0 - \bar{D}^0$ mixing

The phenomenon of meson-antimeson oscillation, being a flavor changing neutral current (FCNC) process, is very sensitive to heavy particles propagating in the mixing amplitude and therefore, it provides a powerful tool to test the SM and a window to observe NP. In the $D^0 - \bar{D}^0$ system, $b$-quark contribution to the fermion loop of the box diagram provides a $\Delta C = 2$ transition which is highly suppressed $\sim \mathcal{O}(\lambda^3)$ (by a tiny $V_{ub}$ CKM

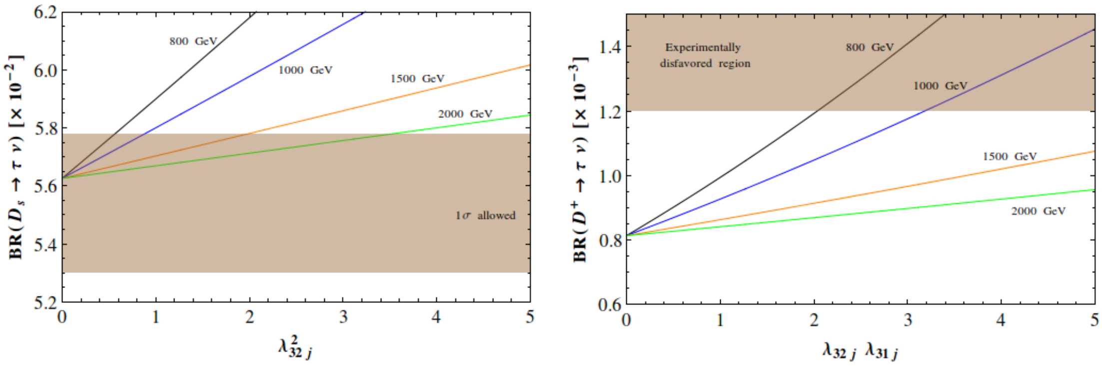


**Figure 7**. Dependence of (left figure) BR($D_s^+ \to \tau\nu$) on the coupling $\lambda_{32j}^2$ [(right figure) BR($D^+ \to \tau\nu$) on the coupling $\lambda_{32j}\lambda_{31j}$] for $m_{\tilde{h}^{j*}}$ = 800, 1000, 1500, 2000 GeV corresponding to black, blue, orange, and green lines respectively. In the left (right) figure the horizontal brown band shows the $1\sigma$ experimentally allowed (disfavored) region.

matrix element). Therefore, the large non-decoupling effects from a heavy fermion in the leading one-loop contributions is small. $D^0 - \bar{D}^0$ mixing involves the dynamical effects of rather light down-type particles and therefore it provides information complementary to the strange and bottom systems where the large effects of heavy top quark in the loops are quintessential. The $D^0 - \bar{D}^0$ mixing is described by $\Delta C = 2$ effective Hamiltonian which induces off-diagonal terms in the mass matrix for neutral D meson pair and typically parametrized in terms of following experimental observables

$$x_D \equiv \frac{\Delta M_D}{\Gamma_D} \quad \text{and} \quad \mathrm{y_D} \equiv \frac{\Gamma_\mathrm{D}}{2\Gamma_\mathrm{D}}, \tag{4.10}$$

where $\Delta M_D$ and $\Delta\Gamma_D$ are the mass and width splittings between mass eigenstates of $D^0 - \bar{D}^0$ systems respectively and $\Gamma_D$ is the average width. The parameters $x_D$ and $y_D$ can be written in terms of the mixing matrix as follows

$$\begin{aligned} x_D &= \frac{1}{2M_D\Gamma_D}\mathrm{Re}\left[2\langle\bar{\mathrm{D}}^0|\mathrm{H}^{|\Delta\mathrm{C}|=2}|\mathrm{D}^0\rangle + \langle\bar{\mathrm{D}}^0|\mathrm{i}\int \mathrm{d}^4\mathrm{x}\mathrm{T}\{\mathcal{H}_\mathrm{w}^{|\Delta\mathrm{C}|=1}(\mathrm{x})\mathcal{H}_\mathrm{w}^{|\Delta\mathrm{C}|=1}(0)\}|\mathrm{D}^0\rangle\right], \\ y_D &= \frac{1}{2M_D\Gamma_D}\mathrm{Im}\langle\bar{\mathrm{D}}^0|\mathrm{i}\int \mathrm{d}^4\mathrm{x} \;\times\; \mathrm{T}\{\mathcal{H}_\mathrm{w}^{|\Delta\mathrm{C}|=1}(\mathrm{x})\mathcal{H}_\mathrm{w}^{|\Delta\mathrm{C}|=1}(0)\}|\mathrm{D}^0\rangle, \end{aligned} \tag{4.11}$$

with $\mathcal{H}_w^{|\Delta C|=1}(x)$ being the Hamiltonian density that describes $|\Delta C| = 1$ transitions at space-point $x$ and T denotes the time ordered product. Since the local $|\Delta C| = 2$ interaction does not contain an absorptive part, this term does not affect $y_D$ and contributes to $x_D$ only. The measured values of $x_D$ and $y_D$ as determined by HFAG are [74]

$$\begin{aligned} x_D &= 0.49^{+0.14}_{-0.15} \times 10^{-2}, \\ y_D &= (0.61 \pm 0.08) \times 10^{-2}, \end{aligned} \tag{4.12}$$

Charm mixing in the SM is highly affected by contributions from intermediate hadronic states, and therefore the theoretical estimations in the SM suffers from large uncertainties and generally stretched over several orders of magnitude (for a review, see ref. [75]). Like

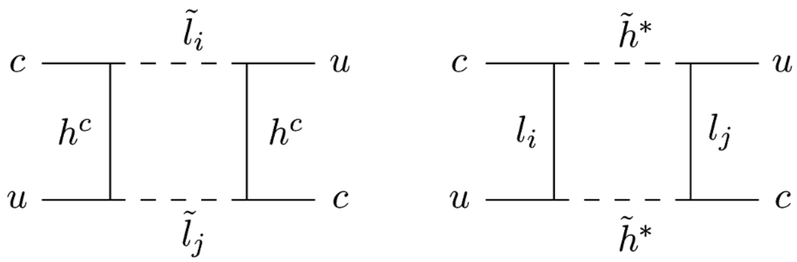


**Figure 8**. Feynman diagrams contributing to $D^0 - \bar{D}^0$ mixing in ALRSM induced by scalar leptoquark and slepton.

in the case of mixing in neutral K and B systems, $D^0 - \bar{D}^0$ mixing is also sensitive to NP effects. Both $x_D$ and $y_D$ can receive large contributions from NP. The contribution to $y_D$ in several NP models including LR models, multi Higgs models, SUSY without R-parity violations and models with extra vector like quarks has been studied in ref. [76], while in ref. [75] the NP contributions to $x_D$ in 21 NP models have been discussed. In this section, we use the neutral D meson mixing to obtain constraints on $\lambda_{32j}\lambda_{31j}$. These bounds are more tighter than those obtained in the previous section from measured BR of $D^+ \to \tau\nu$. The relevant Feynman diagrams which contribute to $D^0 - \bar{D}^0$ mixing in the ALRSM are shown in figure 8. These Box diagrams are similar to the diagrams generated from internal line exchange of lepton-squark pair or slepton-quark pair in the case of R-parity violating models [75, 77]. The mixing is described by the effective Hamiltonian

$$\mathcal{H}_{\text{eff}} = \frac{1}{128\pi^2}(\lambda_{32j}\lambda_{31j})^2 \left(\frac{1}{m_{\tilde{\tau}}^2} + \frac{1}{m_{\tilde{h}^{j*}}^2}\right)(\bar{c}_L\gamma^\mu u_L)(\bar{c}_L\gamma_\mu u_L), \tag{4.13}$$

where we assume that the box diagrams receive contributions from third generation of leptons only. Following ref. [75, 77] and taking $m_{\tilde{h}^{j*}} \simeq m_{\tilde{\tau}}$, the constraints on the size of couplings is given by

$$\lambda_{32j}\lambda_{31j} \leq 0.17\sqrt{x_D^{\text{expt}}}\left(\frac{m_{\tilde{h}^{j*}}}{1000\text{GeV}}\right). \tag{4.14}$$

In figure 9, we plot the dependence of $x_D^{\text{ALRSM}}$ on the product of the couplings $\lambda_{32j}\lambda_{31j}$ for different $m_{\tilde{h}^{j*}}$.

## 5 Results and discussion

Having discussed the allowed region for $C_{V_L}^{\tau}$ which can explain both $\mathcal{R}(D)$ and $\mathcal{R}(D^*)$ data simultaneously in section 3 and the constraints on the couplings $\lambda_{33j}$ and $\lambda_{32j}$ involved in $C_{V_L}^{\tau}$ from the leptonic decays $D_s^+ \to \tau^+\bar{\nu}$, $B^+ \to \tau^+\bar{\nu}$, $D^+ \to \tau^+\bar{\nu}$ and $D^0$-$\bar{D}^0$ mixing in section 4, we are now ready to translate these analysis into a simple $\lambda_{33j}$-$\lambda_{32j}$ parameter space analysis. In figure 10, we plot the range of the couplings $\lambda_{33j}$ and $\lambda_{32j}$ (for $m_{\tilde{h}^j*} =$ 1000 GeV) that can explain both $\mathcal{R}(D)$ and $\mathcal{R}(D^*)$ data over the parameter space allowed by the the leptonic decays and $D^0$-$\bar{D}^0$ mixing. From the decay $D_s^+ \to \tau^+\bar{\nu}$, we constrain the allowed upper limit of the coupling $\lambda_{32j}$. The decay $D^+ \to \tau^+\bar{\nu}$ and $D^0$-$\bar{D}^0$ mixing

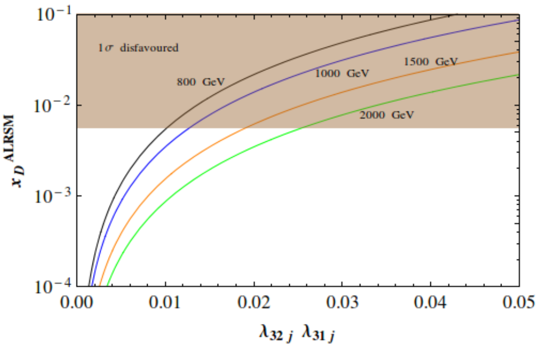


**Figure 9**. Dependence of $x_D^{\rm ALRSM}$ on the coupling $\lambda_{32j}\lambda_{31j}$ for $m_{\tilde{h}^{j*}} = 800, 1000, 1500, 2000\,\text{GeV}$ corresponding to black, blue, orange, and green lines respectively. The horizontal brown (light) band shows the $1\sigma$ experimentally disfavored region.

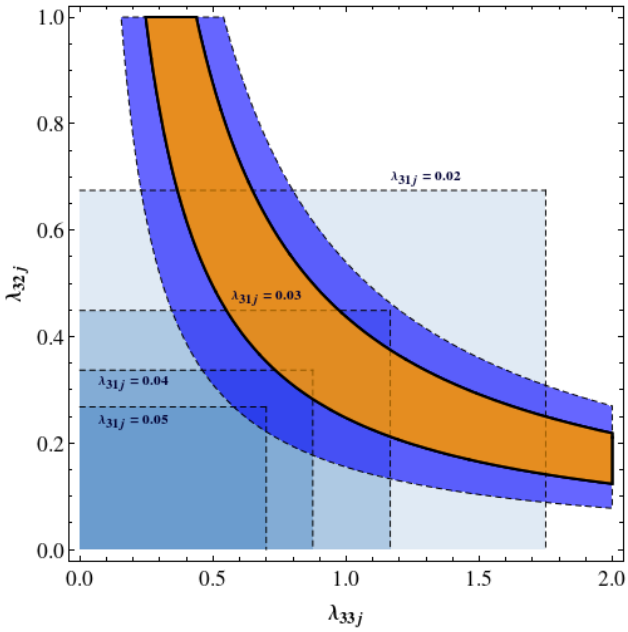


**Figure 10**. The region of $\lambda_{33j}$-$\lambda_{32j}$ parameter space compatible with the experimental data for $\mathcal{R}(D^{(*)})$ and constraints from the leptonic decays $D_s^+ \to \tau^+\bar{\nu}$, $B^+ \to \tau^+\bar{\nu}$, $D^+ \to \tau^+\bar{\nu}$ and $D^0$-$\bar{D}^0$ mixing. We take $m_{\tilde{h}^{j}*} = 1000\,\text{GeV}$ for this plot. Blue band between dashed lines shows allowed values considering constraints from $R_D$ only, Orange band between bold black lines shows allowed region favored by experimental data for both $R_{D^*}$ and $R_D$. The shaded (light blue) rectangles correspond to the allowed regions of $\lambda_{33j}$-$\lambda_{32j}$ parameter space for different values of $\lambda_{31j}$ marked with the corresponding allowed upper boundary shown in dashed lines consistent with the present experimental data on $B \to \tau\nu$, $D_s \to \tau\nu$, $D^+ \to \tau\nu$ and $D - \bar{D}$ mixing.

give constraints on the upper limit of the product of couplings $\lambda_{32j}\lambda_{31j}$. We find that among the two processes the latter gives more stringent constraints and therefore we use the constrains on the allowed upper limit of $\lambda_{32j}\lambda_{31j}$ coming from $D^0$-$\bar{D}^0$ mixing. Finally, we use the decay $B^+ \to \tau^+\bar{\nu}$ to constrain the upper limit of $\lambda_{33j}\lambda_{31j}$. The latter two constraints on the products of couplings have $\lambda_{31j}$ as a common free parameter and the shaded rectangles in figure 10 correspond to the allowed regions of $\lambda_{33j}$-$\lambda_{32j}$ parameter space for different values of $\lambda_{31j}$ marked in the figure with the corresponding allowed upper boundary shown in dashed lines. The blue band corresponds to the allowed band of $\lambda_{33j}$-$\lambda_{32j}$ explaining the $\mathcal{R}(D)$ data and the orange band corresponds to the allowed band of $\lambda_{33j}$-$\lambda_{32j}$ explaining both $\mathcal{R}(D)$ and $\mathcal{R}(D^*)$ data simultaneously. We would like to note that the list of constraints mentioned above is far from exhaustive and many other possible leptonic and semileptonic decays can give independent constrains. For instance, the decay process $\tau^+ \to \pi^+\nu$ can give independent constraint on $\lambda_{31j}$, which we find to be consistent with the values extracted out of the above constraints and used for the parameter space analysis. On the other hand, the semileptonic decay $t \to b\tau\nu$ can give constraint on $\lambda_{33j}$ which we find to be again consistent with the values used in the above parameter space analysis. Also the effective NP operators under consideration may induce $B$-decays such as $b \to s\nu\bar{\nu}$ [78, 79], which can be an interesting channel for the future experiments.

In conclusion, we have studied the superstring inspired $E_6$ motivated Alternative Left-Right Symmetric model to explore if this model can explain the current experimental data for both $\mathcal{R}(D)$ and $\mathcal{R}(D^{(*)})$ simultaneously addressing the excesses over the SM expectations. We use the leptonic decays $D_s^+ \to \tau^+\bar{\nu}$, $B^+ \to \tau^+\bar{\nu}$, $D^+ \to \tau^+\bar{\nu}$ and $D^0$-$\bar{D}^0$ mixing to constrain the couplings involved in the semileptonic $b \to c$ transition in ALRSM. We find that ALRSM can explain the current experimental data on $\mathcal{R}(D^{(*)})$ quite well while satisfying the constraints from the rare $B$, $D$ decays $D^0$-$\bar{D}^0$ mixing. Furthermore, ALRSM can also explain both the $eejj$ and $e\not{p}_T jj$ signals recently reported by CMS and also accommodate successful leptogenesis. If these excess signals are confirmed in future B-physics experiments and at the LHC then ALRSM will be an interesting candidate for NP beyond the Standard Model.


## Acknowledgments

CH would like to thank Utpal Sarkar for many helpful discussions.




## References


[1] LHCb collaboration, *Measurement of the ratio of branching fractions* $\mathcal{B}(\bar{B}^0 \to D^{*+}\tau^-\bar{\nu}_\tau)/\mathcal{B}(\bar{B}^0 \to D^{*+}\mu^-\bar{\nu}_\mu)$, *Phys. Rev. Lett.* **115** (2015) 111803 [arXiv:1506.08614] [INSPIRE].

[2] BaBar collaboration, J.P. Lees et al., *Evidence for an excess of* $\bar{B} \to D^{(*)}\tau^-\bar{\nu}_\tau$ *decays*, *Phys. Rev. Lett.* **109** (2012) 101802 [arXiv:1205.5442] [INSPIRE].

[3] BaBar collaboration, J.P. Lees et al., *Measurement of an excess of* $\bar{B} \to D^{(*)}\tau^-\bar{\nu}_\tau$ *decays and implications for charged Higgs bosons*, *Phys. Rev.* **D 88** (2013) 072012 [arXiv:1303.0571] [INSPIRE].

[4] BELLE collaboration, M. Huschle et al., *Measurement of the branching ratio of $\bar{B} \to D^{(*)}\tau^-\bar{\nu}_\tau$ relative to $\bar{B} \to D^{(*)}\ell^-\bar{\nu}_\ell$ decays with hadronic tagging at Belle*, Phys. Rev. **D 92** (2015) 072014 [arXiv:1507.03233] [INSPIRE].

[5] BABAR collaboration, B. Aubert et al., *Observation of the semileptonic decays $B \to D^*\tau^-\bar{\nu}(\tau)$ and evidence for $B \to D\tau^-\bar{\nu}(\tau)$*, Phys. Rev. Lett. **100** (2008) 021801 [arXiv:0709.1698] [INSPIRE].

[6] BELLE collaboration, A. Bozek et al., *Observation of $B^+ \to \bar{D}^{*0}\tau^+\nu_\tau$ and evidence for $B^+ \to \bar{D}^0\tau^+\nu_\tau$ at Belle*, Phys. Rev. **D 82** (2010) 072005 [arXiv:1005.2302] [INSPIRE].

[7] P. Krawczyk and S. Pokorski, *Strongly coupled charged scalar in $B$ and $t$ decays*, Phys. Rev. Lett. **60** (1988) 182 [INSPIRE].

[8] J. Kalinowski, *Semileptonic decays of $B$ mesons into $\tau\nu_\tau$ in a two Higgs doublet model*, Phys. Lett. **B 245** (1990) 201 [INSPIRE].

[9] W.-S. Hou, *Enhanced charged Higgs boson effects in $B^- \to \tau$ anti-neutrino, $\mu$ anti-neutrino and $b \to \tau$ anti-neutrino $+X$*, Phys. Rev. **D 48** (1993) 2342 [INSPIRE].

[10] M. Tanaka, *Charged Higgs effects on exclusive semitauonic $B$ decays*, Z. Phys. **C 67** (1995) 321 [hep-ph/9411405] [INSPIRE].

[11] J.F. Kamenik and F. Mescia, *$B \to D\tau\nu$ branching ratios: opportunity for lattice QCD and hadron colliders*, Phys. Rev. **D 78** (2008) 014003 [arXiv:0802.3790] [INSPIRE].

[12] U. Nierste, S. Trine and S. Westhoff, *Charged-Higgs effects in a new $B \to D\tau\nu$ differential decay distribution*, Phys. Rev. **D 78** (2008) 015006 [arXiv:0801.4938] [INSPIRE].

[13] M. Tanaka and R. Watanabe, *Tau longitudinal polarization in $B \to D\tau\nu$ and its role in the search for charged Higgs boson*, Phys. Rev. **D 82** (2010) 034027 [arXiv:1005.4306] [INSPIRE].

[14] S. Fajfer, J.F. Kamenik and I. Nisandzic, *On the $B \to D^*\tau\bar{\nu}_\tau$ sensitivity to new physics*, Phys. Rev. **D 85** (2012) 094025 [arXiv:1203.2654] [INSPIRE].

[15] Y. Sakaki and H. Tanaka, *Constraints on the charged scalar effects using the forward-backward asymmetry on $\bar{B} \to D^*\tau\bar{\nu}_\tau$*, Phys. Rev. **D 87** (2013) 054002 [arXiv:1205.4908] [INSPIRE].

[16] S. Fajfer, J.F. Kamenik, I. Nisandzic and J. Zupan, *Implications of lepton flavor universality violations in $B$ decays*, Phys. Rev. Lett. **109** (2012) 161801 [arXiv:1206.1872] [INSPIRE].

[17] A. Datta, M. Duraisamy and D. Ghosh, *Diagnosing new physics in $b \to c\tau\nu_\tau$ decays in the light of the recent BaBar result*, Phys. Rev. **D 86** (2012) 034027 [arXiv:1206.3760] [INSPIRE].

[18] J.A. Bailey et al., *Refining new-physics searches in $B \to D\tau\nu$ decay with lattice QCD*, Phys. Rev. Lett. **109** (2012) 071802 [arXiv:1206.4992] [INSPIRE].

[19] D. Becirevic, N. Kosnik and A. Tayduganov, *$\bar{B} \to D\tau\bar{\nu}_\tau$ vs. $\bar{B} \to D\mu\bar{\nu}_\mu$*, Phys. Lett. **B 716** (2012) 208 [arXiv:1206.4977] [INSPIRE].

[20] M. Tanaka and R. Watanabe, *New physics in the weak interaction of $\bar{B} \to D^{(*)}\tau\bar{\nu}$*, Phys. Rev. **D 87** (2013) 034028 [arXiv:1212.1878] [INSPIRE].

[21] M. Freytsis, Z. Ligeti and J.T. Ruderman, *Flavor models for $\bar{B} \to D^{(*)}\tau\bar{\nu}$*, Phys. Rev. **D 92** (2015) 054018 [arXiv:1506.08896] [INSPIRE].

[22] S. Bhattacharya, S. Nandi and S.K. Patra, *Optimal-observable analysis of possible new physics in $B \to D^{(*)}\tau\nu_\tau$*, arXiv:1509.07259 [INSPIRE].

[23] A. Celis, M. Jung, X.-Q. Li and A. Pich, *Sensitivity to charged scalars in $B \to D^{(*)}\tau\nu_\tau$ and $B \to \tau\nu_\tau$ decays*, JHEP **01** (2013) 054 [arXiv:1210.8443] [INSPIRE].

[24] P. Ko, Y. Omura and C. Yu, *$B \to D^{(*)}\tau\nu$ and $B \to \tau\nu$ in chiral* U(1)′ *models with flavored multi Higgs doublets*, JHEP **03** (2013) 151 [arXiv:1212.4607] [INSPIRE].

[25] A. Crivellin, C. Greub and A. Kokulu, *Explaining $B \to D\tau\nu$, $B \to D^*\tau\nu$ and $B \to \tau\nu$ in a 2HDM of type-III*, Phys. Rev. **D 86** (2012) 054014 [arXiv:1206.2634] [INSPIRE].

[26] N.G. Deshpande and A. Menon, *Hints of R-parity violation in B decays into $\tau\nu$*, JHEP **01** (2013) 025 [arXiv:1208.4134] [INSPIRE].

[27] I. Dorsner, S. Fajfer, J.F. Kamenik and N. Kosnik, *Can scalar leptoquarks explain the $f(D(s))$ puzzle?*, Phys. Lett. **B 682** (2009) 67 [arXiv:0906.5585] [INSPIRE].

[28] Y. Sakaki, M. Tanaka, A. Tayduganov and R. Watanabe, *Testing leptoquark models in $\bar{B} \to D^{(*)}\tau\bar{\nu}$*, Phys. Rev. **D 88** (2013) 094012 [arXiv:1309.0301] [INSPIRE].

[29] A. Greljo, G. Isidori and D. Marzocca, *On the breaking of lepton flavor universality in B decays*, JHEP **07** (2015) 142 [arXiv:1506.01705] [INSPIRE].

[30] I. Doršner, S. Fajfer, N. Košnik and I. Nišandžić, *Minimally flavored colored scalar in $\bar{B} \to D^{(*)}\tau\bar{\nu}$ and the mass matrices constraints*, JHEP **11** (2013) 084 [arXiv:1306.6493] [INSPIRE].

[31] P. Biancofiore, P. Colangelo and F. De Fazio, *On the anomalous enhancement observed in $B \to D^{(*)}\tau\bar{\nu}_\tau$ decays*, Phys. Rev. **D 87** (2013) 074010 [arXiv:1302.1042] [INSPIRE].

[32] Y.-Y. Fan, Z.-J. Xiao, R.-M. Wang and B.-Z. Li, *The $B \to D^{(*)}l\nu_l$ decays in the pQCD approach with the Lattice QCD input*, arXiv:1505.07169 [INSPIRE].

[33] CMS collaboration, *Search for heavy neutrinos and* W *bosons with right-handed couplings in proton-proton collisions at $\sqrt{s} = 8$ TeV*, Eur. Phys. J. **C 74** (2014) 3149 [arXiv:1407.3683] [INSPIRE].

[34] CMS collaboration, *Search for pair-production of first generation scalar leptoquarks in pp collisions at $\sqrt{s} = 8$ TeV*, CMS-PAS-EXO-12-041 (2012).

[35] F.F. Deppisch, T.E. Gonzalo, S. Patra, N. Sahu and U. Sarkar, *Signal of right-handed charged gauge bosons at the LHC?*, Phys. Rev. **D 90** (2014) 053014 [arXiv:1407.5384] [INSPIRE].

[36] F.F. Deppisch, T.E. Gonzalo, S. Patra, N. Sahu and U. Sarkar, *Double beta decay, lepton flavor violation and collider signatures of left-right symmetric models with spontaneous D-parity breaking*, Phys. Rev. **D 91** (2015) 015018 [arXiv:1410.6427] [INSPIRE].

[37] P.S. Bhupal Dev and R.N. Mohapatra, *Unified explanation of the eejj, diboson and dijet resonances at the LHC*, Phys. Rev. Lett. **115** (2015) 181803 [arXiv:1508.02277] [INSPIRE].

[38] J. Gluza and T. Jeliński, *Heavy neutrinos and the $pp \to lljj$ CMS data*, Phys. Lett. **B 748** (2015) 125 [arXiv:1504.05568] [INSPIRE].

[39] B.A. Dobrescu and A. Martin, *Interpretations of anomalous LHC events with electrons and jets*, Phys. Rev. **D 91** (2015) 035019 [arXiv:1408.1082] [INSPIRE].

[40] J.A. Aguilar-Saavedra and F.R. Joaquim, *Closer look at the possible CMS signal of a new gauge boson*, Phys. Rev. **D 90** (2014) 115010 [arXiv:1408.2456] [INSPIRE].

[41] B. Allanach, S. Biswas, S. Mondal and M. Mitra, *Explaining a CMS eejj excess with $\mathcal{R}$-parity violating supersymmetry and implications for neutrinoless double beta decay*, Phys. Rev. **D 91** (2015) 011702 [arXiv:1408.5439] [INSPIRE].

[42] F.S. Queiroz, K. Sinha and A. Strumia, *Leptoquarks, dark matter and anomalous LHC events*, Phys. Rev. **D 91** (2015) 035006 [arXiv:1409.6301] [INSPIRE].

[43] S. Biswas, D. Chowdhury, S. Han and S.J. Lee, *Explaining the lepton non-universality at the LHCb and CMS within a unified framework*, JHEP **02** (2015) 142 [arXiv:1409.0882] [INSPIRE].

[44] B.C. Allanach, S. Biswas, S. Mondal and M. Mitra, *Resonant slepton production yields CMS eejj and ep$_T$jj excesses*, Phys. Rev. **D 91** (2015) 015011 [arXiv:1410.5947] [INSPIRE].

[45] B. Allanach, A. Alves, F.S. Queiroz, K. Sinha and A. Strumia, *Interpreting the CMS $\ell^+\ell^- jj \not{E}_T$ excess with a leptoquark model*, Phys. Rev. **D 92** (2015) 055023 [arXiv:1501.03494] [INSPIRE].

[46] M. Dhuria, C. Hati, R. Rangarajan and U. Sarkar, *Explaining the CMS eejj and e-missing $p_T$ jj excess and leptogenesis in superstring inspired $E_6$ models*, Phys. Rev. **D 91** (2015) 055010 [arXiv:1501.04815] [INSPIRE].

[47] B. Dutta, Y. Gao, T. Ghosh, T. Kamon and N. Kolev, *Explaining the CMS dilepton mass endpoint in the NMSSM*, Phys. Lett. **B 749** (2015) 326 [arXiv:1506.04336] [INSPIRE].

[48] B.A. Dobrescu, *Leptophobic boson signals with leptons, jets and missing energy*, arXiv:1506.04435 [INSPIRE].

[49] J. Berger, J.A. Dror and W.H. Ng, *Sneutrino Higgs models explain lepton non-universality in eejj, eνjj excesses*, JHEP **09** (2015) 156 [arXiv:1506.08213] [INSPIRE].

[50] M.E. Krauss and W. Porod, *Is the CMS eejj excess a hint for light supersymmetry?*, Phys. Rev. **D 92** (2015) 055019 [arXiv:1507.04349] [INSPIRE].

[51] M. Dhuria, C. Hati and U. Sarkar, *Explaining the CMS excesses, baryogenesis and neutrino masses in $E_6$ motivated $U(1)_N$ model*, Phys. Rev. **D 93** (2016) 015001 [arXiv:1507.08297] [INSPIRE].

[52] E. Ma, *Particle dichotomy and left-right decomposition of $E_6$ superstring models*, Phys. Rev. **D 36** (1987) 274 [INSPIRE].

[53] M. Dhuria, C. Hati, R. Rangarajan and U. Sarkar, *The eejj excess signal at the LHC and constraints on leptogenesis*, JCAP **09** (2015) 035 [arXiv:1502.01695] [INSPIRE].

[54] M. Dhuria, C. Hati, R. Rangarajan and U. Sarkar, *Falsifying leptogenesis for a TeV scale $W_R^\pm$ at the LHC*, Phys. Rev. **D 92** (2015) 031701 [arXiv:1503.07198] [INSPIRE].

[55] K. Hagiwara, A.D. Martin and M.F. Wade, *Exclusive semileptonic B meson decays*, Nucl. Phys. **B 327** (1989) 569 [INSPIRE].

[56] M. Neubert, *Model independent extraction of $V(cb)$ from semileptonic decays*, Phys. Lett. **B 264** (1991) 455 [INSPIRE].

[57] I. Caprini, L. Lellouch and M. Neubert, *Dispersive bounds on the shape of $\bar{B} \to D^{(*)}$ lepton anti-neutrino form-factors*, Nucl. Phys. **B 530** (1998) 153 [hep-ph/9712417] [INSPIRE].

[58] N. Isgur and M.B. Wise, *Weak decays of heavy mesons in the static quark approximation*, Phys. Lett. **B 232** (1989) 113 [INSPIRE].

[59] N. Isgur and M.B. Wise, *Weak transition form-factors between heavy mesons*, Phys. Lett. **B 237** (1990) 527 [INSPIRE].

[60] M. Neubert, *Heavy quark symmetry*, Phys. Rept. **245** (1994) 259 [hep-ph/9306320] [INSPIRE].

[61] Heavy Flavor Averaging Group (HFAG) collaboration, Y. Amhis et al., *Averages of b-hadron, c-hadron and τ-lepton properties as of summer 2014*, arXiv:1412.7515 [INSPIRE].

[62] M. Okamoto et al., *Semileptonic $D \to \pi/K$ and $B \to \pi/D$ decays in $2+1$ flavor lattice QCD*, Nucl. Phys. Proc. Suppl. **140** (2005) 461 [hep-lat/0409116] [INSPIRE].


JHEP01(2016)117

[63] Fermilab Lattice, MILC collaboration, J.A. Bailey et al., *Update of $|V_{cb}|$ from the $\bar{B} \to D^* \ell \bar{\nu}$ form factor at zero recoil with three-flavor lattice QCD*, Phys. Rev. **D 89** (2014) 114504 [arXiv:1403.0635] [INSPIRE].

[64] D. London and J.L. Rosner, *Extra gauge bosons in $E_6$*, Phys. Rev. **D 34** (1986) 1530 [INSPIRE].

[65] J.L. Hewett and T.G. Rizzo, *Low-energy phenomenology of superstring inspired $E_6$ models*, Phys. Rept. **183** (1989) 193 [INSPIRE].

[66] Particle Data Group collaboration, K.A. Olive et al., *Review of particle physics*, Chin. Phys. **C 38** (2014) 090001 [INSPIRE].

[67] S.S. Gershtein and M.Yu. Khlopov, SU(4) *symmetry breaking and lepton decays of heavy pseudoscalar mesons*, JETP Lett. **23** (1976) 338 [INSPIRE].

[68] M. Yu. Khlopov, *Effects of symmetry violation in semileptonic meson decays*, Sov. J. Nucl. Phys. **28** (1978) 583 [Yad. Fiz. **28** (1978) 1134] [INSPIRE].

[69] M. Artuso et al., *B, D and K decays*, Eur. Phys. J. **C 57** (2008) 309 [arXiv:0801.1833] [INSPIRE].

[70] G. Burdman, E. Golowich, J.L. Hewett and S. Pakvasa, *Rare charm decays in the standard model and beyond*, Phys. Rev. **D 66** (2002) 014009 [hep-ph/0112235] [INSPIRE].

[71] B.A. Dobrescu and A.S. Kronfeld, *Accumulating evidence for nonstandard leptonic decays of $D_s$ mesons*, Phys. Rev. Lett. **100** (2008) 241802 [arXiv:0803.0512] [INSPIRE].

[72] Y. Kao and T. Takeuchi, *Single-coupling bounds on R-parity violating supersymmetry, an update*, arXiv:0910.4980 [INSPIRE].

[73] J. Barranco, D. Delepine, V. Gonzalez Macias and L. Lopez-Lozano, *Constraining new physics with D meson decays*, Phys. Lett. **B 731** (2014) 36 [arXiv:1303.3896] [INSPIRE].

[74] Heavy Flavor Averaging Group, http://www.slac.stanford.edu/xorg/hfag/charm/CHARM15/results_mix_cpv.html.

[75] E. Golowich, J. Hewett, S. Pakvasa and A.A. Petrov, *Implications of $D^0$-$\bar{D}^0$ mixing for new physics*, Phys. Rev. **D 76** (2007) 095009 [arXiv:0705.3650] [INSPIRE].

[76] E. Golowich, S. Pakvasa and A.A. Petrov, *New physics contributions to the lifetime difference in $D^0$-$\bar{D}^0$ mixing*, Phys. Rev. Lett. **98** (2007) 181801 [hep-ph/0610039] [INSPIRE].

[77] K. Agashe and M. Graesser, *R-parity violation in flavor changing neutral current processes and top quark decays*, Phys. Rev. **D 54** (1996) 4445 [hep-ph/9510439] [INSPIRE].

[78] Y. Grossman, Z. Ligeti and E. Nardi, *New limit on inclusive $B \to X_s$ anti-neutrino neutrino decay and constraints on new physics*, Nucl. Phys. **B 465** (1996) 369 [Erratum ibid. **B 480** (1996) 753] [hep-ph/9510378] [INSPIRE].

[79] A.J. Buras, J. Girrbach-Noe, C. Niehoff and D.M. Straub, *$B \to K^{(*)} \nu \bar{\nu}$ decays in the standard model and beyond*, JHEP **02** (2015) 184 [arXiv:1409.4557] [INSPIRE].

PHYSICAL REVIEW D **94,** 014022 (2016)

# Constraints on a scalar leptoquark from the kaon sector

Girish Kumar[1,2,*]

[1]*Physical Research Laboratory, Navrangpura, Ahmedabad 380 009, India*
[2]*Indian Institute of Technology Gandhinagar, Chandkheda, Ahmedabad 382 424, India*

(Received 4 April 2016; published 19 July 2016)

Recently, several anomalies in flavor physics have been observed, and it was noticed that leptoquarks might account for the deviations from the Standard Model. In this work, we examine the effects of new physics originating from a scalar leptoquark model on the kaon sector. The leptoquark we consider is a TeV-scale particle and within the reach of the LHC. We use the existing experimental data on the several kaon processes including $K^0 - \bar{K}^0$ mixing; rare decays $K^+ \to \pi^+ \nu\bar{\nu}$, $K_L \to \pi^0 \nu\bar{\nu}$; the short-distance part of $K_L \to \mu^+\mu^-$; and lepton-flavor-violating decay $K_L \to \mu^\pm e^\mp$ to obtain useful constraints on the model.

DOI: 10.1103/PhysRevD.94.014022

## I. INTRODUCTION

The discovery of the last missing piece, the Higgs boson, in the first run of the LHC marks the completion of the Standard Model (SM) [1,2]. Though the SM has been exceptionally successful in explaining the experimental data collected so far, there are many evidences which point towards the existence of physics beyond the SM (see, for example, Ref. [3]). Therefore, it is natural to consider the SM as the low-energy limit of a more general theory above the electroweak scale. The direct collider searches at the high-energy frontier (TeVscale) have not found any new particle, but, interestingly, there are some tantalizing hints toward new physics (NP) from high-precision low-energy experiments in the flavor sector. To be specific, in 2012, *BABAR* measured the ratios of branching fractions for the semitauonic decay of the $B$ meson, $\bar{B} \to D^*\tau\bar{\nu}$,

$$\mathcal{R}(D^{(*)}) = \frac{\mathrm{BR}(\bar{B} \to D^{(*)}\tau\bar{\nu})}{\mathrm{BR}(\bar{B} \to D^{(*)}\ell\bar{\nu})}, \tag{1}$$

with $\ell = e, \mu$, and reported $2.0\sigma$ and $2.7\sigma$ excesses over the SM predictions in the measurements of $\mathcal{R}(D)$ and $\mathcal{R}(D^*)$, respectively [4]. Very recently, these decays have been measured by BELLE [5] and LHCb [6]. These results are in agreement with each other and when combined together show a significant deviation from the SM. A summary of the measurements of $\mathcal{R}(D^{(*)})$ done by different collaborations together with the SM predictions is given in Table I.

Another interesting indirect hint of NP comes from the data on $b \to s\mu^+\mu^-$ processes. The LHCb Collaboration has seen a $2.6\sigma$ departure from the SM prediction in the lepton flavor universality ratio $R_K = \mathrm{BR}(\bar{B} \to \bar{K}\mu^+\mu^-)/\mathrm{BR}(\bar{B} \to \bar{K}e^+e^-) = 0.745^{+0.090}_{-0.074} \pm 0.036$ in the dilepton invariant mass bin $1\ \mathrm{GeV}^2 < q^2 < 6\ \mathrm{GeV}^2$ [8]. Though the individual branching fractions for $\bar{B} \to \bar{K}\mu^+\mu^-$ and $\bar{B} \to \bar{K}e^+e^-$ are marred with large hadronic uncertainties in the SM [9], their ratio is a very clean observable and predicted to be $R_K = 1.0003 \pm 0.0001$ [9,10]. Also, the recent data on angular observables of four-body distribution in the process $(B \to K^*(\to K \to)\ell^+\ell^-$ indicate some tension with the SM [11,12], particularly the deviation of $\sim 3\sigma$ in two of the $q^2$ bins of angular observable $P_5'$ [13]. In the decay $B_s \to \phi\mu^+\mu^-$, a deviation of $3.5\sigma$ significance with respect to the SM prediction has also been reported by LHCb [14]. The model-independent global fits to the updated data on $b \to s\mu^+\mu^-$ observables point toward a solution with NP that is favored over the SM by $\sim 4\sigma$ [13].

Several NP scenarios have been proposed to explain these discrepancies. The excesses in $\mathcal{R}(D^{(*)})$ have been explained in a generalized framework of 2HDM (two Higgs doublet model) in Refs. [15–17], in the framework of the $R$-parity-violating minimal supersymmetric Standard Model in Ref. [18], in the $E_6$-motivated alternative left right symmetric model in Ref. [19], and using a model-independent approach [20–23], while in Refs. [24–27] the excesses in $\mathcal{R}(D^{(*)})$ have been addressed in the context of leptoquark models. The possible explanation for the observed anomalies in $b \to s\mu^+\mu^-$ processes preferably demands a negative contribution to the Wilson coefficient of semileptonic operator $(\bar{s}b)_{\mathrm{V-A}}(\bar{\mu}\gamma_\alpha\mu)$ [13,28]. Several NP models, generally involving $Z'$ vector bosons [29–35] or leptoquarks [36–44], are able to produce such operators with the required effects to explain the present data.

In view of this, we are motivated to study a TeV-scale leptoquark model and analyze NP effects on the kaon sector. It is known that the studies of kaon decays have played a vital role in retrieving information on the flavor structure of the SM. In particular, neutral kaon mixing and the rare decays of the kaon have been analyzed in various extensions of the SM and are known to provide some of the most stringent constraints on NP [45–56]. The NP model we consider in this paper is a simple extension of the SM by a single scalar leptoquark. The leptoquark $\phi$ with mass $M_\phi$

*girishk@prl.res.in

TABLE I. Summary of experimental measurement for the ratios $R(D^{(*)})$ and the expectation in the SM. Here, the first (second) errors are statistical (systematic).

| | $\mathcal{R}(D^*)$ | $\mathcal{R}(D)$ |
|---|---|---|
| LHCb [6] | $0.336 \pm 0.027 \pm 0.030$ | $\cdots$ |
| *BABAR* [4] | $0.332 \pm 0.024 \pm 0.018$ | $0.440 \pm 0.058 \pm 0.042$ |
| BELLE [5] | $0.293 \pm 0.038 \pm 0.015$ | $0.375 \pm 0.064 \pm 0.026$ |
| SM Pred.[7] | $0.252 \pm 0.003$ | $0.300 \pm 0.010$ |

has $(SU(3), SU(2))_{U(1)}$ quantum numbers $(3,1)_{-1/3}$. This model is interesting, considering that it has all the necessary ingredients accommodating semileptonic $b \to c$ and $b \to s$ decays to explain the anomalies in the LFU (lepton flavor universality) ratios discussed above [40,41]. To this end, we must mention that, along with anomalies observed in the flavor sector, the leptoquark model under study is also capable of explaining the new diphoton excess recently reported by the ATLAS and CMS collaborations in their analysis of $\sqrt{s} = 13$ TeV $pp$ collision [57].

Following the conventions of Ref. [40], the Lagrangian governing the leptoquark interaction with first-family fermions is given by

$$\mathcal{L}^{(\phi)} \ni \lambda^L_{ue} \bar{u}^c_L e_L \phi^* + \lambda^R_{ue} \bar{u}^c_R e_R \phi^* - \lambda^L_{d\nu} \bar{d}^c_L \nu_L \phi^* + \text{H.c.}, \qquad (2)$$

where L/R are the left/right projection operators $(1 \mp \gamma_5)/2$. The couplings $\lambda$'s are family dependent, and $u^c = C\bar{u}^T$ are the charge-conjugated spinors. Similar interaction terms for the second and third families can also be written down. In this model, $B \to D^{(*)}\tau\bar{\nu}$ proceeds at tree level through the exchange of leptoquark $(\phi)$. Integrating out the heavy particles gives rise to low-energy six-dimension effective operators, which can produce the required effects to satisfy the experimental data. In Ref. [40], it was shown that with $O(1)$ left-handed and relatively suppressed right-handed couplings one can explain the observed excesses in the rate of $B \to D^{(*)}\tau\bar{\nu}$ decays. The authors of Ref. [40] were also able to simultaneously explain the observed anomalies in $R_K$ with large $[\sim O(1)]$ left-handed couplings for a TeV scale leptoquark. In this model, such large couplings are possible because the leading contribution to $\bar{B} \to \bar{K}\mu^+\mu^-$ comes from one-loop diagrams and therefore additional GIM (Glashow-Iliopoulos-Maiani) and CKM (Cabibbo-Kobayashi-Maskawa) suppression compensates for the "largeness" of the couplings. This is in contrast to NP models [37,41,58] in which $R_K$ arises at tree level, which renders the couplings very small in order to have leptoquarks within the reach of the LHC. Apart from the B system, this model has also been explored in the context of flavor changing neutral current (FCNC) decays of the D meson. In Refs. [59–61], the impact of scalar (as well as vector) leptoquarks on the FCNC processes $D^0 \to \mu^+\mu^-$ and $D^+ \to \pi^+\mu^+\mu^-$ have been studied, and using the existing experimental results, strong bounds on the leptoquark coupling have been derived. However, to the best of our knowledge, the effects of new physics on the kaon sector have not been investigated before in the scalar leptoquark $(3,1)_{-1/3}$ model. We start by writing the effective Hamiltonian relevant for each case and discuss the effective operators and corresponding coupling strengths (Wilson coefficients) generated in the model. The explicit expressions of new contributions in terms of parameters of the model are derived. We then discuss NP affecting the various kaon processes such as $K^+ \to \pi^+\nu\bar{\nu}$, $K_L \to \pi^0\nu\bar{\nu}$, $K_L \to \mu^+\mu^-$, and LFV (lepton flavor violating) decay $K_L \to \mu^\pm e^\mp$. Using the existing experimental information on these processes, the constraints on the leptoquark couplings are obtained.

The rest of the article is organized in the following way. In Sec. II, we study the $K^0 - \bar{K}^0$ mixing in this model and obtain constraints on the couplings. In Secs. III and IV, we constrain the parameter space using information on $\text{BR}(K^+ \to \pi^+\nu\bar{\nu})$ and $CP$-violating $\text{BR}(K_L \to \pi^0\nu\bar{\nu})$, respectively. In Sec. V, we discuss the new contribution to the short-distance part of rare decay $K_L \to \mu^+\mu^-$ in this model and obtain constraints on the generation-diagonal leptoquark couplings using the bounds on $\text{BR}(K_L \to \mu^+\mu^-)_{\text{SD}}$. In Sec. VI, we discuss the LFV process $K_L \to \mu^\mp e^\pm$ and constrain the off-diagonal couplings of the leptoquark contributing to NP Wilson coefficients. Finally, we summarize our results in the last section.

## II. CONSTRAINTS FROM $K^0 - \bar{K}^0$ MIXING

The phenomenon of meson-antimeson oscillation, being a FCNC process, is very sensitive to heavy particles propagating in the mixing amplitude, and therefore it provides a powerful tool to test the SM and a window to observe NP. In this section, we focus on the mixing of the neutral kaon meson. The experimental measurement of the $K^0 - \bar{K}^0$ mass difference $\Delta m_K$ and of $CP$-violating parameter $\epsilon_K$ has been instrumental in not only constraining the parameters of the unitarity triangle but also providing stringent constraints on NP. The theoretical calculations for $K^0 - \bar{K}^0$ mixing are done in the framework of effective field theories (EFT), which allow one to separate long- and short-distance contributions. The leading contribution to $K^0 - \bar{K}^0$ oscillations in the SM comes from the so-called box diagrams generated through internal line exchange of the W boson and up-type quark pair. The effective SM Hamiltonian for $|\Delta S| = 2$ resulting from the evaluation of box diagrams is written as [62,63]

$$\mathcal{H}^{|\Delta S|=2}_{\text{eff}} = \frac{G_F^2 M_W^2}{4\pi^2}(\lambda_c^2 \eta_{cc} S_0(x_c) + \lambda_t^2 \eta_{tt} S_0(x_t) + 2\lambda_t\lambda_c\eta_{ct} S_0(x_c, x_t))K(\mu)Q_s(\mu), \qquad (3)$$

where $G_F$ is the Fermi constant and $\lambda_i = V_{is}^* V_{id}$ contains CKM matrix elements. $Q_s(\mu)$ is a dimension-6, four-fermion local operator $(\bar{s}\gamma_\mu L d)(\bar{s}\gamma^\mu L d)$, and $K(\mu)$ is the relevant short-distance factor which makes product $K(\mu)Q_s(\mu)$ independent of $\mu$. The Inami-Lim functions $S_0(x)$ and $S_0(x_i, x_j)$ [64] contain contributions of loop diagrams and are given by [65]

$$S(x_c, x_t) = x_c x_t \left[ -\frac{3}{4(1-x_c)(1-x_t)} + \frac{\mathrm{Ln} x_t}{(x_t - x_c)(1-x_t)^2}\left(1 - 2x_t + \frac{x_t^2}{4}\right) + \frac{\mathrm{Ln} x_c}{(x_c - x_t)(1-x_c)^2}\left(1 - 2x_c + \frac{x_c^2}{4}\right)\right], \tag{4}$$

and the function $S_0(x)$ is the limit when $y \to x$ of $S_0(x, y)$, while $\eta_i$ in Eq. (3) are the short-distance QCD correction factors $\eta_{cc} = 1.87$, $\eta_{tt} = 0.57$, and $\eta_{ct} = 0.49$ [66–68]. The hadronic matrix element $\langle \bar{K}^0 | Q_s | K^0 \rangle$ is parametrized in terms of decay constant $f_K$ and kaon bag parameter $B_K$ in the following way:

$$B_K = \frac{3}{2} K(\mu) \frac{\langle \bar{K}^0 | Q_s | K^0 \rangle}{f_K^2 m_K^2}. \tag{5}$$

The contribution of NP to $|\Delta S| = 2$ transition can be parametrized as the ratio of the full amplitude to the SM one as follows [69]:

$$C_{\Delta m_K} = \frac{\mathrm{Re}\langle K | H_{\mathrm{eff}}^{\mathrm{Full}} | \bar{K} \rangle}{\mathrm{Re}\langle K | H_{\mathrm{eff}}^{\mathrm{SM}} | \bar{K} \rangle}, \qquad C_{\varepsilon_K} = \frac{\mathrm{Im}\langle K | H_{\mathrm{eff}}^{\mathrm{Full}} | \bar{K} \rangle}{\mathrm{Im}\langle K | H_{\mathrm{eff}}^{\mathrm{SM}} | \bar{K} \rangle}. \tag{6}$$

In the SM, $C_{\Delta m_K}$ and $C_{\varepsilon_K}$ are unity. The effective Hamiltonian $\langle \bar{K}^0 | H_{\mathrm{eff}} | K^0 \rangle$ can be related to the off-diagonal element $M_{12}$ through the relation[1]

$$\langle \bar{K}^0 | H_{\mathrm{eff}}^{\mathrm{Full}} | K^0 \rangle = 2 m_K M_{12}^*, \tag{7}$$

with $M_{12} = (M_{12})_{\mathrm{SM}} + (M_{12})_{NP}$. In the SM, the theoretical expression of $(M_{12})_{\mathrm{SM}}$ reads [54]

$$(M_{12})_{\mathrm{SM}} = \frac{G_F^2}{12\pi^2} f_K^2 B_K m_K M_W^2 F^*(\lambda_c, \lambda_t, x_c, x_t), \tag{8}$$

where the function $F(\lambda_c, \lambda_t, x_c, x_t)$ stands for

[1]The observables mass difference $\Delta m_K$ and $CP$-violating parameter $\varepsilon_K$ are related to off-diagonal element $M_{12}$ through the following relations: $\Delta m_K = 2[\mathrm{Re}(M_{12})_{\mathrm{SM}} + \mathrm{Re}(M_{12})_{NP}]$ and $\varepsilon_K = \frac{k_\varepsilon \exp^{i\phi_\varepsilon}}{\sqrt{2}(\Delta m_K)_{\mathrm{exp}}}[\mathrm{Im}(M_{12})_{\mathrm{SM}} + \mathrm{Im}(M_{12})_{NP}]$, where $\phi_\varepsilon \simeq 43°$ and $k_\varepsilon \simeq 0.94$ [70–72].

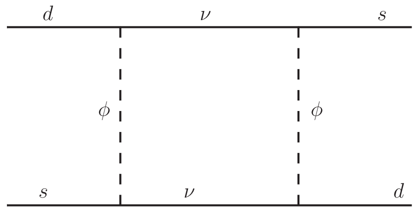


FIG. 1. New contribution to $K - \bar{K}$ mixing induced by the scalar leptoquark ($\phi$).

$$F(\lambda_c, \lambda_t, x_c, x_t) = \lambda_c^2 \eta_{cc} S_0(x_c) + \lambda_t^2 \eta_{tt} S_0(x_t) + 2\lambda_t \lambda_c \eta_{ct} S_0(x_c, x_t), \tag{9}$$

with $x_i = m_i^2 / M_W^2$.

In the $(3,1)_{-1/3}$ leptoquark model, the internal line exchange of the neutrino-leptoquark pair induces new Feynman diagrams, which contributes to $K^0 - \bar{K}^0$ mixing. The diagrams are shown in Fig. 1. The new effects modify the observables $C_{\Delta m_K}$ and $C_{\varepsilon_K}$, and in the approximation $M_\phi^2 \gg m_{t,W}^2$, their expressions are given by

$$C_{\Delta m_K} = 1 + \frac{1}{g_2^4} \frac{M_W^2}{M_\phi^2} \frac{\eta_{tt}}{\mathrm{Re}(F^*)} \mathrm{Re}(\xi_{ds})^2, \tag{10}$$

$$C_{\varepsilon_K} = 1 + \frac{1}{g_2^4} \frac{M_W^2}{M_\phi^2} \frac{\eta_{tt}}{\mathrm{Im}(F^*)} \mathrm{Im}(\xi_{ds})^2, \tag{11}$$

where we have used notation $F$ for $F(\lambda_c, \lambda_t, x_c, x_t)$ for simplicity. $g_2$ is the SU(2) gauge coupling, and we define

$$\xi_{ds} \equiv (\lambda^L \lambda^{L\dagger})_{ds} = \sum_i \lambda_{d\nu_i}^L \lambda_{s\nu_i}^{L*}. \tag{12}$$

Solving Eqs. (10) and (11) for real and imaginary parts of $\xi_{ds}$ in terms of the experimental observables $C_{\Delta m_K}$ and $C_{\varepsilon_K}$, we obtain the following expressions:

$$(\mathrm{Re}\xi_{ds})^2 = \left(\frac{g_2^4}{2} \frac{M_\phi^2}{M_W^2}\right)\left(\frac{\mathrm{Re}(F^*)}{\eta_{tt}}\left(-1 + C_{\Delta m_K}\right)\right) \times \left(1 + \sqrt{1 + \left(\frac{\mathrm{Im}F^*}{\mathrm{Re}F^*} \cdot \frac{C_{\varepsilon_K} - 1}{C_{\Delta m_K} - 1}\right)^2}\right), \tag{13}$$

$$(\mathrm{Im}\xi_{ds})^2 = \left(\frac{g_2^4}{2} \frac{M_\phi^2}{M_W^2}\right)\left(\frac{\mathrm{Re}(F^*)}{\eta_{tt}}\left(-1 + C_{\Delta m_K}\right)\right) \times \left(-1 + \sqrt{1 + \left(\frac{\mathrm{Im}F^*}{\mathrm{Re}F^*} \cdot \frac{C_{\varepsilon_K} - 1}{C_{\Delta m_K} - 1}\right)^2}\right). \tag{14}$$

To constrain the leptoquark couplings $\mathrm{Re}\xi_{\mathrm{ds}}$ and $\mathrm{Im}\xi_{\mathrm{ds}}$, we use the latest global fit results provided by the UTfit collaboration and to be conservative evaluate the constraints at the $2\sigma$ level: $C_{\Delta m_K} = 1.10 \pm 0.44$ and $C_{\varepsilon_K} = 1.05 \pm 0.32$ [69]. Here, to account for the significant uncertainties from poorly known long-distance effects [73], we allow for a $\pm 40\%$ uncertainty in the case of $\Delta M_K$. For $\mathrm{Re}\xi_{\mathrm{ds}}$ and $\mathrm{Im}\xi_{\mathrm{ds}}$, we obtain the following upper bounds:

$$(\mathrm{Re}\xi_{\mathrm{ds}})^2 \leq 6.0 \times 10^{-4} \left(\frac{M_\phi}{1000\ \mathrm{GeV}}\right)^2, \qquad (15)$$

$$(\mathrm{Im}\xi_{\mathrm{ds}})^2 \leq 3.8 \times 10^{-4} \left(\frac{M_\phi}{1000\ \mathrm{GeV}}\right)^2. \qquad (16)$$

As discussed in the next section, we find that a more constraining bound on the product of the couplings $\mathrm{Re}(\xi_{\mathrm{ds}})$ and $\mathrm{Im}(\xi_{\mathrm{ds}})$ can be obtained from theoretically rather clean rare processes $K^+ \to \pi^+ \nu\bar{\nu}$ and $K_L \to \pi^0 \nu\bar{\nu}$ as compared to $K - \bar{K}$ mixing.

## III. CONSTRAINTS FROM RARE DECAY $K^+ \to \pi^+ \nu\bar{\nu}$

The charged and neutral $K \to \pi\nu\bar{\nu}$ are in many ways interesting FCNC processes and considered as *golden* modes. Both the decays can play an important role in indirect searches for NP because these decays are theoretically very clean and their branching ratio can be computed with an exceptionally high level of precision (for a review, see Ref. [74]). In the SM, these decays are dominated by Z-penguin and box diagrams, which exhibit hard, powerlike GIM suppression as compared to logarithmic GIM suppression generally seen in other loop-induced meson decays. At the leading order, both modes are induced by a single dimension-6 local operator $(\bar{s}d)_{\mathrm{V-A}}(\bar{\nu}\nu)_{\mathrm{V-A}}$. The hadronic matrix element of this operator can be measured precisely in $K^+ \to \pi^0 e^+ \nu$ decays, including isospin breaking corrections [75,76]. The principal contribution to the error in theoretical predictions originates from the uncertainties on the current values of $\lambda_t$ and $m_c$. The long-distance effects are rather suppressed and have been found to be small [77–79].

In the SM, the effective Hamiltonian for $K \to \pi\nu\bar{\nu}$ decays is written as [80]

$$\mathcal{H}_{\mathrm{eff}}^{\mathrm{SM}} = \frac{G_F}{\sqrt{2}} \frac{2\alpha}{\pi \sin^2\theta_W} \sum_{\ell = e,\mu,\tau} (\lambda_c X_{\mathrm{NNL}}^{\ell} + \lambda_t X(x_t)) \times (\bar{s}_L \gamma_\mu d_L)(\bar{\nu}_{\ell L} \gamma^\mu \nu_{\ell L}). \qquad (17)$$

The index $\ell = e, \mu, \tau$ denotes the lepton flavor. The short-distance function $X(x_t)$ corresponds to the loop-function containing top contribution and is given by

$$X(x_t) = \eta_X \cdot \frac{x_t}{8} \left[\frac{x_t + 2}{x_t - 1} + \frac{3x_t - 6}{(x_t - 1)^2} \mathrm{Ln} x_t\right], \qquad (18)$$

where the factor $\eta_X$ includes the next-to-leading-order (NLO) correction and is close to unity ($\eta_X = 0.995$), while the remaining part describes the contribution of top quark without QCD correction. The NLO QCD corrections have been computed in Refs. [81–83], while two-loop electroweak corrections have been studied in Ref. [84]. The loop-function $X_{\mathrm{NNL}}$ summarizes the contribution from the charm quark and can be written as [55]

$$X_{\mathrm{NNL}} = \frac{2}{3} X_{\mathrm{NNL}}^{e} + \frac{1}{3} X_{\mathrm{NNL}}^{\tau} \equiv \lambda^4 P_c^{\mathrm{SD}}(X), \qquad (19)$$

where $\lambda = |V_{us}|$. The NLO results for the function $X_{\mathrm{NNL}}$ can be found in Refs. [80,83], while next-to-next-to-leading-order (NNLO) calculations are done in Refs. [85,86].

In the considered model, leptoquark $\phi$ mediates $K^+ \to \pi^+ \nu\bar{\nu}$ at tree level. The corresponding Feynman diagram is shown in Fig 2. Integrating out the heavy degrees of freedom, we obtain the following NP effective Hamiltonian relevant for $K^+ \to \pi^+ \nu\bar{\nu}$ decay:

$$\mathcal{H}_{\mathrm{eff}}^{\mathrm{NP}} = -\frac{\lambda_{s\nu_\ell}^{L*} \lambda_{d\nu_\ell}^{L}}{2M_\phi^2} (\bar{s}\gamma_\mu L d)(\bar{s}\gamma^\mu L d). \qquad (20)$$

The new contribution alters the SM branching ratio of $K^+ \to \pi^+ \nu\bar{\nu}$ [87] as

$$\mathrm{BR}(K^+ \to \pi^+ \nu\bar{\nu}) = \kappa_+ (1 + \Delta_{\mathrm{EM}}) \left[\left(\frac{\mathrm{Im}\lambda_t}{\lambda^5} X_{\mathrm{new}}\right)^2 + \left(\frac{\mathrm{Re}\lambda_c}{\lambda} P_c(X) + \frac{\mathrm{Re}\lambda_t}{\lambda^5} X_{\mathrm{new}}\right)^2\right], \qquad (21)$$

where $\kappa_+$ contains relevant hadronic matrix elements extracted from the decay rate of $K^+ \to \pi^0 e^+ \nu$ along with an isospin-breaking correction factor. The explicit form of $\kappa_+$ can be found in Ref. [88]. $\Delta_{\mathrm{EM}}$ describes the electromagnetic radiative correction from photon exchanges and amounts to -0.3%. The charm contribution $P_c(X)$ includes the short-distance part $P_c^{\mathrm{SD}}(X)$ plus the long-distance contribution $\delta P_c$ (calculated in Ref. [76]). We use $P_c(X) = 0.404$ given in Ref. [87]. The function $X_{\mathrm{new}}$ contains a new short-distance contribution from the leptoquark-mediated diagram and modifies the SM contribution through

$$X_{\mathrm{new}} = X(x_t) + \frac{X_\phi}{\lambda_t}, \qquad (22)$$

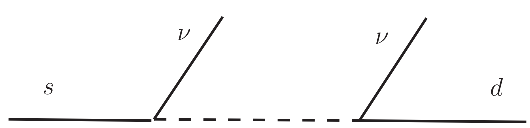


FIG. 2. Feynman diagrams for the decay $K \to \pi\nu\bar{\nu}$ induced by the exchange of scalar leptoquark $\phi$.

where $X(x_t)$ is the top contribution in the SM already defined in Eq. (18) and $X_\phi$ is the contribution due to leptoquark exchange. In terms of the model parameters, $X_\phi$ is given by

$$X_\phi = -\frac{\sqrt{2}}{4G_F}\frac{\pi \sin^2\theta_W}{\alpha}\frac{\xi_{\rm ds}}{M_\phi^2}, \tag{23}$$

where $\alpha(M_Z) = 1/127.9$ is the electromagnetic coupling constant and $\sin^2\theta_W = 0.23$ is the weak mixing angle. Using the experimental value of the branching ratio from the Particle Data Group, $\mathrm{BR}(K^+ \to \pi^+\nu\bar{\nu}) = (1.7 \pm 1.1) \times 10^{-10}$ [89], we obtain the constraint on $\mathrm{Re}\xi_{\rm ds}$ and $\mathrm{Im}\xi_{\rm ds}$, shown in Fig 3. A most conservative bound on individual couplings $\mathrm{Re}\xi_{\rm ds}$ and $\mathrm{Im}\xi_{\rm ds}$ can be obtained by taking only one set to be nonzero at a time. We find that for a leptoquark of 1 TeV mass the constraints are given by $-7.2 \times 10^{-4} < \mathrm{Re}\xi_{\rm ds} < 2.2 \times 10^{-4}$ and $-3.3 \times 10^{-4} < \mathrm{Im}\xi_{\rm ds} < 4.9 \times 10^{-4}$. As pointed out before, these bounds rule out a large parameter space allowed from $K^0 - \bar{K}^0$ mixing. The coupling $\mathrm{Im}\xi_{\rm ds}$ can also be probed independently through the decay $K_L \to \pi^0\nu\bar{\nu}$, which is the subject of our next section.

## IV. CONSTRAINTS FROM $K_L \to \pi^0\nu\bar{\nu}$

The neutral decay mode $K_L \to \pi^0\nu\bar{\nu}$ is *CP* violating. In contrast to the decay rate of $K^+ \to \pi^+\nu\bar{\nu}$ which depends on the real and imaginary parts of $\lambda_t$, with a small contribution from the real part of $\lambda_c$, the rate of $K_L \to \pi^0\nu\bar{\nu}$ depends only on $\mathrm{Im}\lambda_t$. Because of the absence of the charm contribution, the prediction for $\mathrm{BR}(K_L \to \pi^0\nu\bar{\nu})$ is theoretically cleaner. The principal sources of error are the uncertainties on $\mathrm{Im}\lambda_t$ and $m_t$. In the SM, the branching ratio is given by [74]

$$\mathrm{BR}(K_L \to \pi\nu\bar{\nu}) = \kappa_L\left(\frac{\mathrm{Im}\lambda_t}{\lambda^5}X(x_t)\right)^2, \tag{24}$$

with [87]

$$\kappa_L = 2.231 \times 10^{-10}\left(\frac{\lambda}{0.225}\right)^8. \tag{25}$$

The exchange of leptoquark $\phi$ induces new contribution to the rate which can be accommodated in the expression of branching ratio by replacing $X(x_t)$ with $X_{\rm new}$ given in Eq. (22). Experimentally, only a upper bound on the branching ratio is available: $\mathrm{BR}(K_L \to \pi^0\nu\bar{\nu}) < 2.8 \times 10^{-8}$ at 90% C.L. [89]. In Fig 4, we plot the dependence of the $K_L \to \pi\nu\bar{\nu}$ branching ratio on the imaginary part of the effective couplings $\xi_{\rm ds}$. Numerically, the constraints are given by

$$-0.0021 < \frac{\mathrm{Im}\xi_{\rm ds}}{\left(\frac{M_\phi}{1000\ \mathrm{GeV}}\right)^2} < 0.0023. \tag{26}$$

Since the decay has not been observed so far and the present experimental limits are 3 orders of magnitude above the SM predictions [87], we find that constraints from $K_L \to \pi^0\nu\bar{\nu}$ are weaker compared to those obtained in the case of $K^+ \to \pi^+\nu\bar{\nu}$.

## V. CONSTRAINTS FROM $K_L \to \mu^+\mu^-$

The decay $K_L \to \mu^+\mu^-$ is sensitive to much of the same short-distance physics (i.e., $\lambda_t$ and $m_t$) as $K \to \pi\nu\bar{\nu}$ and therefore provides complementary information on the structure of FCNC $|\Delta S| = 1$ transitions. This is important

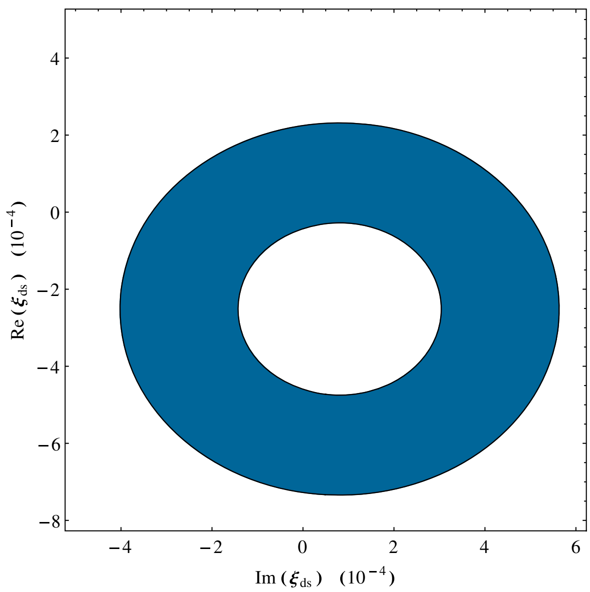


FIG. 3. The constraints on $\mathrm{Re}(\xi_{\rm ds}) - \mathrm{Im}(\xi_{\rm ds})$ parameter space from the measured value of $\mathrm{BR}(K^+ \to \pi^+\nu\bar{\nu})$. The blue colored region shows experimentally allowed values at the $1\sigma$ level.

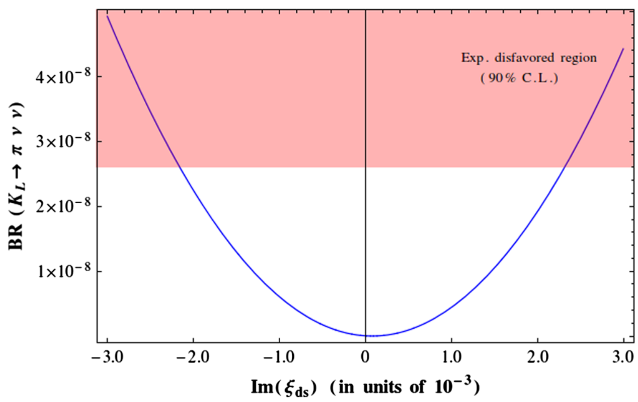


FIG. 4. The dependence of $\mathrm{BR}(K_L \to \pi^0\nu\bar{\nu})$ on $\mathrm{Im}\xi_{\rm ds}$. The red shaded region is currently disfavored by the experimental data at 90% C.L.

because experimentally a much more precise measurement compared to $K \to \pi\nu\bar{\nu}$ is available: $\mathrm{BR}(K_L \to \mu\mu) = (6.84 \pm 0.11) \times 10^{-9}$ [89]. However, the theoretical situation is far more complex (for a review, see Refs. [90,91]). The amplitude for $K_L \to \mu^+\mu^-$ can be decomposed into a dispersive (real) and an absorptive (imaginary) part. The dominant contribution to the absorptive part [as well as to total decay rate $(K_L \to \mu^+\mu^-)$] comes from the real two-photon intermediate state. The dispersive amplitude is the sum of the so-called long-distance and the short-distance contributions. Only the short-distance (SD) part can be reliably calculated. The most recent estimates of the SD part from the data give $\mathrm{BR}(K_L \to \mu^+\mu^-)_{\mathrm{SD}} \leq 2.5 \times 10^{-9}$ [92]. The effective Hamiltonian relevant for the decay $K_L \to \mu^+\mu^-$ is given by [80]

$$\begin{aligned}\mathcal{H}_{\mathrm{eff}}&(K_L \to \mu^+\mu^-)\\ &= \frac{G_F}{\sqrt{2}}\frac{\alpha}{2\pi\sin^2\theta_W}(\lambda_c Y_{\mathrm{NL}} + \lambda_t Y(x_t))(\bar{s}\gamma^\mu(1-\gamma_5)d)(\bar{\mu}\gamma_\mu\gamma_5\mu),\\ &= \frac{G_F}{\sqrt{2}} V_{us}^* V_{ud} \Delta_{\mathrm{SM}}^K (\bar{s}\gamma^\mu(1-\gamma_5)d)(\bar{\mu}\gamma_\mu\gamma_5\mu),\end{aligned} \tag{27}$$

where $\Delta^K_{\mathrm{SM}}$ describes the Wilson coefficient (WC) of the effective local operator $(\bar{s}d)_{\mathrm{V-A}}(\bar{\mu}\gamma_\mu\gamma_5\mu)$ and is given as

$$\Delta^K_{\mathrm{SM}} = \frac{\alpha(\lambda_c Y_{\mathrm{NL}} + \lambda_t Y(x_t))}{2\pi\sin^2\theta_w V_{us}^* V_{ud}}. \tag{28}$$

The short-distance function $Y(x_t)$ describes contribution from Z-penguin and box diagrams with an internal top quark with QCD corrections. Its expression in NLO can be written as [82,83]

$$Y(x_t) = \eta_Y \cdot \frac{x_t}{8}\left(\frac{4-x_t}{1-x_t} + \frac{3x_t}{(1-x_t)^2}\mathrm{Ln}x_t\right), \tag{29}$$

where the factor $\eta_Y$ summarizes the QCD corrections ($\eta_Y = 1.012$). The function $Y_{\mathrm{NL}}$ represents the contribution of loop-diagrams involving internal charm-quark exchange and is known to NLO [80,83] and recently to NNLO [93]. The charm contribution is also often denoted by $P_c(Y)$ and is related to $Y_{\mathrm{NL}}$ analogous to the relation in Eq (19). In the SM, the branching ratio for the SD part is written as [93,94]

$$\begin{aligned}\mathrm{BR}(K_L \to \mu^+\mu^-)_{\mathrm{SM}}(\mathrm{SD}) &= \frac{N_K^2}{2\pi\Gamma_{K_L}}\left(\frac{m_\mu}{m_K}\right)^2\sqrt{1-\frac{4m_\mu^2}{m_K^2}}\\ &\quad\times f_K^2 m_K^3 (\mathrm{Re}\Delta^K_{\mathrm{SM}})^2,\end{aligned} \tag{30}$$

where $N_K = G_F V_{us}^* V_{ud}$ and $\Gamma_{K_L}$ is the decay width of $K_L$. Before proceeding to discuss the constraints on leptoquark couplings from $K_L \to \mu^+\mu^-$, we give a description of the “operator basis” we use in the present and next sections. The effective Hamiltonian for $K_L \to \mu^+\mu^-$ in Eq. (27) is written in the operator basis of $\{Q_{7V}, Q_{7A}\}$ following Ref. [94]. In what follows, we will switch to the $\{Q^K_{\mathrm{VLL}}, Q^K_{\mathrm{VLR}}\}$ operator basis. The operators in both bases are written as

$$\begin{aligned}Q_{7V} &= (\bar{s}\gamma_\alpha(1-\gamma_5)d)(\bar{\mu}\gamma^\alpha\mu),\\ Q_{7A} &= (\bar{s}\gamma_\alpha(1-\gamma_5)d)(\bar{\mu}\gamma^\alpha\gamma_5\mu),\end{aligned} \tag{31}$$

and

$$\begin{aligned}Q^K_{\mathrm{VLL}} &= (\bar{s}\gamma_\alpha L d)(\bar{\mu}\gamma^\alpha L\mu),\\ Q^K_{\mathrm{VLR}} &= (\bar{s}\gamma_\alpha L d)(\bar{\mu}\gamma^\alpha R\mu).\end{aligned} \tag{32}$$

To change from the basis $\{Q_{7V}, Q_{7A}\}$ to the basis $\{Q^K_{\mathrm{VLL}}, Q^K_{\mathrm{VLR}}\}$, the following transformation rules hold:

$$\begin{aligned}Q^K_{\mathrm{VLL}} &= \frac{1}{4}(Q_{7V} - Q_{7A}),\\ Q^K_{\mathrm{VLR}} &= \frac{1}{4}(Q_{7V} + Q_{7A}).\end{aligned} \tag{33}$$

The scalar leptoquark $\phi$ contributes to the quark-level transition $\bar{s} \to \bar{d}\mu^+\mu^-$ at the leading order through loop diagrams. The Feynman diagrams relevant for $K_L \to \mu^+\mu^-$ are shown in Fig 5. These diagrams are similar to the ones calculated in the case of $b \to s\mu\mu$ in Ref. [40]. We adapt the results in Ref. [40] to the case of $s \to d\mu^+\mu^-$ to obtain the NP Wilson coefficients of effective operators $Q^K_{\mathrm{VLL}}$ and $Q^K_{\mathrm{VLR}}$ given by,

$$C^{K(\mathrm{new})}_{\mathrm{VLL}} = -\frac{1}{8\pi^2}\frac{\lambda_t}{\lambda_u}\frac{m_t^2}{M_\phi^2}|\lambda^L_{t\mu}|^2 + \frac{\sqrt{2}}{64G_F\pi^2 M_\phi^2}\frac{\xi_{\mathrm{ds}}\xi^L_{\mu\mu}}{\lambda_u}, \tag{34}$$

$$\begin{aligned}C^{K(\mathrm{new})}_{\mathrm{VLR}} &= -\frac{1}{16\pi^2}\frac{\lambda_t}{\lambda_u}\frac{m_t^2}{M_\phi^2}|\lambda^R_{t\mu}|^2\left(\mathrm{Ln}\frac{M_\phi^2}{m_t^2} - f(x_t)\right)\\ &\quad + \frac{\sqrt{2}}{64G_F\pi^2 M_\phi^2}\frac{\xi_{\mathrm{ds}}\xi^R_{\mu\mu}}{\lambda_u},\end{aligned} \tag{35}$$

where the function $f(x_t)$ depends on the top-quark mass and is given in Ref. [40] and we define

$$\xi^{L(R)}_{\ell\ell'} = \sum_i \lambda^{L(R)*}_{u_i\ell}\lambda^{L(R)}_{u_i\ell'}. \tag{36}$$

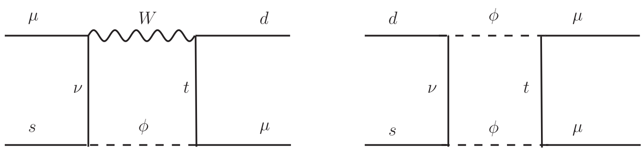


FIG. 5. Feynman diagrams relevant for the decay $K_L \to \mu^+\mu^-$ induced by the scalar leptoquark $\phi$.

The one advantage we get by the change of basis is that the contribution of right-handed interaction terms in the Lagrangian [Eq. (2)] is contained only in $C_{\mathrm{VLR}}^{K(\mathrm{new})}$. After accommodating the leptoquark contribution to the SM value, the total SD branching ratio for the decay $K_L \to \mu^+\mu^-$ is given by

$$\begin{aligned}\mathrm{BR}(K_L \to \mu^+\mu^-)_{\mathrm{SD}} = & \frac{N_K^2}{2\pi\Gamma_{K_L}}\left(\frac{m_\mu}{m_K}\right)^2\sqrt{1-\frac{4m_\mu^2}{m_K^2}} \\ & \times f_K^2 m_K^3 \lambda^{10}\left\{\frac{\mathrm{Re}\lambda_c}{\lambda}\frac{\alpha P_c(Y)}{2\pi\sin^2\theta_W\lambda_u}\right. \\ & +\frac{1}{\lambda^5}\left(\mathrm{Re}\lambda_t\frac{\alpha Y(x_t)}{2\pi\sin^2\theta_W\lambda_u}\right. \\ & \left.\left.+\frac{1}{4}\mathrm{Re}(C_{\mathrm{VLR}}^{K(\mathrm{new})}-C_{\mathrm{VLL}}^{K(\mathrm{new})})\right)\right\}^2. \end{aligned} \tag{37}$$

To simplify further the analysis, we invoke the assumption that, except the SM contribution, only one of the NP operators contributes dominantly. This assumption helps us in determining the limits on the dominant WC from $\mathrm{BR}(K_L \to \mu^+\mu^-)_{\mathrm{SD}}$, and the generalization of this situation to incorporate more than one NP operator contribution is straight forward. Therefore, in what follows, we will ignore the contribution of the right-handed operator in further analysis. In Fig. 6, we show the dependence of the SD part of $\mathrm{BR}(K_L \to \mu^+\mu^-)$ on $\mathrm{Re}C_{\mathrm{VLL}}^{K(\mathrm{new})}$. Numerically, the bound on the WC reads $-1.00\times10^{-4} < \mathrm{Re}C_{\mathrm{VLL}}^{K(\mathrm{new})} < 0.27\times10^{-4}$. We use the upper bound to constrain the generation-diagonal leptoquark couplings in the following way. Employing Eq. (34), the upper bound on the WC can be written in terms of model parameters as

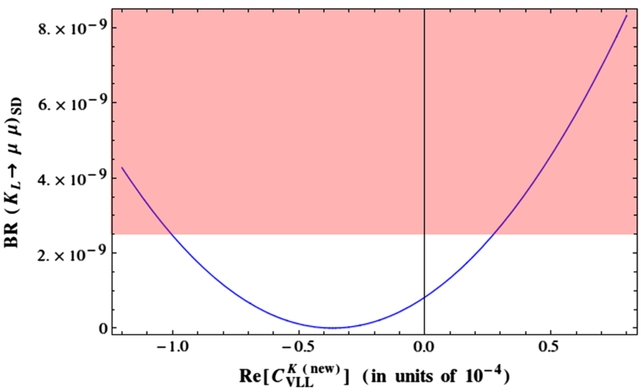


FIG. 6. The dependence of $\mathrm{BR}(K_L \to \mu^+\mu^-)$ on the Wilson coefficient $C_{\mathrm{VLL}}^{K(\mathrm{new})}$. We have assumed one-operator dominance as discussed in the text. The red shaded region shows the experimentally disallowed values at $1\sigma$.

$$\left(-\frac{1}{8\pi^2}\frac{\mathrm{Re}\lambda_t}{\lambda_u}\frac{m_t^2}{M_\phi^2}|\lambda_{t\mu}^L|^2+\frac{\sqrt{2}}{64G_F\pi^2M_\phi^2}\frac{\mathrm{Re}\xi_{\mathrm{ds}}}{\lambda_u}\xi_{\mu\mu}^L\right) < 0.27\times10^{-4}. \tag{38}$$

Assuming the worst possible case in which the bound on $\mathrm{Re}\xi_{\mathrm{ds}}$ from $K^+ \to \pi^+\nu\bar{\nu}$ (as obtained in Sec. III) is saturated, i.e., using $\mathrm{Re}\xi_{\mathrm{ds}} = 2.2\times10^{-4}$ in the above equation, we get

$$\sqrt{|\lambda_{u\mu}^L|^2+|\lambda_{c\mu}^L|^2+\left(1+\frac{2.52}{(\frac{M_\phi}{1000\ \mathrm{GeV}})^2}\right)|\lambda_{t\mu}^L|^2} < 11.83. \tag{39}$$

We find that constraints from the SD branching ratio of $K_L \to \mu^+\mu^-$ are not severe and large $\sim O(1)$ generation-diagonal leptoquark couplings are allowed. To this end, we must mention that the above bound is in agreement with the constraint obtained in Ref. [40] [see Eq. (17) therein] while explaining the anomaly in $R_K$ in this model. We also note from Eq. (39) that the top contribution to $\bar{s} \to \bar{d}\mu^+\mu^-$ for the considered masses of the leptoquark ($\sim$1 TeV) is largely enhanced in contrast to the effects found in the case of $b \to s\mu^+\mu^-$ processes [40] where the top contribution is suppressed for the same choice of the leptoquark masses.

## VI. CONSTRAINTS FROM LFV DECAY $K_L \to \mu^\mp e^\pm$

In this section, we discuss the effects of the leptoquark $\phi$ on LFV process $K \to \mu^\mp e^\pm$. Experimentally, there is only an upper bound on this process: $\mathrm{BR}(K_L \to \mu^\mp e^\pm) < 4.7\times10^{-12}$ [89]. LFV processes are interesting because in the SM they are forbidden. Therefore, any observation of such process immediately indicates toward the presence of NP. The leptoquark $\phi$ can mediate $K_L \to \mu e$ decay through similar diagrams shown in Fig. 5 with one of the $\mu$ lines being replaced with $e$. After integrating out heavy particles, new effective operators relevant for $K_L \to \mu e$ are generated. The operators are similar to those in Eq. (32) but with one of the $\mu$ changed to $e$. The branching ratio in terms of the new Wilson coefficients $C_{\mathrm{VLL}}^{\mu e}$ and $C_{\mathrm{VLR}}^{\mu e}$ is given by [94]

$$\begin{aligned}\mathrm{BR}(K_L \to \mu e) = & \frac{N_K^2 f_K^2}{64\pi\Gamma_{K_L}}\left(\frac{m_\mu}{m_K}\right)^2\left(1-\frac{m_\mu^2}{m_K^2}\right)^2 \\ & \times(|C_{\mathrm{VLL}}^{\mu e}|^2+|C_{\mathrm{VLR}}^{\mu e}|^2). \end{aligned} \tag{40}$$

Adjusting the results of Eq. (34) to the LFV case, we find

$$\begin{aligned}C_{\mathrm{VLL}}^{\mu e} = & -\frac{1}{8\pi^2}\frac{\lambda_t}{\lambda_u}\frac{m_t^2}{M_\phi^2}(\lambda_{te}^L\lambda_{t\mu}^{L*}) \\ & +\frac{\sqrt{2}}{64G_F\pi^2M_\phi^2}\frac{\xi_{\mathrm{ds}}\xi_{\mu e}^L}{\lambda_u}, \end{aligned} \tag{41}$$

$$C_{\mathrm{VLR}}^{\mu e} = -\frac{1}{16\pi^2}\frac{\lambda_t}{\lambda_u}\frac{m_t^2}{M_\phi^2}(\lambda_{t\mu}^R\lambda_{te}^R)\left(\mathrm{Ln}\frac{M_\phi^2}{m_t^2} - f(x_t)\right) + \frac{\sqrt{2}}{64 G_F \pi^2 M_\phi^2}\frac{\xi_{\mathrm{ds}}\xi_{\mu e}^R}{\lambda_u}. \quad (42)$$

Using the current experimental bound on $K_L \to \mu e$, we get $[|C_{\mathrm{VLL}}^{\mu e}|^2 + |C_{\mathrm{VLR}}^{\mu e}|^2]^{1/2} < 3.9 \times 10^{-6}$. Following the similar analysis as done in Sec. V for the case of $K_L \to \mu\mu$, we obtain the constraints on the leptoquark couplings,

$$\left(\sqrt{(\lambda_{u\mu}^L\lambda_{ue}^L) + (\lambda_{c\mu}^L\lambda_{ce}^L) + \left(1 + \frac{2.52}{(\frac{M_\phi}{1000\ \mathrm{GeV}})^2}\right)(\lambda_{t\mu}^L\lambda_{te}^L)}\right) < 4.49, \quad (43)$$

where the top contribution is again enhanced. For simplicity, we assumed the couplings to be real. Here, we would like to mention that the same Wilson coefficients also contribute to other LFV processes such as $K \to \pi\mu e$. However, as pointed out in Ref. [94], the constraints on Wilson coefficients $(|C_{\mathrm{VLL}}^{\mu e}|^2 + |C_{\mathrm{VLR}}^{\mu e}|^2)^{1/2}$ are about an order of magnitude weaker than the one from $K_L \to \mu^\mp e^\pm$. Therefore, experimental data on $K \to \pi\mu e$ do not improve the constraints obtained in Eq. (43).

## VII. RESULTS AND DISCUSSION

In light of several anomalies observed in semileptonic B decays, often explained by invoking leptoquark NP models, we have studied a scalar leptoquark model in the context of rare decays of kaons and neutral kaon mixing. The model is interesting because it can provide one of the possible explanations for the observed discrepancies in semileptonic B decays. We examined the effects of leptoquark contribution to the several kaon processes involving $K^0 - \bar{K}^0$ mixing, $K^+ \to \pi^+\nu\bar{\nu}$, $K_L \to \pi^0\nu\bar{\nu}$, $K_L \to \mu^+\mu^-$, and LFV decay $K_L \to \mu^\mp e^\pm$. Working in the framework of EFT, we have discussed the effective operators generated after integrating out heavy particles and written down the explicit expressions of the corresponding Wilson coefficient in terms of the leptoquark couplings. Using the present experimental information on these decays, we derived bounds on the couplings relevant for kaon processes. We found that the constraints from $K^0 - \bar{K}^0$ on the real and imaginary parts of left-handed coupling $\xi_{\mathrm{ds}}$ are $\sim O(10^{-2})$. However, the same set of couplings can also be constrained from $\mathrm{BR}(K^+ \to \pi^+\nu\bar{\nu})$, $\mathrm{BR}(K_L \to \pi^0\nu\bar{\nu})$, and it was found that constraints from the rare process $\mathrm{BR}(K^+ \to \pi^+\nu\bar{\nu})$ are about 2 orders of magnitude more severe than those obtained from the mixing of neutral kaons. In fact, the decay $\mathrm{BR}(K^+ \to \pi^+\nu\bar{\nu})$ gives the most stringent constraints on the leptoquark couplings among all the processes studied in this work and therefore is the most interesting observable to test the NP effects of a scalar leptoquark in the kaon sector. Assuming a one-operator dominance scenario, we constrained the NP Wilson coefficient contributing to the rate of $K_L \to \mu^+\mu^-$. We further used the bounds on the NP Wilson coefficient to obtain the constraints on generation-diagonal leptoquark couplings. We found that the present measured value of $\mathrm{BR}(K_L \to \mu^+\mu^-)$ allows generation-diagonal coupling of the leptoquark to be $\sim O(1)$. The constraint on the combination of generation-diagonal couplings from $K_L \to \mu^+\mu^-$ is in agreement with the one obtained in Ref. [40] for explaining experimental data on $R_K$. However, whereas the top contribution to $b \to s\mu^+\mu^-$ is suppressed, we found that in the case of $\bar{s} \to \bar{d}\mu^+\mu^-$ the top contribution is enhanced for the considered range of leptoquark masses. We also did a similar analysis for the case of LFV decay $K_L \to \mu^\mp e^\pm$, which involves generation-diagonal as well as off-diagonal couplings. We found that present experimental limits on $\mathrm{BR}(K_L \to \mu^\mp e^\pm)$ do not provide very strong constraints, and involved couplings can be as large as $\sim O(1)$.

## ACKNOWLEDGMENTS

The author would like to thank Namit Mahajan, Anjan Joshipura, and Saurabh Rindani for many helpful discussions. The author would like to thank Monika Blanke for a very useful communication regarding kaon mixing observables. The author also thanks Abhaya Swain and Chandan Hati for help with the preparation of this manuscript.

[1] G. Aad *et al.* (ATLAS Collaboration), Phys. Lett. B **716**, 1 (2012).
[2] S. Chatrchyan *et al.* (CMS Collaboration), Phys. Lett. B **716**, 30 (2012).
[3] G. Ricciardi *et al.*, Eur. Phys. J. Plus **130**, 209 (2015); J. Ellis, arXiv:1604.00333.
[4] J. P. Lees *et al.* (*BABAR* Collaboration), Phys. Rev. Lett. **109**, 101802 (2012); J. P. Lees *et al.* (*BABAR* Collaboration), Phys. Rev. D **88**, 072012 (2013).
[5] M. Huschle *et al.* (Belle Collaboration), Phys. Rev. D **92**, 072014 (2015).

[6] R. Aaij *et al.* (LHCb Collaboration), Phys. Rev. Lett. **115**, 111803 (2015).
[7] S. Fajfer, J. F. Kamenik, and I. Nisandzic, Phys. Rev. D **85**, 094025 (2012); H. Na, C. M. Bouchard, G. P. Lepage, C. Monahan, and J. Shigemitsu (HPQCD Collaboration), Phys. Rev. D **92**, 054510 (2015).
[8] R. Aaij *et al.* (LHCb Collaboration), Phys. Rev. Lett. **113**, 151601 (2014).
[9] C. Bobeth, G. Hiller, and G. Piranishvili, J. High Energy Phys. 12 (2007) 040.
[10] G. Hiller and F. Kruger, Phys. Rev. D **69**, 074020 (2004).
[11] R. Aaij *et al.* (LHCb Collaboration), Phys. Rev. Lett. **111**, 191801 (2013).
[12] R. Aaij *et al.* (LHCb Collaboration), J. High Energy Phys. 02 (2016) 104.
[13] W. Altmannshofer and D. M. Straub, arXiv:1503.06199.
[14] R. Aaij *et al.* (LHCb Collaboration), J. High Energy Phys. 09 (2015) 179.
[15] A. Celis, M. Jung, X. Q. Li, and A. Pich, J. High Energy Phys. 01 (2013) 054.
[16] P. Ko, Y. Omura, and C. Yu, J. High Energy Phys. 03 (2013) 151.
[17] A. Crivellin, C. Greub, and A. Kokulu, Phys. Rev. D **86**, 054014 (2012).
[18] N. G. Deshpande and A. Menon, J. High Energy Phys. 01 (2013) 025.
[19] C. Hati, G. Kumar, and N. Mahajan, J. High Energy Phys. 01 (2016) 117.
[20] A. Datta, M. Duraisamy, and D. Ghosh, Phys. Rev. D **86**, 034027 (2012).
[21] M. Tanaka and R. Watanabe, Phys. Rev. D **87**, 034028 (2013).
[22] M. Freytsis, Z. Ligeti, and J. T. Ruderman, Phys. Rev. D **92**, 054018 (2015).
[23] S. Bhattacharya, S. Nandi, and S. K. Patra, Phys. Rev. D **93**, 034011 (2016).
[24] I. Dorsner, S. Fajfer, J. F. Kamenik, and N. Kosnik, Phys. Lett. B **682**, 67 (2009).
[25] Y. Sakaki, M. Tanaka, A. Tayduganov, and R. Watanabe, Phys. Rev. D **88**, 094012 (2013).
[26] S. Fajfer, J. F. Kamenik, I. Nisandzic, and J. Zupan, Phys. Rev. Lett. **109**, 161801 (2012).
[27] I. Dorner, S. Fajfer, N. Konik, and I. Niandi, J. High Energy Phys. 11 (2013) 084.
[28] T. Blake, T. Gershon, and G. Hiller, Annu. Rev. Nucl. Part. Sci. **65**, 113 (2015).
[29] R. Gauld, F. Goertz, and U. Haisch, J. High Energy Phys. 01 (2014) 069.
[30] S. L. Glashow, D. Guadagnoli, and K. Lane, Phys. Rev. Lett. **114**, 091801 (2015).
[31] A. Crivellin, G. D'Ambrosio, and J. Heeck, Phys. Rev. D **91**, 075006 (2015).
[32] W. Altmannshofer, S. Gori, M. Pospelov, and I. Yavin, Phys. Rev. D **89**, 095033 (2014).
[33] A. J. Buras and J. Girrbach, J. High Energy Phys. 12 (2013) 009.
[34] A. Crivellin, G. D'Ambrosio, and J. Heeck, Phys. Rev. Lett. **114**, 151801 (2015).
[35] C. W. Chiang, X. G. He, and G. Valencia, Phys. Rev. D **93**, 074003 (2016).
[36] B. Gripaios, M. Nardecchia, and S. A. Renner, J. High Energy Phys. 05 (2015) 006.
[37] D. Beirevi, S. Fajfer, and N. Konik, Phys. Rev. D **92**, 014016 (2015).
[38] R. Alonso, B. Grinstein, and J. M. Camalich, J. High Energy Phys. 10 (2015) 184.
[39] L. Calibbi, A. Crivellin, and T. Ota, Phys. Rev. Lett. **115**, 181801 (2015).
[40] M. Bauer and M. Neubert, Phys. Rev. Lett. **116**, 141802 (2016).
[41] G. Hiller and M. Schmaltz, Phys. Rev. D **90**, 054014 (2014).
[42] R. Barbieri, G. Isidori, A. Pattori, and F. Senia, Eur. Phys. J. C **76**, 67 (2016).
[43] S. Fajfer and N. Konik, Phys. Lett. B **755**, 270 (2016).
[44] I. de Medeiros Varzielas and G. Hiller, J. High Energy Phys. 06 (2015) 072.
[45] M. Blanke, *Proc. Sci.* KAON13 (2013) 010.
[46] A. J. Buras and J. Girrbach, Acta Phys. Pol. B **43**, 1427 (2012).
[47] A. J. Buras, T. Ewerth, S. Jager, and J. Rosiek, Nucl. Phys. **B714**, 103 (2005).
[48] M. Blanke, A. J. Buras, B. Duling, S. Recksiegel, and C. Tarantino, Acta Phys. Pol. B **41**, 657 (2010).
[49] M. Blanke, A. J. Buras, B. Duling, K. Gemmler, and S. Gori, J. High Energy Phys. 03 (2009) 108.
[50] M. Bauer, S. Casagrande, U. Haisch, and M. Neubert, J. High Energy Phys. 09 (2010) 017.
[51] C. J. Lee and J. Tandean, J. High Energy Phys. 08 (2015) 123.
[52] A. J. Buras, F. De Fazio, J. Girrbach, and M. V. Carlucci, J. High Energy Phys. 02 (2013) 023.
[53] A. J. Buras, F. De Fazio, and J. Girrbach-Noe, J. High Energy Phys. 08 (2014) 039.
[54] A. J. Buras and J. Girrbach, Rep. Prog. Phys. **77**, 086201 (2014).
[55] A. J. Buras, A. Romanino, and L. Silvestrini, Nucl. Phys. **B520**, 3 (1998).
[56] F. S. Queiroz, K. Sinha, and A. Strumia, Phys. Rev. D **91**, 035006 (2015).
[57] For ATLAS and CMS physics results from Run-II, see http://indico.cern.ch/event/442432/.
[58] S. Sahoo and R. Mohanta, Phys. Rev. D **91**, 094019 (2015).
[59] S. Fajfer and N. Kosnik, Phys. Rev. D **79**, 017502 (2009).
[60] S. de Boer and G. Hiller, Phys. Rev. D **93**, 074001 (2016).
[61] S. Fajfer and N. Konik, Eur. Phys. J. C **75**, 567 (2015).
[62] M. Antonelli, D. M. Asner, D. Bauer, T. Becher, M. Beneke, A.J. Bevan, M. Blanke, C. Bloise, M. Bona, and A. Bondar, Phys. Rep. **494**, 197 (2010).
[63] G. Buchalla, A. J. Buras, and M. E. Lautenbacher, Rev. Mod. Phys. **68**, 1125 (1996).
[64] T. Inami and C. S. Lim, Prog. Theor. Phys. **65**, 297 (1981); **65**, 1772 (1981).
[65] G. C. Branco, L. Lavoura, and J. P. Silva, Int. ser. monogr. phys. **103**, 1 (1999).
[66] A. J. Buras, M. Jamin, and P. H. Weisz, Nucl. Phys. **B347**, 491 (1990).
[67] J. Brod and M. Gorbahn, Phys. Rev. Lett. **108**, 121801 (2012).
[68] J. Brod and M. Gorbahn, Phys. Rev. D **82**, 094026 (2010).

[69] M. Bona *et al.* (UTfit Collaboration), J. High Energy Phys. 03 (2008) 049.
[70] A. J. Buras and D. Guadagnoli, Phys. Rev. D **78**, 033005 (2008).
[71] A. J. Buras, D. Guadagnoli, and G. Isidori, Phys. Lett. B **688**, 309 (2010).
[72] Z. Ligeti and F. Sala, arXiv:1602.08494.
[73] A. J. Buras, J. M. Grard, and W. A. Bardeen, Eur. Phys. J. C **74**, 2871 (2014).
[74] A. J. Buras, F. Schwab, and S. Uhlig, Rev. Mod. Phys. **80**, 965 (2008).
[75] F. Mescia and C. Smith, Phys. Rev. D **76**, 034017 (2007).
[76] G. Isidori, F. Mescia, and C. Smith, Nucl. Phys. **B718**, 319 (2005).
[77] G. Buchalla and G. Isidori, Phys. Lett. B **440**, 170 (1998).
[78] C. Q. Geng, I. J. Hsu, and Y. C. Lin, Phys. Rev. D **54**, 877 (1996).
[79] G. Buchalla and A. J. Buras, Phys. Rev. D **57**, 216 (1998).
[80] G. Buchalla and A. J. Buras, Nucl. Phys. **B412**, 106 (1994).
[81] G. Buchalla and A. J. Buras, Nucl. Phys. **B400**, 225 (1993).
[82] M. Misiak and J. Urban, Phys. Lett. B **451**, 161 (1999).
[83] G. Buchalla and A. J. Buras, Nucl. Phys. **B548**, 309 (1999).
[84] J. Brod, M. Gorbahn, and E. Stamou, Phys. Rev. D **83**, 034030 (2011).
[85] A. J. Buras, M. Gorbahn, U. Haisch, and U. Nierste, Phys. Rev. Lett. **95**, 261805 (2005).
[86] A. J. Buras, M. Gorbahn, U. Haisch, and U. Nierste, J. High Energy Phys. 11 (2016) 002; J. High Energy Phys.11 (2012) 167.
[87] A. J. Buras, D. Buttazzo, J. Girrbach-Noe, and R. Knegjens, J. High Energy Phys. 11 (2015) 03.
[88] A. J. Buras, arXiv:hep-ph/9806471.
[89] K. A. Olive *et al.* (Particle Data Group Collaboration), Chin. Phys. C **38**, 090001 (2014).
[90] J. L. Ritchie and S. G. Wojcicki, Rev. Mod. Phys. **65**, 1149 (1993).
[91] V. Cirigliano, G. Ecker, H. Neufeld, A. Pich, and J. Portoles, Rev. Mod. Phys. **84**, 399 (2012).
[92] G. Isidori and R. Unterdorfer, J. High Energy Phys. 01 (2004) 009.
[93] M. Gorbahn and U. Haisch, Phys. Rev. Lett. **97**, 122002 (2006).
[94] A. Crivellin, G. D'Ambrosio, M. Hoferichter, and L. C. Tunstall, Phys. Rev. D **93**, 074038 (2016).